Pacific Northwest
NATIONAL LABORATORY

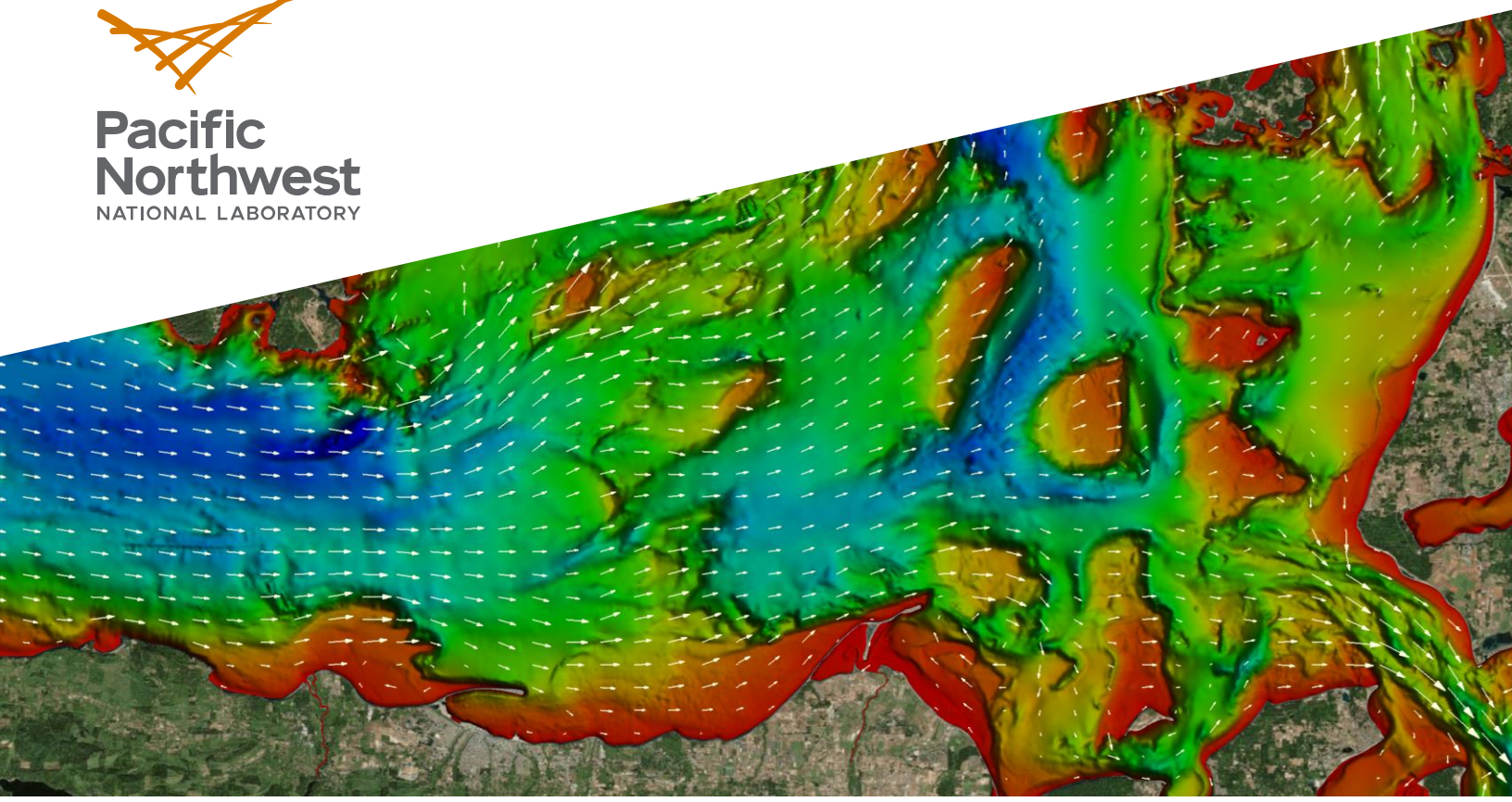

PNNL-30448

Validation of the High-Resolution Salish Sea Tidal Hydrodynamic Model

September 2020

Z Yang
T Wang
R Branch
Z Xiao

U.S. DEPARTMENT OF ENERGY

Prepared for the U.S. Department of Energy
under Contract DE-AC05-76RL01830

DISCLAIMER

PACIFIC NORTHWEST NATIONAL LABORATORY
operated by
BATTELLE
for the
UNITED STATES DEPARTMENT OF ENERGY
under Contract DE-AC05-76RL01830

Printed in the United States of America

Available to DOE and DOE contractors from the
Office of Scientific and Technical Information,
P.O. Box 62, Oak Ridge, TN 37831-0062;
ph: (865) 576-8401
fax: (865) 576-5728
email: reports@adonis.osti.gov

Available to the public from the National Technical Information Service
5301 Shawnee Rd., Alexandria, VA 22312
ph: (800) 553-NTIS (6847)
email: orders@ntis.gov <https://www.ntis.gov/about>
Online ordering: http://www.ntis.gov

PNNL-30448

Validation of the High-Resolution Salish Sea Tidal Hydrodynamic Model

September 2020

Z Yang
T Wang
R Branch
Z Xiao

Prepared for
the U.S. Department of Energy
under Contract DE-AC05-76RL01830

Pacific Northwest National Laboratory
Richland, Washington 99354

Summary

In this study, a tidal hydrodynamic model was developed and validated to simulate tidal currents in Puget Sound, Washington, to support tidal energy resource characterization using the unstructured-grid, Finite Volume Community Ocean Model (FVCOM). The Salish Sea tidal hydrodynamic model was driven by tides along two open boundaries at the entrance of the Strait of Juan de Fuca and north end of Georgia Strait, and river flows from 19 major rivers in the Salish Sea. To simulate the tidal current in Puget Sound, a high-resolution model grid is required to accurately represent the complex coastlines and bathymetry. The spatial resolution of the model grid varies from ~10 m near river boundaries and ~30 m in small tidal channels and estuaries to near 1000 m inside Georgia Strait and at the open boundaries.

Model validation was carried out by comparing simulated and observed water levels at 12 tidal stations and currents at 135 Acoustic Doppler Current Profiler stations in the model domain. A set of model performance metrics, including root mean square error, scatter index, bias, and linear correlation coefficient, were used to quantify the model skills in simulating the tidal hydrodynamics in Puget Sound. Error statistics showed an overall good agreement between simulated and observed tidal elevations and currents, which demonstrated that the Puget Sound tidal model can be used to accurately characterize the tidal stream energy resource in Puget Sound.

Acknowledgments

The project is funded by the U.S. Department of Energy, Office of Energy Efficiency and Renewable Energy, Water Power Technologies Office under Contract DE AC05-76RL01830 to Pacific Northwest National Laboratory.

Acronyms and Abbreviations

ADCP	acoustic Doppler current profiler
CFSR	Climate Forecast System Reanalysis
C-MIST	currents measurement interface for the study of tides
DFO	Fisheries and Oceans Canada (Department of Fisheries and Oceans)
FVCOM	finite volume community ocean model
MSL	mean sea level
NAVD88	North American Vertical Datum of 1988
NOAA	National Oceanic and Atmospheric Administration
RMSE	root mean square error
SI	scatter index
SJDF	Strait of Juan de Fuca

Contents

Summary iii
Acknowledgments iv
Acronyms and Abbreviations v
1.0 Introduction 1
2.0 Methodology 2
2.1 Hydrodynamic Model of the Salish Sea 2
2.2 Tidal Elevation and Current Data 3
2.3 Model Forcing and Boundary Conditions 9
2.4 Model Performance Metrics 11
3.0 Results and Discussion 12
3.1 Model Validation – Water Levels 12
3.2 Model Validation – Currents 13
4.0 Conclusion 24
5.0 References 26
Appendix A – Velocity Comparison A.1
Appendix B – Error Statistics Parameters B.1

Figures

Figure 2.1. Study domain, model bathymetry, and major rivers discharged into Salish Sea 2
Figure 2.2. Salish Sea tidal hydrodynamic model grids for selected sub-basins 3

Figure 2.3. Distribution of tide-gauge stations and ADCP stations in the Salish Sea.....5
Figure 2.4. Discharge of 19 rivers during 2016 10
Figure 3.1. Time-series comparisons of simulated and observed total water levels at 12 tidal stations in the model domain.....12
Figure 3.2. Model seabed depth as defined by NAVD88 vs. the ADCP deployment depth 14
Figure 3.3. Comparisons of simulated and observed velocities at Lopez Passage (PUG1730): (a) velocity histograms, (b) scatter plot, (c) vertical profiles, and (d) time series of depth-averaged principal velocities.....15
Figure 3.4. Comparisons of simulated and observed velocities at Rosario Strait (PUG1702): (a) velocity histograms, (b) scatter plot, (c) vertical profiles, and (d) time series of depth-averaged principal velocities.....15
Figure 3.5. Comparisons of simulated and observed velocities at Admiralty Inlet (PUG1624): (a) velocity histograms;, (b) scatter plot, (c) vertical profiles, and (d) time series of depth-averaged principal velocities.....16
Figure 3.6. Comparisons of simulated and observed velocities at Agate Passage (PUG1501): (a) station location, (b) scatter plot, (c) vertical profiles, and (d) time series of depth-averaged principal velocities.....16
Figure 3.7. Comparisons of simulated and observed velocities at The Narrows (PUG1524): (a) velocity histograms;, (b) scatter plot, (c) vertical profiles, and (d) time series of depth-averaged principal velocities.....17
Figure 3.8. Comparisons of simulated and observed velocities at Hale Passage (PUG1710): (a) velocity histograms, (b) scatter plot, (c) vertical profiles, and (d) time series of depth-averaged principal velocities.....17
Figure 3.9. RMSE of depth-averaged principal velocity comparison: (a) map and (b) histogram.....22
Figure 3.10. *SI* of depth-averaged principal velocity comparison: (a) map and (b) histogram.....22
Figure 3.11. Bias of depth-averaged principal velocity comparison: (a) map and (b) histogram.....23
Figure 3.12. *R* of depth-averaged principal velocity comparison: (a) map and (b) histogram.....23
Figure 4.1. Simulated tidal elevation at (a) high tide at 6/17/2015 19:00:00 (PST) and (b) low tide 6/17/2015 11:00:00 (PST)24
Figure 4.2. Simulated depth-averaged tidal currents at 6/16/2015 14:00:00 (PST) and (b) ebb tide at 6/17/2015 08:00:00 (PST).....25
Figure 5.1. Locations of the ADCP measurements. (a-c) 1500 series: Central Sound and South Sound; (d-f) 1600 series: Admiralty Inlet, Hood Canal, Whidbey Basin and San Juan de Fuca; (g-i) 1700 series: San Juan Islands and Georgia Strait..... A.1

Tables

Table 2.1. Tide gauges (12 stations) in the model domain.....3

Table 2.2. NOAA C-MIST ADCP stations for model validation in Puget Sound.....5
Table 2.3. Flow rates of major rivers included in the Salish Sea tidal model.....9
Table 3.1. Error statistics of total water level predictions at 12 tide gauges 13
Table 3.2. Error statistics for modeled depth-averaged tidal velocities.....18

1.0 Introduction

Salish Sea is a large estuary located on the Pacific Northwest coast of Washington State, USA and British Columbia, Canada. It has been identified as one of the top sites in terms of maximum tidal energy potential (Defne et al. 2012) and for early deployment of tidal turbine farms (Kilcher et al. 2016) because of its strong tidal currents and the presence of numerous waterways. To characterize and assess the tidal energy potential, especially at a basin scale, numerical models are often used to simulate tidal currents at desired spatial and temporal resolutions. Over the past decade a number of modeling studies have been conducted to simulate the circulation and tidal energy extraction in Puget Sound using an unstructured-grid modeling approach (Wang and Yang 2017; Yang and Khangaonkar 2010; Yang et al. 2014). However, systematic model validation with current data were not conducted in these modeling studies, and model resolution was not fine enough to resolve the details of tidal channels and Islands in the model domain. To improve the tidal stream resource characterization, a high-resolution, validated tidal hydrodynamic model for the Puget Sound is needed.

The overall objective of this study is to refine and validate the Salish Sea tidal hydrodynamic model and generate high-resolution (Wang and Yang 2017; Yang et al. 2020) tidal current data to support tidal resource characterization and assessment in the Puget Sound. Specifically, high grid resolution (~50 m) was specified in many of the tidal channels and estuaries in the Salish Sea model and the model was validated by extensive water level and current measurements in the modal domain.

This report summarizes the model refinement and validation efforts, including model configuration, boundary forcing, and the error statistics of model performance in simulating water level and currents.

2.0 Methodology

The hydrodynamic model, data used in model validation, model configuration and forcing, and model performance metrics are described in the following sections.

2.1 Hydrodynamic Model of the Salish Sea

The Salish Sea is a complex estuarine system with many islands and complex tidal channels of different widths and depths (Figure 2.1). The hydrodynamics are dominated by strong tidal currents and modulated by density-driven estuarine circulation (Babson et al. 2006; Khangaonkar et al. 2011; Sutherland et al. 2011; Yang and Khangaonkar 2010). The Salish Sea consists of three large sub-basins, including Puget Sound, the Strait of Juan de Fuca (SJDF), and Georgia Strait. Puget Sound can be further divided into four deep sub-basins connected by shallower sills: Hood Canal, Whidbey Basin, South Sound, and the Main Basin, which is subdivided into Admiralty Inlet and the Central Basin. Tides in Puget Sound are classified as a mixed semidiurnal meso-tidal regime.

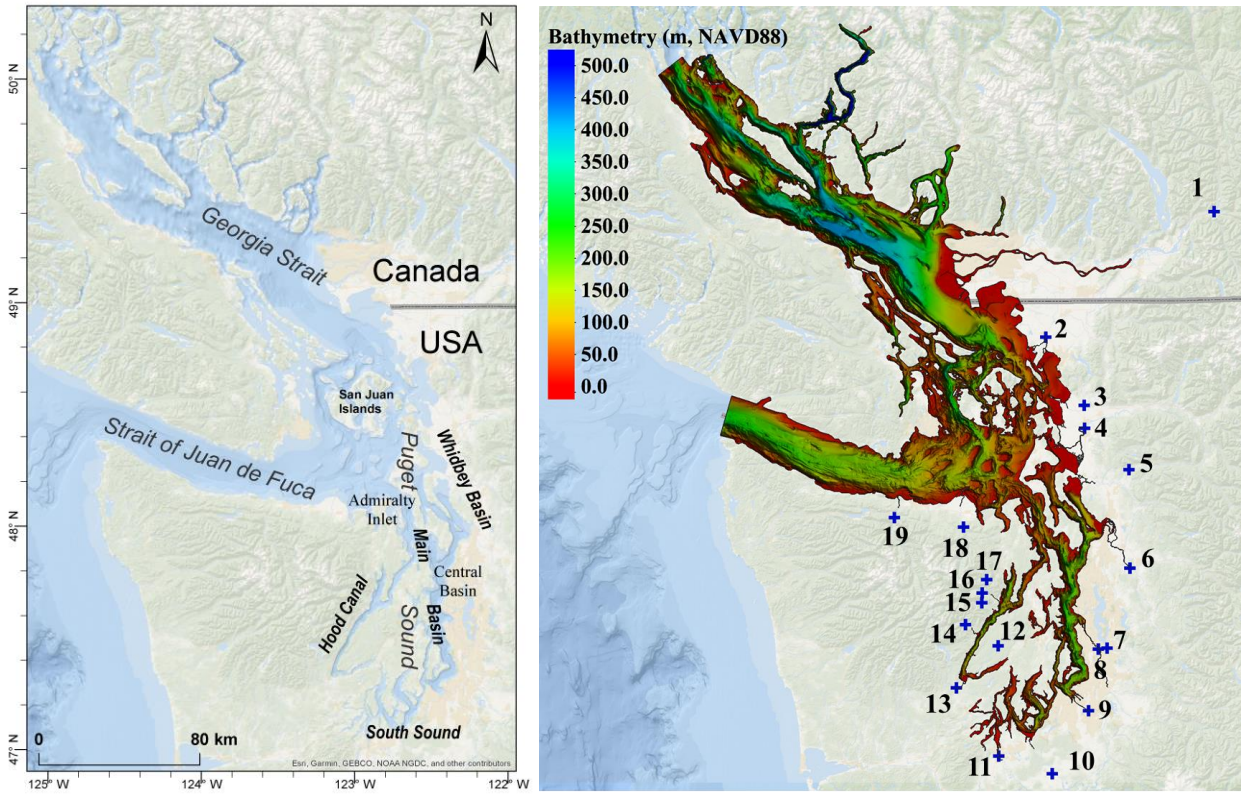

Figure 2.1. Study domain (left), model bathymetry, and major rivers discharged into Salish Sea (right).

The Salish Sea hydrodynamic model was implemented using the Finite Volume Community Ocean Model (FVCOM) (Chen et al. 2013). The model domain and bathymetry are shown in Figure 2.1. There are two open boundaries in the Salish Sea model; one is at the entrance of the SJDF and the other is at the north end of the Strait of Georgia. Water depths in the Salish Sea varies from 0 in the large tide flats areas, such as Skagit Bay and Bellingham Bay, to more than 200 m in the deep sub-basins, such as Central Sound, SJDF, and Georgia Strait. The

major rivers that discharge into the Salish Sea are also marked in Figure 2.1. Because FVCOM employs the unstructured-grid modeling framework, it allows for the use of flexible mesh with various spatial resolutions in complex water bodies. Figure 2.2 shows examples of unstructured model grids and the associated bathymetric features in selected sub-basins of the model domain. The model grid consists of approximately 843,000 nodes and 1,631,000 elements. The model resolution (length of the triangular element) varies from as fine as 30 m at small channels to ~1000 m near the open boundaries and inside Georgia Strait.

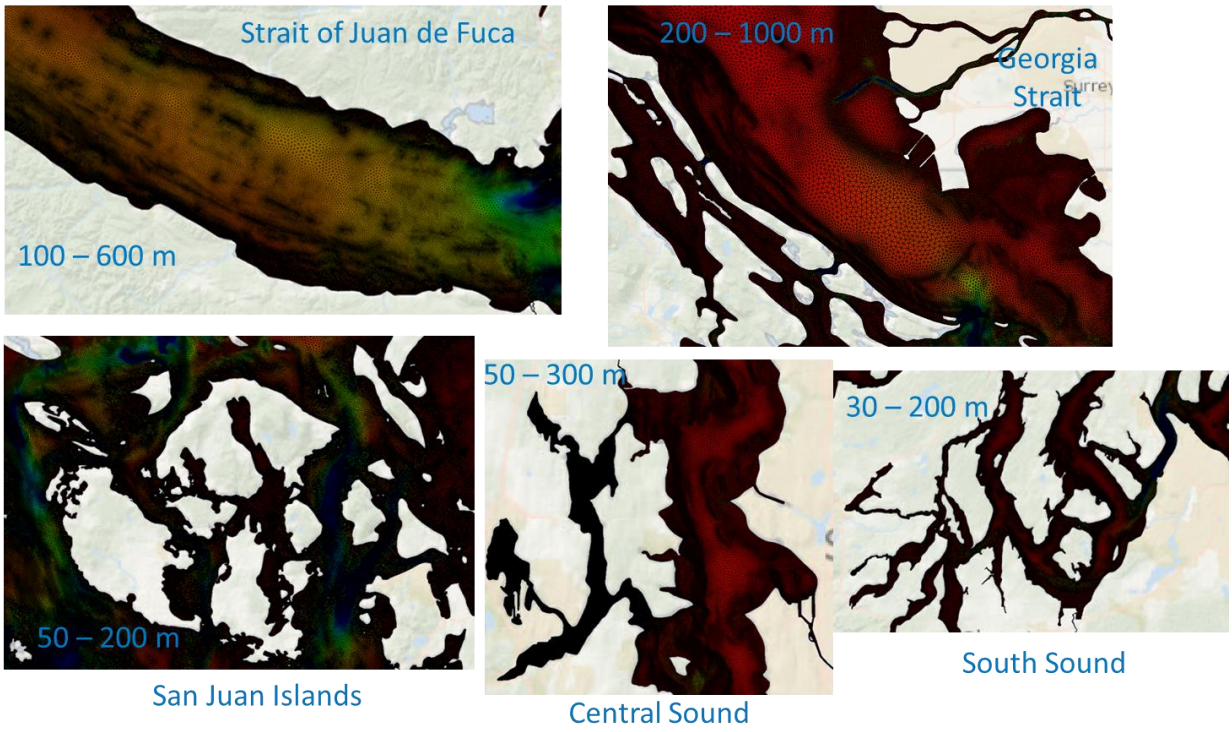

Figure 2.2. Salish Sea tidal hydrodynamic model grids for selected sub-basins.

2.2 Tidal Elevation and Current Data

Tidal elevation and current data are used to validate the Salish Sea tidal hydrodynamic model. There are 12 tide stations in the model domain, including 10 long-term real-time tide-gauge stations, managed by the U.S. National Oceanic and Atmospheric Administration (NOAA) and Fisheries and Oceans Canada (DFO; Canada's Department of Fisheries and Oceans), and two XTIDE stations (Table 2.1 and Figure 2.3). These 12 stations cover the major basins of Salish Sea, including SJDF, Puget Sound, San Juan Islands, and Georgia Strait.

Table 2.1. Tide gauges (12 stations) in the model domain.

Station ID	Lat	Long	Data Source
Point Atkinson	49.3372	-123.2539	DFO
Nanaimo Harbor	49.1628	-123.9235	DFO
Cherry Point	48.8633	-122.7583	NOAA

Station ID	Lat	Long	Data Source
Patricia Bay	48.6536	-123.4517	DFO
Friday Harbor	48.5450	-123.0133	NOAA
Victoria	48.4242	-123.3708	DFO
Yokeko Point	48.4133	-122.6150	XTIDE
Port Angeles	48.1250	-123.4417	NOAA
Port Townsend	48.1133	-122.7600	NOAA
Seattle	47.6017	-122.3383	NOAA
Lynch Cove Dock	47.4183	-122.9017	XTIDE
Tacoma	47.2700	-122.4133	NOAA

There are 135 acoustic Doppler current profiler (ADCP) data sets collected by NOAA in SJDF, Puget Sound and San Juan Islands. Measurements spanned more than three years—2015, 2016 and 2017 (Figure 2.3). In each year, the measurements were typically taken for two separate periods and each period covered a subset of the stations. At each ADCP station, the measurement period varied and mostly lasted for two to three months during the sampling window from late spring (May) to early fall (September). Detailed information about all NOAA C-MIST (currents measurement interface for the study of tides) ADCP stations are listed in Table 2.2, including station names and ID numbers, locations (latitude and longitude), water depths, and measurement periods. These data sets were used to validate the Salish Sea hydrodynamic model.

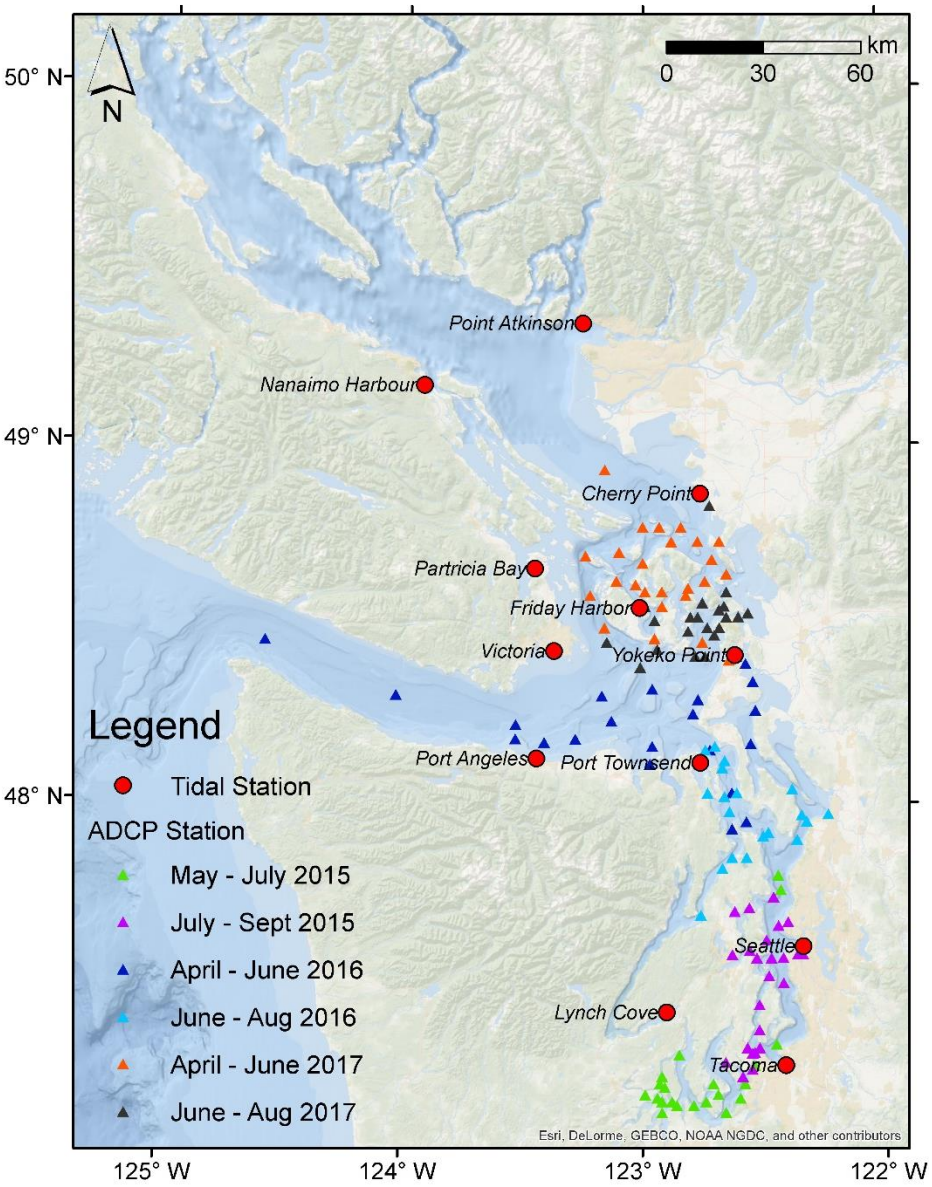

Figure 2.3. Distribution of tide-gauge stations and ADCP stations in the Salish Sea.

Table 2.2. NOAA C-MIST ADCP stations for model validation in Puget Sound.

Station Number	Station Name	Latitude	Longitude	Water Depth (m)	Start Date	End Date
PUG1501	Agate Passage	47.71	-122.57	9	7/27/15	9/9/15
PUG1502	Alki Point	47.58	-122.45	232	5/29/15	9/14/15
PUG1503	Edmonds	47.81	-122.44	182	5/28/15	9/11/15
PUG1504	Ballard Locks	47.67	-122.41	9	7/28/15	9/10/15
PUG1505	Eagle Harbor	47.62	-122.50	12	7/28/15	9/10/15
PUG1506	Harbor Island East	47.59	-122.34	13	7/25/15	9/10/15
PUG1507	Harbor Island West	47.58	-122.36	17	7/25/15	9/10/15

Station Number	Station Name	Latitude	Longitude	Water Depth (m)	Start Date	End Date
PUG1508	Liberty Bay	47.71	-122.63	13	7/27/15	9/15/15
PUG1509	Point Jefferson	47.74	-122.47	31	7/27/15	9/11/15
PUG1510	Port Washington Narrows	47.58	-122.63	8	7/26/15	9/9/15
PUG1511	President Point	47.77	-122.43	198	5/29/15	9/11/15
PUG1512	Restoration Point	47.58	-122.47	53	7/26/15	9/10/15
PUG1513	Rich Passage, E	47.57	-122.53	32	7/26/15	9/9/15
PUG1514	Rich Passage, W	47.59	-122.56	26	7/26/15	9/9/15
PUG1515	West Point	47.66	-122.44	41	7/27/15	9/10/15
PUG1516	Alki Point	47.58	-122.43	95	7/25/15	9/14/15
PUG1517	Blake Island	47.52	-122.49	83	7/26/15	9/10/15
PUG1518	Anderson Point	47.44	-122.53	115	7/23/15	9/12/15
PUG1519	Point Richmond	47.38	-122.53	106	7/23/15	9/12/15
PUG1520	Dolphin Point	47.50	-122.42	184	7/24/15	9/14/15
PUG1521	Browns Point	47.33	-122.45	178	5/29/15	7/23/15
PUG1522	Dalco Passage	47.33	-122.52	73	7/23/15	9/13/15
PUG1523	Gig Harbor Entrance	47.32	-122.57	19	7/24/15	9/14/15
PUG1524	The Narrows, A	47.31	-122.55	48	5/29/15	9/12/15
PUG1525	The Narrows, B	47.31	-122.54	26	7/24/15	9/12/15
PUG1526	The Narrows, C	47.30	-122.56	75	7/24/15	9/14/15
PUG1527	The Narrows, D	47.27	-122.55	53	5/29/15	9/13/15
PUG1528	The Narrows, E	47.26	-122.56	50	7/20/15	9/13/15
PUG1529	Hale Passage, E	47.25	-122.60	37	7/20/15	9/12/15
PUG1530	Hale Passage, W	47.28	-122.66	22	7/20/15	9/12/15
PUG1531	Gibson Point	47.22	-122.59	73	5/29/15	7/17/15
PUG1532	Steilacoom	47.18	-122.61	106	5/29/15	7/17/15
PUG1533	Ketron Island	47.15	-122.66	126	5/30/15	7/17/15
PUG1534	Nisqually Reach	47.12	-122.70	64	5/30/15	7/17/15
PUG1535	Balch Passage	47.19	-122.69	21	5/30/15	7/19/15
PUG1536	Pitt Passage	47.22	-122.71	9	6/3/15	7/17/15
PUG1537	Drayton Passage	47.17	-122.74	54	5/30/15	7/17/15
PUG1538	Devil’s Head	47.16	-122.79	81	5/30/15	7/17/15
PUG1539	Dana Passage	47.16	-122.87	36	5/31/15	9/13/15
PUG1540	Budd Inlet Entrance	47.14	-122.92	31	5/31/15	7/16/15
PUG1541	Peale Passage, S	47.17	-122.89	13	6/1/15	7/16/15
PUG1542	Peale Passage, N	47.22	-122.91	8	6/1/15	7/15/15
PUG1543	Squaxin Passage	47.18	-122.92	13	6/1/15	7/15/15
PUG1544	Totten Inlet Entrance	47.19	-122.95	24	6/2/15	7/15/15
PUG1545	Libby Point	47.20	-122.99	7	6/2/15	7/21/15
PUG1546	Pickering Passage, W	47.22	-122.93	18	6/2/15	7/18/15
PUG1547	Pickering Passage	47.25	-122.93	21	5/31/15	7/16/15
PUG1548	Pickering Passage, N	47.31	-122.85	34	5/30/15	7/16/15
PUG1601	Hazel Point	47.69	-122.76	97	6/16/16	8/25/16
PUG1602	South Point	47.82	-122.68	63	6/16/16	8/25/16

Station Number	Station Name	Latitude	Longitude	Water Depth (m)	Start Date	End Date
PUG1603	Hood Canal Bridge	47.85	-122.63	96	6/17/16	8/26/16
PUG1604	Port Gamble Bay	47.85	-122.58	12	6/17/16	8/26/16
PUG1605	Possession Sound	47.90	-122.36	203	6/15/16	8/28/16
PUG1606	Point No Point, A	47.91	-122.50	201	6/17/16	8/28/16
PUG1607	Point No Point, B	47.92	-122.48	115	6/17/16	8/27/16
PUG1608	Hood Canal Entrance	47.93	-122.64	92	4/20/16	8/26/16
PUG1609	West of Mukilteo	47.95	-122.33	185	6/15/16	8/27/16
PUG1610	Foulweather Bluff	47.95	-122.58	110	4/20/16	8/26/16
PUG1611	Olele Point	47.98	-122.65	62	6/21/16	8/25/16
PUG1612	Clinton Ferry Terminal	47.97	-122.35	33	6/15/16	8/27/16
PUG1613	Everett	47.98	-122.24	87	6/15/16	8/27/16
PUG1614	Port Townsend Canal	48.03	-122.73	5	6/18/16	8/23/16
PUG1615	Nodule Point	48.03	-122.66	21	6/17/16	8/20/16
PUG1616	Admiralty Inlet	48.03	-122.64	108	4/20/16	8/20/16
PUG1617	Bush Point Light	48.03	-122.61	94	6/18/16	8/20/16
PUG1618	Camano Head-Sandy Point	48.05	-122.39	147	6/16/16	8/27/16
PUG1619	Marrowstone Point, A	48.11	-122.67	65	6/18/16	8/21/16
PUG1620	Marrowstone Point, B	48.12	-122.66	101	6/19/16	8/20/16
PUG1622	West of Camano Island	48.17	-122.55	84	4/27/16	6/8/16
PUG1623	Point Wilson, A	48.15	-122.75	63	6/19/16	8/21/16
PUG1624	Point Wilson, B	48.16	-122.73	67	4/26/16	8/21/16
PUG1625	Point Wilson, C	48.17	-122.71	63	6/19/16	8/21/16
PUG1626	Skagit Bay, N	48.15	-122.75	33	4/27/16	6/8/16
PUG1627	Skagit Bay, S	48.27	-122.53	18	4/27/16	6/8/16
PUG1628	Skagit Bay channel	48.34	-122.55	16	4/27/16	6/9/16
PUG1629	Yokeko Point	48.40	-122.58	19	4/27/16	6/8/16
PUG1630	Kanem Point	48.41	-122.61	69	4/25/16	6/20/16
PUG1631	Violet Point	48.11	-122.97	46	4/25/16	6/12/16
PUG1632	Smith Island	48.16	-122.97	128	4/26/16	6/12/16
PUG1633	Point Partridge	48.32	-122.96	78	4/26/16	6/9/16
PUG1634	Smith Island	48.26	-122.79	50	4/26/16	6/9/16
PUG1635	New Dungeness Light	48.30	-122.78	155	4/25/16	6/11/16
PUG1636	Discovery Island	48.23	-123.13	113	4/25/16	6/11/16
PUG1637	Ediz Hook Light, ENE	48.30	-123.17	72	4/23/16	6/9/16
PUG1638	Ediz Hook Light, N	48.18	-123.28	90	4/23/16	6/11/16
PUG1639	Angeles Pt.	48.17	-123.42	29	4/23/16	6/11/16
PUG1640	Race Rocks	48.18	-123.53	148	4/23/16	8/24/16
PUG1641	Pillar Point	48.30	-124.04	189	4/22/16	6/10/16
PUG1642	Strait of Juan de Fuca	48.45	-124.58	251	4/22/16	8/24/16
PUG1701	Deception Pass	48.41	-122.64	37	4/20/17	9/7/17
PUG1702	Rosario Strait	48.46	-122.75	70	4/20/17	8/23/17
PUG1703	San Juan Channel	48.46	-122.95	129	4/22/17	8/27/17
PUG1704	Peavine Pass	48.59	-122.82	17	4/19/17	6/15/17

Station Number	Station Name	Latitude	Longitude	Water Depth (m)	Start Date	End Date
PUG1705	Obstruction Pass	48.60	-122.81	19	4/19/17	6/14/17
PUG1706	Peapod Rocks Light	48.62	-122.75	64	4/19/17	8/25/17
PUG1707	Sinclair Island	48.64	-122.66	73	4/24/17	6/14/17
PUG1708	Lawrence Point	48.68	-122.71	87	4/24/17	8/25/17
PUG1709	Clark Island	48.73	-122.77	102	4/24/17	6/18/17
PUG1710	Hale Passage	48.73	-122.68	17	4/24/17	6/14/17
PUG1711	Matia Island	48.77	-122.84	124	4/23/17	6/18/17
PUG1712	Parker Reef Light	48.73	-122.89	66	4/23/17	6/17/17
PUG1713	Patos Island	48.77	-122.93	30	4/23/17	6/16/17
PUG1714	Patos Island Light	48.77	-123.01	138	4/21/17	6/16/17
PUG1715	President Channel	48.67	-123.01	196	4/23/17	6/16/17
PUG1716	Waldron Island	48.70	-123.10	69	4/21/17	6/16/17
PUG1717	Turn Point	48.69	-123.25	145	4/21/17	6/17/17
PUG1718	Haro Strait	48.59	-123.23	257	4/20/17	6/16/17
PUG1719	Spieden Channel	48.63	-123.11	110	4/23/17	6/16/17
PUG1720	Spring Passage	48.61	-123.03	36	4/22/17	6/15/17
PUG1721	Wasp Passage narrows	48.59	-122.99	23	4/22/17	6/15/17
PUG1722	Harney Channel, north of Point Hudson	48.59	-122.92	32	4/22/17	6/19/17
PUG1723	Upright Channel narrows	48.55	-122.92	46	4/22/17	6/15/17
PUG1724	South Haro Strait	48.50	-123.16	302	4/20/17	8/28/17
PUG1725	Cherry Point	48.83	-122.73	18	6/21/17	8/25/17
PUG1726	Strait of Georgia	48.94	-123.17	117	4/21/17	6/17/17
PUG1727	Point Colville, A	48.41	-122.74	82	6/24/17	8/23/17
PUG1728	Point Colville, B	48.42	-122.78	67	6/24/17	8/23/17
PUG1729	Belle Rock Light	48.50	-122.73	57	6/23/17	8/26/17
PUG1730	Lopez Pass	48.48	-122.82	22	6/24/17	8/29/17
PUG1731	Fauntleroy Point Light	48.52	-122.77	51	6/23/17	8/26/17
PUG1732	Strawberry Island	48.56	-122.75	67	6/23/17	8/25/17
PUG1733	Thatcher Pass	48.53	-122.80	61	6/23/17	8/26/17
PUG1734	Guemes Channel, W	48.52	-122.65	20	6/22/17	8/26/17
PUG1735	Guemes Channel, E	48.53	-122.61	20	6/24/17	8/26/17
PUG1736	Saddle Bag Island Passage	48.54	-122.56	84	6/22/17	8/27/17
PUG1737	Allan Pass	48.47	-122.70	36	6/23/17	8/29/17
PUG1738	Burrows Pass	48.49	-122.69	32	6/24/17	8/29/17
PUG1739	Bellingham Channel South	48.54	-122.68	44	6/23/17	8/25/17
PUG1740	Bellingham Channel	48.56	-122.66	88	6/23/17	8/24/17
PUG1741	Bellingham Channel North	48.59	-122.66	70	6/22/17	8/24/17
PUG1742	Cattle Point, SE	48.43	-122.95	113	6/21/17	8/27/17
PUG1743	Cattle Point, SW	48.38	-123.02	154	6/20/17	8/28/17
PUG1744	Discovery Island	48.45	-123.16	141	6/20/17	8/28/17
PUG1745	Point George	48.56	-123.00	162	6/21/17	8/27/17
PUG1746	Pear Point	48.51	-122.95	72	6/20/17	8/27/17

2.3 Model Forcing and Boundary Conditions

The hydrodynamics in the Salish Sea is driven by tides, river discharge, and surface wind as well as density stratification. Tidal forcing is the dominant mechanism (Sutherland et al. 2011; Wang and Yang 2017; Yang and Khangaonkar 2010). River discharge can affect the flow field near the estuaries and induce two-layer circulation in the entire system, especially during high river flow seasons (Khangaonkar et al. 2011; Lavelle et al. 1991; Yang et al. 2015). The effect of wind forcing is generally small because of the deep water depths in Salish Sea but could result in noticeable storm surge during episodic storm events, which typically occur during winter (Bromirski et al. 2017; Yang et al. 2020).

In this study, only tides and river discharge were considered. The model open boundary conditions were specified by observed water levels at two tidal stations—Neah Bay, Washington and Campbell River, British Columbia (Figure 2.3). A total of 19 major rivers that discharged into the Salish Sea were considered in the model (Figure 2.1). The annual mean flows for all 19 rivers are listed in Table 2.3, and the seasonal distributions of the flow rates in 2016 are shown in Figure 2.4. River flow from Fraser River is about an order of magnitude greater than that from the Skagit River, the largest river discharged into Puget Sound. Fraser River peaks in the summer, but rivers in Puget Sound generally exhibit a two-peak pattern, one in winter due to rainfall and one in spring due to snowmelt. River flows in Puget Sound are the lowest in the summer and early fall.

Table 2.3. Flow rates of major rivers included in the Salish Sea tidal model.

ID	River Name	Long-Term Daily Mean Flow (m^3/s)
1	Fraser	2713
2	Nooksack	108
3	Samish	7
4	Skagit	469
5	Stillaguamish	55
6	Snohomish	270
7	Cedar	19
8	Duwamish	46
9	Puyallup	94
10	Nisqually	36
11	Deschutes	12
12	Tahuya	1
13	Skokomish	35
14	Hamma Hamma	10
15	Duckabush	12
16	Dosewallips	13
17	Big Quilcene	4
18	Dungeness	11
19	Elwha	43

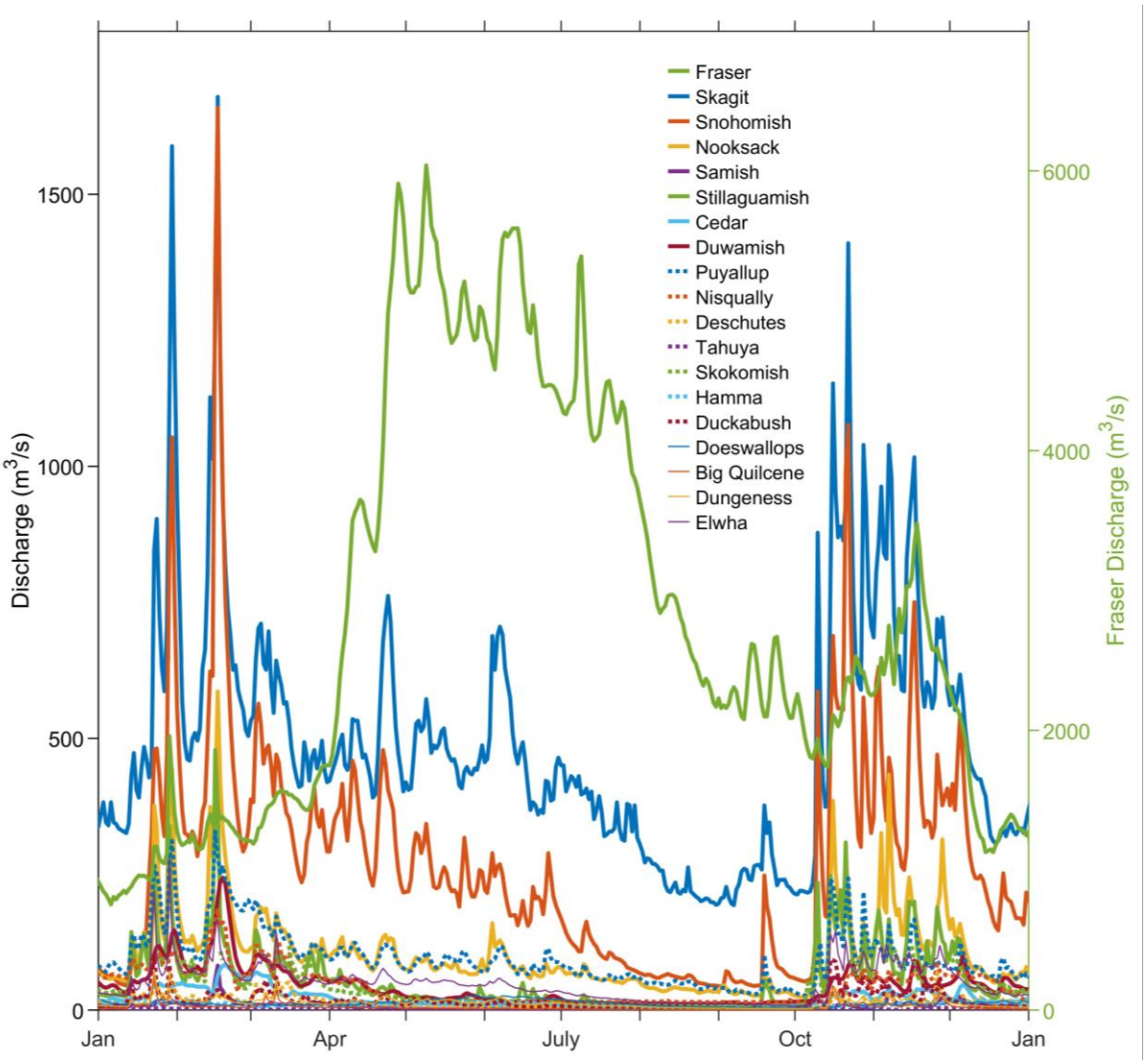

Figure 2.4. Discharge of 19 rivers during 2016. The Fraser River discharge is shown on the right axis and the other rivers on the left axis.

Model configurations and parameterizations are summarized below:

- Open boundary condition: observed 6 min resolution water levels at Neah Bay, Washington, and Campbell River, British Columbia
- Upstream boundary condition: daily river flows from 19 rivers
- Simulation period: six 1-month (30 days plus 4 days spin-up time) long simulation periods in 2015, 2016, and 2017
- Model time step: 0.2 second for the barotropic (external) mode
- Number of vertical layers: 20 uniform sigma layers
- Bottom drag coefficient and roughness height: C_d = 0.0025; and Z_0 = 0.001 m
- Model output frequency: 30 min interval at every grid point/element and every vertical layer.

All model runs were conducted in the barotropic mode without considering the effect of water density variation caused by salinity and temperature. Surface wind forcing was not included either.

2.4 Model Performance Metrics

A set of model performance metrics were used to assess the model skills in simulating water levels and currents in the Salish Sea. The following four commonly used error statistics were used in this study to quantify the accuracy of model simulations of water levels and currents.

The root mean square error ($RMSE$) is defined as:

$$RMSE = \sqrt{\frac{\sum_{i=1}^{N}(P_i - M_i)^2}{N}}$$

where N is the number of observations, M_i is the measured value, and P_i is the model-predicted value.

The scatter index (SI) is the $RMSE$ normalized by the average magnitude of measurements:

$$SI = \frac{RMSE}{abs(M)}$$

The bias is defined as:

$$Bias = \frac{\sum_{i=1}^{N}(P_i - M_i)}{N}$$

The linear correlation coefficient (R) is a measure of the linear relationship between the predictions and the measurements where 1 is a perfect positive correlation and -1 is a perfect negative correlation:

$$R = \frac{\sum_{i=1}^{N}\left(P_i - \overline{P}\right)\left(M_i - \overline{M}\right)}{\sqrt{\left(\sum_{i=1}^{N}\left(M_i - \overline{M}\right)^2\right)\left(\sum_{i=1}^{N}\left(P_i - \overline{P}\right)^2\right)}}$$

3.0 Results and Discussion

Model validation of water levels and tidal currents are described in the following sections.

3.1 Model Validation – Water Levels

Simulated water levels were compared to observed data at all 12 tide stations for the period of 6/10/2015 – 7/10/2015. Overall, model-predicted water levels matched observed data and captured the distribution pattern of tides in the Salish Sea very well (Figure 3.1). The model successfully reproduced the spring-neap tidal cycle and diurnal inequality in the entire system. The model also accurately simulated tidal amplification, as tides propagated from SJDF (Port Angeles) to Georgia Strait (Point Atkinson) and South Puget Sound (Tacoma) (Figure 3.1).

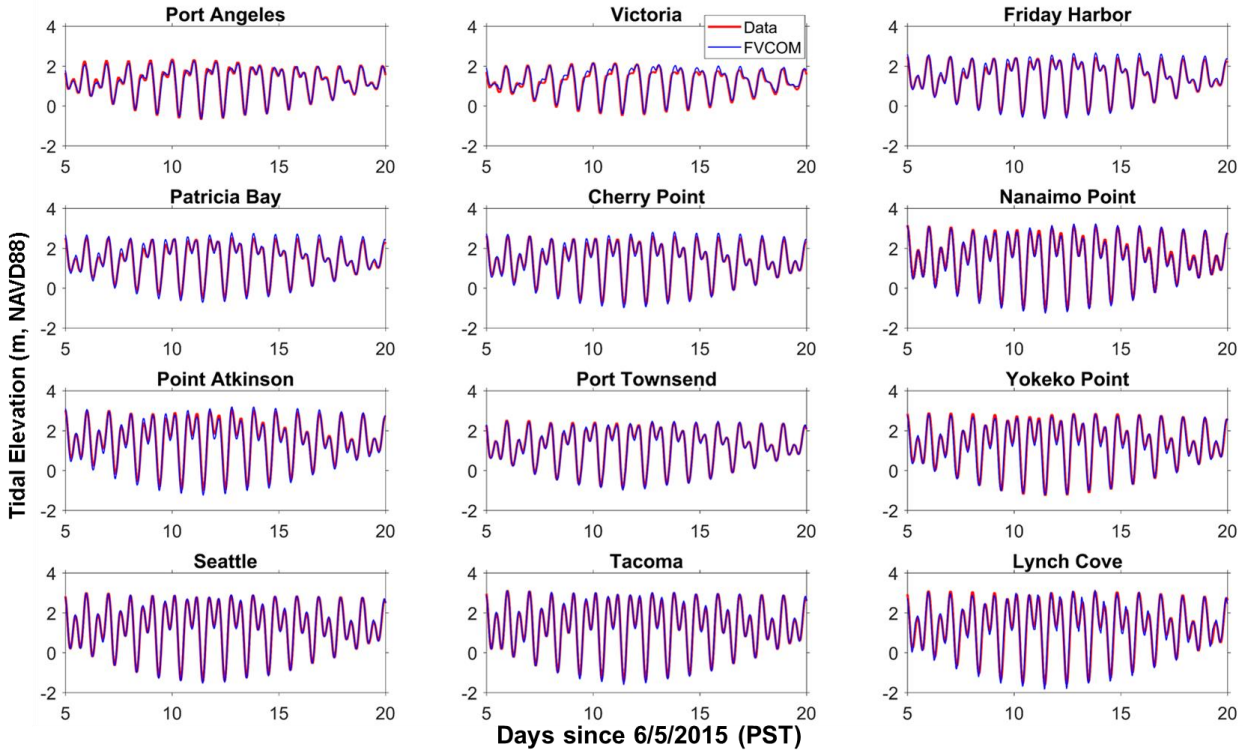

Figure 3.1. Time-series comparisons of simulated and observed total water levels at 12 tidal stations in the model domain.

Error statistics for simulated wave levels at the 12 tide gauges are provided in Table 3.1. The calculated RMSE is less than 0.2 m, which is very satisfactory given the large tidal range in Salish Sea. The SI, which measures the normalized RMSE, is less than 0.14. It should be noted that the maximum RMSE and SI occurred at Yoketo Point and in Lynch Cove, for which XTIDE stations collect data that are not as accurate as other real-time observed data. Biases at all stations are very small, with a range of -0.06 m to 0.06 m. The linear correlation coefficient, is greater than 0.98 for the stations, indicating the model has a strong correlation with field observations.

Table 3.1. Error statistics of total water level predictions at 12 tide gauges.

Station Name	RMSE (m)	SI	Bias (m)	R
Point Atkinson	0.14	0.09	-0.05	0.993
Nanaimo Harbor	0.13	0.08	-0.06	0.994
Cherry Point	0.10	0.07	0.02	0.995
Patricia Bay	0.11	0.07	0.05	0.996
Friday Harbor	0.09	0.06	0.05	0.996
Victoria	0.13	0.11	0.06	0.983
Yokeko Point	0.20	0.14	-0.03	0.980
Port Angeles	0.10	0.08	-0.01	0.990
Port Townsend	0.05	0.04	-0.02	0.998
Seattle	0.06	0.04	0.02	0.999
Lynch Cove Dock	0.20	0.13	0.02	0.985
Tacoma	0.07	0.05	0.01	0.998

3.2 Model Validation – Currents

Model skill for simulating tidal currents was evaluated using the same model performance metrics as water level, i.e., $RMSE$, SI, bias, and R, at all 135 ADCP stations. In addition, graphic comparisons of velocity probability distribution (%), scatter plot, time series, and vertical profiles of the principal velocity components were also plotted at all ADCP stations, and are provided in Appendix A. It is worth noting that ADCP measurement depth was recorded based on the vessel depth when the ADCP was deployed and no referenced datum was provided. However, the model depth was configured relative to the North American Vertical Datum of 1988 (NAVD88). Therefore, there is a discrepancy between the model and ADCP depths. To evaluate this discrepancy, a correlation between the model and ADCP depths was plotted (Figure 3.2). In general, the model depth correlates well with the ADCP deployment depth, with a linear correlation coefficient of 0.9974. However, the model depth is slightly shallower than the ADCP depth; the former has a slope of less than 1 (0.98) and a negative intersect (-0.32). The trend of the smaller model depth is expected because the NAVD88 datum is approximately in the range of–1.5 m below mean sea level (MSL) in the Salish Sea. For example, NAVD88 at Seattle is 1.31 m below MSL (https://tidesandcurrents.noaa.gov/datums.html?id=9447130) and 1.16 m at Port Angeles (https://tidesandcurrents.noaa.gov/datums.html?id=9444090).

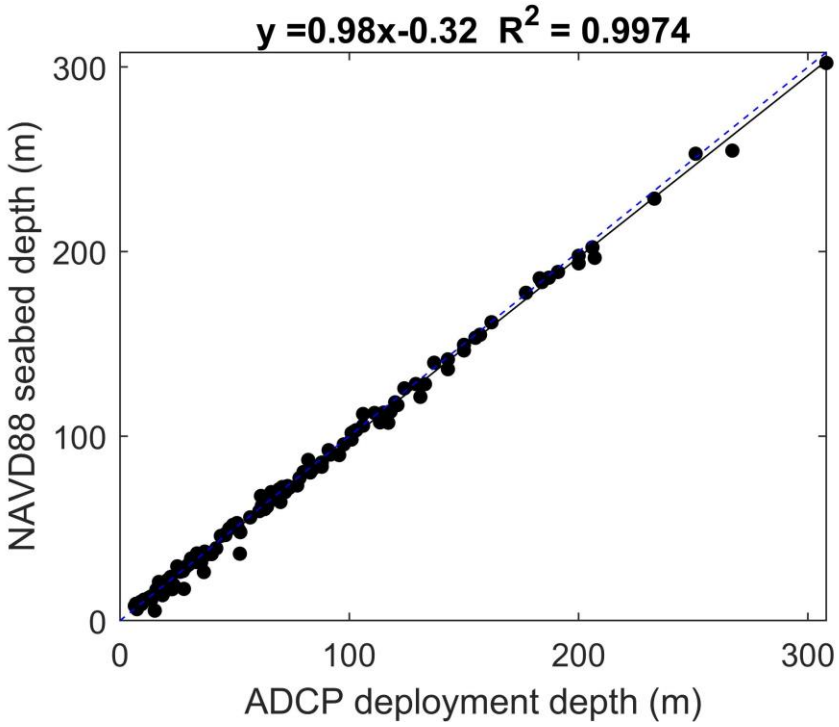

Figure 3.2. Model seabed depth as defined by NAVD88 vs. the ADCP deployment depth. The dashed line represents the 1 to 1 correlation and the solid line is the linear fit.

Examples of model and data comparisons at six selected stations are shown in Figure 3.3 through Figure 3.8. These six stations are spread across a large area of the Salish Sea, from Lopez Passage in the San Juan Islands, and Rosario Strait in the eastern SJDF, to Admiralty Inlet and Agate Passage in the Main Basin, and further down to Tacoma Narrows and Hale Passage in the South Puget Sound. Overall, the model predicted the velocity time histories, magnitudes, and directions at all six stations well (see panels c and d in Figure 3.3 through Figure 3.8). For tidal energy extraction and site optimization, velocity probability and vertical profiles distributions are important. In general, the model successfully reproduced velocity vertical profiles through the water column (see panel b in Figure 3.3 through). The model also successfully predicted the strong velocity asymmetry at Agate Passage (Figure 3.6b, negative velocity indicated flood) and Hale Passage (Figure 3.8b, positive indicated flood). It is interesting to see that the velocity probability showed different distribution patterns at different locations (see panel a in Figure 3.3 through). At Lopez Passage, Admiralty Inlet, and Hale Passage, relatively high velocity percentiles occurred in the low- to mid-range of current speed, and a small peak around mid-range current magnitude (see Figure 3.3a, Figure 3.5a, and Figure 3.8a). At Rosario Strait, the probability of low current speed is dominant (Figure 3.4a). At Agate Passage, the high probability distribution is centered around the mid-range current speed (Figure 3.6a), likely due to the dominant semidiurnal tide. At Tacoma Narrows, the velocity probability distribution showed a two-peak pattern, likely due to the strong diurnal inequality at the site (Figure 3.7a). Further study is necessary to investigate how the probability distribution of current speed correlates to tidal harmonics distribution at a study site.

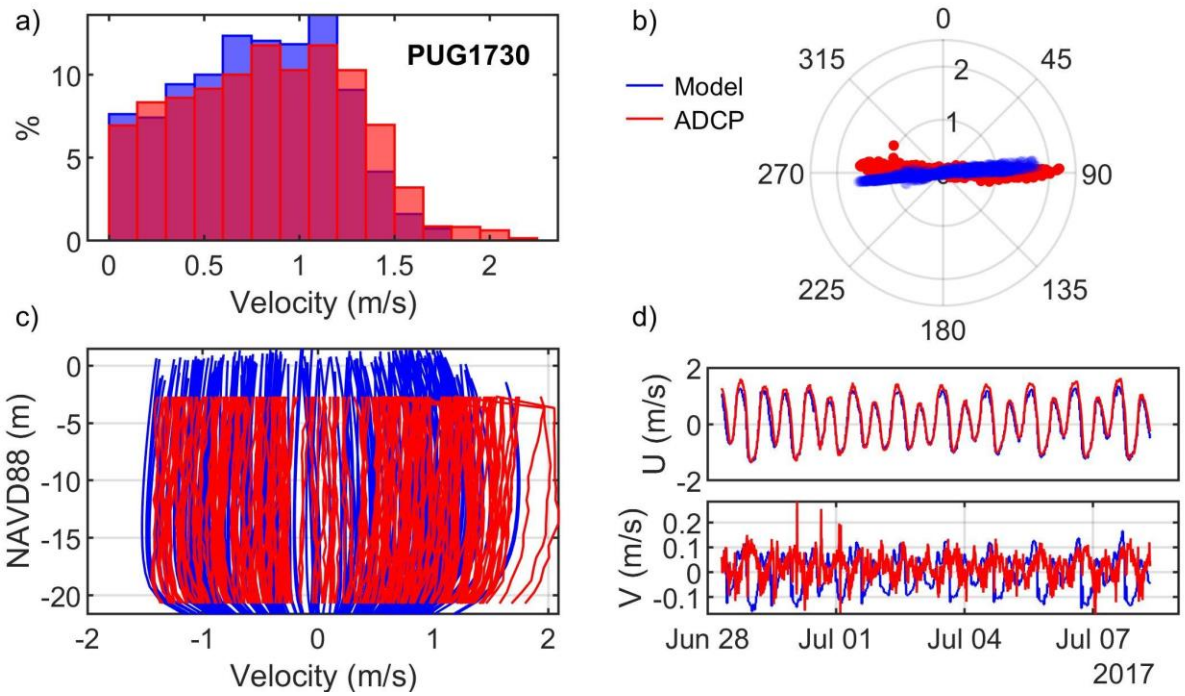

Figure 3.3. Comparisons of simulated and observed velocities at Lopez Passage (PUG1730): (a) velocity histograms, (b) scatter plot, (c) vertical profiles, and (d) time series of depth-averaged principal velocities.

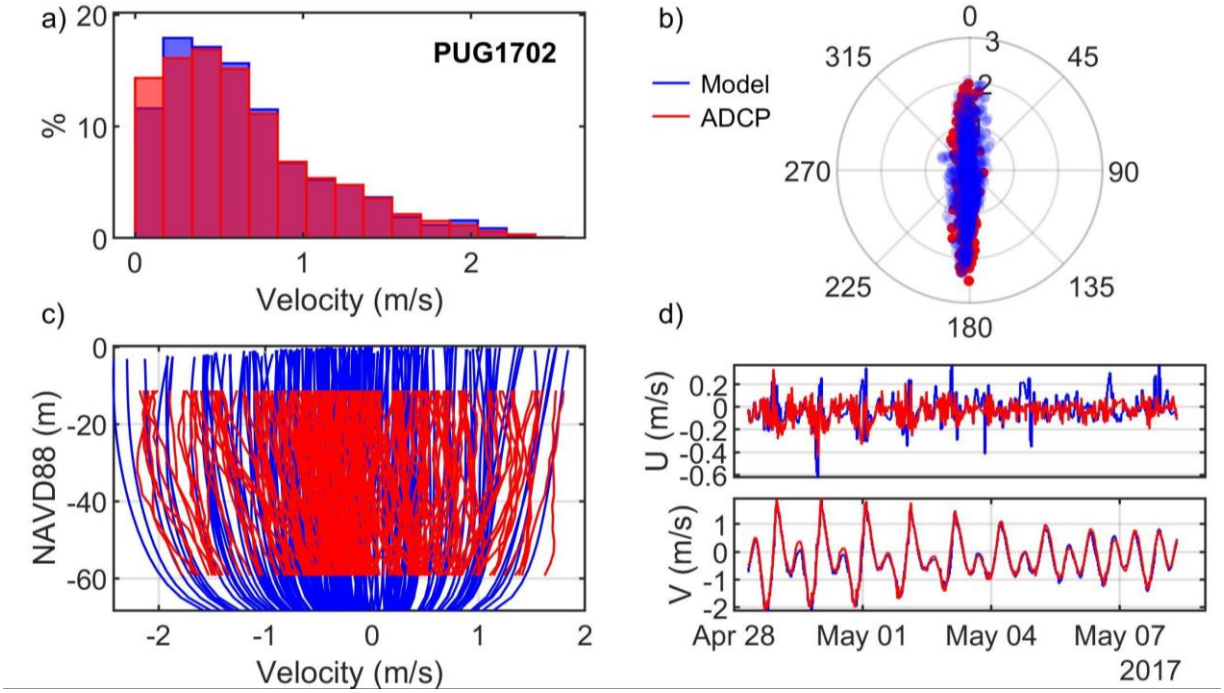

Figure 3.4. Comparisons of simulated and observed velocities at Rosario Strait (PUG1702): (a) velocity histograms, (b) scatter plot, (c) vertical profiles, and (d) time series of depth-averaged principal velocities.

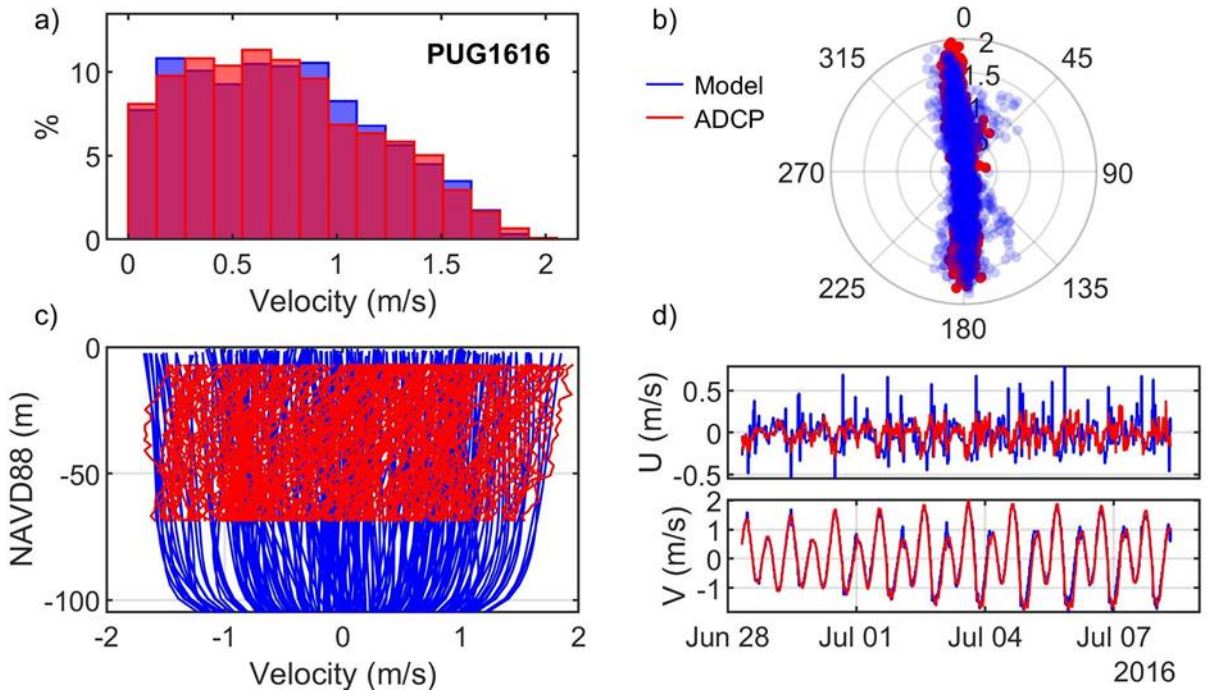

Figure 3.5. Comparisons of simulated and observed velocities at Admiralty Inlet (PUG1616): (a) velocity histograms;, (b) scatter plot, (c) vertical profiles, and (d) time series of depth-averaged principal velocities.

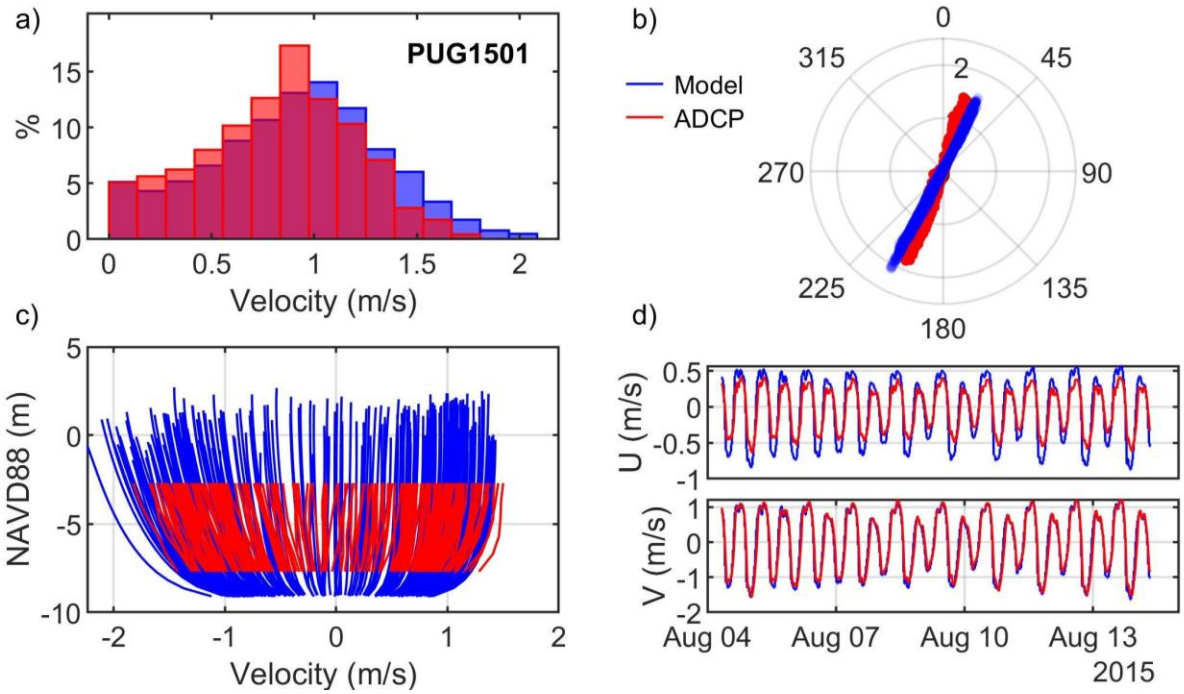

Figure 3.6. Comparisons of simulated and observed velocities at Agate Passage (PUG1501): (a) station location, (b) scatter plot, (c) vertical profiles, and (d) time series of depth-averaged principal velocities.

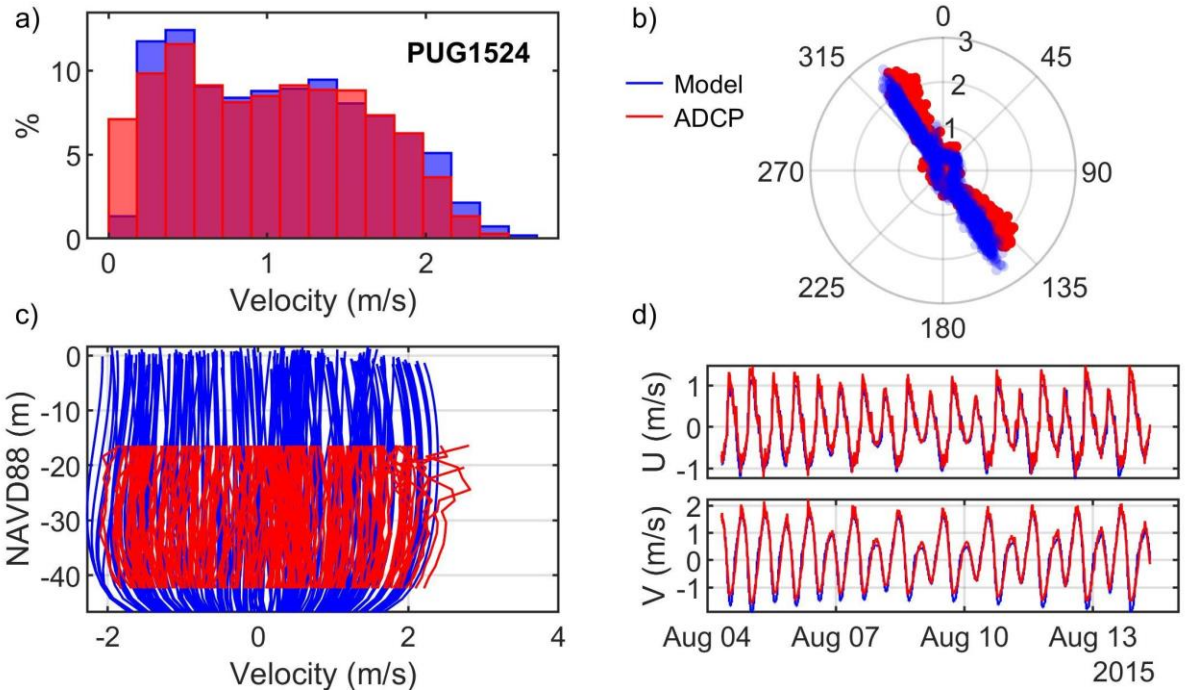

Figure 3.7. Comparisons of simulated and observed velocities at The Narrows (PUG1524): (a) velocity histograms;, (b) scatter plot, (c) vertical profiles, and (d) time series of depth-averaged principal velocities.

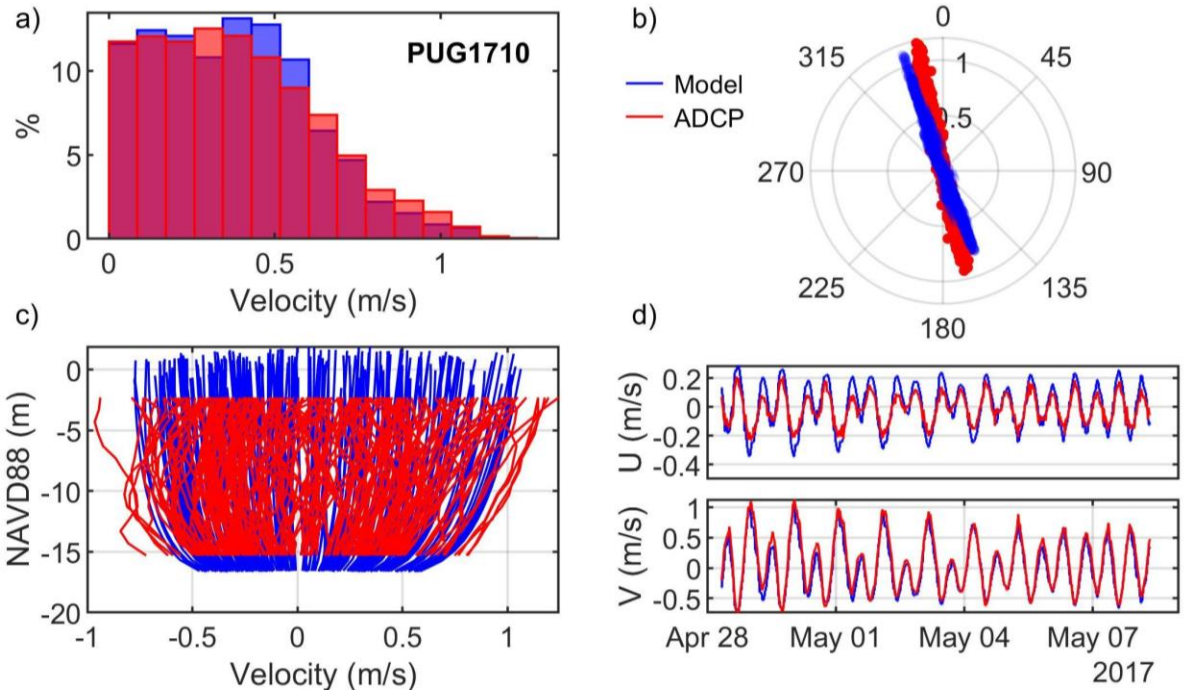

Figure 3.8. Comparisons of simulated and observed velocities at Hale Passage (PUG1710): (a) velocity histograms, (b) scatter plot, (c) vertical profiles, and (d) time series of depth-averaged principal velocities.

Error statistics for simulated velocities were calculated at the surface layer, mid-depth, and bottom layer, as were depth-averaged values. Table 3.2 shows the error statistics for the simulated depth-averaged velocities at all 135 ADCP stations, and the error statistics for the surface, mid-depth, and bottom layer velocities are provided in Appendix B. The range of RMSE varies from 0.02 m/s (Station 1622) to 0.67 m/s (Station 1545). The SI varies from 0.16 (ST 1735) to 1.74 (Station 1532). Bias varies from -0.31 (Station 1735) to 0.3 (Station 1701). R varies from 0.34 (Station 1532) to 0.99 (Station 1722). Although there are a few outliers in terms error statistics, the overall model performance for simulating velocity field in the Salish Sea is good, as demonstrated by the station-averaged values of the RMSE (0.2 m/s), SI (0.5), Bias (-0.02 m/s), and R (0.92).

Table 3.2. Error statistics for modeled depth-averaged tidal velocities.

Station ID	Station Name	RMSE (m/s)	SI	Bias (m/s)	R
1501	Agate Passage, south end	0.24	0.29	-0.02	0.97
1502	Alki Point	0.07	0.49	0.04	0.94
1503	Edmonds	0.04	0.30	-0.01	0.97
1504	Entrance to Ballard Locks	0.03	0.58	0.02	0.56
1505	Entrance to Eagle Harbor	0.04	0.71	-0.01	0.86
1506	Harbor Island East	0.04	1.11	0.00	0.83
1507	Harbor Island West	0.04	0.61	0.04	0.96
1508	Liberty Bay	0.07	0.28	0.02	0.98
1509	Point Jefferson	0.20	0.66	-0.08	0.87
1510	Port Washington Narrows	0.32	0.38	-0.03	0.99
1511	President Point	0.05	0.32	-0.01	0.96
1512	Restoration Point	0.21	1.03	-0.13	0.91
1513	Rich Passage, East	0.17	0.70	-0.02	0.83
1514	Rich Passage, West	0.13	0.16	-0.05	0.99
1515	West Point	0.20	1.08	0.04	0.84
1516	Alki Point	0.17	0.80	-0.04	0.88
1517	Blake Island	0.11	0.38	0.07	0.95
1518	Anderson Point	0.07	0.25	0.02	0.96
1519	Point Richmond	0.13	0.43	0.06	0.90
1520	Dolphin Point	0.05	0.59	0.00	0.88
1521	Browns Point	0.08	0.68	-0.03	0.84
1522	Dalco Passage	0.13	0.48	-0.05	0.90
1523	Gig Harbor Entrance	0.14	0.61	-0.01	0.86
1524	The Narrows, North	0.19	0.20	0.01	0.99
1525	The Narrows, East	0.23	0.25	-0.01	0.93
1526	The Narrows, West	0.25	0.33	-0.02	0.95
1527	The Narrows	0.28	0.22	-0.07	0.99
1528	The Narrows, South	0.26	0.22	-0.05	0.99
1529	Hale Passage, East	0.12	0.52	0.01	0.92
1530	Hale Passage, West	0.16	0.34	0.08	0.96
1531	Gibson Point	0.40	0.55	-0.02	0.89
1532	Steilacoom	0.19	1.74	0.07	0.34

Station ID	Station Name	RMSE (m/s)	SI	Bias (m/s)	R
1533	Ketron Island	0.11	1.02	-0.03	0.82
1534	Nisqually Reach	0.25	0.56	-0.01	0.88
1535	Balch Passage	0.33	0.53	0.02	0.91
1536	Pitt Passage	0.14	0.39	0.01	0.94
1537	Drayton Passage	0.08	0.66	0.01	0.87
1538	Devil's Head	0.08	0.53	0.00	0.90
1539	Dana Passage	0.16	0.24	-0.02	0.98
1540	Budd Inlet Entrance	0.07	0.61	0.03	0.92
1541	Peale Passage	0.10	0.75	0.00	0.78
1542	Peale Passage	0.16	1.08	0.01	0.64
1543	Squaxin Passage	0.29	0.60	0.04	0.87
1544	Totten Inlet Entrance	0.21	0.54	0.03	0.90
1545	Libby Point	0.67	0.79	-0.09	0.85
1546	Pickering Passage, West	0.27	0.56	0.06	0.89
1547	Pickering Passage	0.26	0.58	0.05	0.90
1548	Pickering Passage, North	0.12	0.58	0.01	0.88
1601	Hazel Point	0.06	0.31	-0.02	0.97
1602	South Point	0.06	0.24	0.02	0.98
1603	Hood Canal Bridge	0.07	0.26	0.02	0.98
1604	Port Gamble	0.12	0.44	0.04	0.94
1605	Possession Sound	0.05	0.54	-0.05	0.97
1606	Point No Point, 1.2 mi.	0.16	0.60	-0.01	0.93
1607	Point No Point, 2.1 mi.	0.15	0.48	0.04	0.93
1608	Hood Canal Entrance	0.07	0.30	-0.01	0.97
1609	West of Mukilteo	0.03	0.23	-0.01	0.98
1610	Foulweather Bluff	0.16	0.25	0.01	0.98
1611	Olele Point	0.17	0.53	-0.07	0.93
1612	Clinton	0.06	0.51	0.00	0.91
1613	Everett	0.03	1.22	0.01	0.43
1614	Port Townsend Canal	0.34	0.29	-0.02	0.96
1615	Nodule Point	0.43	0.63	-0.26	0.91
1616	Admiralty Inlet	0.17	0.24	0.02	0.98
1617	Bush Point Light	0.28	0.34	0.04	0.96
1618	Camano Head-Sandy Point,	0.04	0.39	0.02	0.95
1619	Marrowstone Point, 0.8 mi.	0.25	0.27	0.03	0.98
1620	Marrowstone Point, 1.65 mi.	0.20	0.26	-0.02	0.98
1622	West of Camano Island	0.02	0.29	-0.01	0.98
1623	Point Wilson, A	0.28	0.34	-0.04	0.97
1624	Point Wilson, B	0.28	0.27	-0.05	0.98
1625	Point Wilson, C	0.46	0.48	-0.14	0.92
1626	Skagit Bay, N	0.07	0.42	0.00	0.94
1627	Skagit Bay, S	0.18	0.34	-0.01	0.97
1628	Skagit Bay, SW	0.37	0.60	-0.22	0.90

Station ID	Station Name	RMSE (m/s)	SI	Bias (m/s)	R
1629	Yokeko Point	0.33	0.35	-0.04	0.96
1630	Kanem Point	0.15	0.58	-0.02	0.88
1631	Violet Point	0.12	0.67	0.07	0.90
1632	Smith Island, WNW	0.11	0.51	0.03	0.92
1633	Point Partridge	0.16	0.79	0.13	0.83
1634	Smith Island, ESE	0.21	0.79	0.20	0.92
1635	New Dungeness Light	0.13	0.34	-0.07	0.97
1636	Discovery Island	0.11	0.33	-0.03	0.97
1637	Ediz Hook Light, ENE	0.15	0.29	-0.09	0.98
1638	Ediz Hook Light, N	0.19	0.52	0.15	0.97
1639	Angeles Pt.	0.46	0.75	0.21	0.91
1640	Race Rocks	0.18	0.32	-0.13	0.98
1641	Pillar Point	0.11	0.33	-0.09	0.99
1642	Strait of Juan de Fuca	0.12	0.36	-0.11	0.99
1701	Deception Pass	0.63	0.32	0.30	0.97
1702	Rosario Strait	0.16	0.25	-0.09	0.98
1703	San Juan Channel	0.54	0.68	-0.01	0.92
1704	Peavine Pass	0.49	0.64	0.14	0.91
1705	Obstruction Pass	0.22	0.45	-0.08	0.93
1706	Peapod Rocks Light	0.23	0.36	-0.15	0.98
1707	Sinclair Island	0.09	0.37	-0.01	0.93
1708	Lawrence Point	0.16	0.34	-0.01	0.97
1709	Clark Island	0.16	0.39	-0.03	0.95
1710	Hale Passage	0.11	0.29	-0.06	0.98
1711	Matia Island	0.17	0.54	-0.05	0.91
1712	Parker Reef Light	0.34	0.87	-0.26	0.90
1713	Patos Island	0.26	0.54	-0.14	0.93
1714	Patos Island Light	0.25	0.54	-0.10	0.93
1715	President Channel	0.35	0.76	-0.31	0.95
1716	Waldron Island	0.31	0.80	0.02	0.88
1717	Turn Point	0.45	0.70	-0.22	0.92
1718	Haro Strait	0.36	0.62	-0.30	0.96
1719	Spieden Channel	0.32	0.37	-0.11	0.97
1720	Spring Passage	0.16	0.45	0.02	0.95
1721	Wasp Passage	0.14	0.22	-0.01	0.98
1722	Harney Channel	0.08	0.23	0.01	0.99
1723	Upright Channel	0.16	0.35	0.02	0.96
1724	South Haro Strait	0.35	0.83	-0.19	0.93
1725	Cherry Point	0.09	0.46	-0.01	0.94
1726	Strait of Georgia	0.20	0.70	0.19	0.98
1727	Point Colville, 3.0	0.14	0.36	0.04	0.96
1728	Point Colville, 1.4	0.15	0.26	0.04	0.98
1729	Belle Rock Light	0.20	0.28	-0.02	0.97

Station ID	Station Name	RMSE (m/s)	SI	Bias (m/s)	R
1730	Lopez Pass	0.21	0.25	-0.12	0.98
1731	Fauntleroy Point	0.24	0.55	0.03	0.90
1732	Strawberry Island	0.26	0.31	-0.05	0.97
1733	Thatcher Pass	0.16	0.48	0.02	0.94
1734	Guemes Channel, W	0.14	0.22	-0.04	0.98
1735	Guemes Channel, E	0.10	0.16	-0.02	0.99
1736	Saddle Bag Island Passage	0.12	0.46	0.03	0.95
1737	Allan Pass	0.40	0.77	-0.17	0.88
1738	Burrows Pass	0.30	0.46	-0.13	0.93
1739	Bellingham Channel S	0.24	0.29	-0.01	0.97
1740	Bellingham Channel	0.27	0.30	-0.05	0.98
1741	Bellingham Channel N	0.26	0.36	0.02	0.96
1742	Cattle Point, SE	0.47	1.30	-0.26	0.90
1743	Cattle Point SW	0.20	0.88	-0.07	0.75
1744	Discovery Island	0.37	0.74	-0.18	0.92
1745	Point George	0.17	0.55	-0.04	0.96
1746	Pear Point	0.24	0.55	-0.02	0.92
	Spatial Averaged Values	**0.20**	**0.50**	**-0.02**	**0.92**

To better understand the distributions of model error in simulating currents in the Salish Sea, spatial distributions for each of the depth-averaged error statistical parameters as well as probability distributions are shown in Figure 3.9 through Figure 3.12. As can be seen, more than 80% of the RMSEs are within 0.30 m/s. Three stations—San Juan Channel (PUG1703); Deception Pass (PUG1701) and Libby Point (PUG1545)—have an RMSE greater than 0.5 m/s (Figure 3.8a). The *SI* has a relatively large range because it is a normalized quantity. Some of the large values can be attributed to the small current magnitudes in the low current sub-basins, such as the Central Basin (Figure 3.10a). About 75% of the SI values are in the range of 0.25 to 0.75 (Figure 3.10b). The bias between predicted and observed velocities is generally very good, ranging from -03 to 0.3. Figure 3.11a indicates that the model, in general, overpredicts them in Puget Sound and underpredicts in San Juan Islands. However, the overall model bias is centered around 0, as shown in Figure 3.11b. *R* for the modeled velocity is high; more than 80% of the stations have an *R* value greater than 0.9 (Figure 3.12).

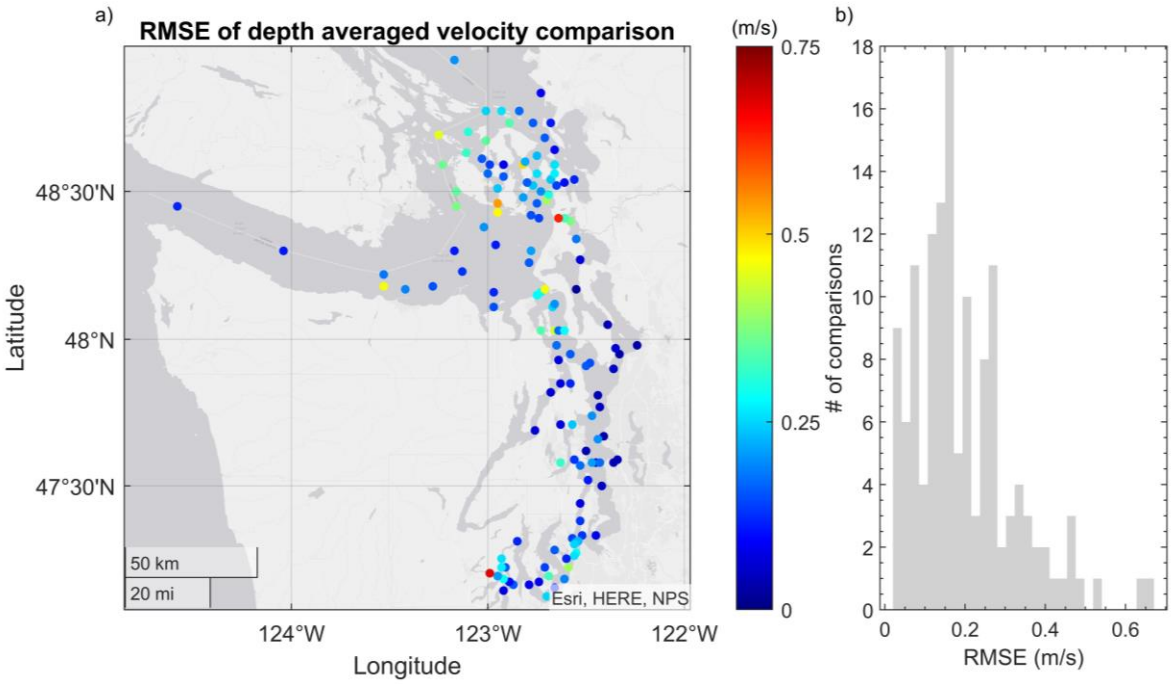

Figure 3.9. *RMSE* of depth-averaged principal velocity comparison: (a) map and (b) histogram.

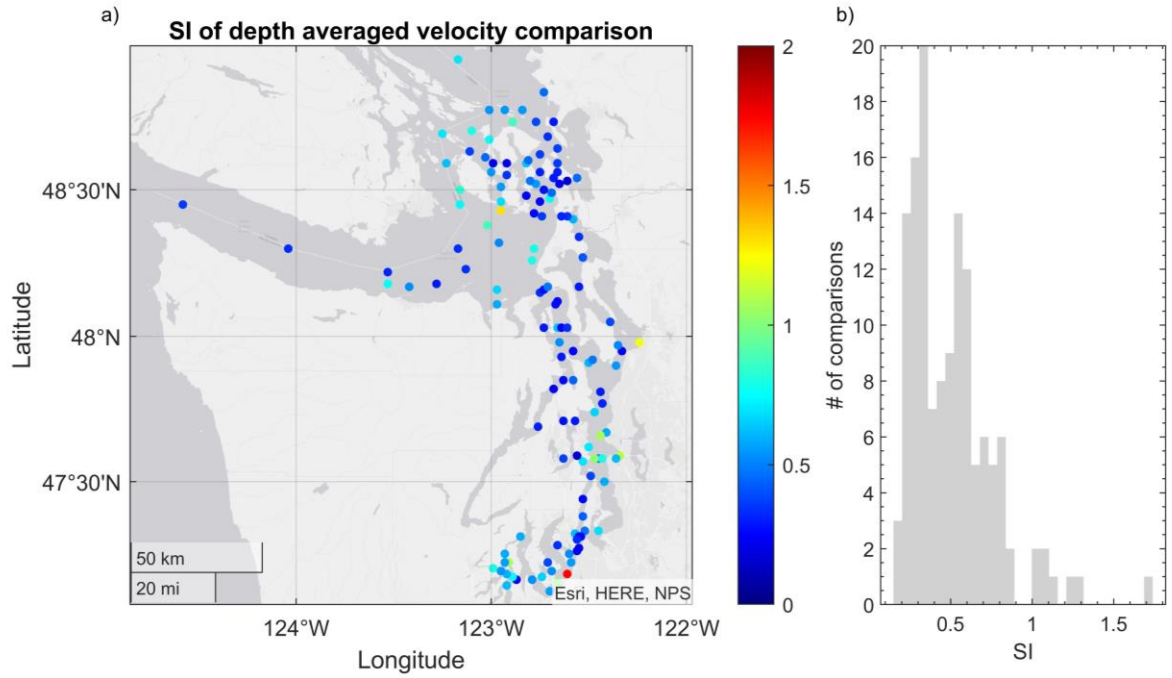

Figure 3.10. *SI* of depth-averaged principal velocity comparison: (a) map and (b) histogram.

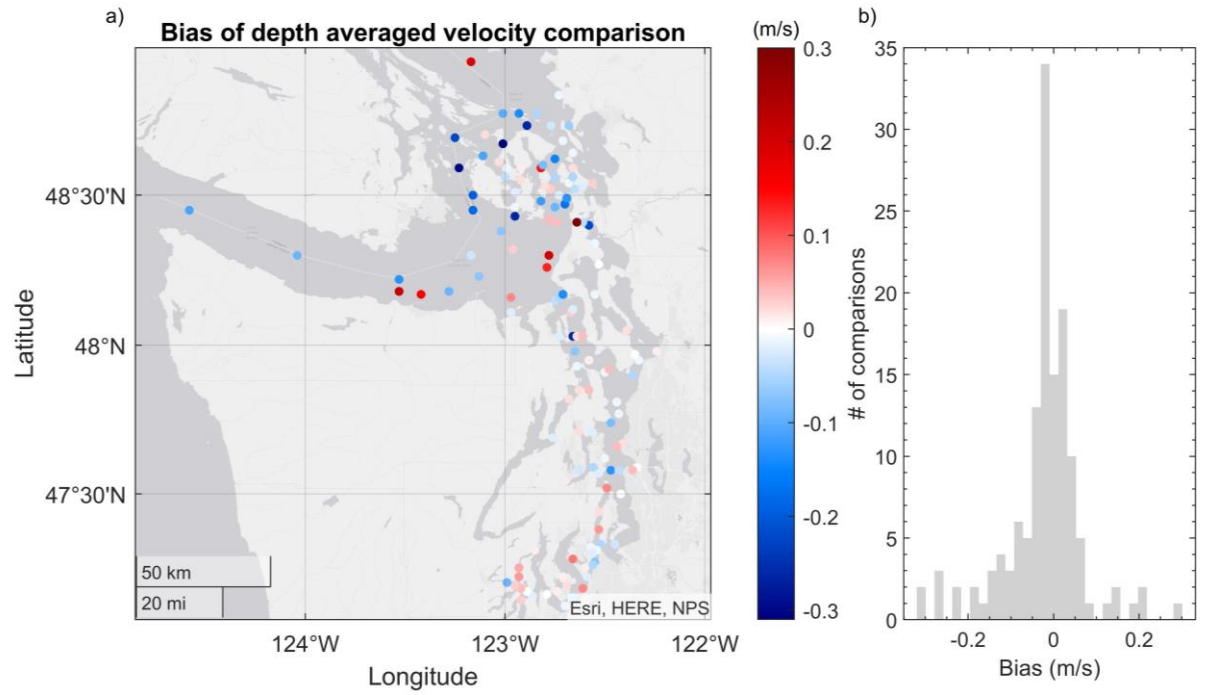

Figure 3.11. Bias of depth-averaged principal velocity comparison: (a) map and (b) histogram.

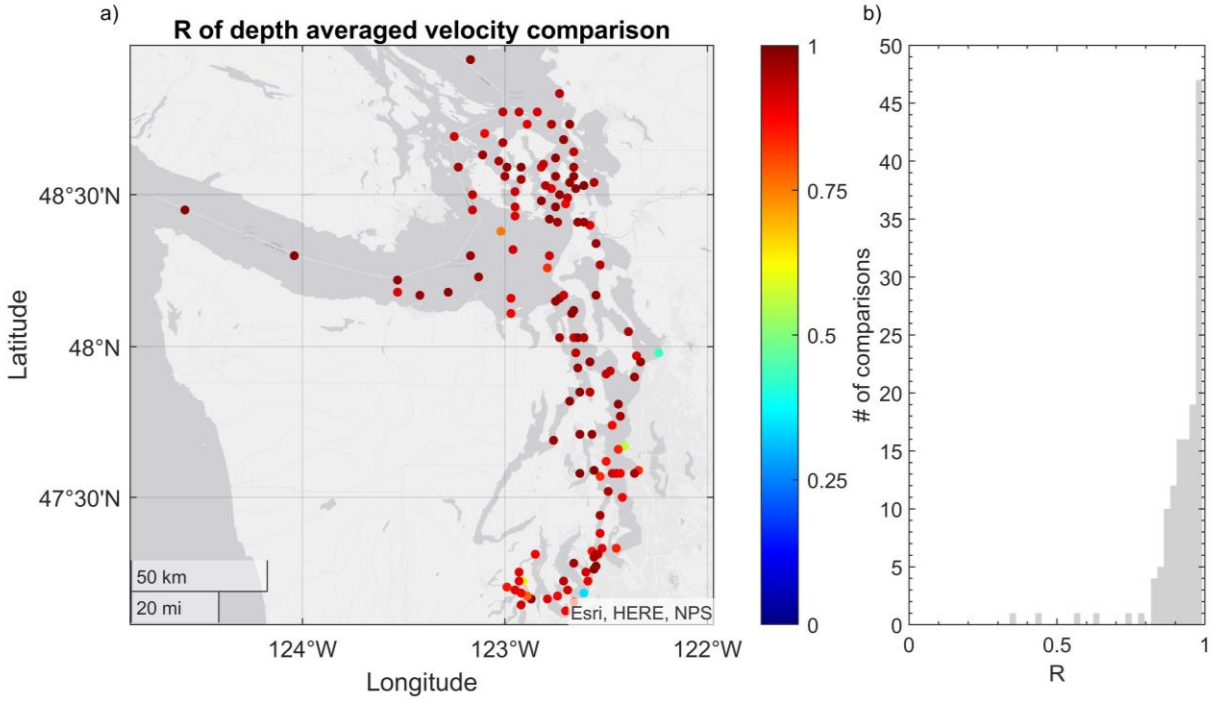

Figure 3.12. *R* of depth-averaged principal velocity comparison: (a) map and (b) histogram.

4.0 Conclusion

To support tidal stream resource characterization and assessment in Puget Sound, a high-resolution, three-dimensional tidal hydrodynamic model for the Salish Sea was developed and validated using extensive water level and ADCP data. To provide detailed tidal current data, the unstructured-grid coastal ocean model FVCOM was used and high grid-resolution was specified in the tidal channels, inlets, and estuaries. Model validation results indicated the Salish Sea hydrodynamic model is able to accurately simulate the distributions of water levels and tidal currents in the Salish Sea. Therefore, model outputs can be used with confidence to support detailed tidal energy resource characterization and assessment and to identify hotspots for tidal energy development in the Salish Sea. Specific model outputs include water level and three-dimensional velocity distributions in the entire Salish Sea at hourly temporal resolution. Examples of instantaneous water level at high tide and low tide, and depth-averaged velocity distributions at flood tide and ebb tide are shown in Figure 4.1 and Figure 4.2, respectively.

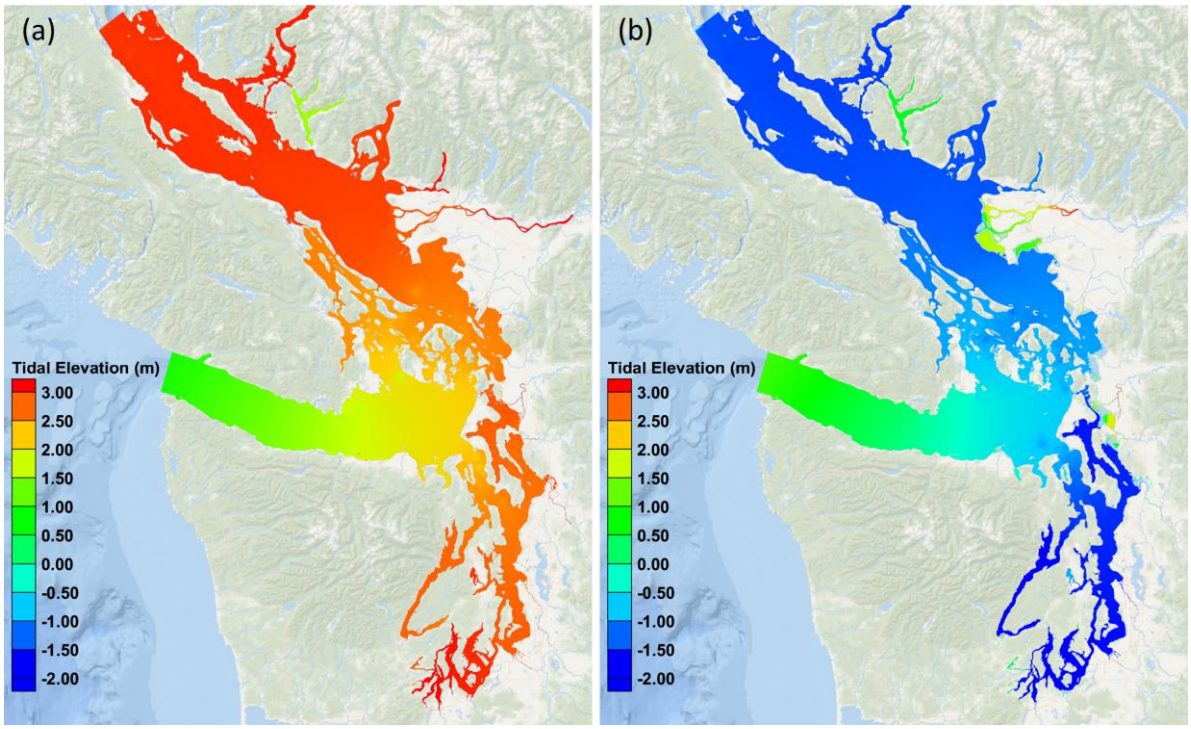

Figure 4.1. Simulated tidal elevation at (a) high tide at 6/17/2015 19:00:00 (PST) and (b) low tide 6/17/2015 11:00:00 (PST). Note: High tide and low tide are relative to South Puget Sound.

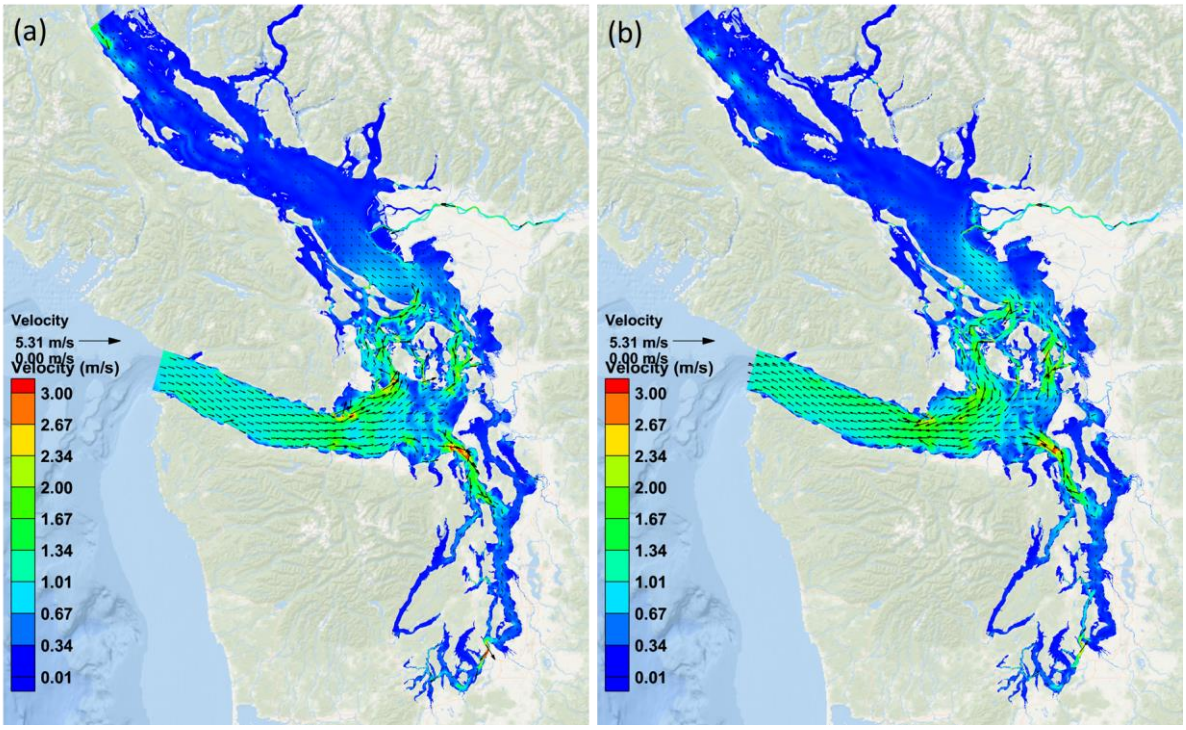

Figure 4.2. Simulated depth-averaged tidal currents at 6/16/2015 14:00:00 (PST) and (b) ebb tide at 6/17/2015 08:00:00 (PST). Note: High tide and low tide are relative to South Puget Sound.

Although the Salish Model validation is overall satisfactory, it can be further improved in following areas.

1. Include salinity and temperature simulations to account for the baroclinic motion.
2. Include high-resolution sea surface wind forcing to improve surface velocity prediction.
3. Obtain more accurate bathymetric data to improve the model bathymetry, especially at the stations where model performance is poor.
4. Conduct thorough quality assurance and quality control on the ADCP data and eliminate those with high uncertainty of data quality.

5.0 References

Babson, A.L., Kawase, A. and MacCready, P. (2006) Seasonal and interannual variability in the circulation of Puget Sound, Washington: A box model study. Atmosphere-Ocean 44(1), 29-45.

Bromirski, P.D., Flick, R.E. and Miller, A.J. (2017) Storm surge along the Pacific coast of North America. Journal of Geophysical Research-Oceans 122(1), 441-457.

Chen, C., Beardsley, R.C., Cowles, G., Qi, J., Lai, Z., Gao, G., Stuebe, D., Xu, Q., Xue, P., Ge, J., Ji, R., Hu, S., Tian, R., Huang, H., Wu, L. and Lin, H. (2013) An Unstructured Grid, Finite-Volume Community Ocean Model - FVCOM p. 416.

Defne, Z., Haas, K.A., Fritz, H.M., Jiang, L., French, S.P., Shi, X., Smith, B.T., Neary, V.S. and Stewart, K.M. (2012) National geodatabase of tidal stream power resource in USA. Renewable and Sustainable Energy Reviews 16(5), 3326-3338.

Khangaonkar, T., Yang, Z., Kim, T. and Roberts, M. (2011) Tidally averaged circulation in Puget Sound sub-basins: Comparison of historical data, analytical model, and numerical model. Estuarine, Coastal and Shelf Science 93(4), 305-319.

Kilcher, K., Thresher, R. and Tinnesand, H. (2016) Marine Hydrokinetic Energy Site Identification and Ranking Methodology Part II: Tidal Energy, p. 30, National Renewable Energy Laboratory, Golden, CO.

Lavelle, J.W., Cokelet, E.D. and Cannon, G.A. (1991) A Model Study of Density Intrusions into and Circulation within a Deep, Silled Estuary - Puget Sound. Journal of Geophysical Research-Oceans 96(C9), 16779-16800.

Sutherland, D.A., MacCready, P., Banas, N.S. and Smedstad, L.F. (2011) A Model Study of the Salish Sea Estuarine Circulation. Journal of Physical Oceanography 41(6), 1125-1143.

Wang, T.P. and Yang, Z.Q. (2017) A modeling study of tidal energy extraction and the associated impact on tidal circulation in a multi-inlet bay system of Puget Sound. Renewable Energy 114, 204-214.

Yang, Z.Q. and Khangaonkar, T. (2010) Multi-scale modeling of Puget Sound using an unstructured-grid coastal ocean model: from tide flats to estuaries and coastal waters. Ocean Dynamics 60(6), 1621-1637.

Yang, Z.Q., Wang, T.P., Castrucci, L. and Miller, I. (2020) Modeling assessment of storm surge in the Salish Sea. Estuarine Coastal and Shelf Science 238.

Yang, Z.Q., Wang, T.P., Copping, A. and Geerlofs, S. (2014) Modeling of in-stream tidal energy development and its potential effects in Tacoma Narrows, Washington, USA. Ocean & Coastal Management 99, 52-62.

Yang, Z.Q., Wang, T.P., Voisin, N. and Copping, A. (2015) Estuarine response to river flow and sea-level rise under future climate change and human development. Estuarine Coastal and Shelf Science 156, 19-30.

Appendix A – Velocity Comparison

This appendix contains the comparisons of simulated and observed velocities at 135 acoustic Doppler current profiler (ADCP) stations. The station numbers identify the station locations in the sub-basins of the Salish Sea, grouped by 1500, 1600, and 1700 series. The latitude and longitude coordinates of each station are listed in Table 2.1.

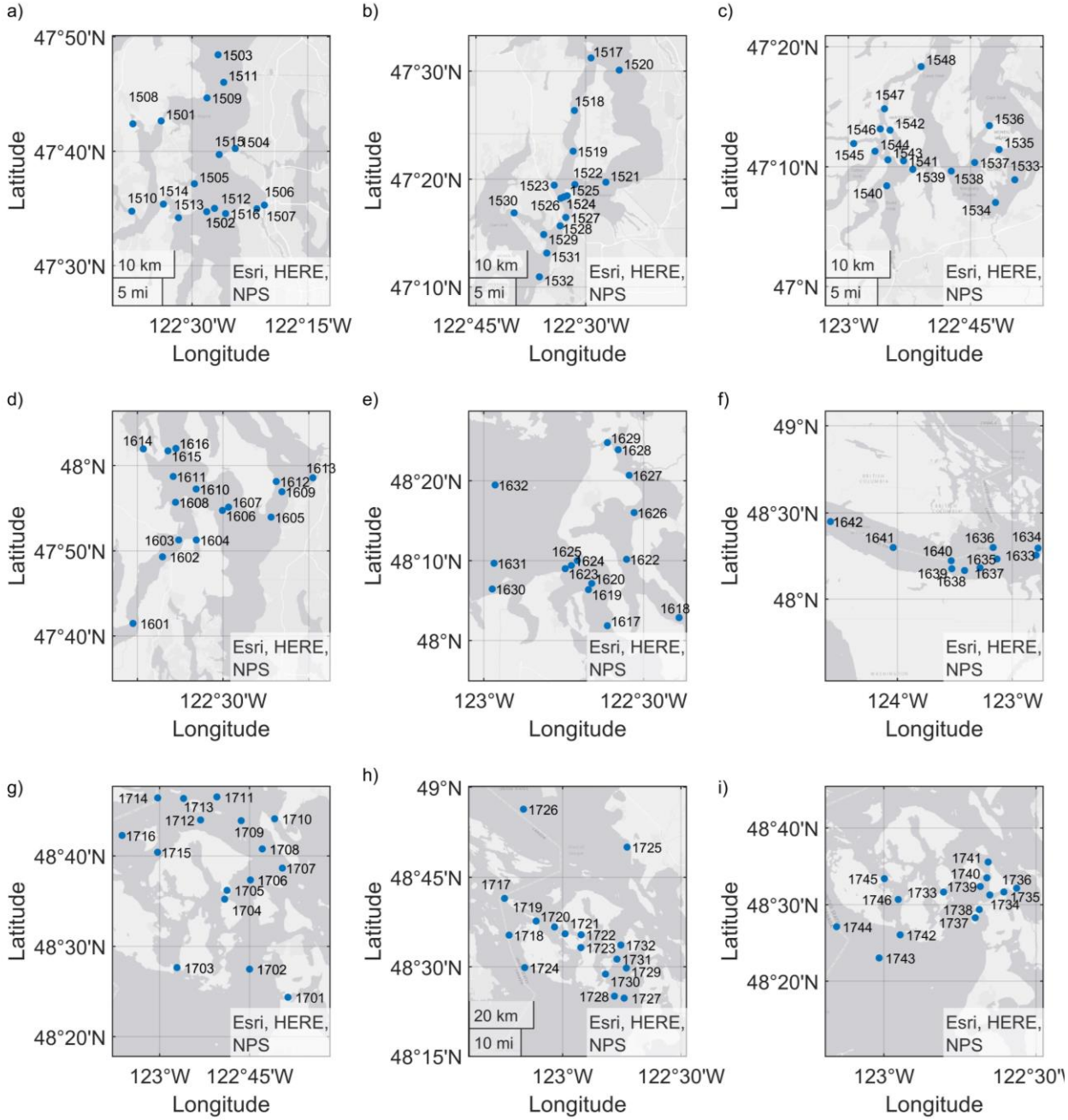

Figure 5.1. Locations of the ADCP measurements. (a-c) 1500 series: Central Sound and South Sound; (d-f) 1600 series: Admiralty Inlet, Hood Canal, Whidbey Basin and San Juan de Fuca; (g-i) 1700 series: San Juan Islands and Georgia Strait.

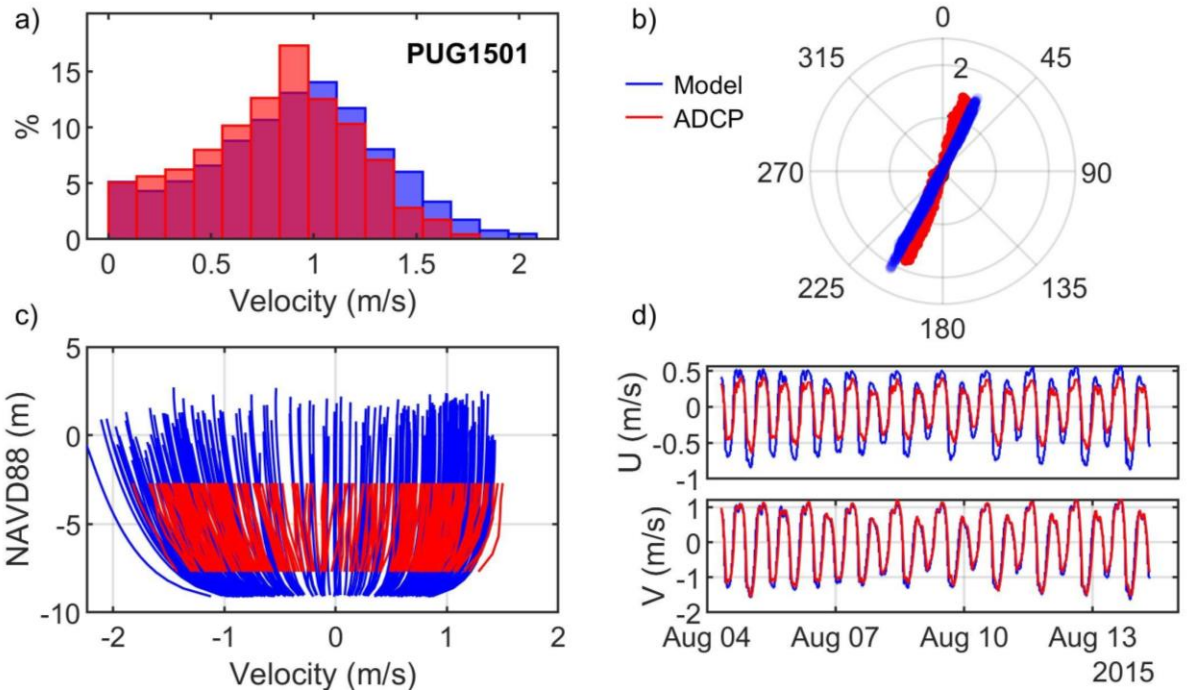

Figure A.1. Comparisons of simulated and observed velocities at Agate Passage (PUG1501): (a) velocity histograms, (b) scatter plot, (c) vertical profiles, and (d) time series of depth-averaged principal velocities.

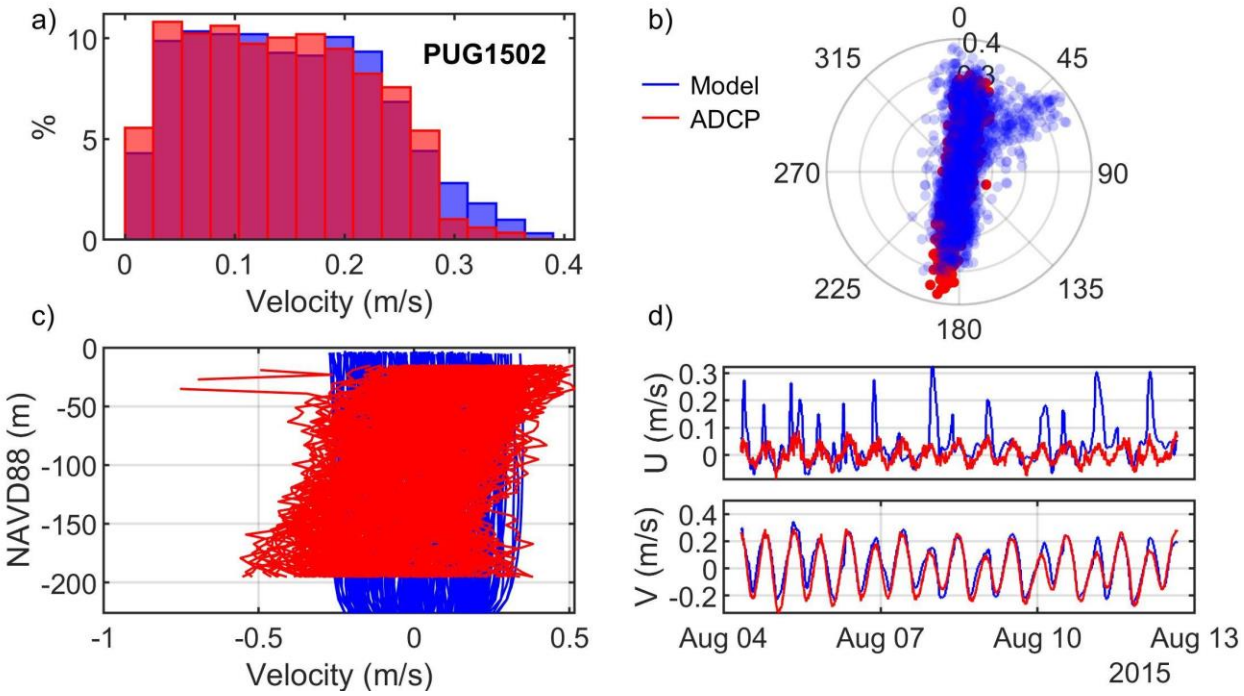

Figure A.2. Comparisons of simulated and observed velocities at Alki Point (PUG1502): (a) velocity histograms, (b) scatter plot, (c) vertical profiles, and (d) time series of depth-averaged principal velocities.

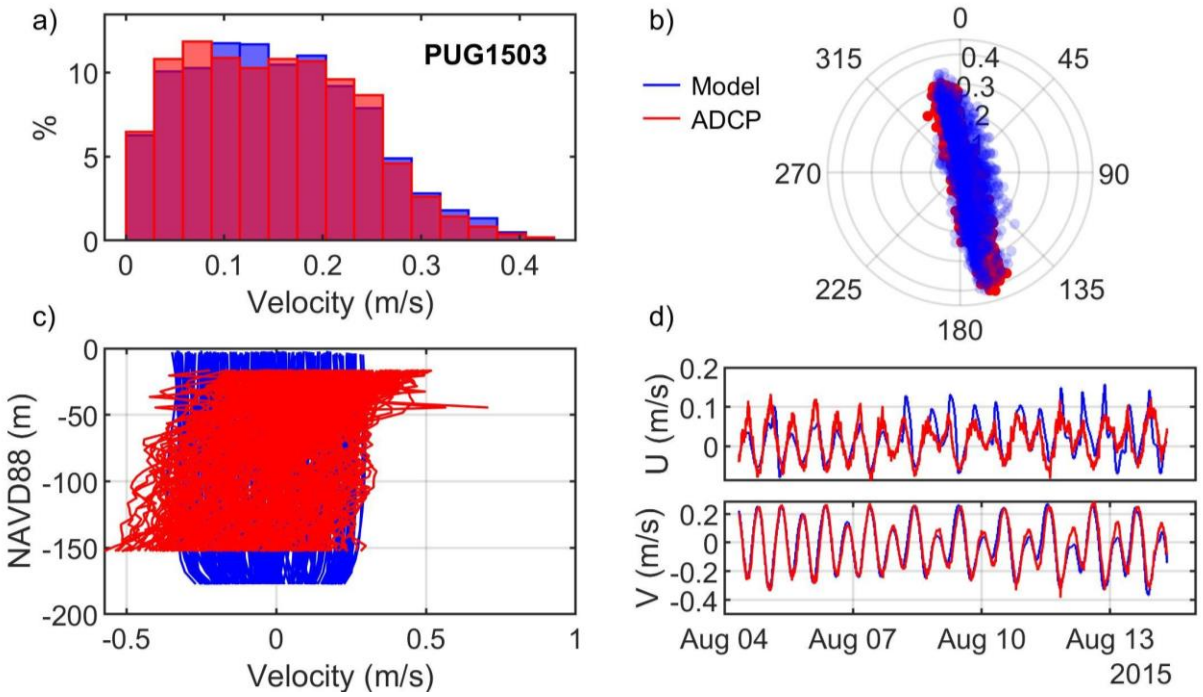

Figure A.3. Comparisons of simulated and observed velocities at Edmonds (PUG1503): (a) velocity histograms, (b) scatter plot, (c) vertical profiles, and (d) time series of depth-averaged principal velocities.

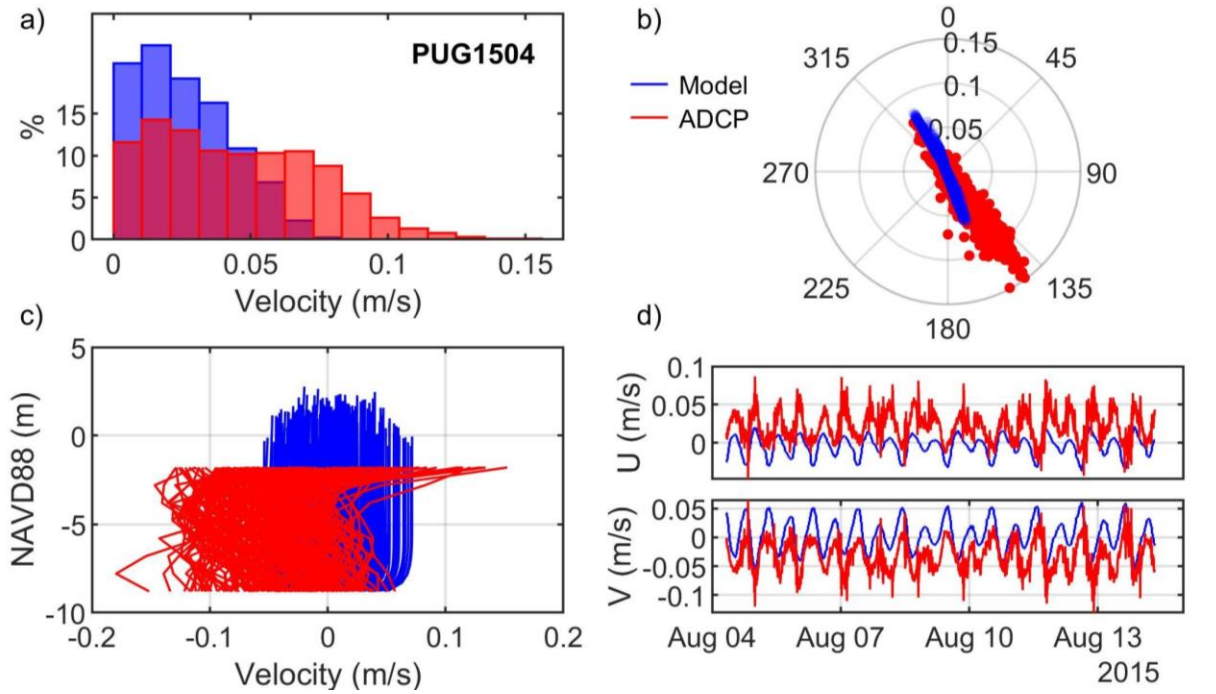

Figure A.4. Comparisons of simulated and observed velocities at Ballard Locks (PUG1504): (a) velocity histograms, (b) scatter plot, (c) vertical profiles, and (d) time series of depth-averaged principal velocities.

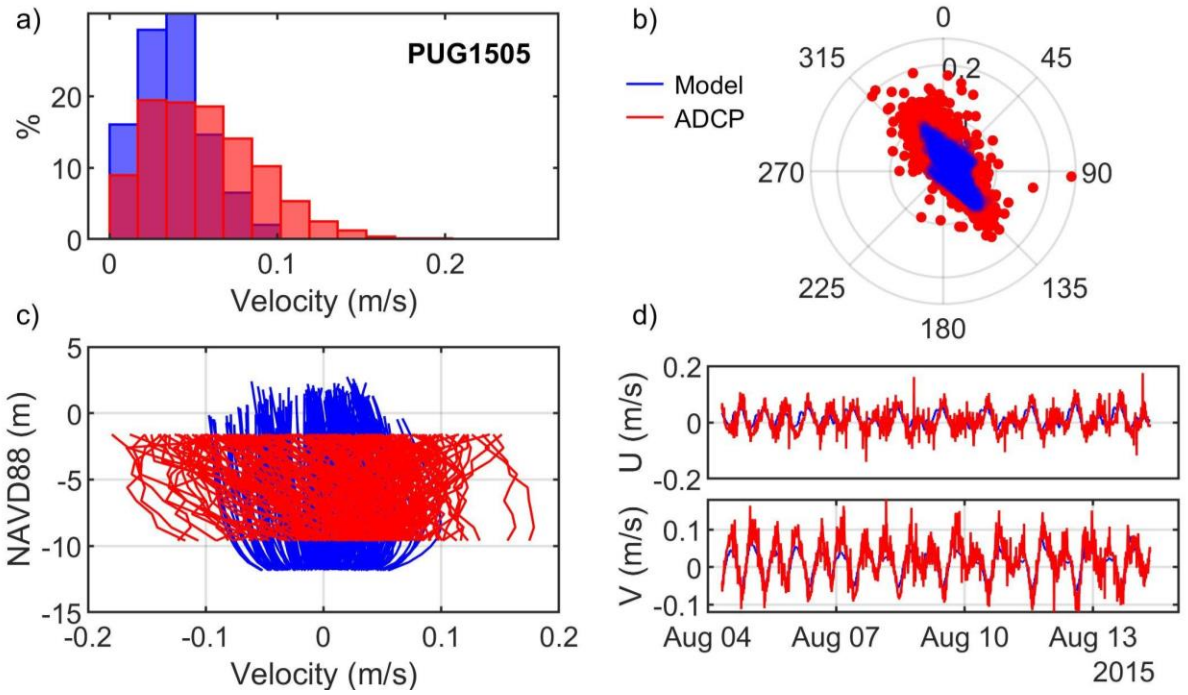

Figure A.5. Comparisons of simulated and observed velocities at Eagle Harbor (PUG1505): (a) velocity histograms, (b) scatter plot, (c) vertical profiles, and (d) time series of depth-averaged principal velocities.

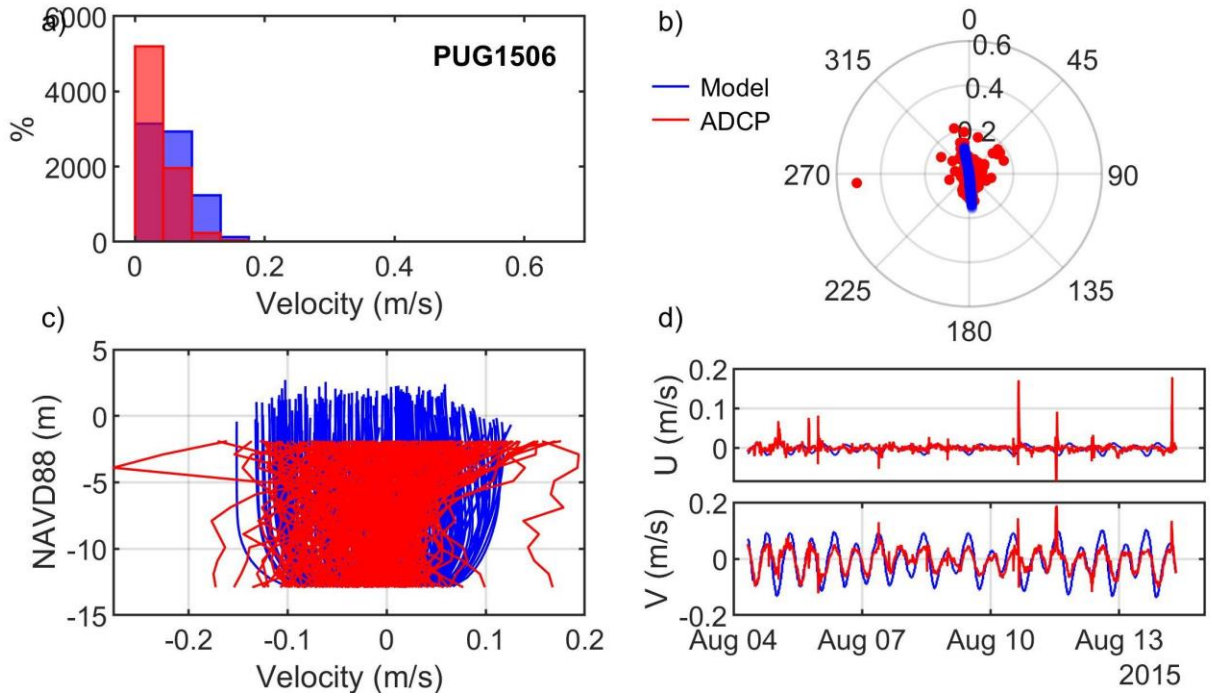

Figure A.6. Comparisons of simulated and observed velocities at Harbor Island (PUG1506): (a) velocity histograms, (b) scatter plot, (c) vertical profiles, and (d) time series of depth-averaged principal velocities.

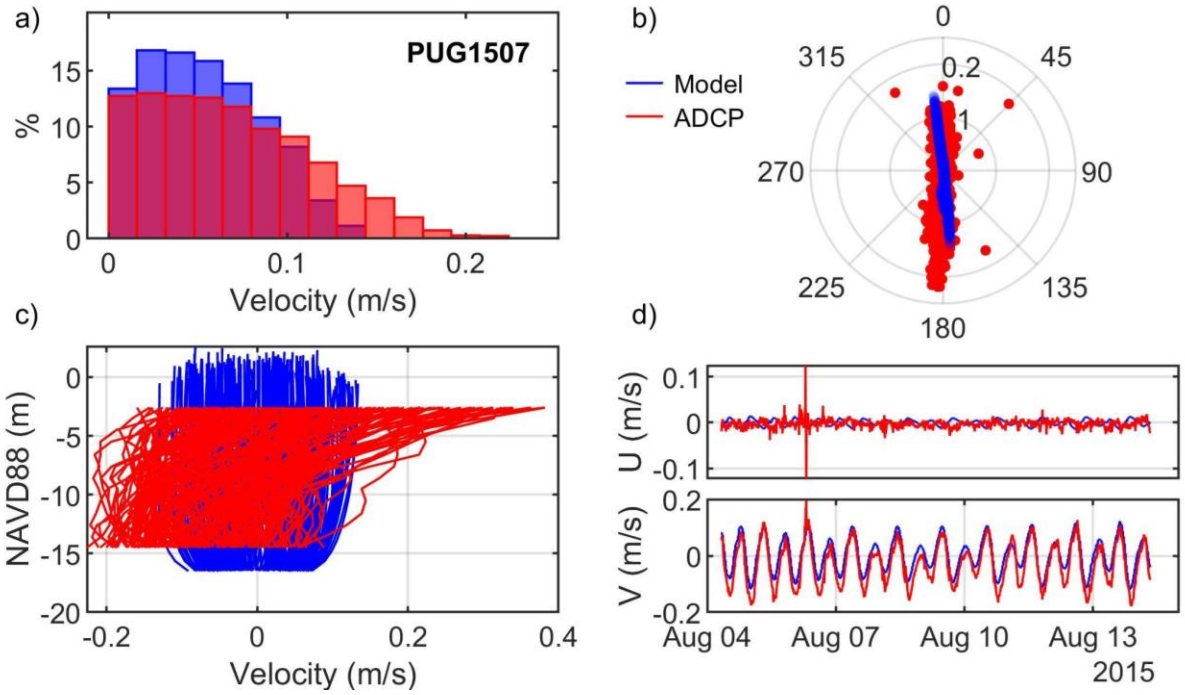

Figure A.7. Comparisons of simulated and observed velocities at Harbor Island (PUG1507): (a) velocity histograms, (b) scatter plot, (c) vertical profiles, and (d) time series of depth-averaged principal velocities.

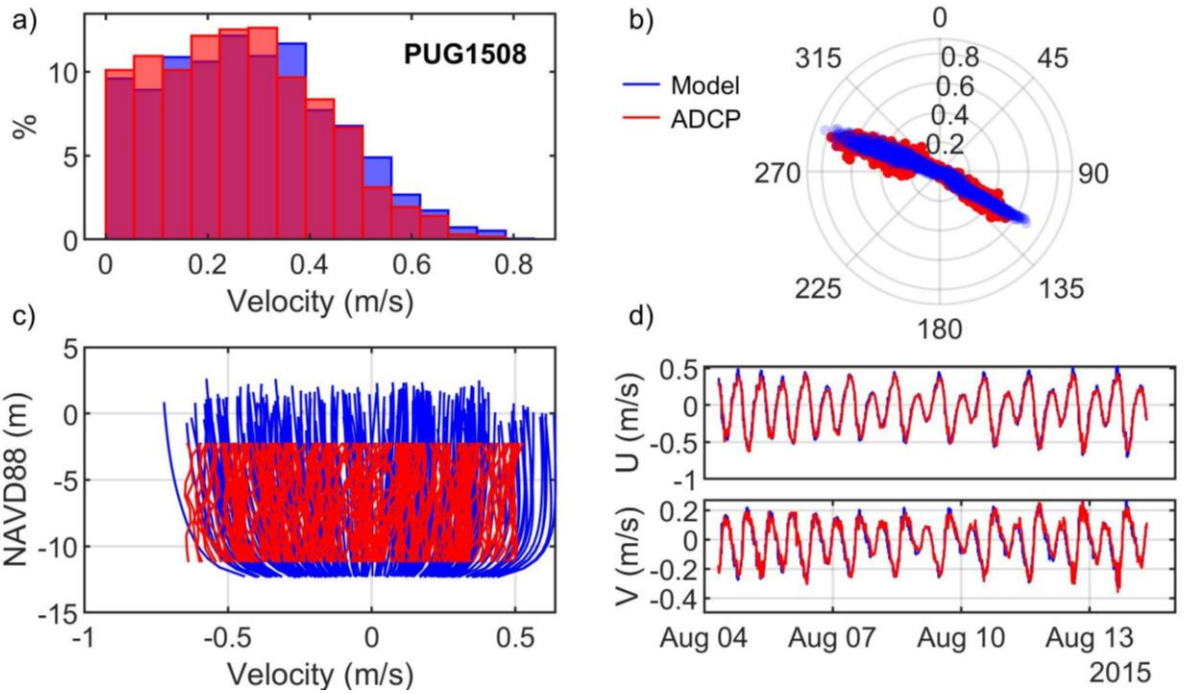

Figure A.8. Comparisons of simulated and observed velocities at Liberty Bay (PUG1508): (a) velocity histograms, (b) scatter plot, (c) vertical profiles, and (d) time series of depth-averaged principal velocities.

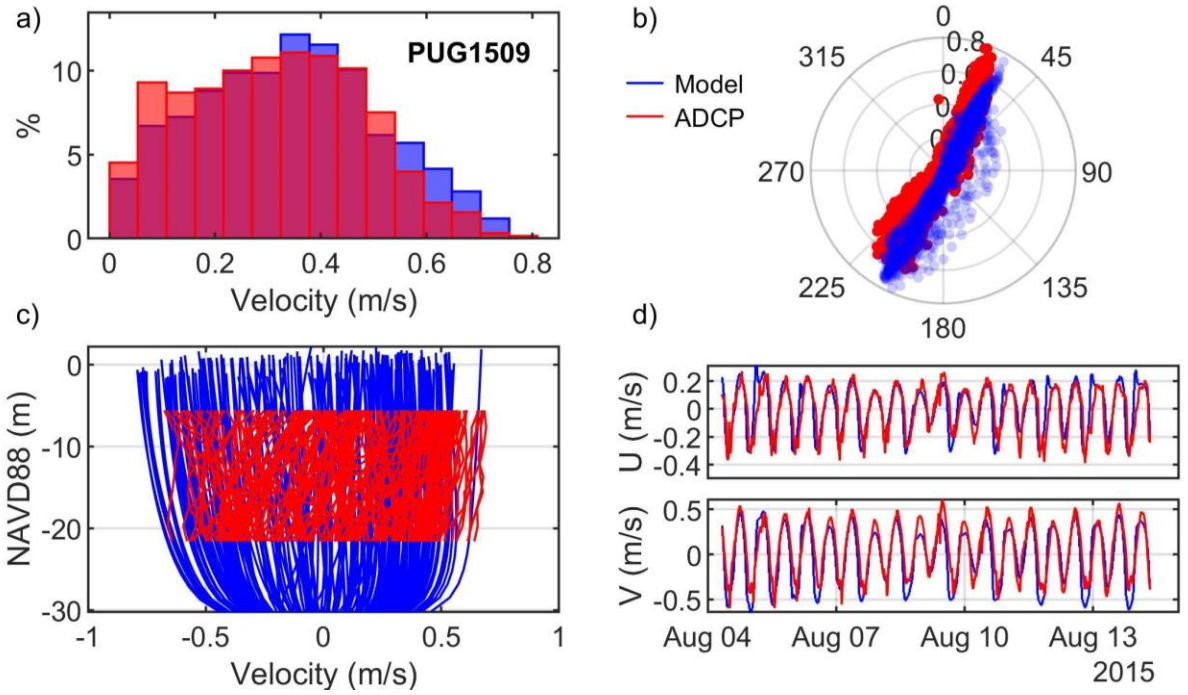

Figure A.9. Comparisons of simulated and observed velocities at Point Jefferson (PUG1509): (a) velocity histograms, (b) scatter plot, (c) vertical profiles, and (d) time series of depth-averaged principal velocities.

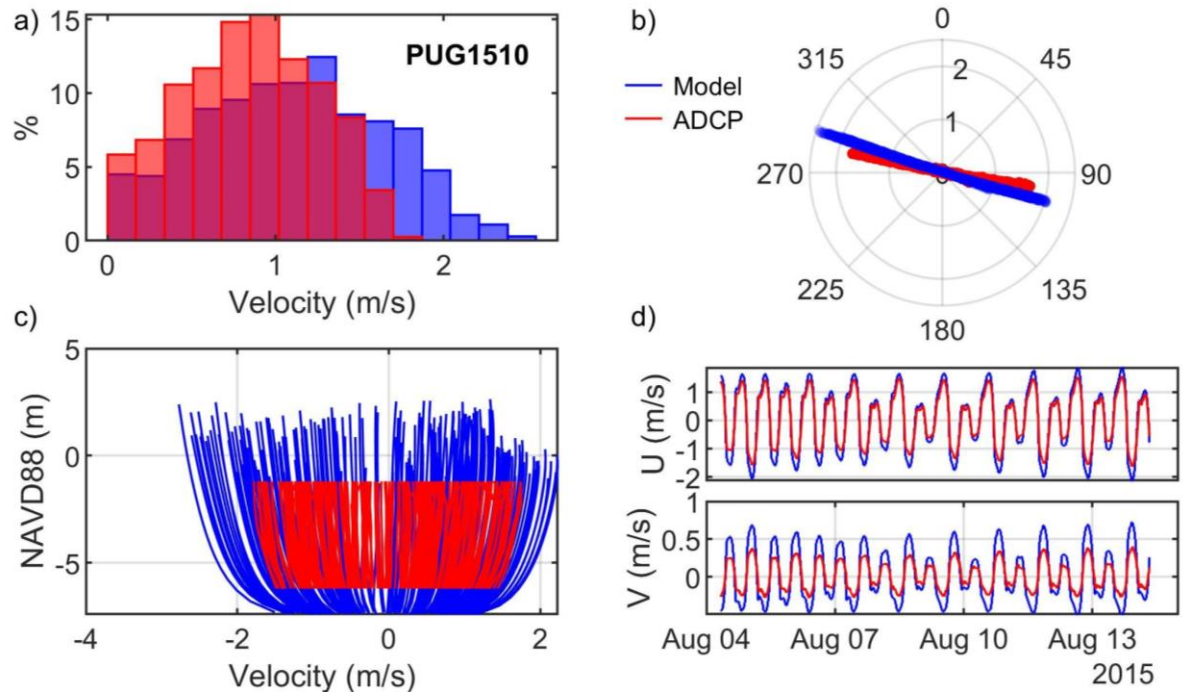

Figure A.10. Comparisons of simulated and observed velocities at Point Washington (PUG1510): (a) velocity histograms, (b) scatter plot, (c) vertical profiles, and (d) time series of depth-averaged principal velocities.

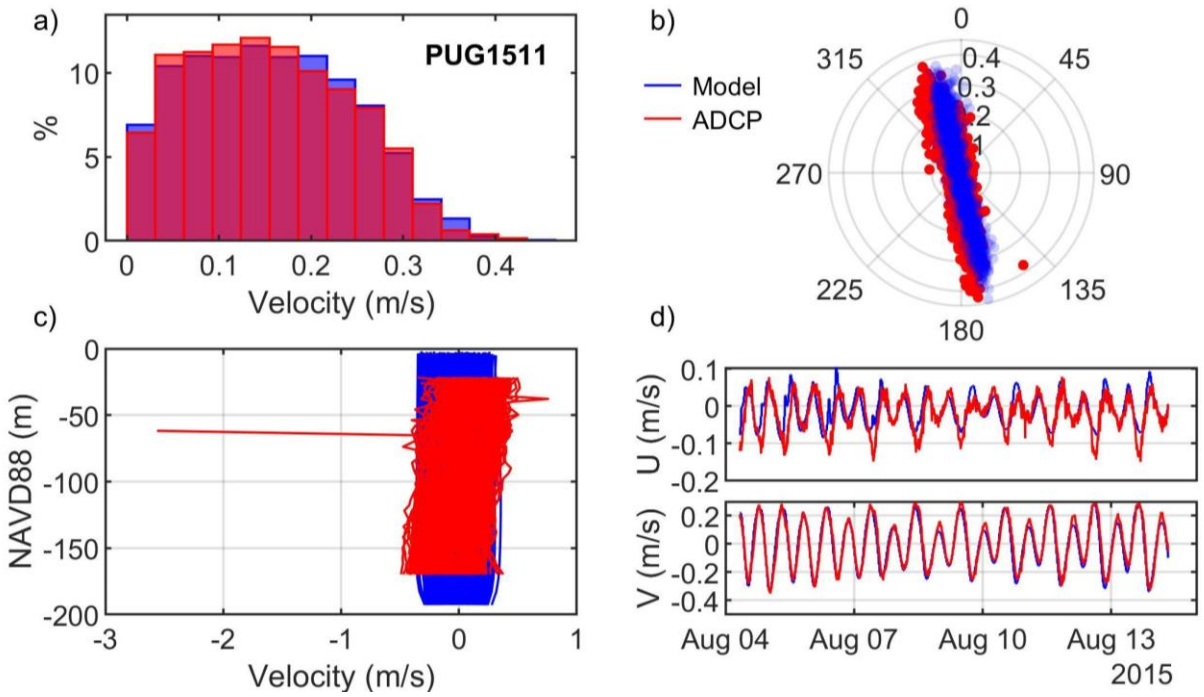

Figure A.11. Comparisons of simulated and observed velocities at President Point (PUG1511): (a) velocity histograms, (b) scatter plot, (c) vertical profiles, and (d) time series of depth-averaged principal velocities.

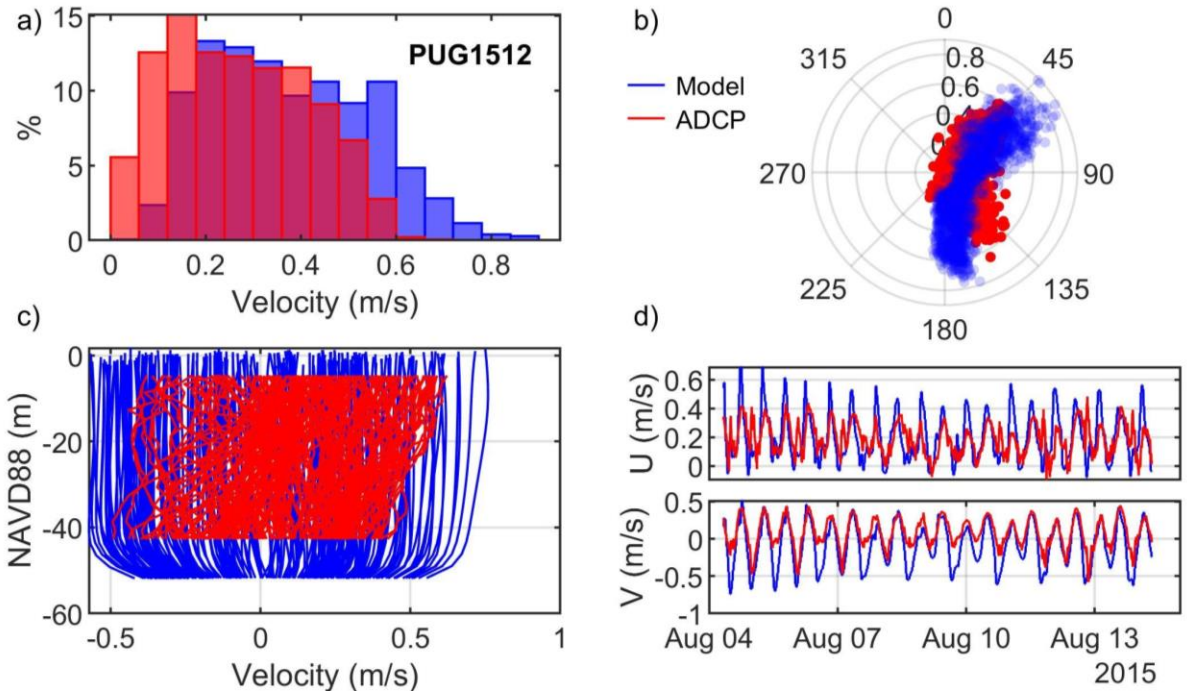

Figure A.12. Comparisons of simulated and observed velocities at Restoration Point (PUG1512): (a) velocity histograms, (b) scatter plot, (c) vertical profiles, and (d) time series of depth-averaged principal velocities.

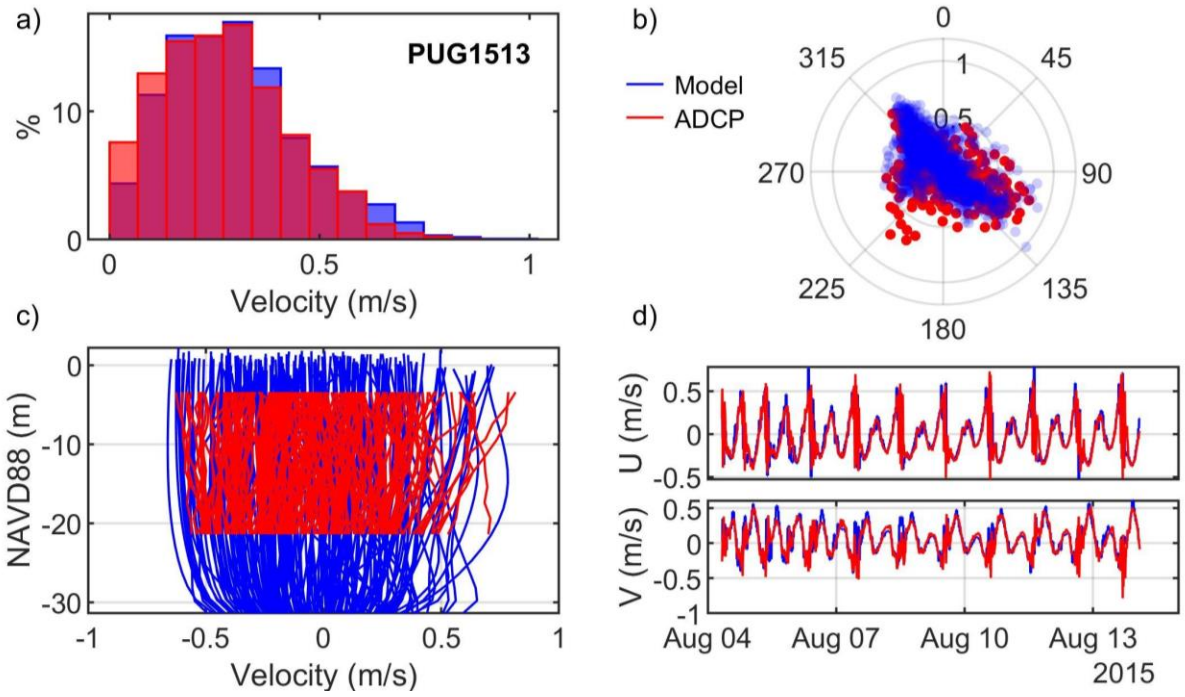

Figure A.13. Comparisons of simulated and observed velocities at Rich Passage (PUG1513): (a) velocity histograms, (b) scatter plot, (c) vertical profiles, and (d) time series of depth-averaged principal velocities.

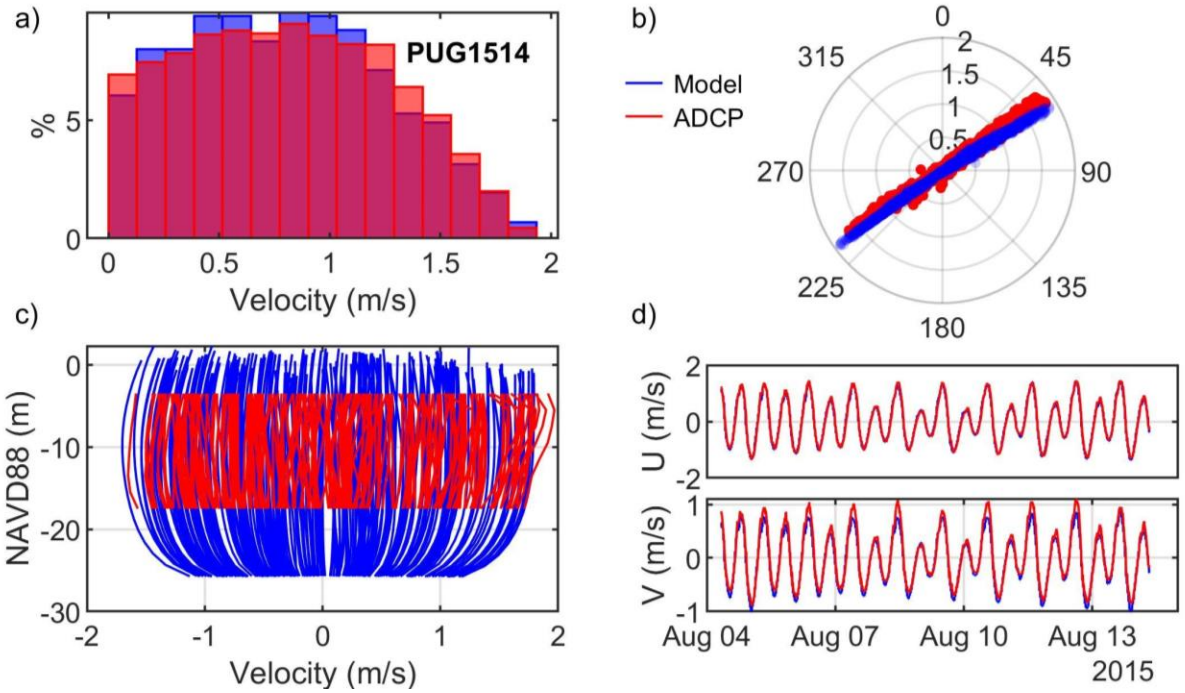

Figure A.14. Comparisons of simulated and observed velocities at Rich Passage (PUG1514): (a) velocity histograms, (b) scatter plot, (c) vertical profiles, and (d) time series of depth-averaged principal velocities.

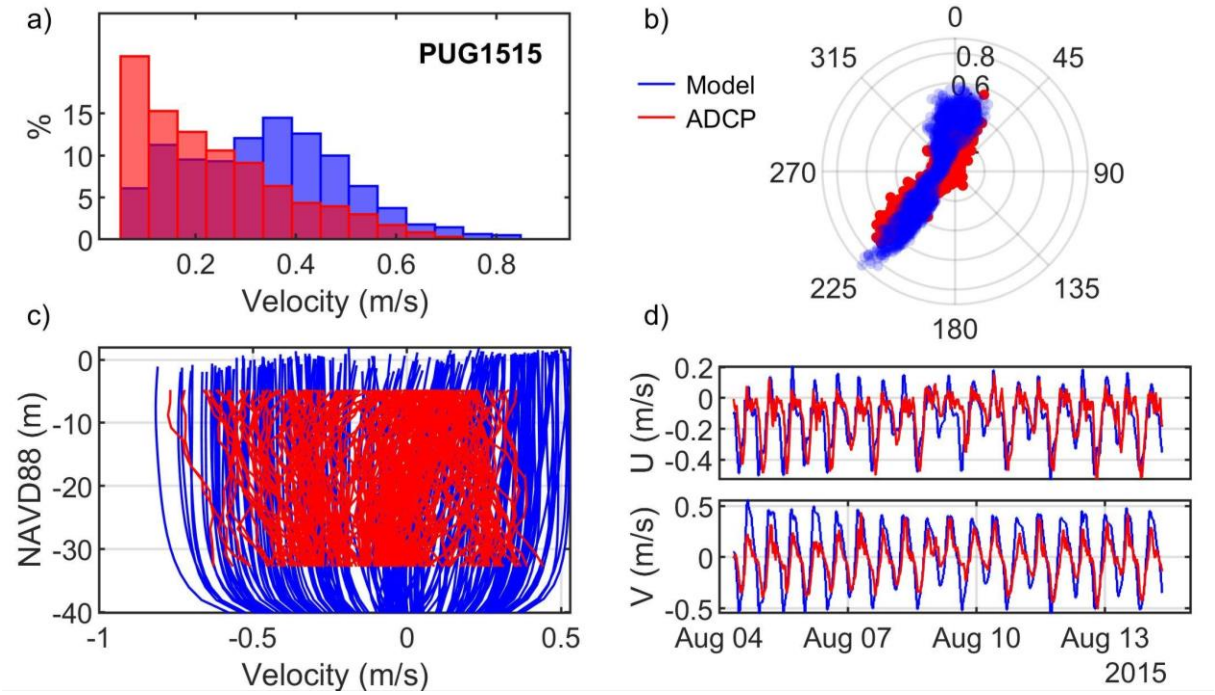

Figure A.15. Comparisons of simulated and observed velocities at West Point (PUG1515): (a) velocity histograms, (b) scatter plot, (c) vertical profiles, and (d) time series of depth-averaged principal velocities.

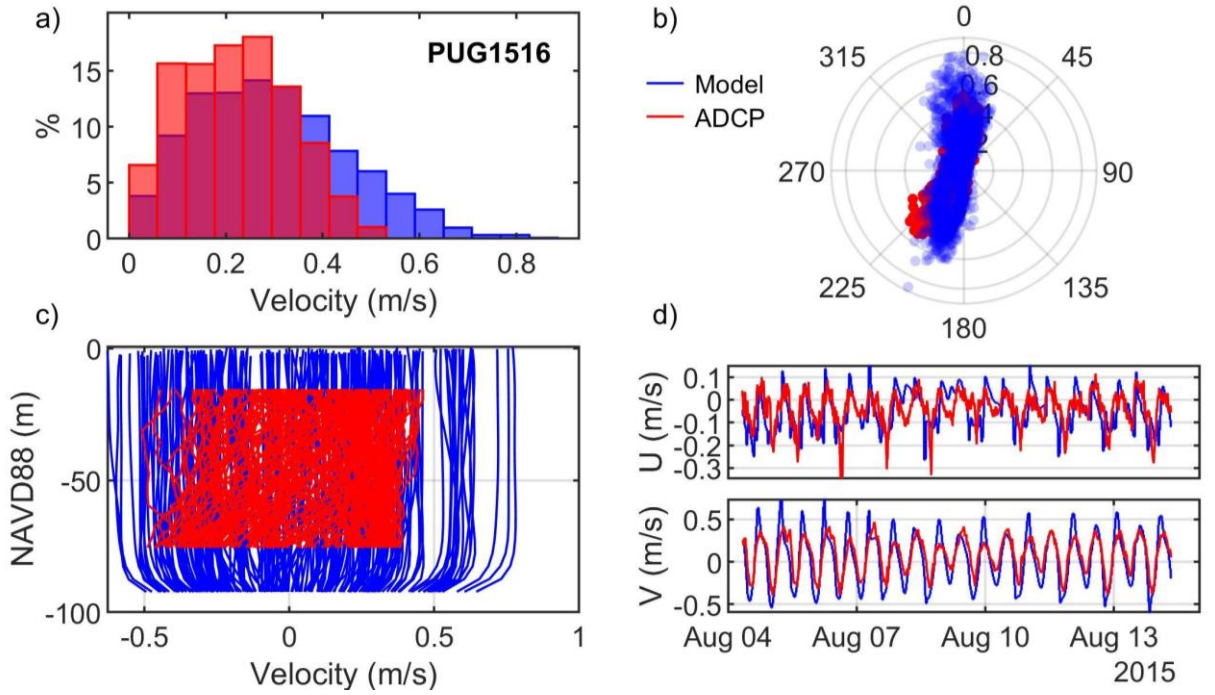

Figure A.16. Comparisons of simulated and observed velocities at Alki Point (PUG1516): (a) velocity histograms, (b) scatter plot, (c) vertical profiles, and (d) time series of depth-averaged principal velocities.

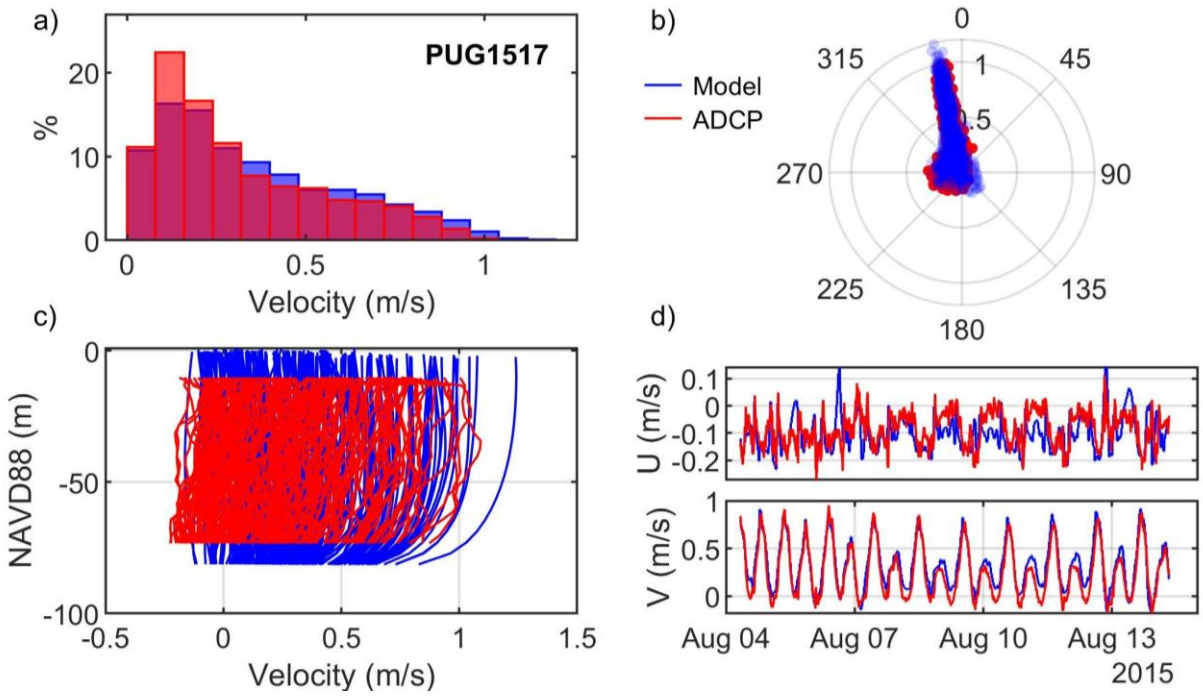

Figure A.17. Comparisons of simulated and observed velocities at Blake Island (PUG1517): (a) velocity histograms, (b) scatter plot, (c) vertical profiles, and (d) time series of depth-averaged principal velocities.

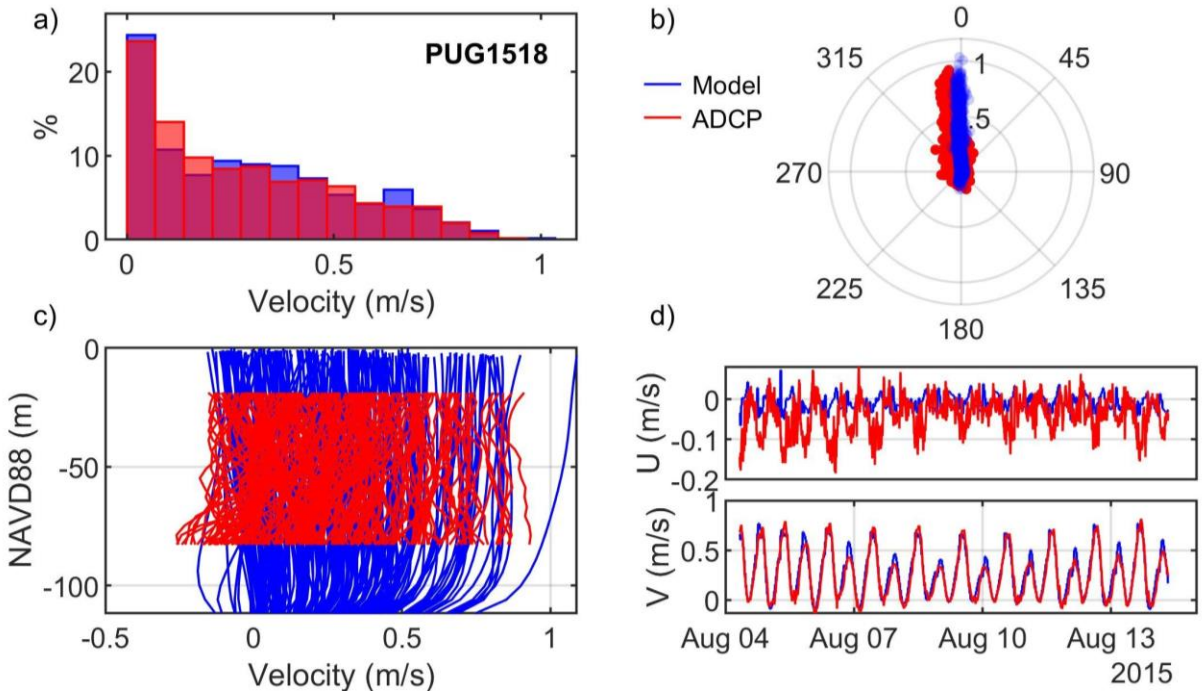

Figure A.18. Comparisons of simulated and observed velocities at Anderson Point (PUG1518): (a) velocity histograms, (b) scatter plot, (c) vertical profiles, and (d) time series of depth-averaged principal velocities.

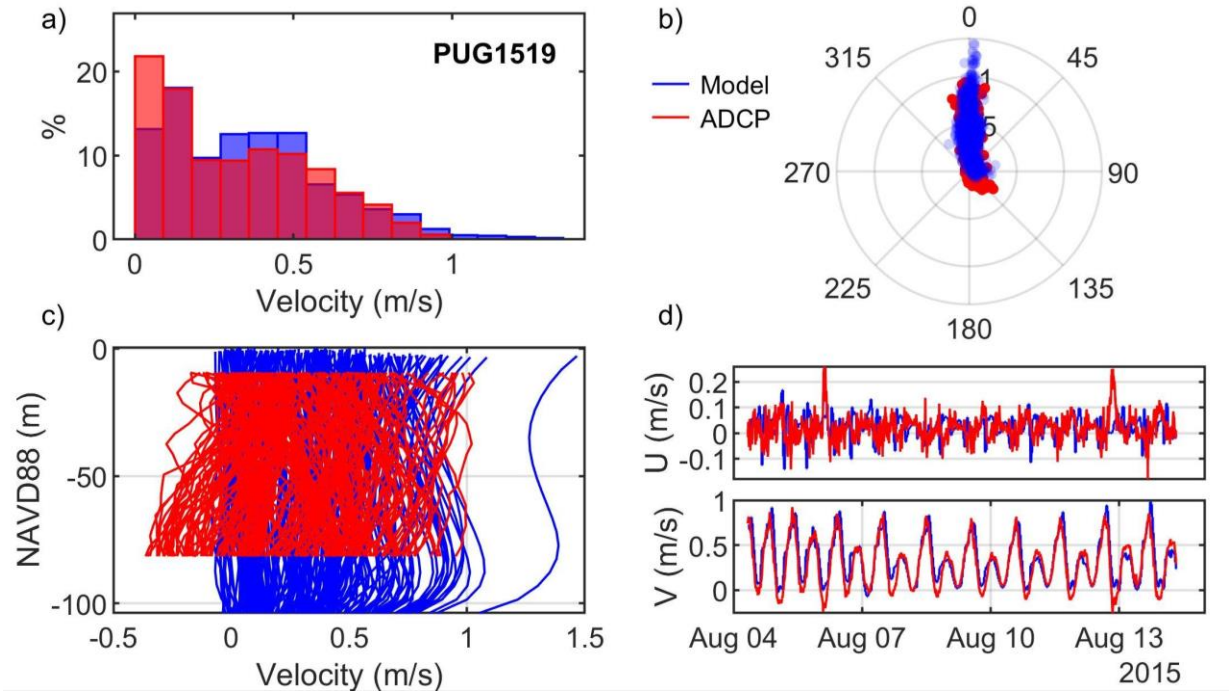

Figure A.19. Comparisons of simulated and observed velocities at Point Richmond (PUG1519): (a) velocity histograms, (b) scatter plot, (c) vertical profiles, and (d) time series of depth-averaged principal velocities.

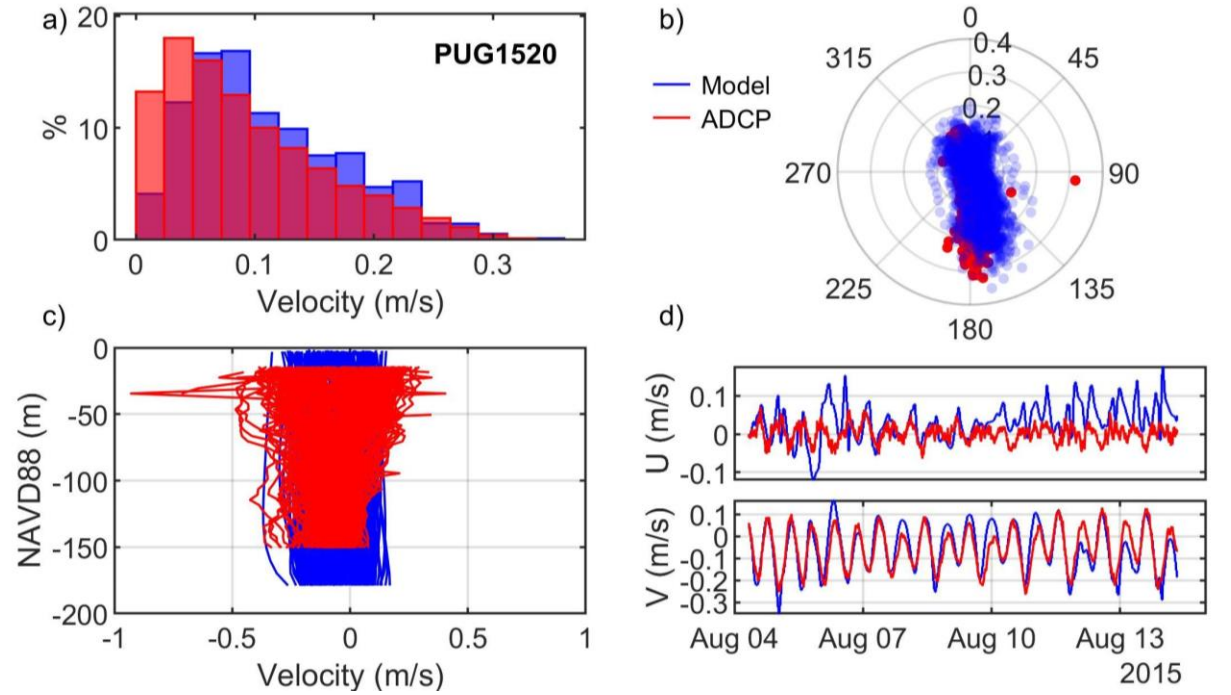

Figure A.20. Comparisons of simulated and observed velocities at Dolphin Point (PUG1520): (a) velocity histograms, (b) scatter plot, (c) vertical profiles, and (d) time series of depth-averaged principal velocities.

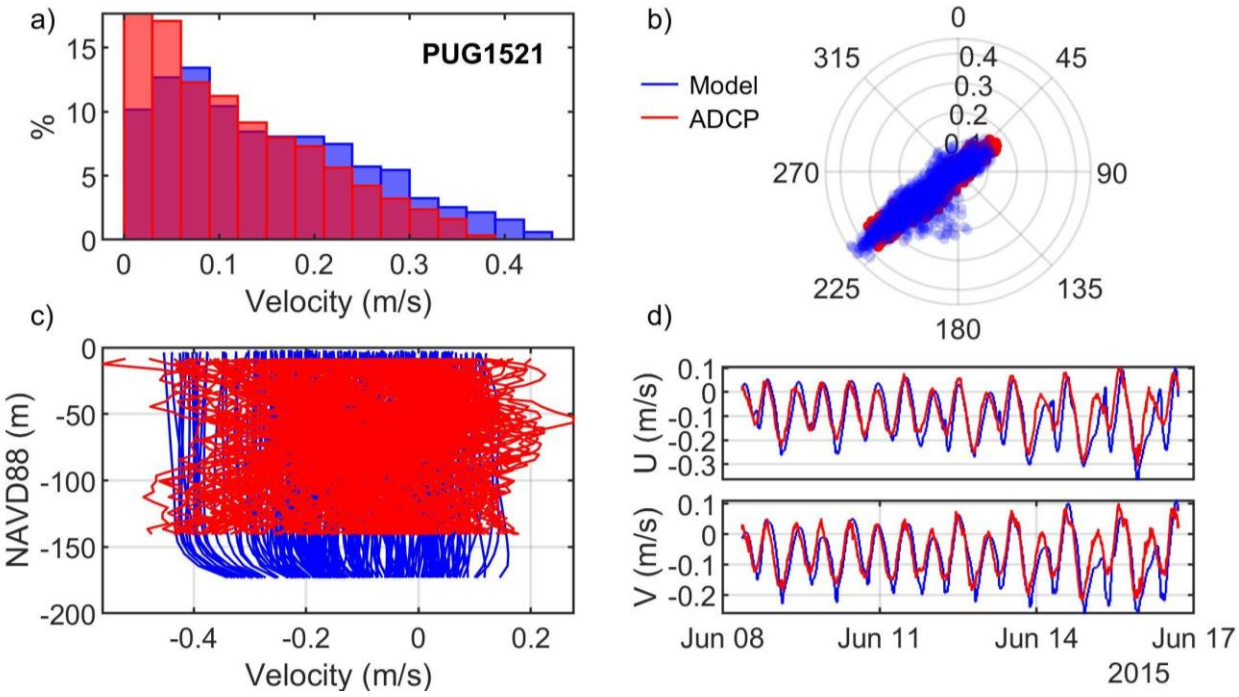

Figure A.21. Comparisons of simulated and observed velocities at Browns Point (PUG1521): (a) velocity histograms, (b) scatter plot, (c) vertical profiles, and (d) time series of depth-averaged principal velocities.

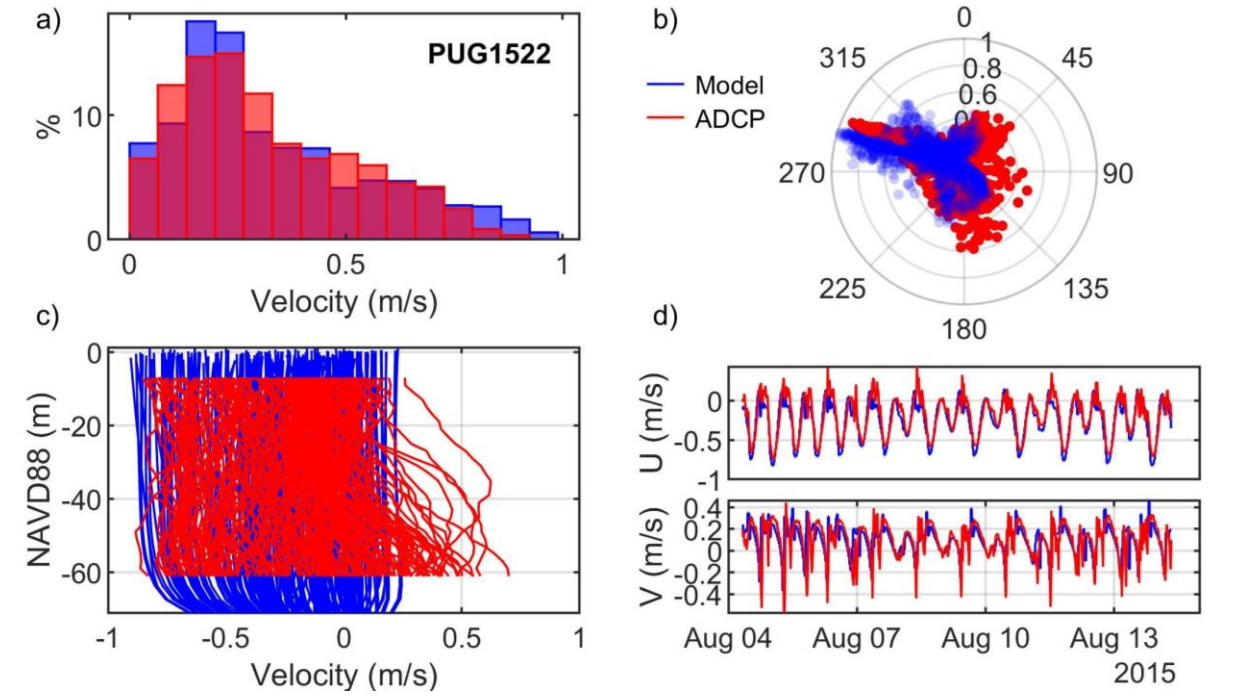

Figure A.22. Comparisons of simulated and observed velocities at Dalco Passage (PUG1522): (a) velocity histograms, (b) scatter plot, (c) vertical profiles, and (d) time series of depth-averaged principal velocities.

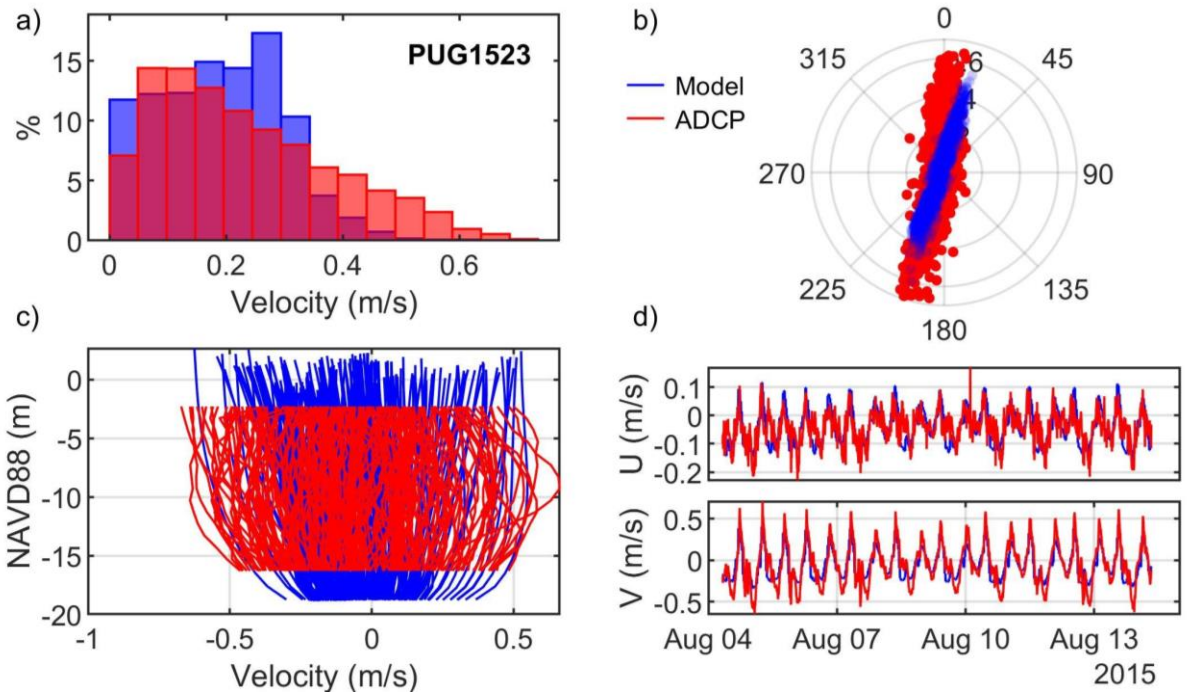

Figure A.23. Comparisons of simulated and observed velocities at Gig Harbor (PUG1523): (a) velocity histograms, (b) scatter plot, (c) vertical profiles, and (d) time series of depth-averaged principal velocities.

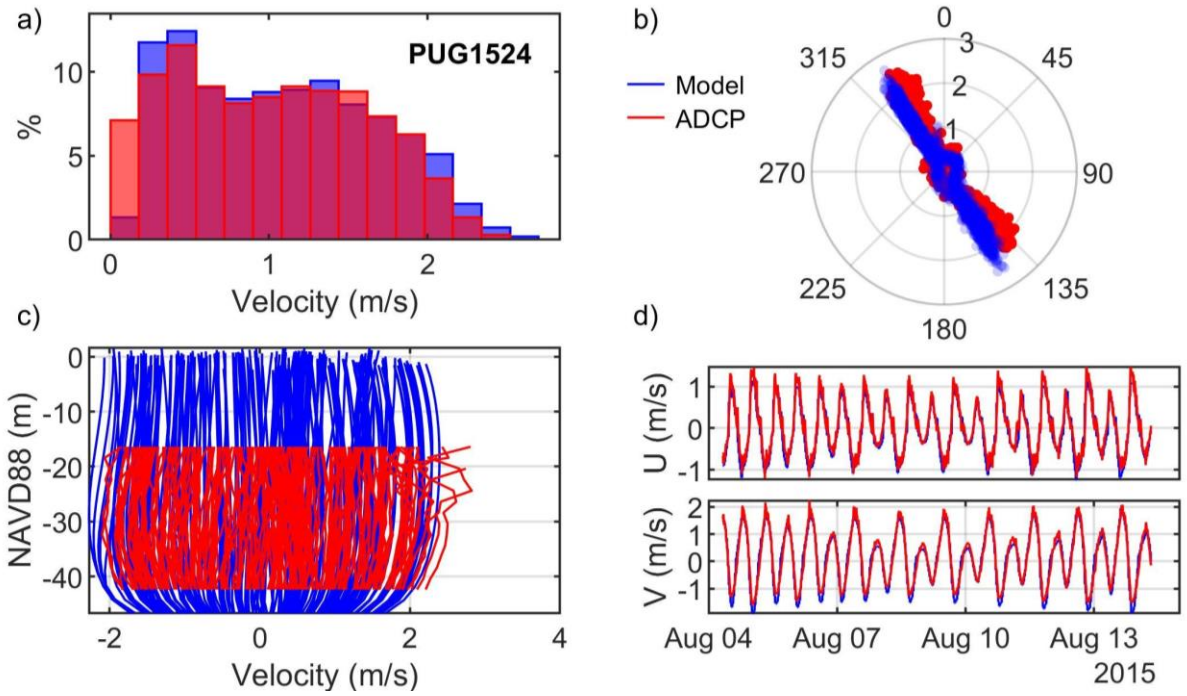

Figure A.24. Comparisons of simulated and observed velocities at The Narrows (PUG1524): (a) velocity histograms, (b) scatter plot, (c) vertical profiles, and (d) time series of depth-averaged principal velocities.

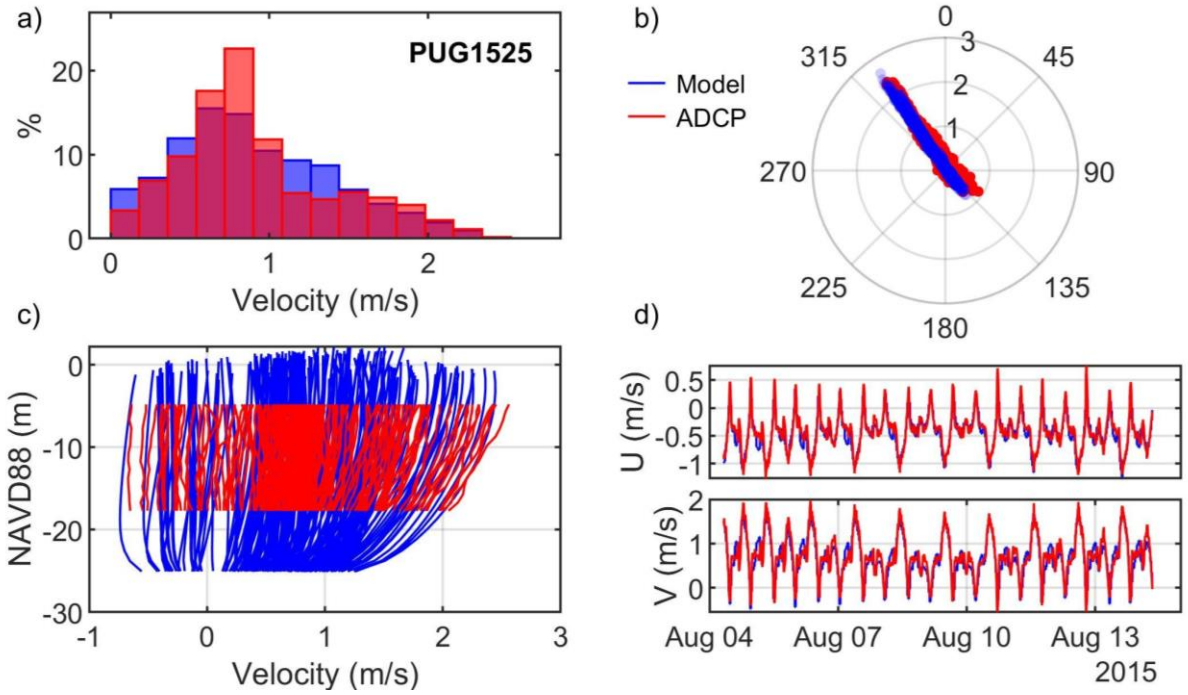

Figure A.25. Comparisons of simulated and observed velocities at The Narrows (PUG1525): (a) velocity histograms, (b) scatter plot, (c) vertical profiles, and (d) time series of depth-averaged principal velocities.

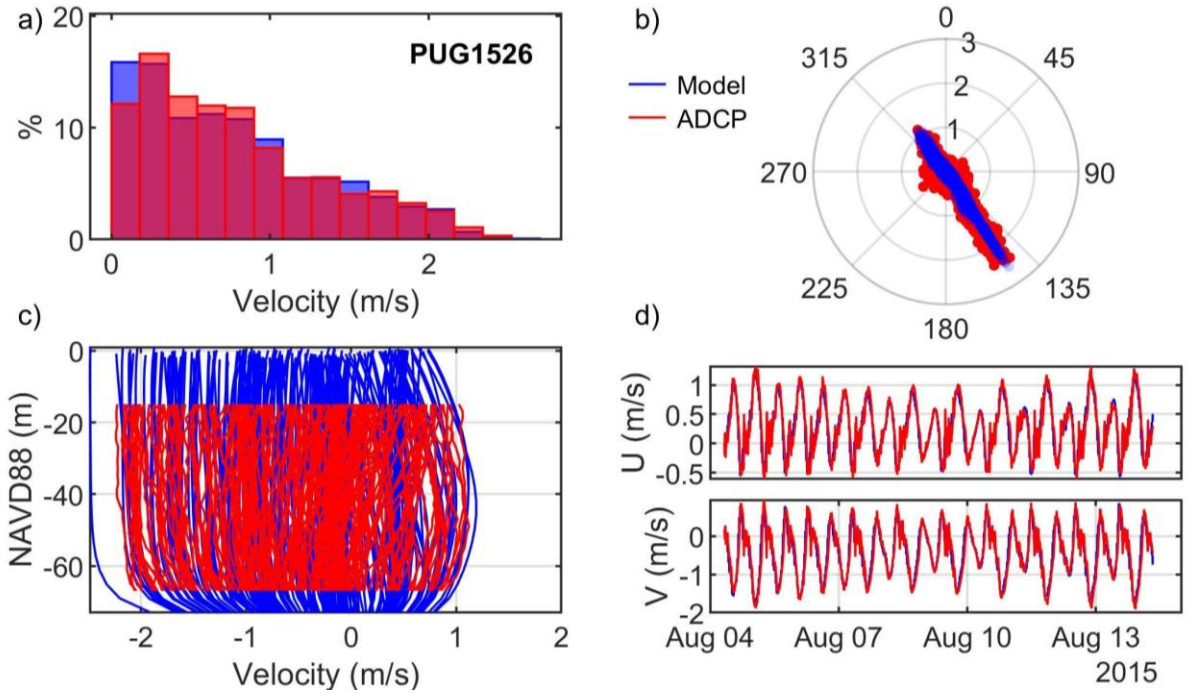

Figure A.26. Comparisons of simulated and observed velocities at The Narrows (PUG1526): (a) velocity histograms, (b) scatter plot, (c) vertical profiles, and (d) time series of depth-averaged principal velocities.

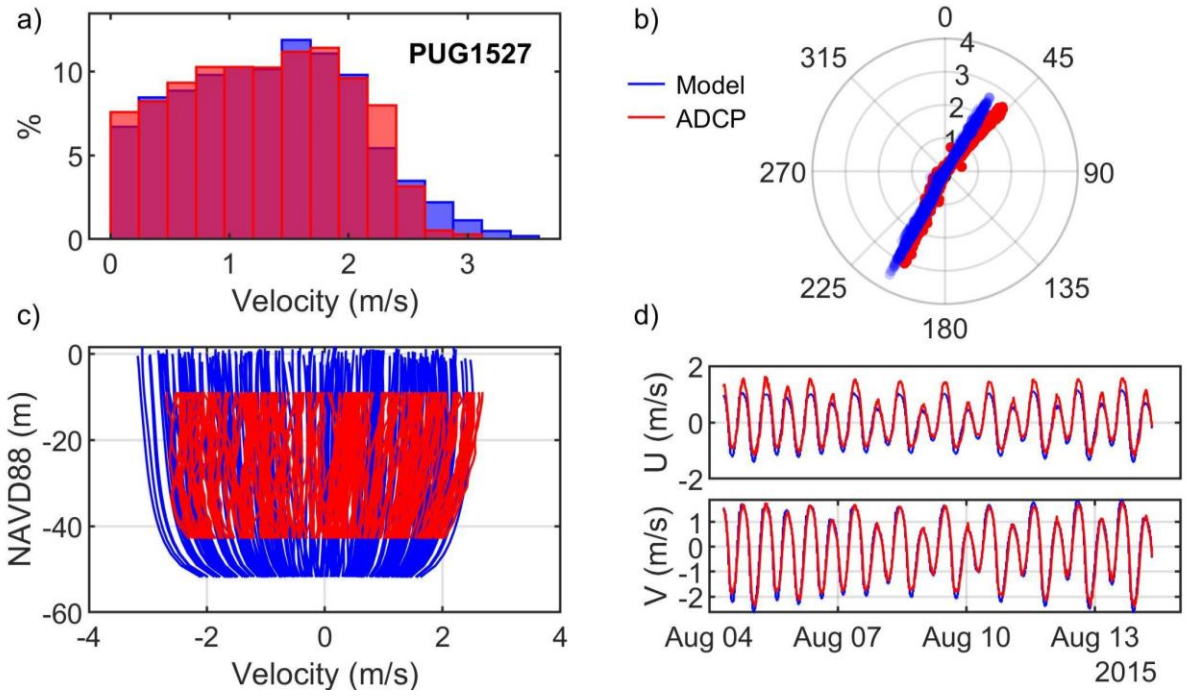

Figure A.27. Comparisons of simulated and observed velocities at The Narrows (PUG1527): (a) velocity histograms, (b) scatter plot, (c) vertical profiles, and (d) time series of depth-averaged principal velocities.

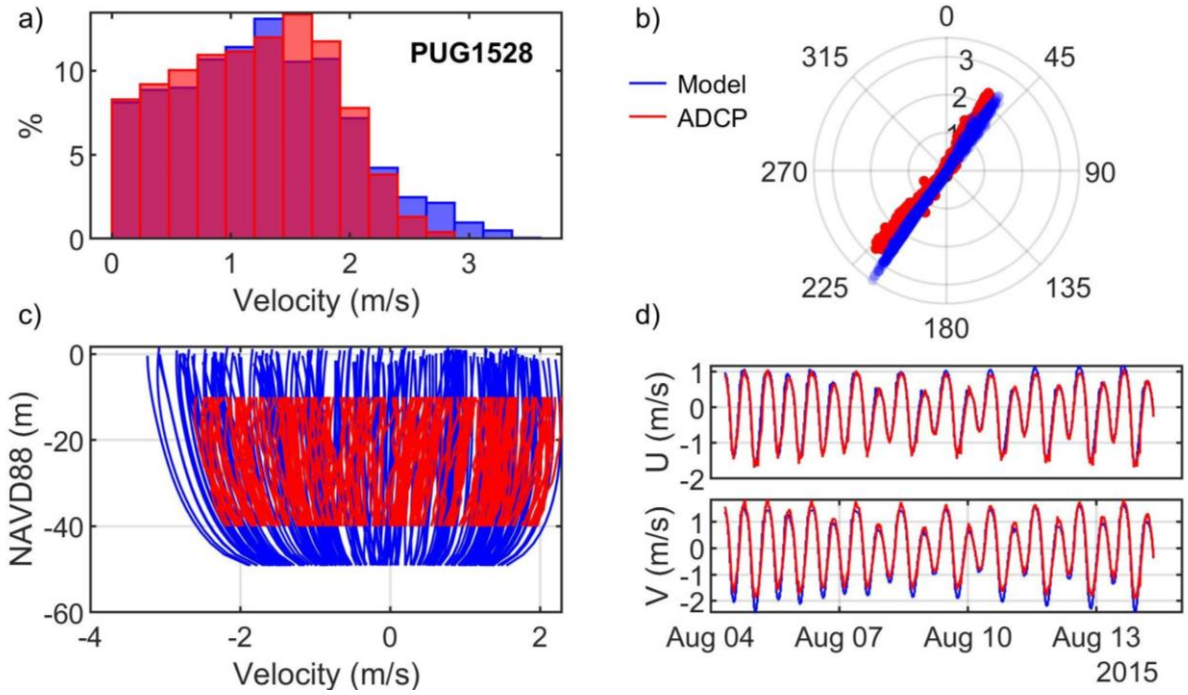

Figure A.28. Comparisons of simulated and observed velocities at The Narrows (PUG1528): (a) velocity histograms, (b) scatter plot, (c) vertical profiles, and (d) time series of depth-averaged principal velocities.

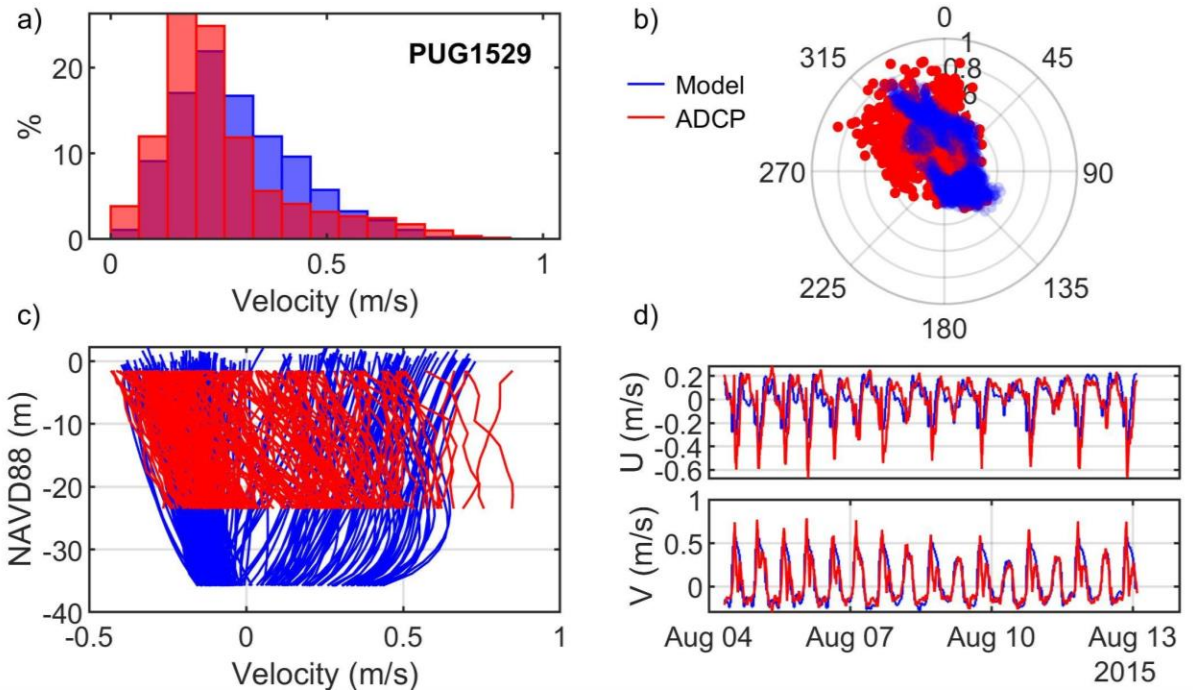

Figure A.29. Comparisons of simulated and observed velocities at Hale Passage (PUG1529): (a) velocity histograms, (b) scatter plot, (c) vertical profiles, and (d) time series of depth-averaged principal velocities.

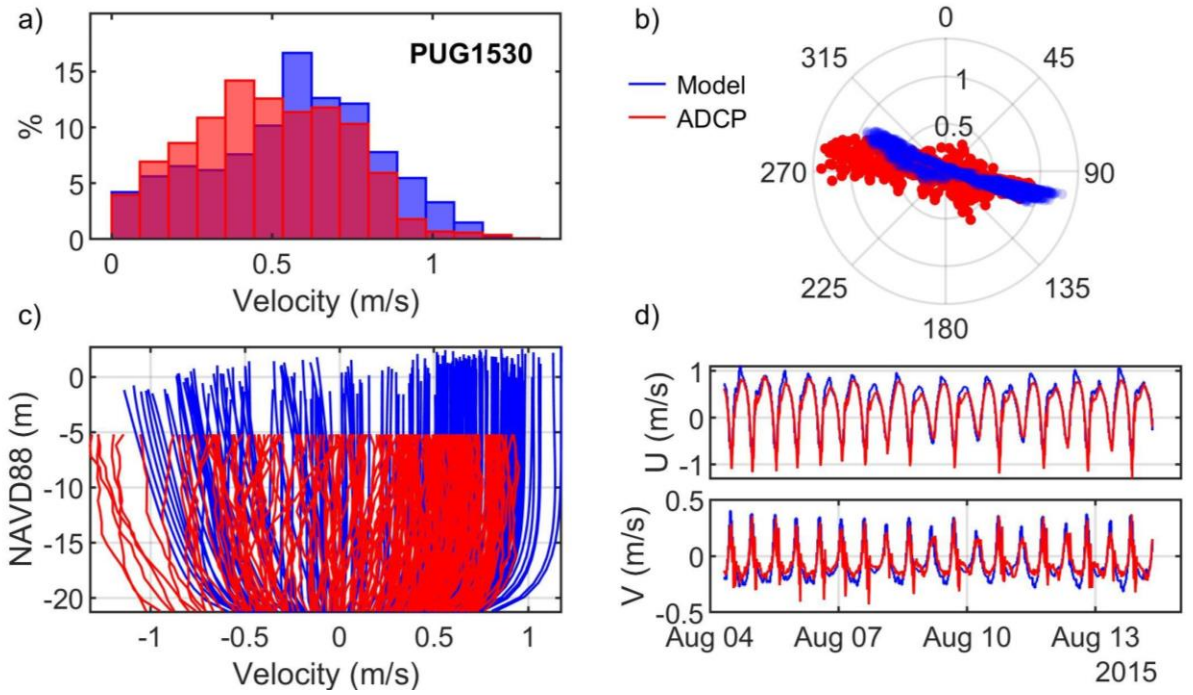

Figure A.30. Comparisons of simulated and observed velocities at Hale Passage (PUG1530): (a) velocity histograms, (b) scatter plot, (c) vertical profiles, and (d) time series of depth-averaged principal velocities.

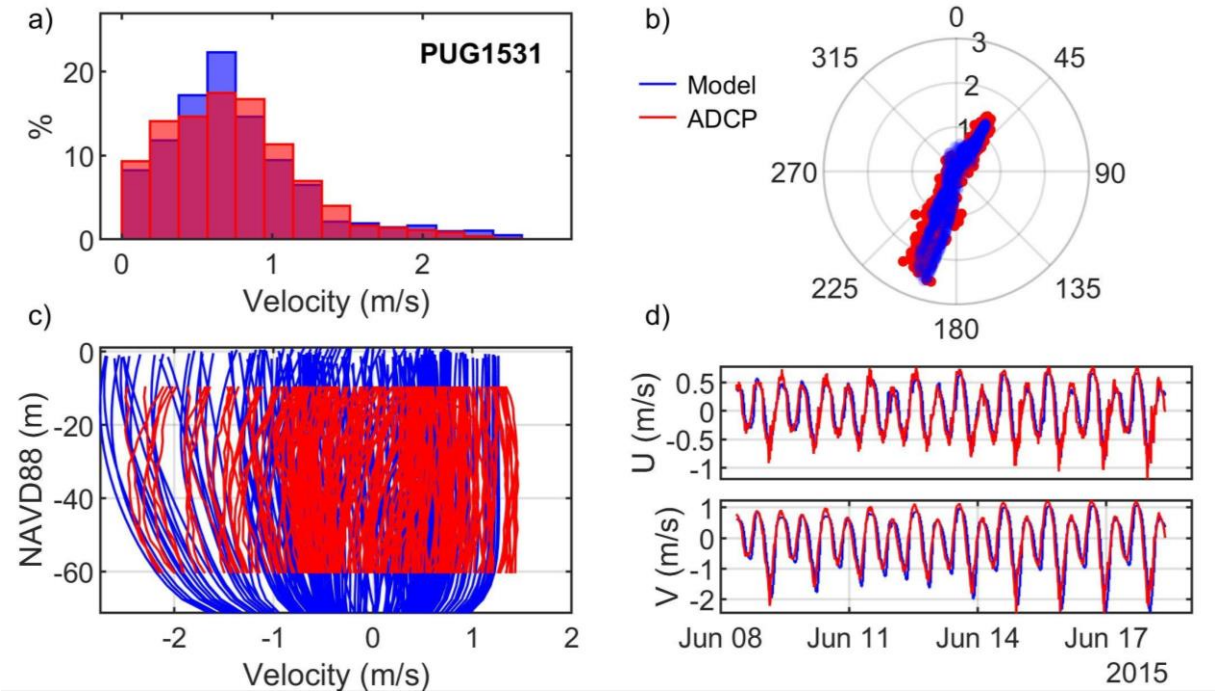

Figure A.31. Comparisons of simulated and observed velocities at Gibson Point (PUG1531): (a) velocity histograms, (b) scatter plot, (c) vertical profiles, and (d) time series of depth-averaged principal velocities.

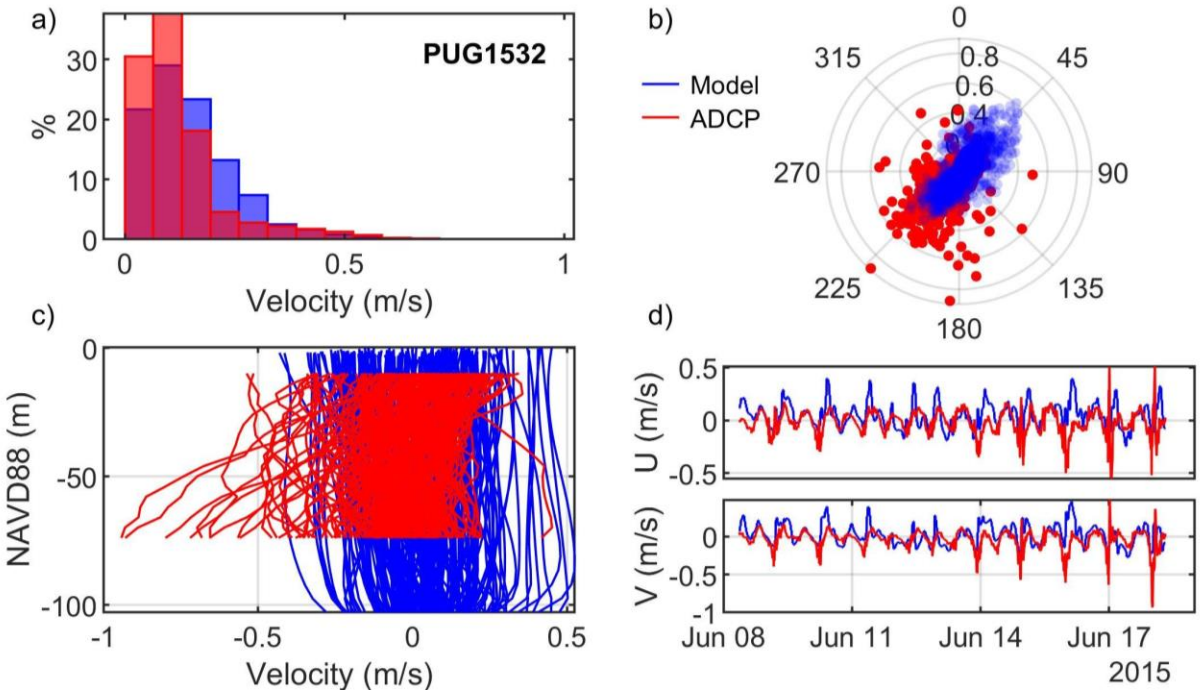

Figure A.32. Comparisons of simulated and observed velocities at Steilacoom (PUG1532): (a) velocity histograms, (b) scatter plot, (c) vertical profiles, and (d) time series of depth-averaged principal velocities.

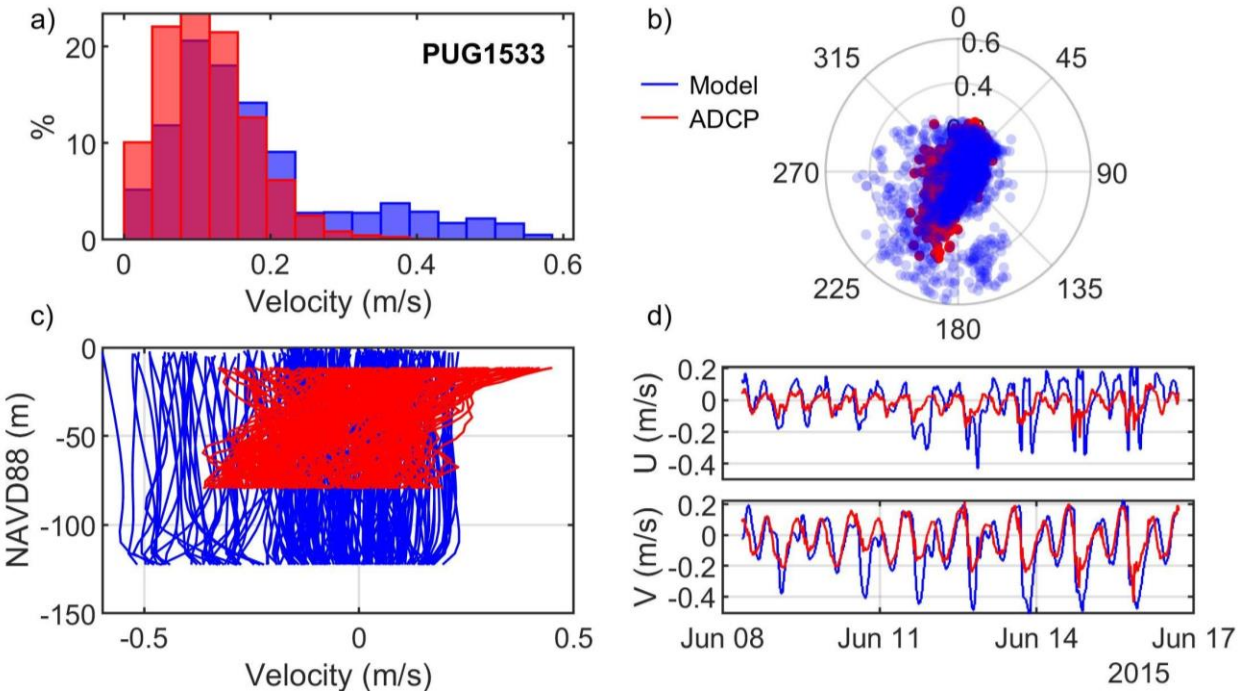

Figure A.33. Comparisons of simulated and observed velocities at Ketron Island (PUG1533): (a) velocity histograms, (b) scatter plot, (c) vertical profiles, and (d) time series of depth-averaged principal velocities.

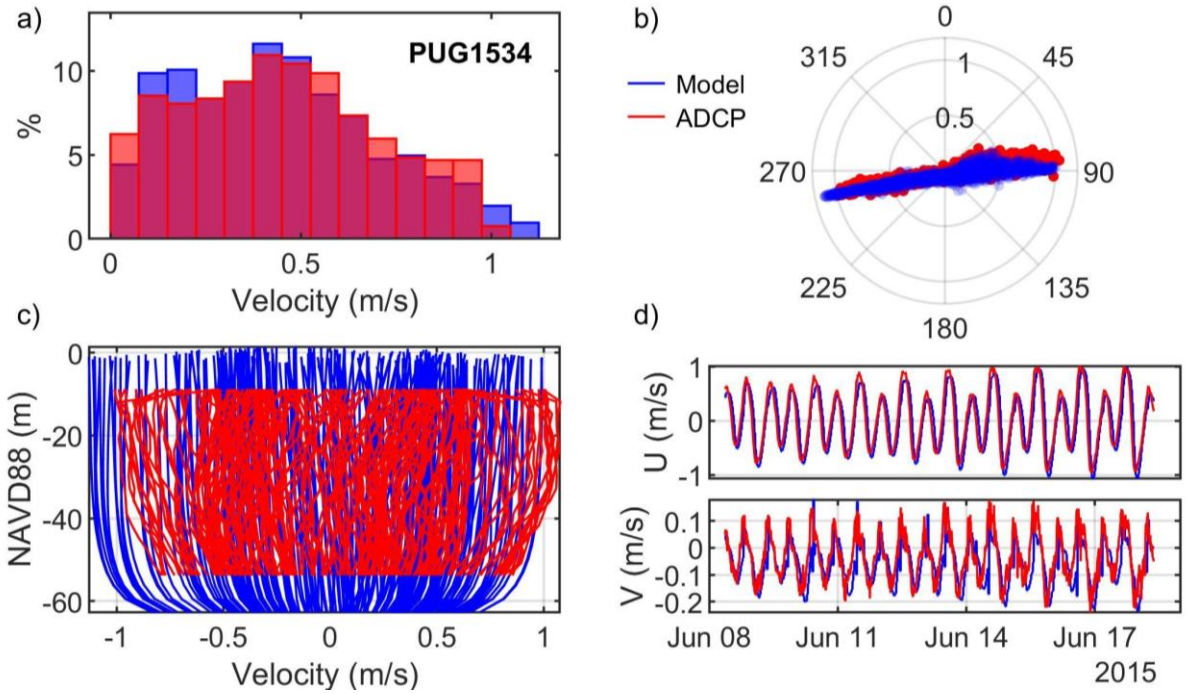

Figure A.34. Comparisons of simulated and observed velocities at Nisqually Reach (PUG1534): (a) velocity histograms, (b) scatter plot, (c) vertical profiles, and (d) time series of depth-averaged principal velocities.

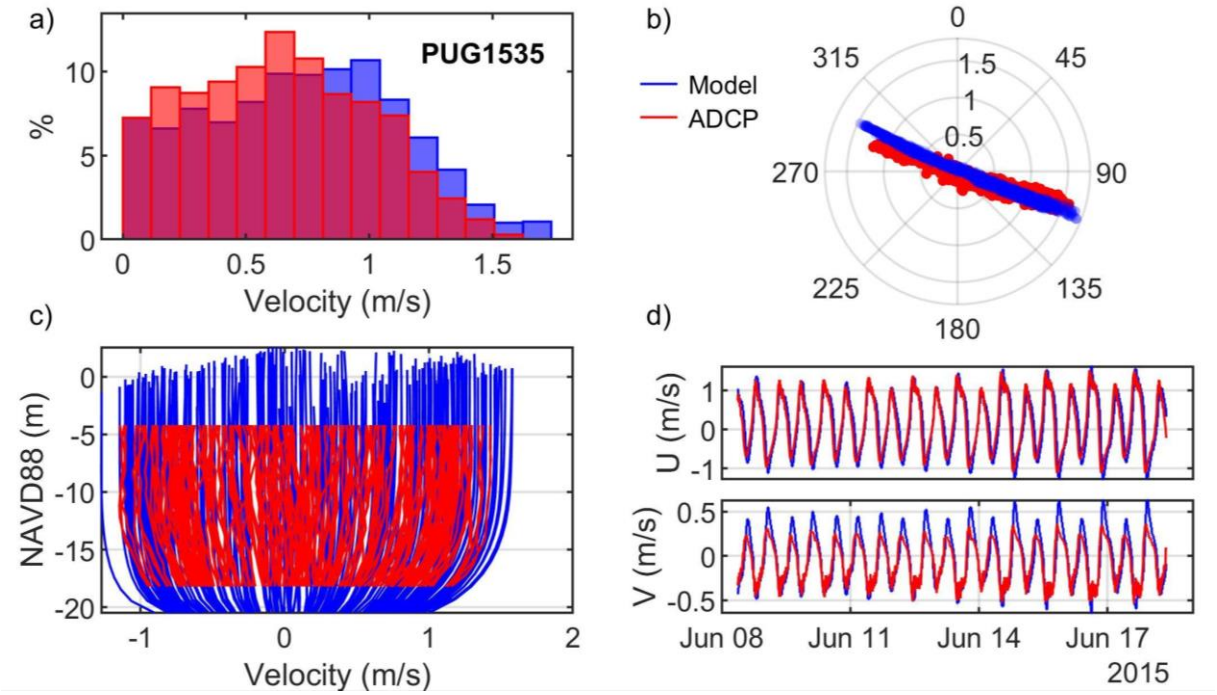

Figure A.35. Comparisons of simulated and observed velocities at Balch Passage (PUG1535): (a) velocity histograms, (b) scatter plot, (c) vertical profiles, and (d) time series of depth-averaged principal velocities.

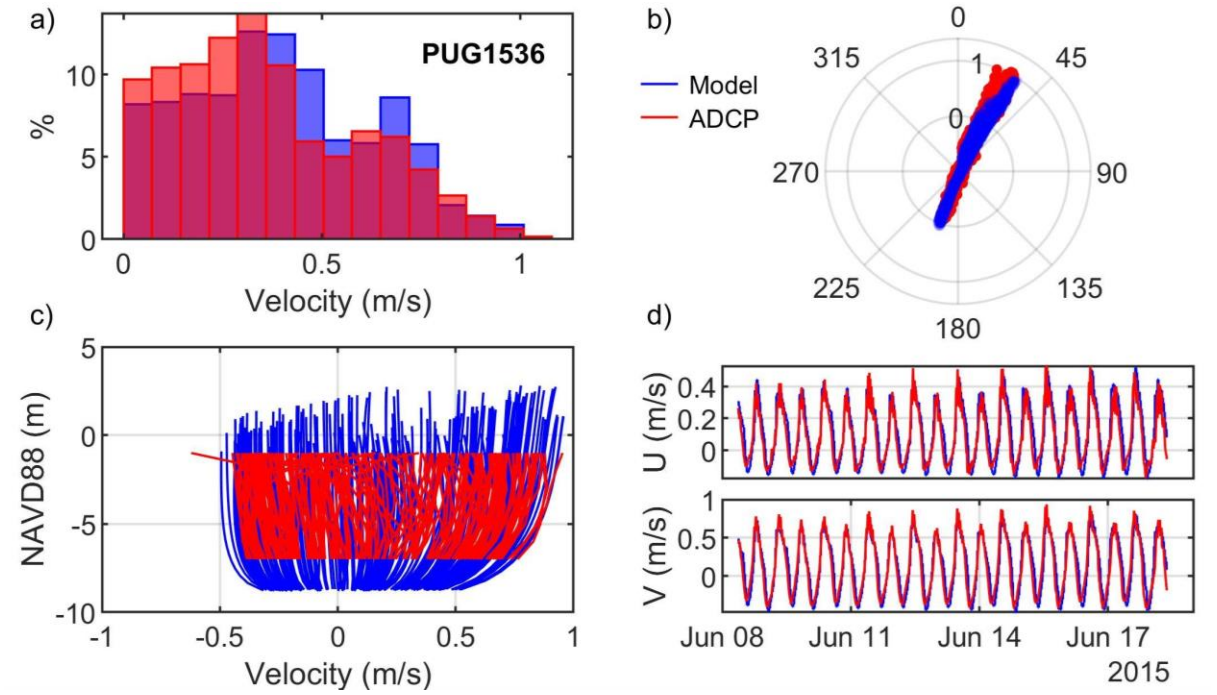

Figure A.36. Comparisons of simulated and observed velocities at Pitt Passage (PUG1536): (a) velocity histograms, (b) scatter plot, (c) vertical profiles, and (d) time series of depth-averaged principal velocities.

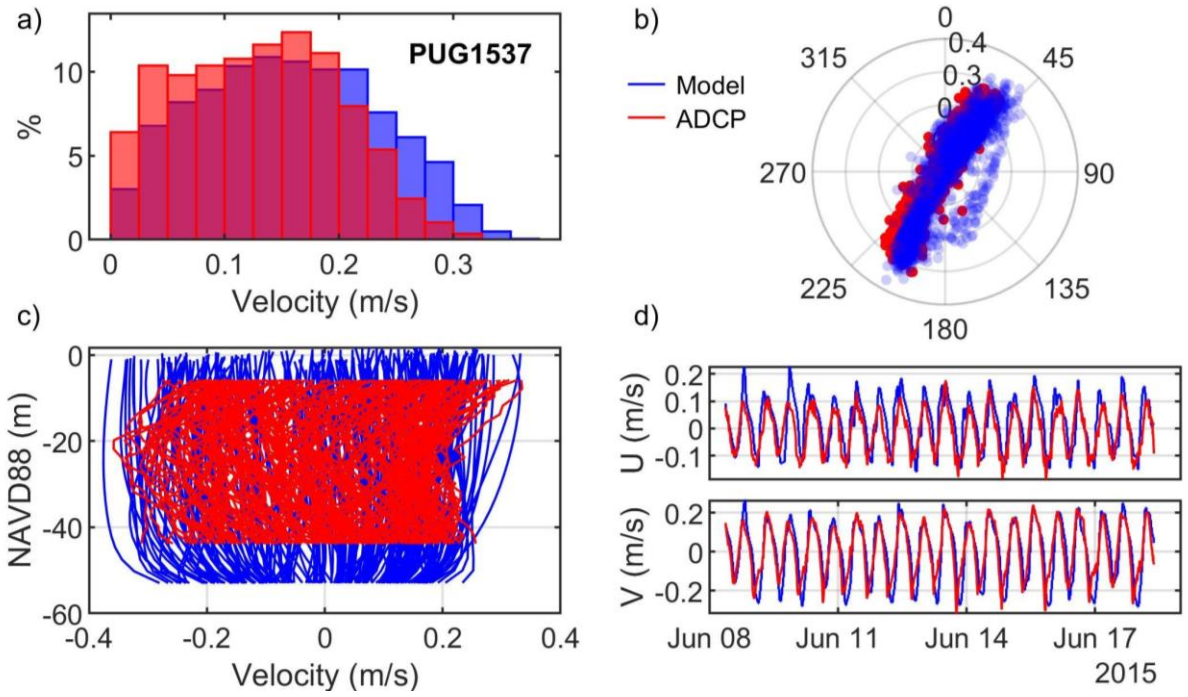

Figure A.37. Comparisons of simulated and observed velocities at Drayton Passage (PUG1537): (a) velocity histograms, (b) scatter plot, (c) vertical profiles, and (d) time series of depth-averaged principal velocities.

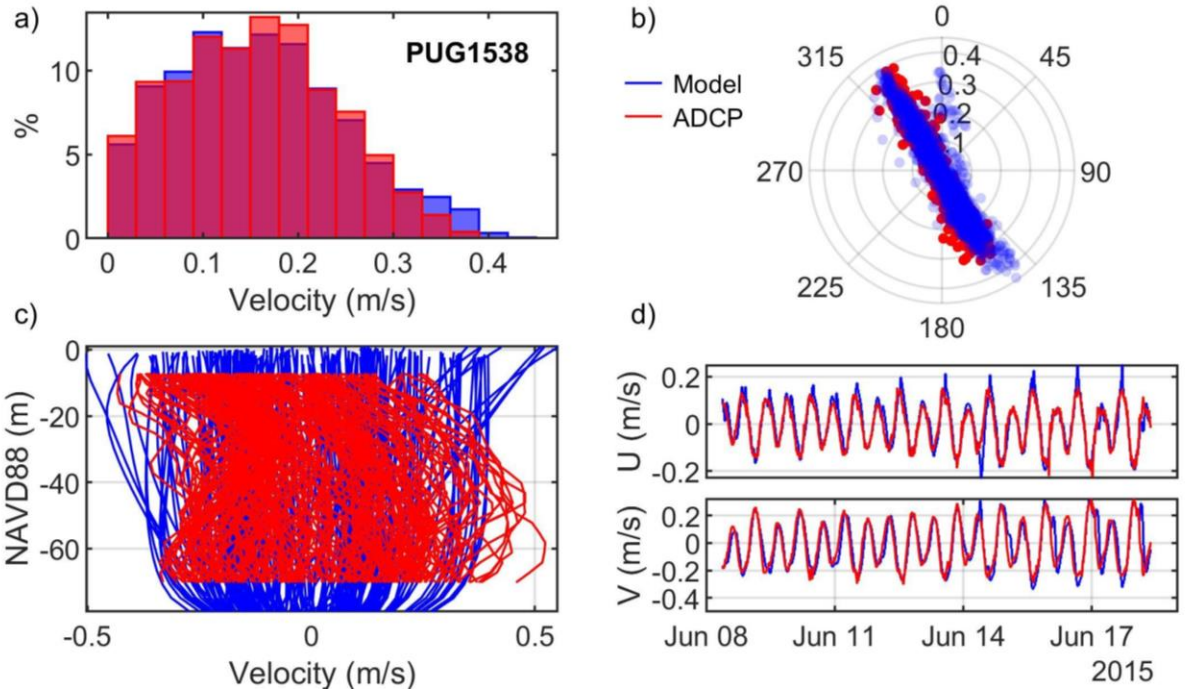

Figure A.38. Comparisons of simulated and observed velocities at Devil's Head (PUG1538): (a) velocity histograms, (b) scatter plot, (c) vertical profiles, and (d) time series of depth-averaged principal velocities.

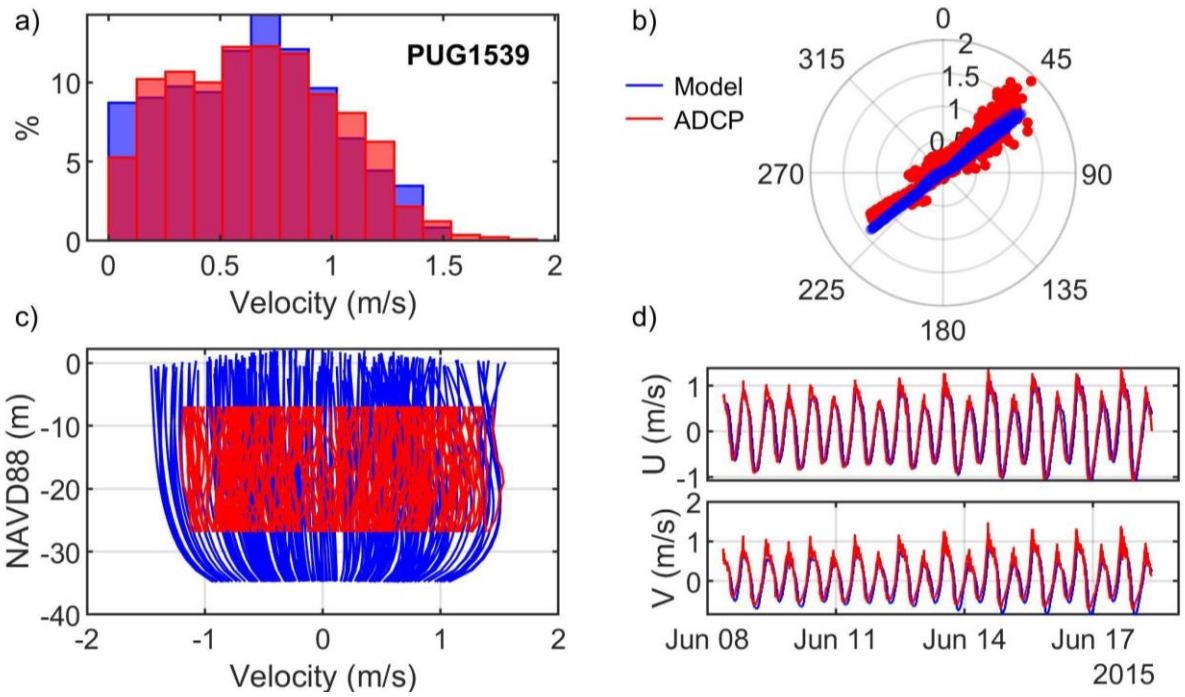

Figure A.39. Comparisons of simulated and observed velocities at Dana Passage (PUG1539): (a) velocity histograms, (b) scatter plot, (c) vertical profiles, and (d) time series of depth-averaged principal velocities.

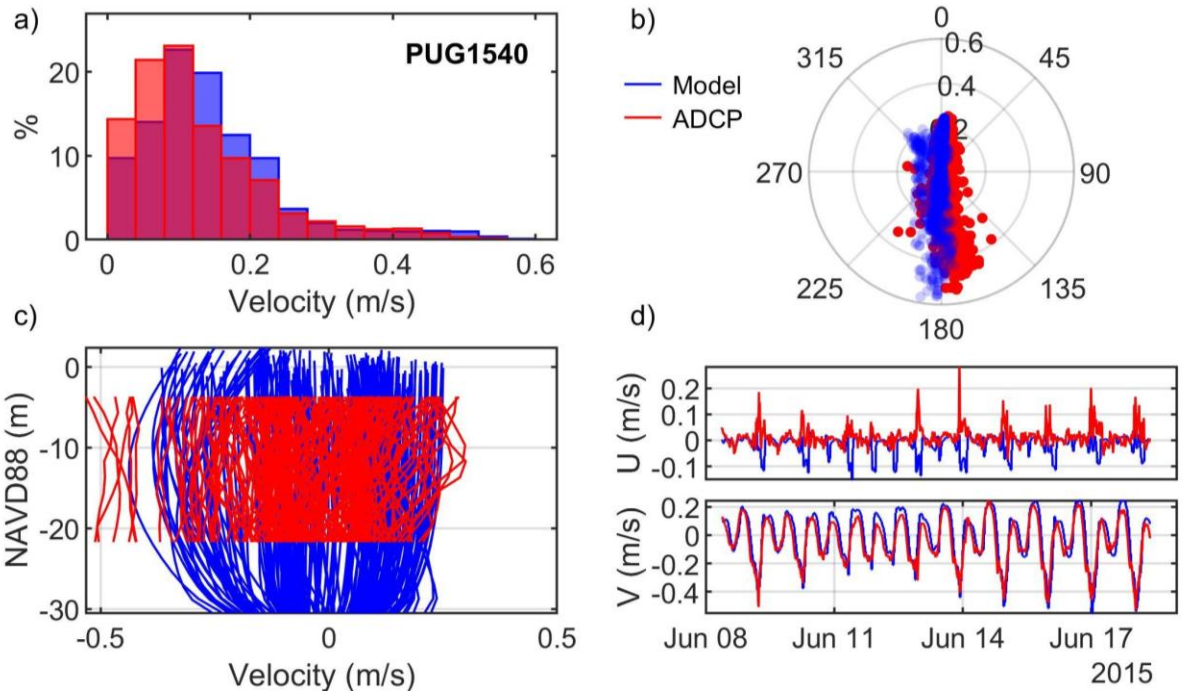

Figure A.40. Comparisons of simulated and observed velocities at Budd Inlet (PUG1540): (a) velocity histograms, (b) scatter plot, (c) vertical profiles, and (d) time series of depth-averaged principal velocities.

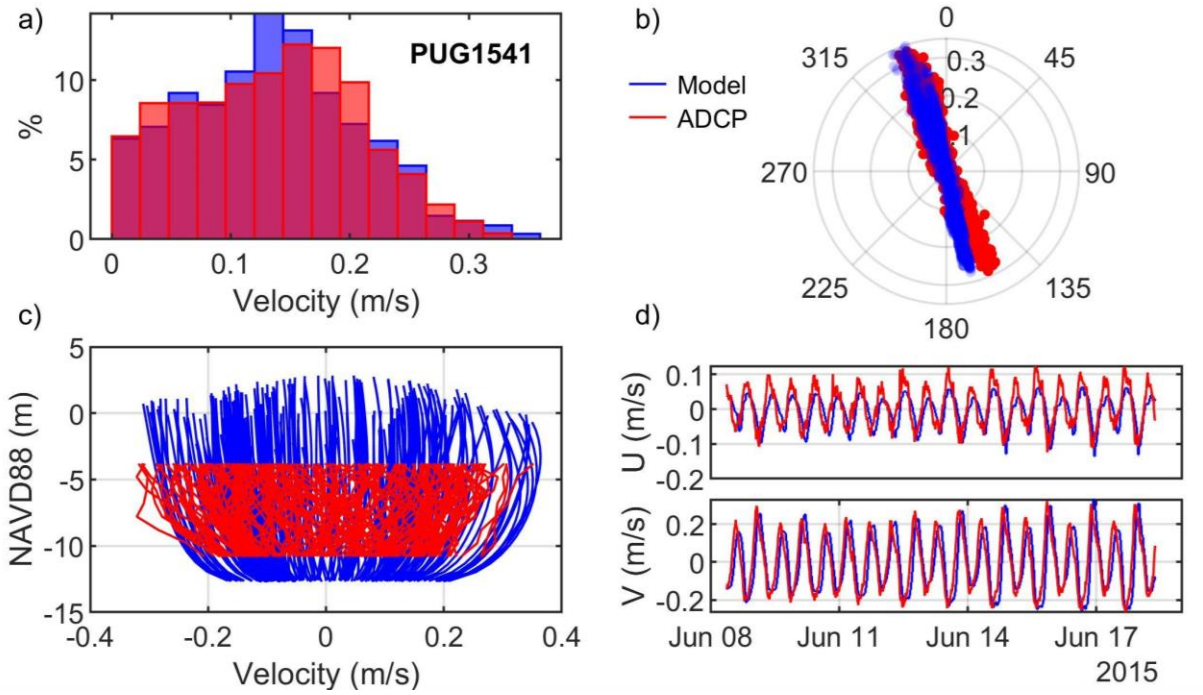

Figure A.41. Comparisons of simulated and observed velocities at Peal Passage (PUG1541): (a) velocity histograms, (b) scatter plot, (c) vertical profiles, and (d) time series of depth-averaged principal velocities.

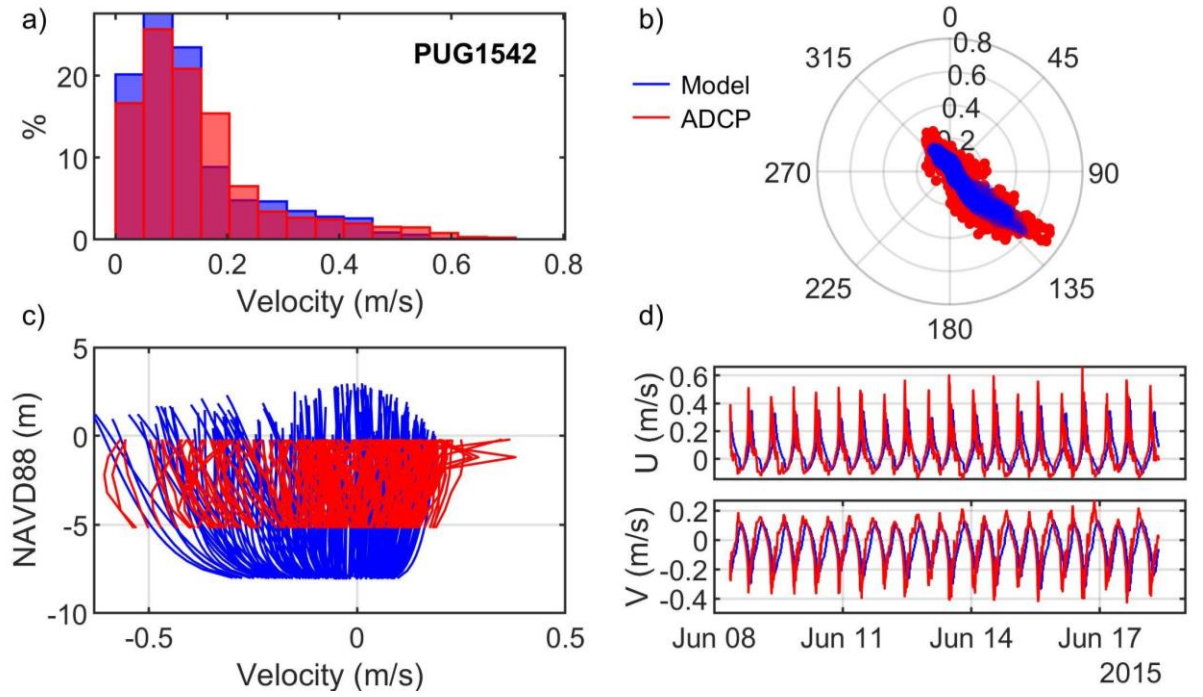

Figure A.42. Comparisons of simulated and observed velocities at Peal Passage (PUG1542): (a) velocity histograms, (b) scatter plot, (c) vertical profiles, and (d) time series of depth-averaged principal velocities.

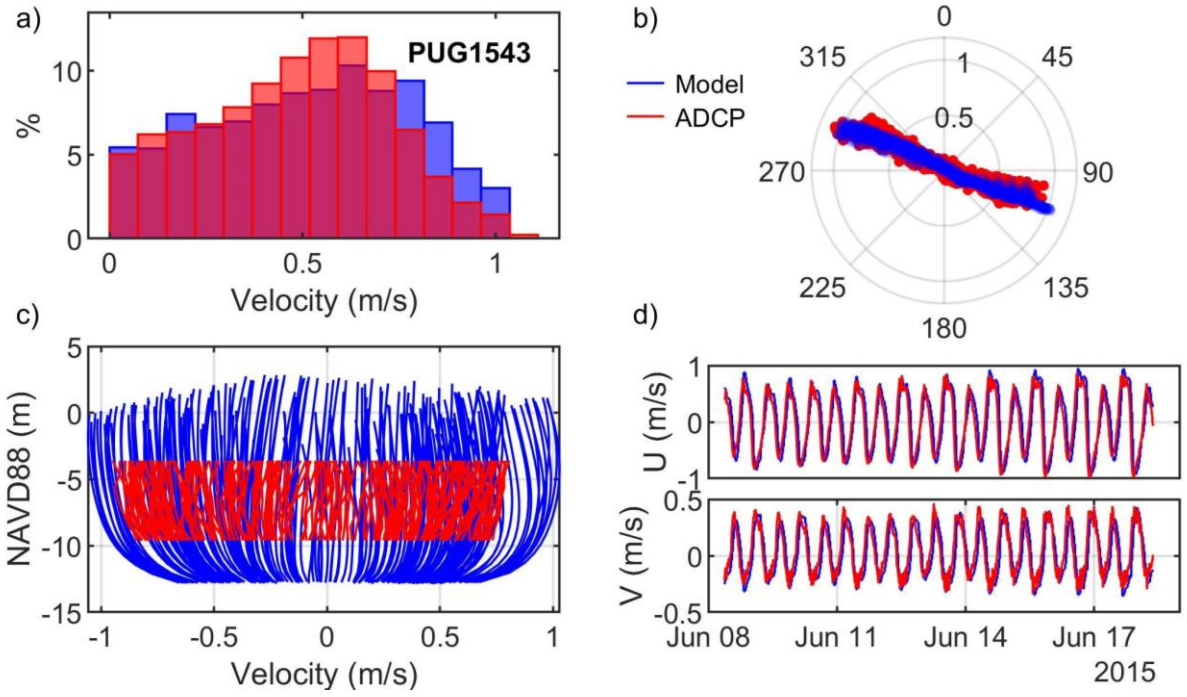

Figure A.43. Comparisons of simulated and observed velocities at Squaxin Passage (PUG1543): (a) velocity histograms, (b) scatter plot, (c) vertical profiles, and (d) time series of depth-averaged principal velocities.

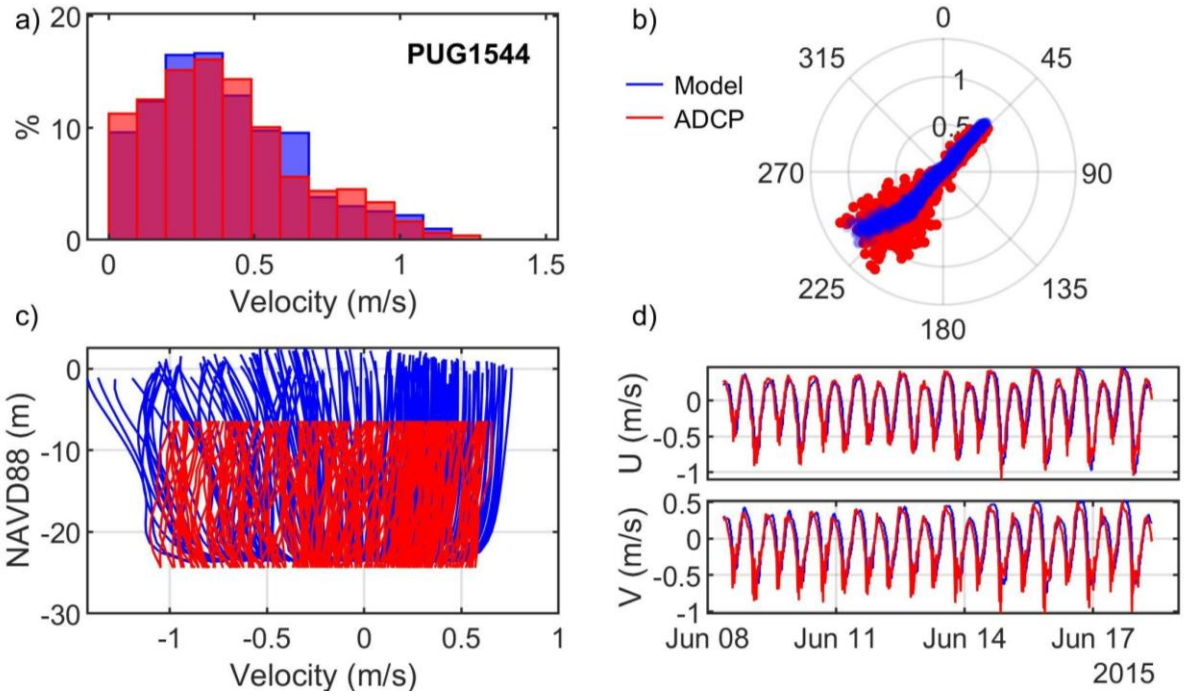

Figure A.44. Comparisons of simulated and observed velocities at Totten Inlet (PUG1544): (a) velocity histograms, (b) scatter plot, (c) vertical profiles, and (d) time series of depth-averaged principal velocities.

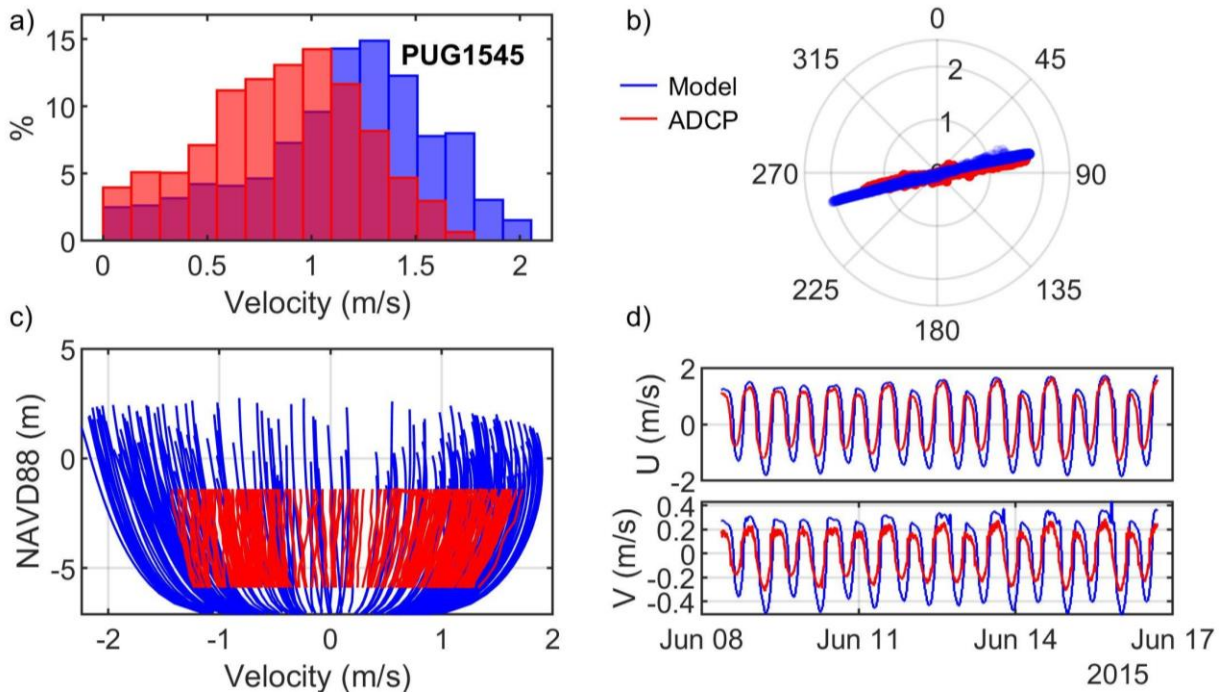

Figure A.45. Comparisons of simulated and observed velocities at Libby Point (PUG1545): (a) velocity histograms, (b) scatter plot, (c) vertical profiles, and (d) time series of depth-averaged principal velocities.

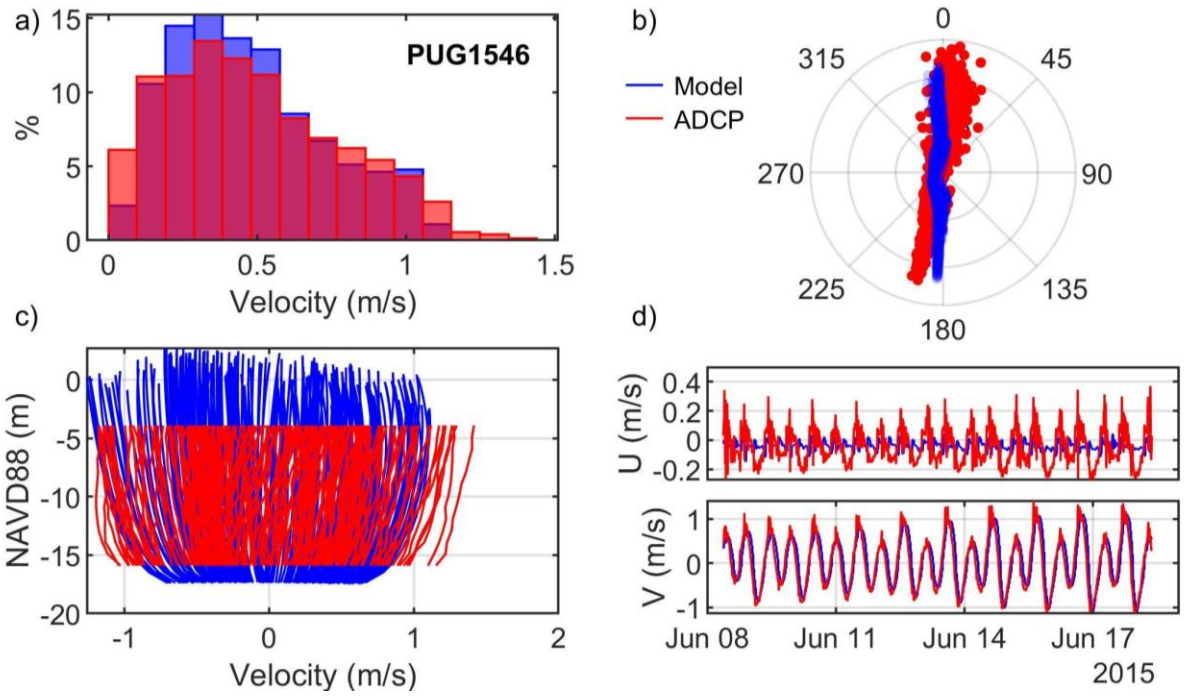

Figure A.46. Comparisons of simulated and observed velocities at Pickering Passage (PUG1546): (a) velocity histograms, (b) scatter plot, (c) vertical profiles, and (d) time series of depth-averaged principal velocities.

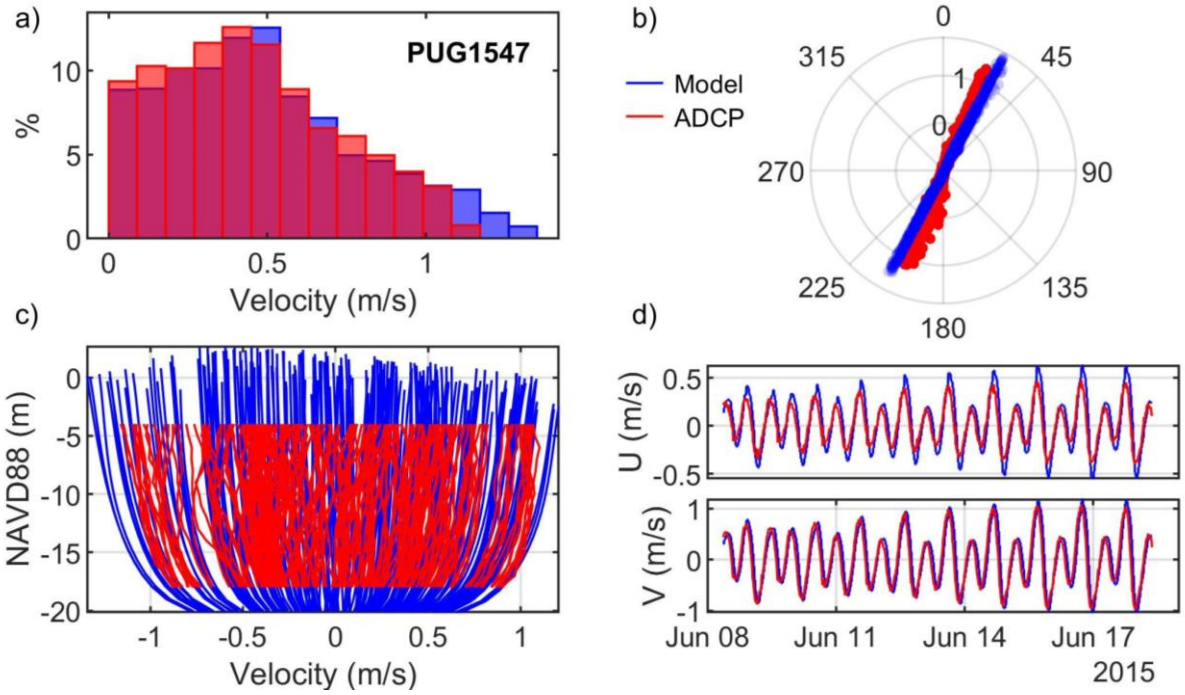

Figure A.47. Comparisons of simulated and observed velocities at Pickering Passage (PUG1547): (a) velocity histograms, (b) scatter plot, (c) vertical profiles, and (d) time series of depth-averaged principal velocities.

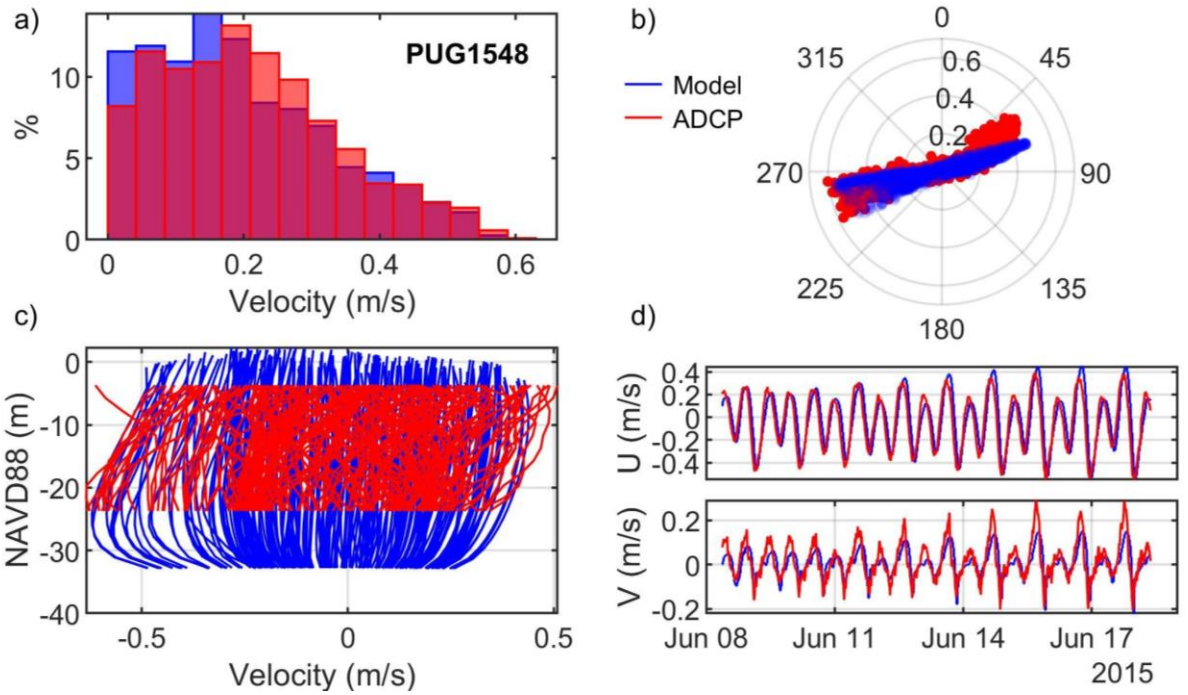

Figure A.48. Comparisons of simulated and observed velocities at Pickering Passage (PUG1548): (a) velocity histograms, (b) scatter plot, (c) vertical profiles, and (d) time series of depth-averaged principal velocities.

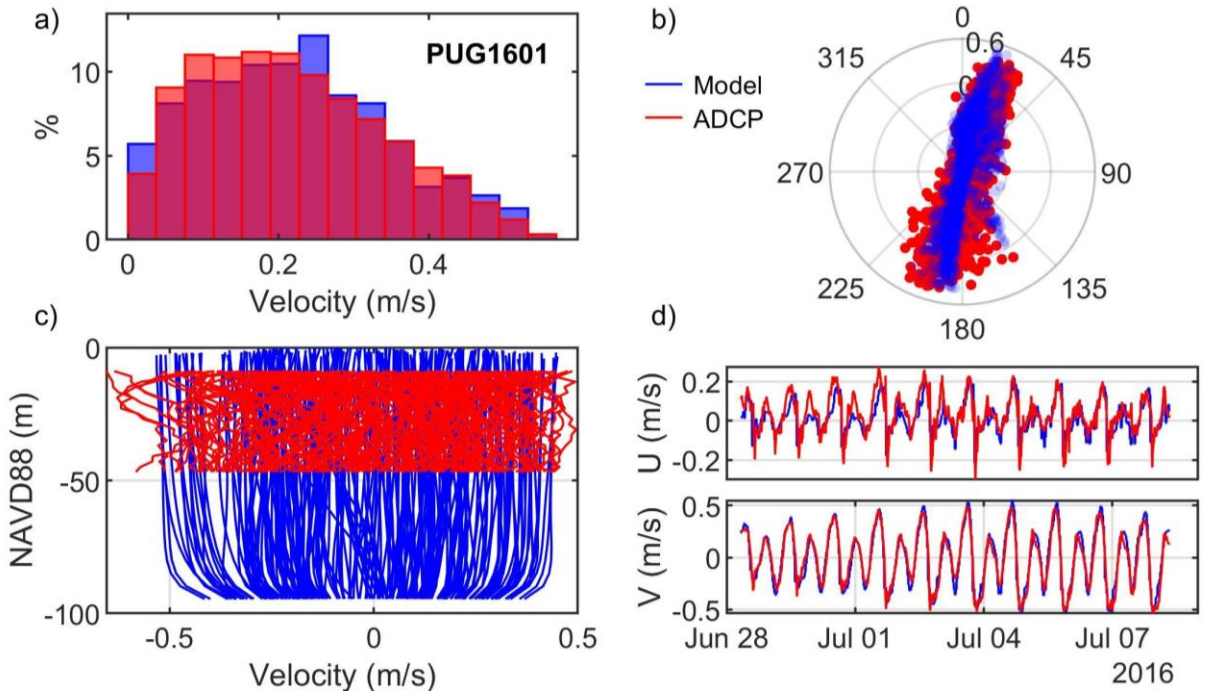

Figure A.49. Comparisons of simulated and observed velocities at Hazel Point (PUG1601): (a) velocity histograms, (b) scatter plot, (c) vertical profiles, and (d) time series of depth-averaged principal velocities.

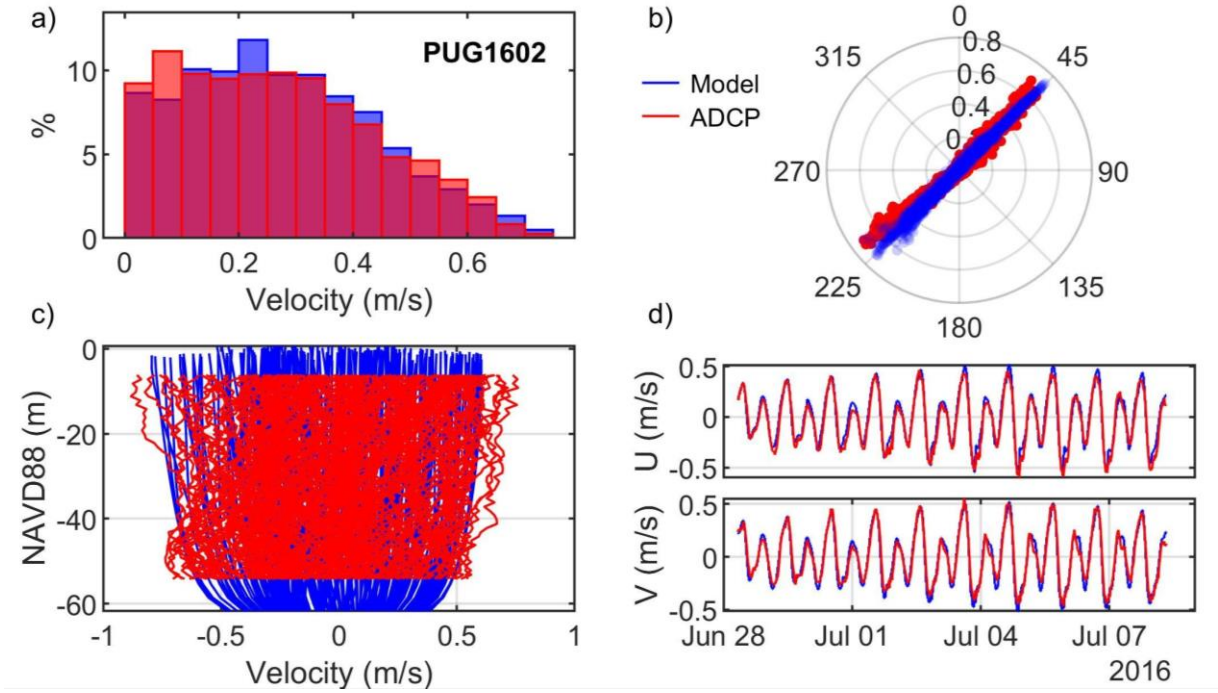

Figure A.50. Comparisons of simulated and observed velocities at South Point (PUG1602): (a) velocity histograms, (b) scatter plot, (c) vertical profiles, and (d) time series of depth-averaged principal velocities.

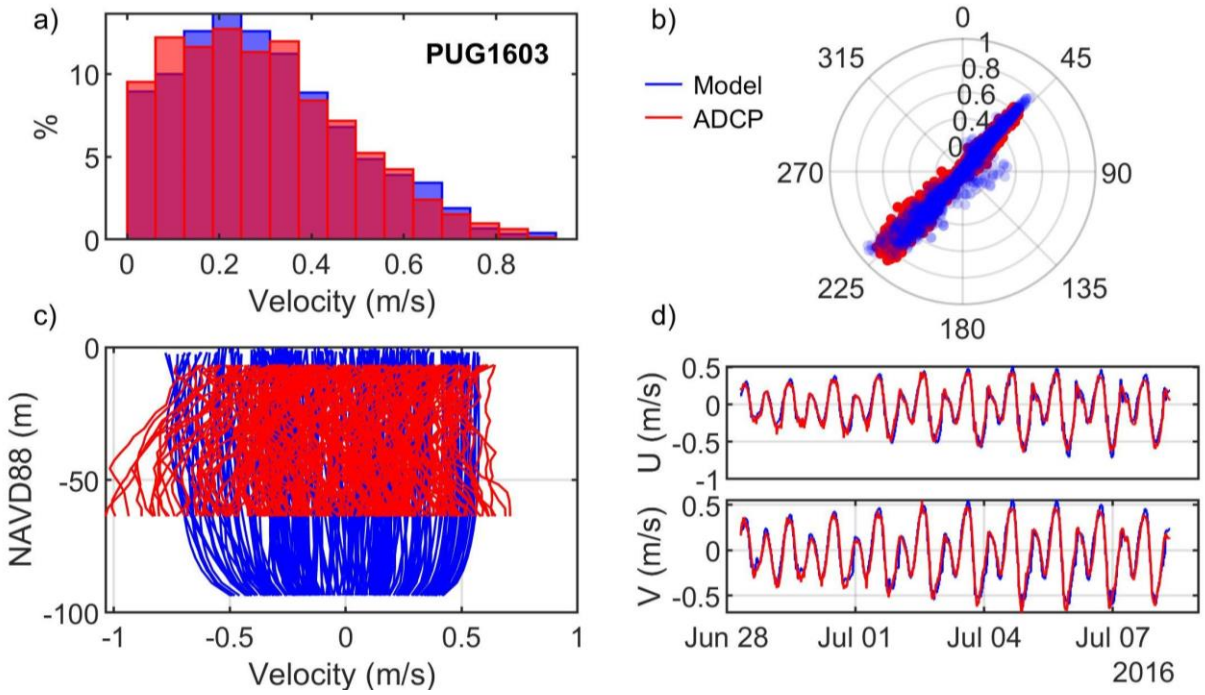

Figure A.51. Comparisons of simulated and observed velocities at Hood Canal Bridge (PUG1603): (a) velocity histograms, (b) scatter plot, (c) vertical profiles, and (d) time series of depth-averaged principal velocities.

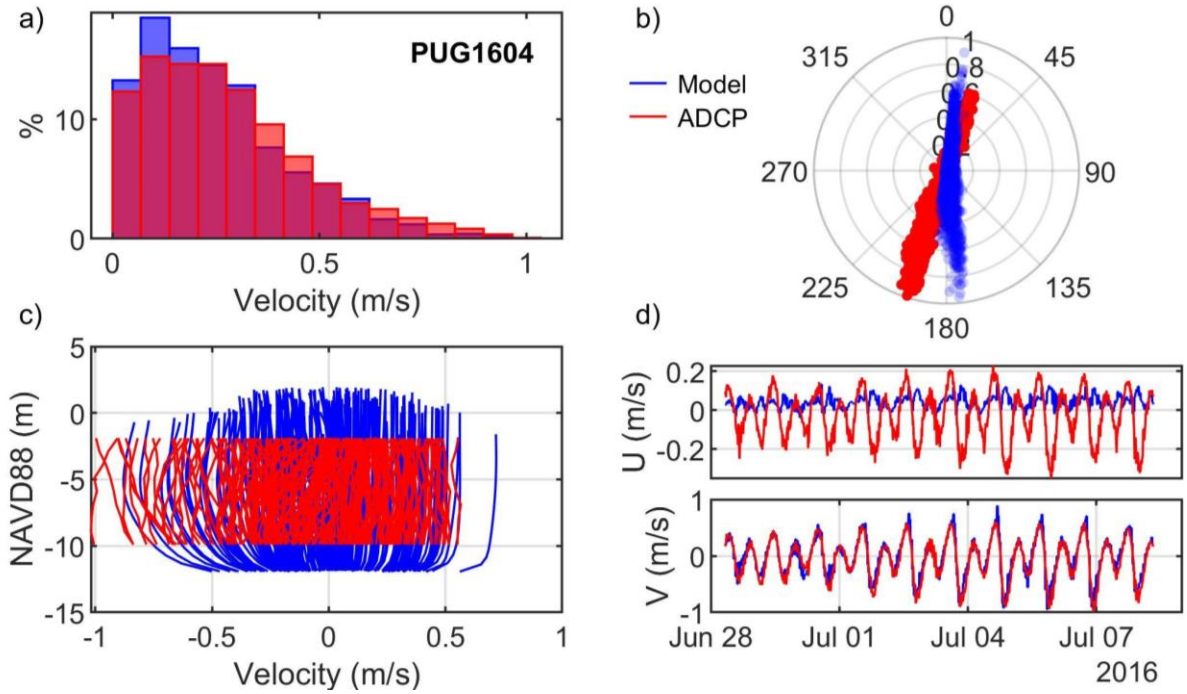

Figure A.52. Comparisons of simulated and observed velocities at Port Gamble (PUG1604): (a) velocity histograms, (b) scatter plot, (c) vertical profiles, and (d) time series of depth-averaged principal velocities.

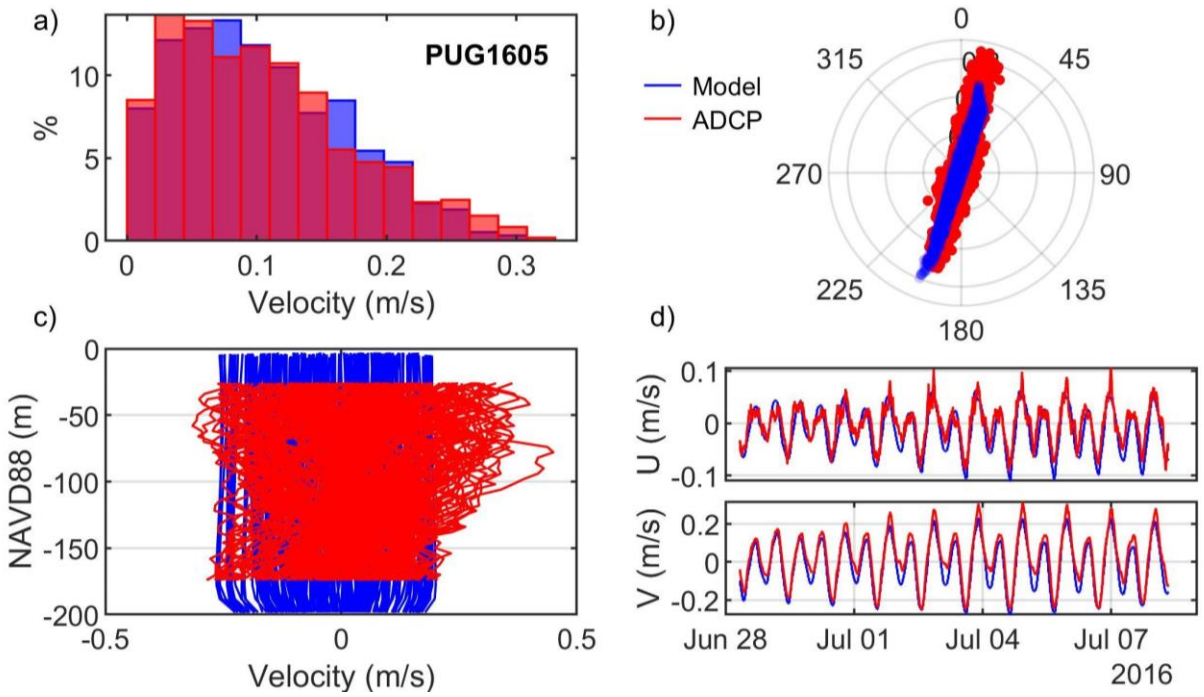

Figure A.53. Comparisons of simulated and observed velocities at Possession Sound (PUG1605): (a) velocity histograms, (b) scatter plot, (c) vertical profiles, and (d) time series of depth-averaged principal velocities.

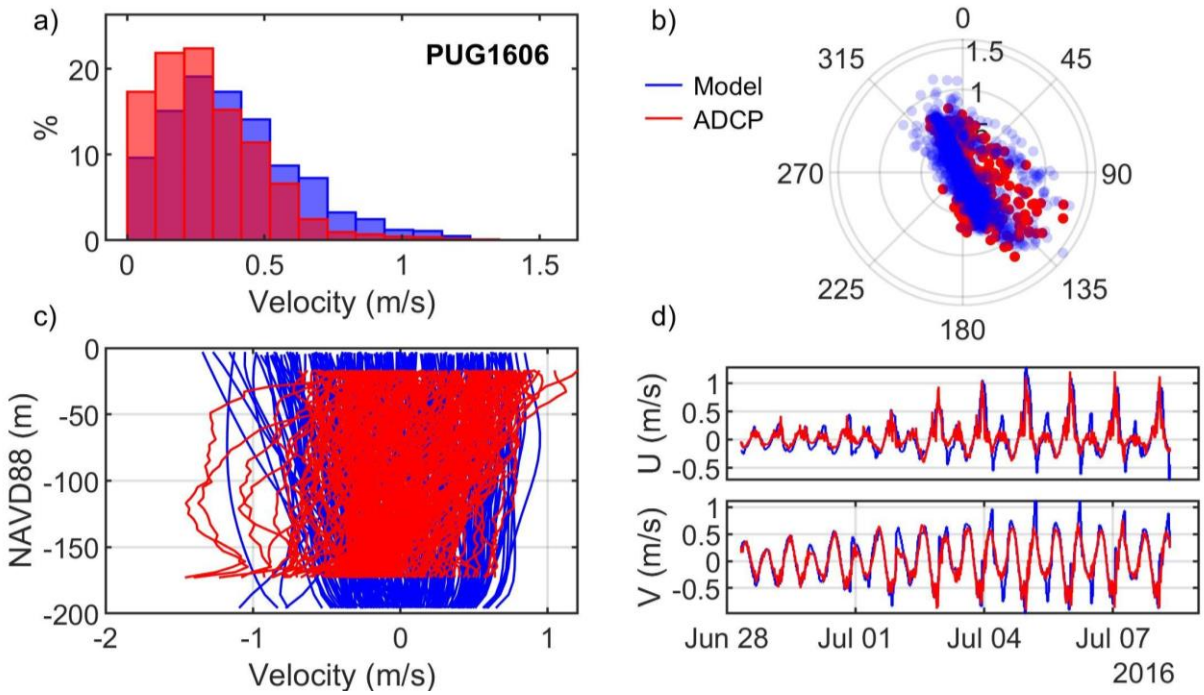

Figure A.54. Comparisons of simulated and observed velocities at Point No Point (PUG1606): (a) velocity histograms, (b) scatter plot, (c) vertical profiles, and (d) time series of depth-averaged principal velocities.

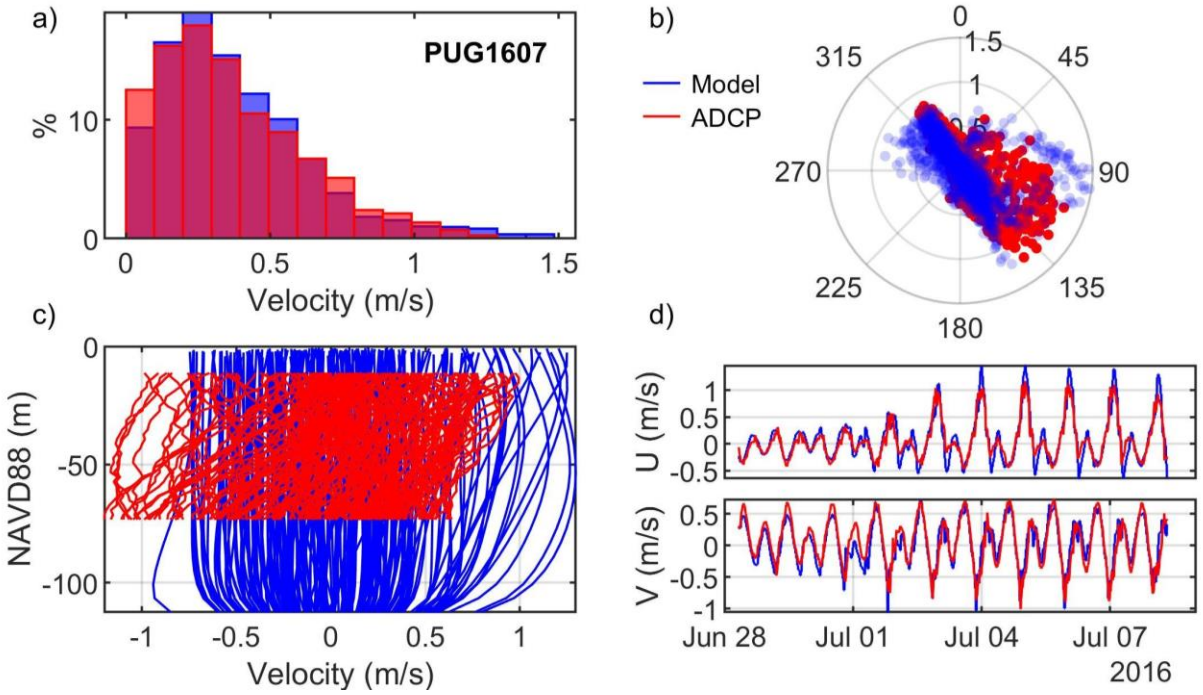

Figure A.55. Comparisons of simulated and observed velocities at Point No Point (PUG1607): (a) velocity histograms, (b) scatter plot, (c) vertical profiles, and (d) time series of depth-averaged principal velocities.

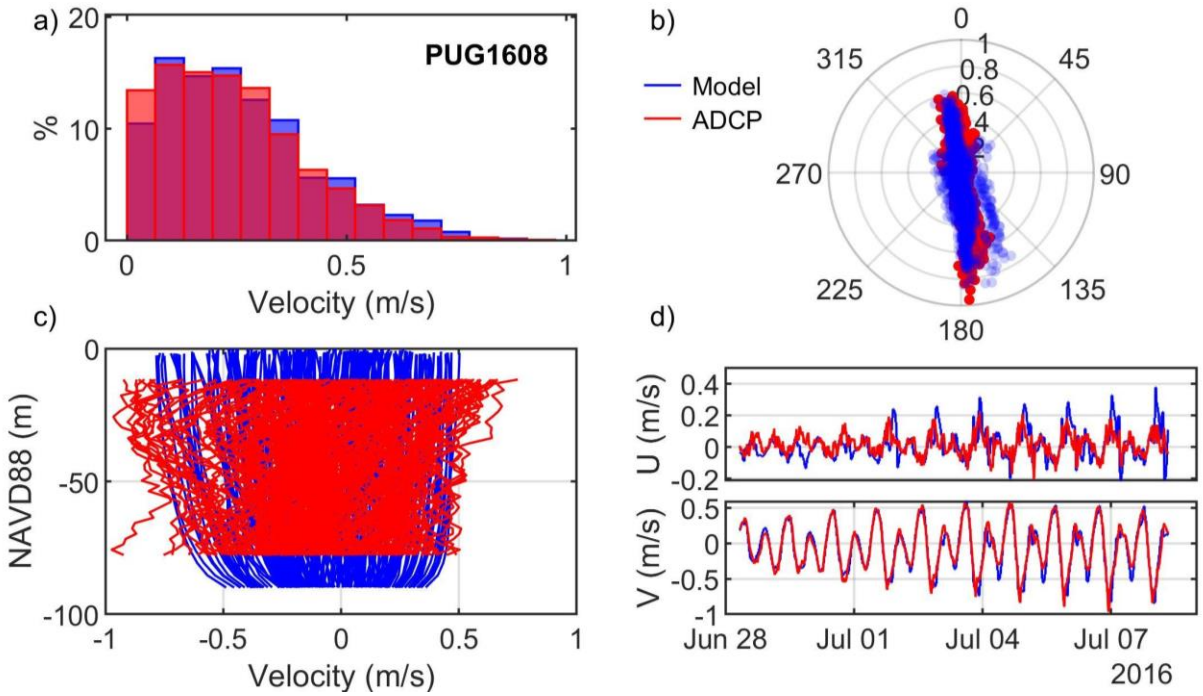

Figure A.56. Comparisons of simulated and observed velocities at Hood Canal (PUG1608): (a) velocity histograms, (b) scatter plot, (c) vertical profiles, and (d) time series of depth-averaged principal velocities.

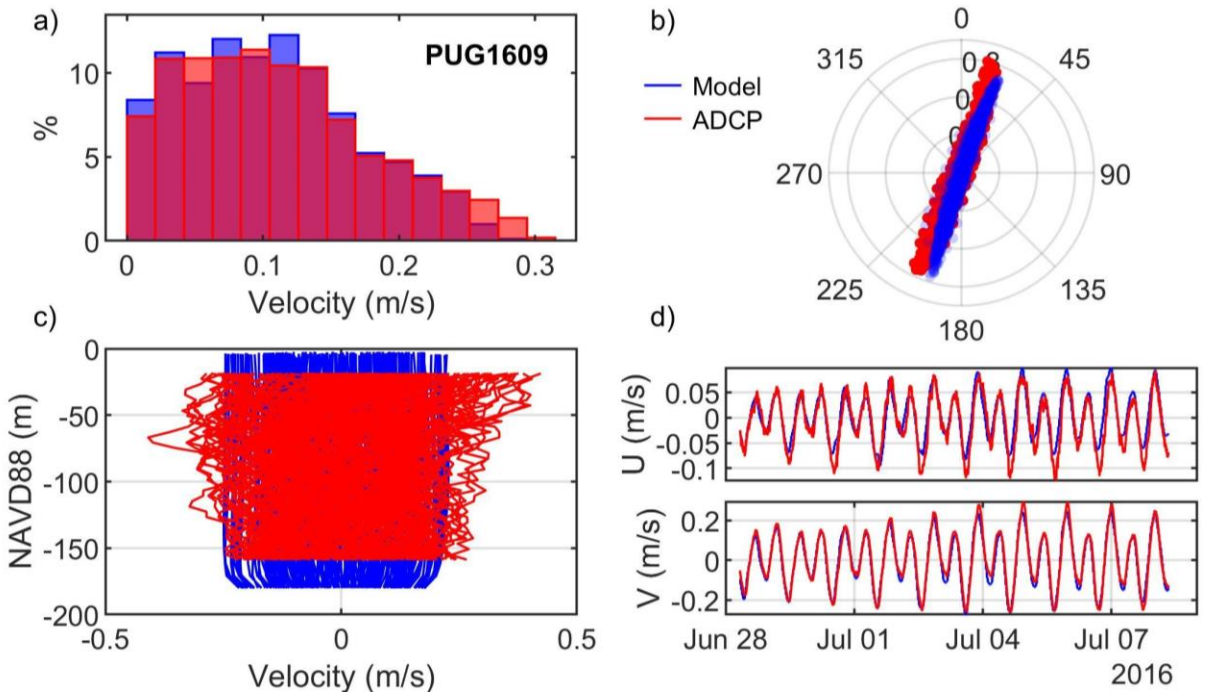

Figure A.57. Comparisons of simulated and observed velocities at Mukilteo (PUG1609): (a) velocity histograms, (b) scatter plot, (c) vertical profiles, and (d) time series of depth-averaged principal velocities.

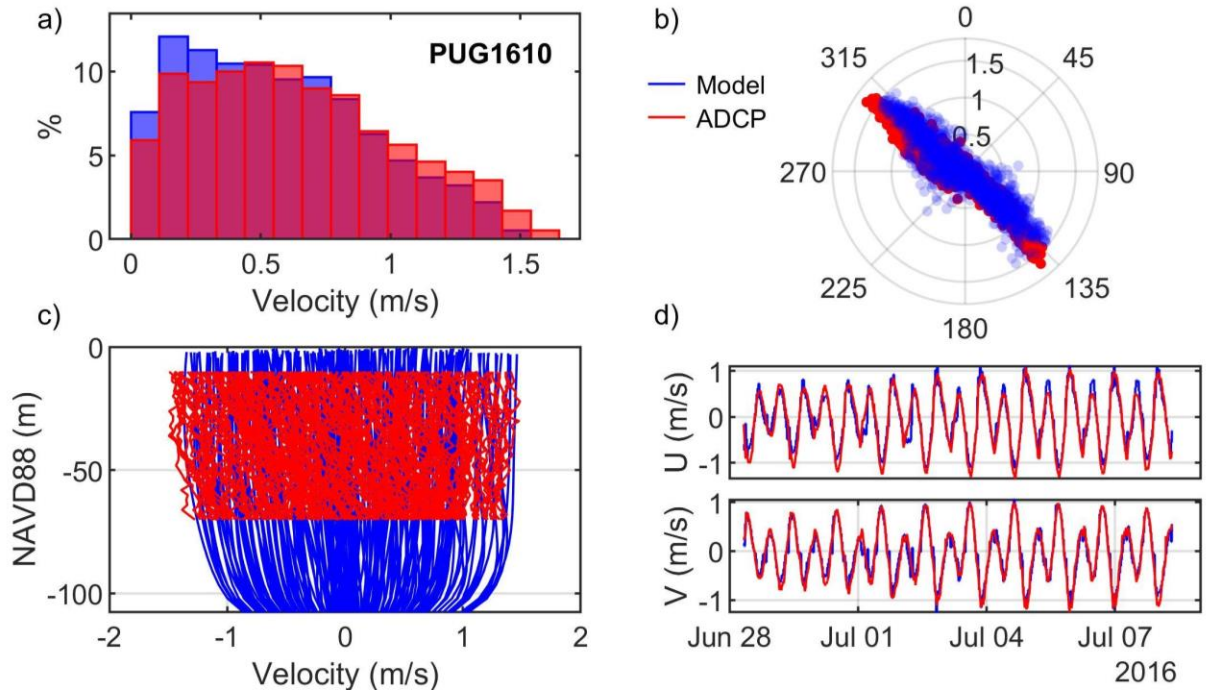

Figure A.58. Comparisons of simulated and observed velocities at Foulweather Bluff (PUG1610): (a) velocity histograms, (b) scatter plot, (c) vertical profiles, and (d) time series of depth-averaged principal velocities.

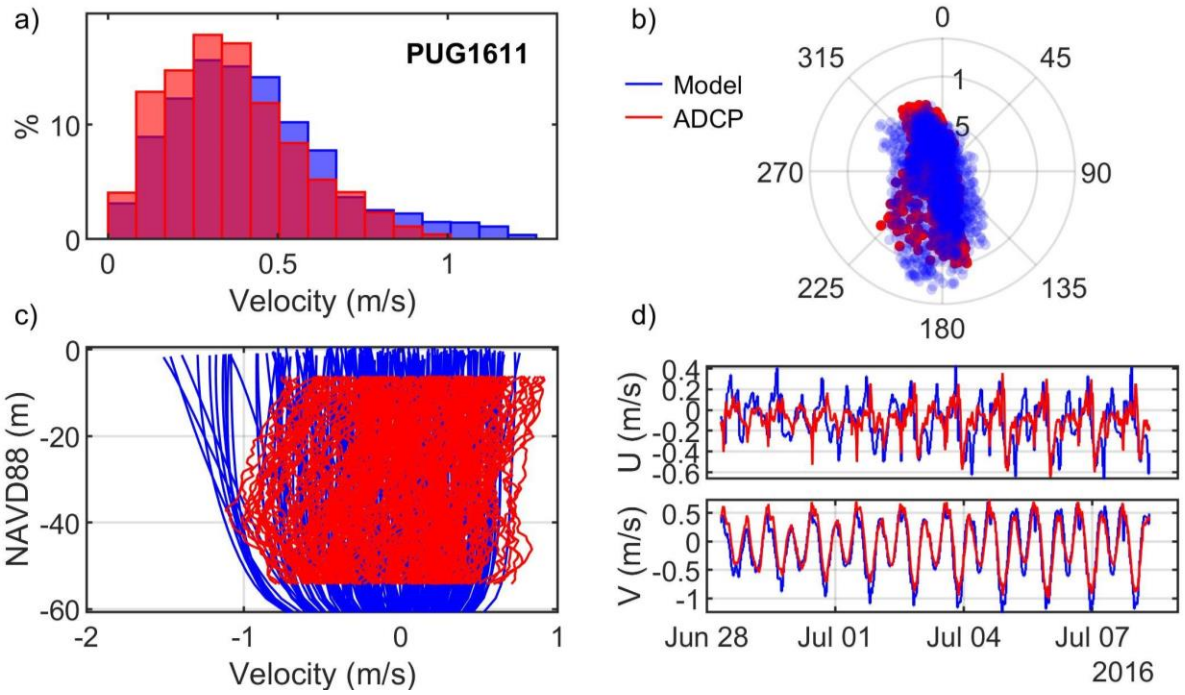

Figure A.59. Comparisons of simulated and observed velocities at Olele Point (PUG1611): (a) velocity histograms, (b) scatter plot, (c) vertical profiles, and (d) time series of depth-averaged principal velocities.

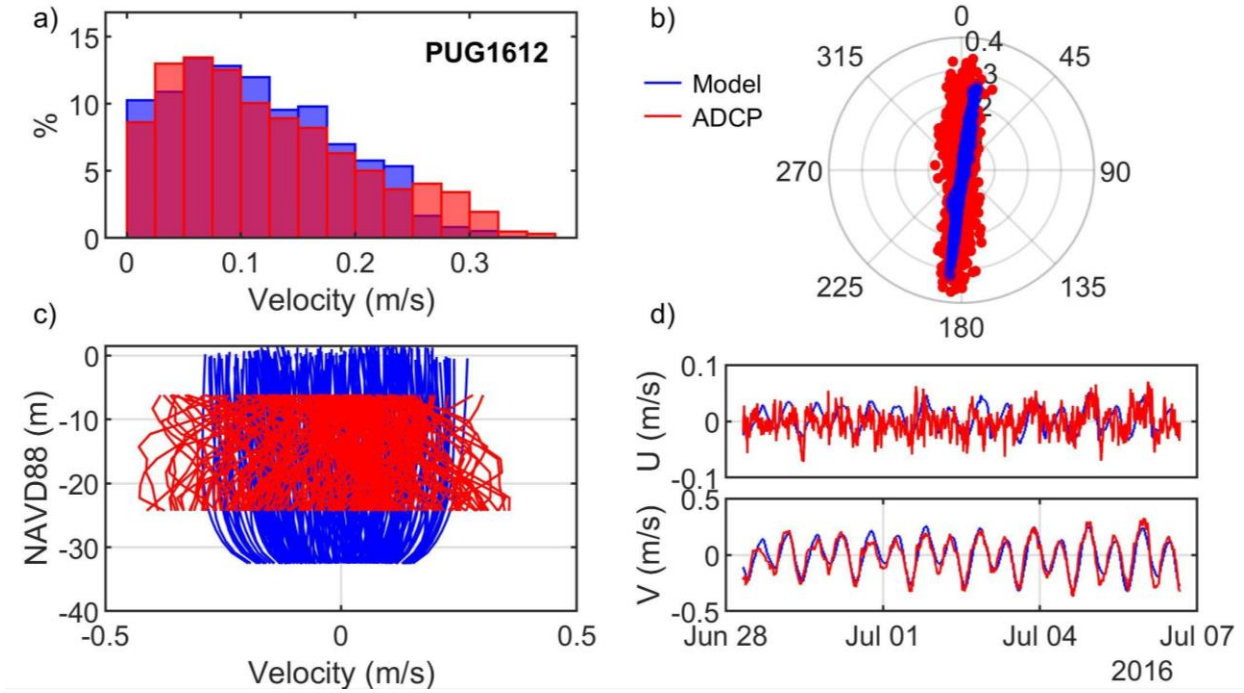

Figure A.60. Comparisons of simulated and observed velocities at Clinton (PUG1612): (a) velocity histograms, (b) scatter plot, (c) vertical profiles, and (d) time series of depth-averaged principal velocities.

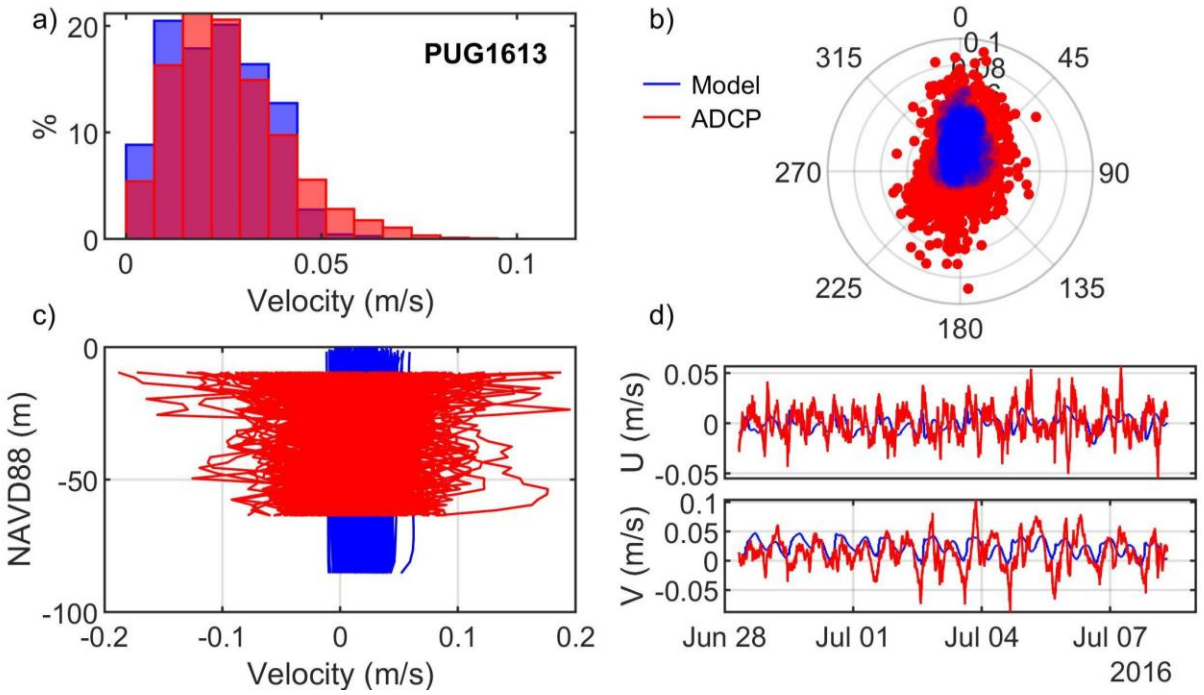

Figure A.61. Comparisons of simulated and observed velocities at Everett (PUG1613): (a) velocity histograms, (b) scatter plot, (c) vertical profiles, and (d) time series of depth-averaged principal velocities.

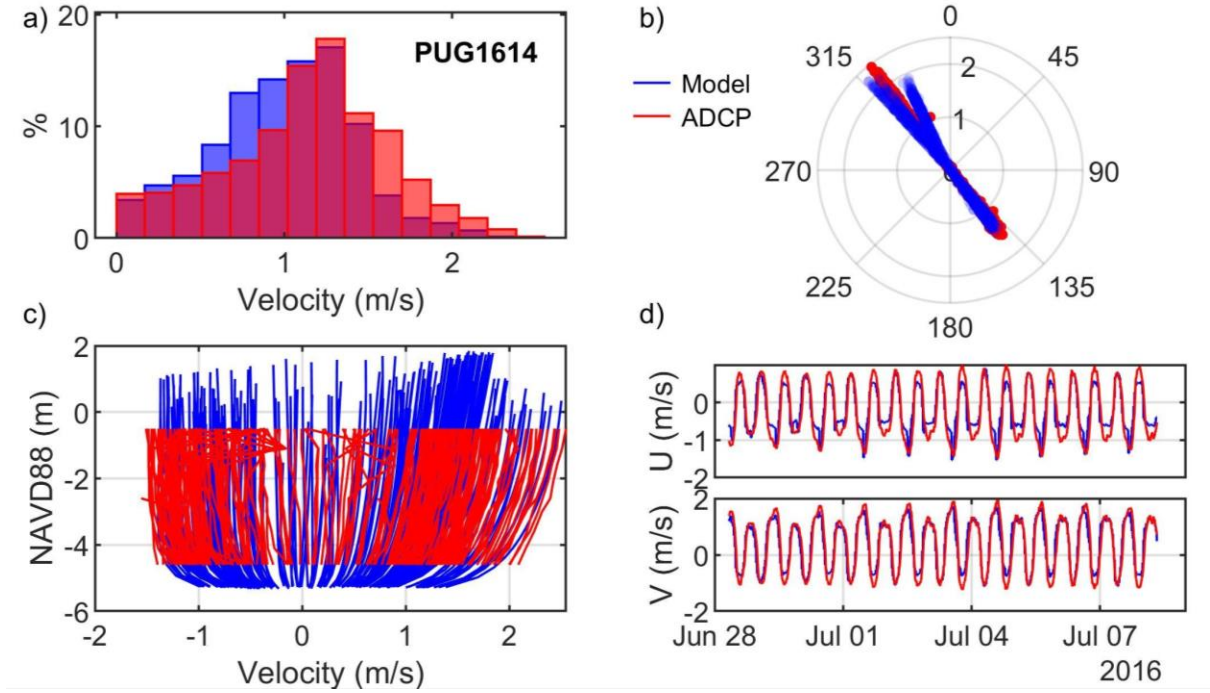

Figure A.62. Comparisons of simulated and observed velocities at Port Townsend (PUG1614): (a) velocity histograms, (b) scatter plot, (c) vertical profiles, and (d) time series of depth-averaged principal velocities.

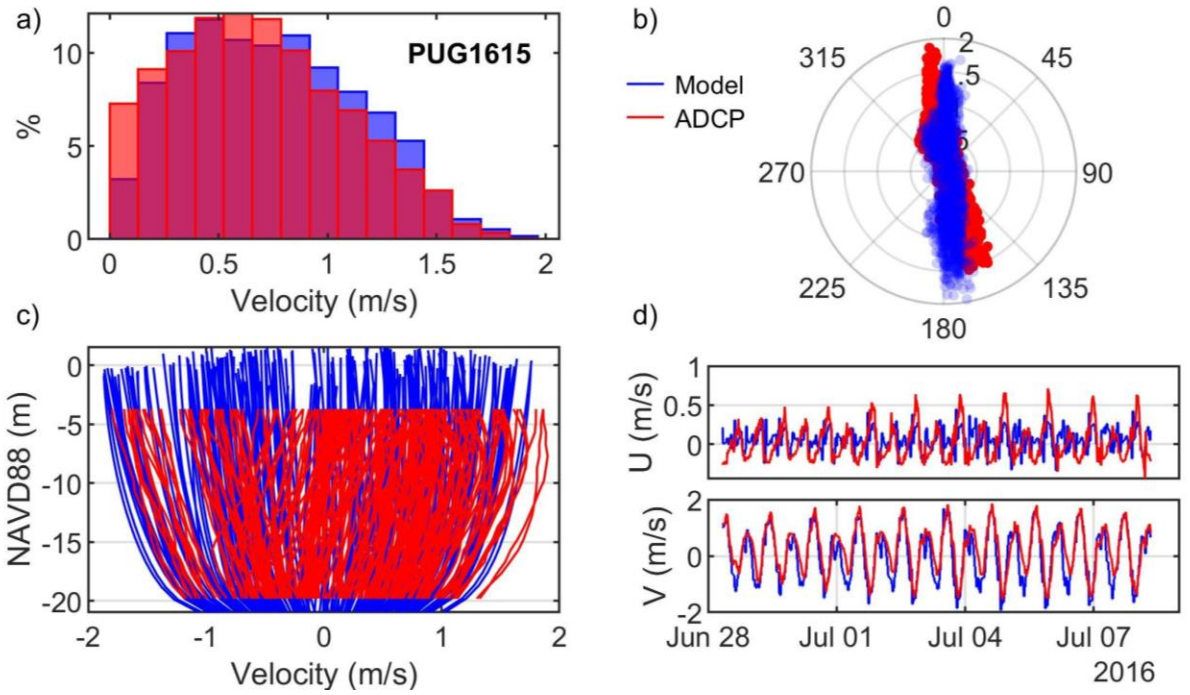

Figure A.63. Comparisons of simulated and observed velocities at Nodule Point (PUG1615): (a) velocity histograms, (b) scatter plot, (c) vertical profiles, and (d) time series of depth-averaged principal velocities.

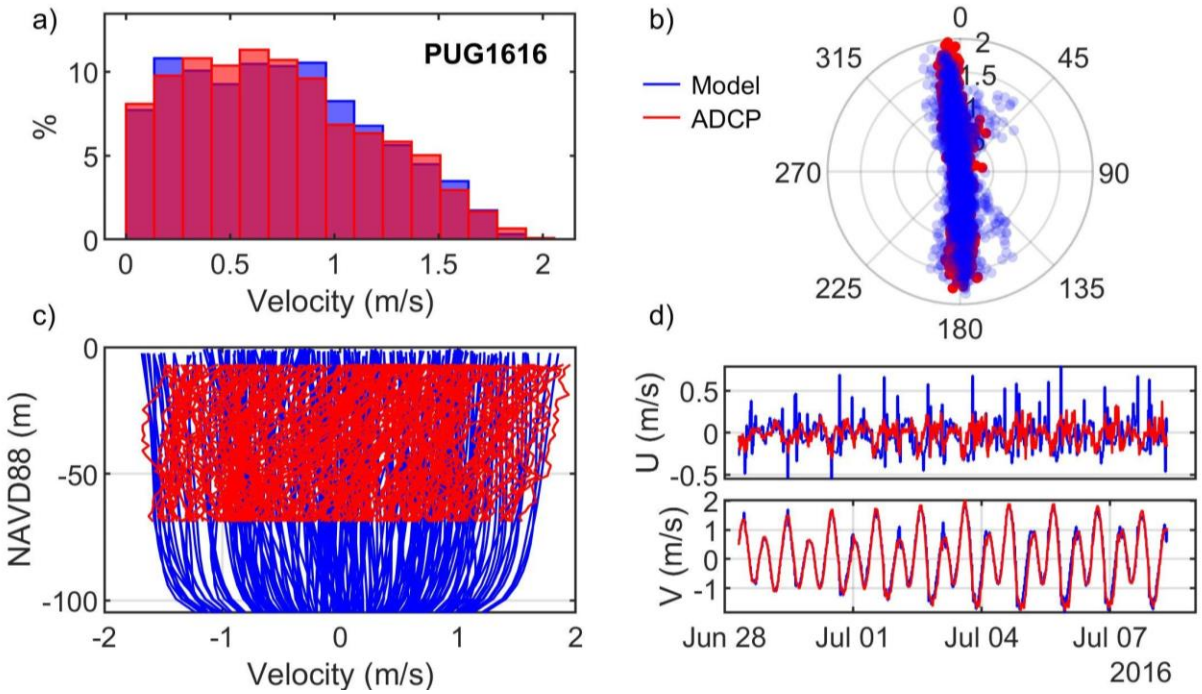

Figure A.64. Comparisons of simulated and observed velocities at Admiralty Inlet (PUG1616): (a) velocity histograms, (b) scatter plot, (c) vertical profiles, and (d) time series of depth-averaged principal velocities.

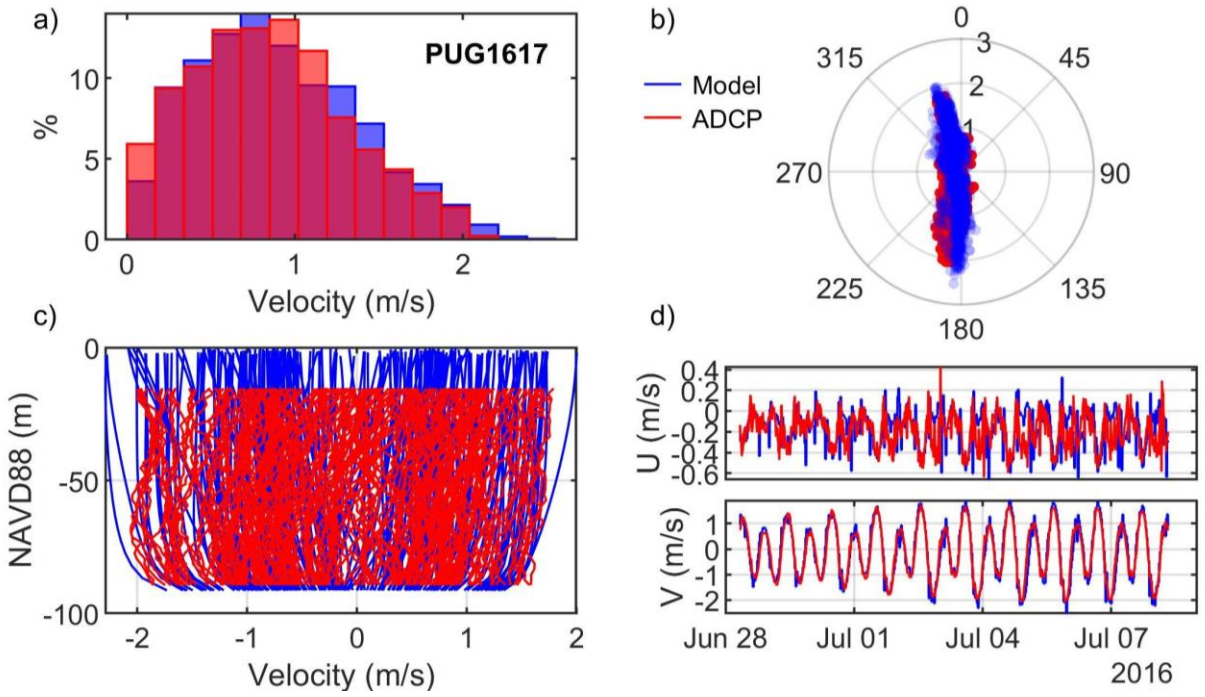

Figure A.65. Comparisons of simulated and observed velocities at Bush Point (PUG1617): (a) velocity histograms, (b) scatter plot, (c) vertical profiles, and (d) time series of depth-averaged principal velocities.

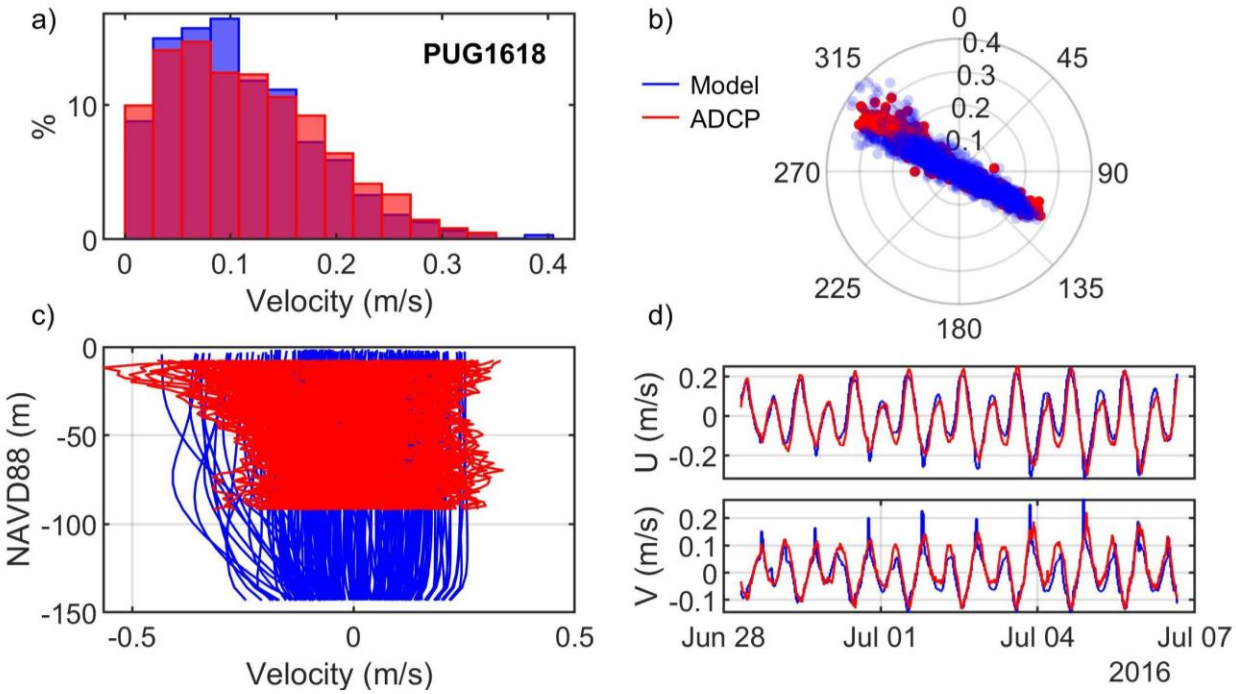

Figure A.66. Comparisons of simulated and observed velocities at Camano Head (PUG1618): (a) velocity histograms, (b) scatter plot, (c) vertical profiles, and (d) time series of depth-averaged principal velocities.

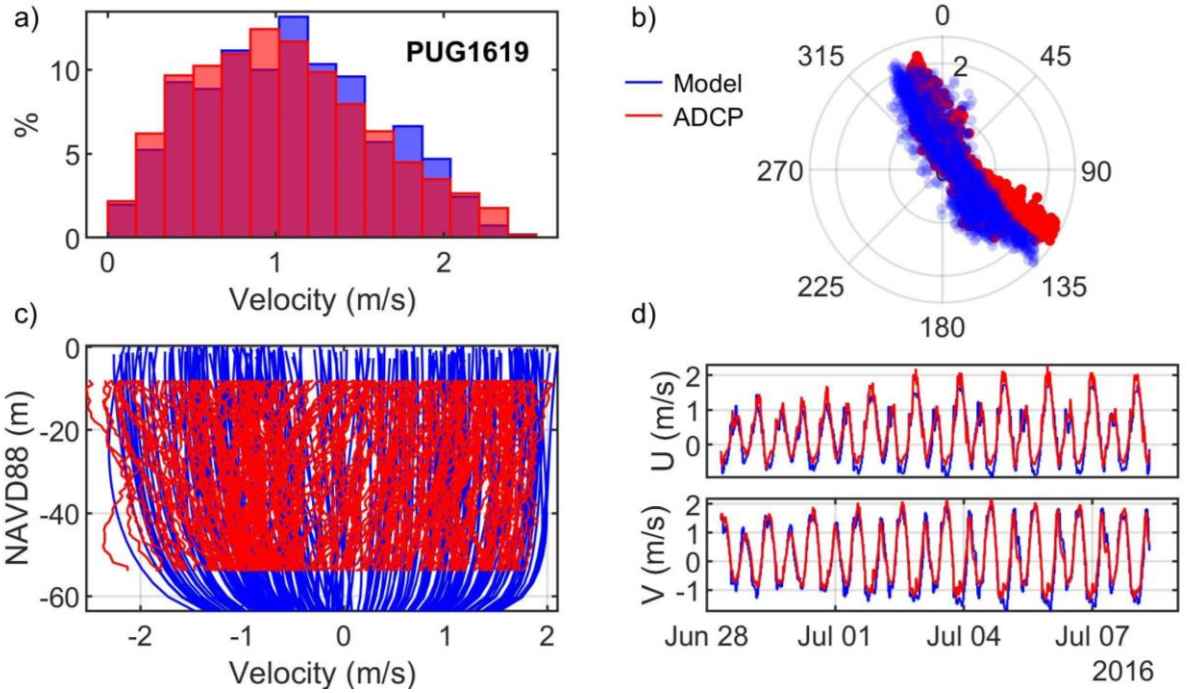

Figure A.67. Comparisons of simulated and observed velocities at Marrowstone Point (PUG1619): (a) velocity histograms, (b) scatter plot, (c) vertical profiles, and (d) time series of depth-averaged principal velocities.

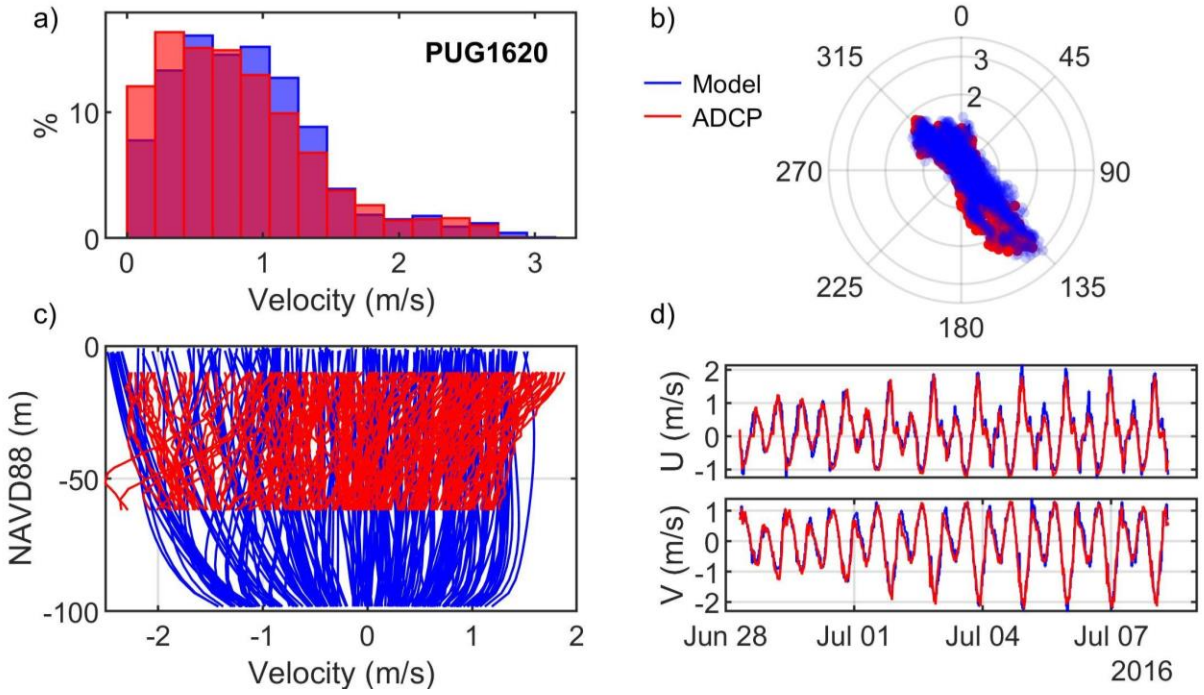

Figure A.68. Comparisons of simulated and observed velocities at Marrowstone Point (PUG1620): (a) velocity histograms, (b) scatter plot, (c) vertical profiles, and (d) time series of depth-averaged principal velocities.

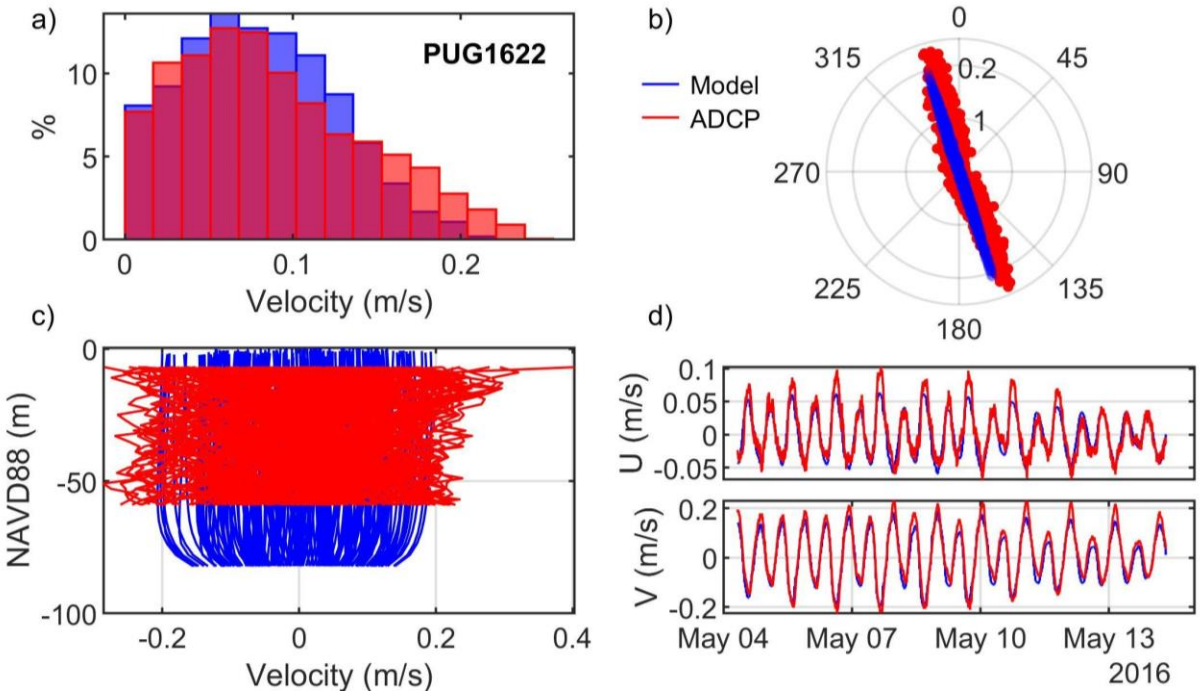

Figure A.69. Comparisons of simulated and observed velocities at Camano Island (PUG1622): (a) velocity histograms, (b) scatter plot, (c) vertical profiles, and (d) time series of depth-averaged principal velocities.

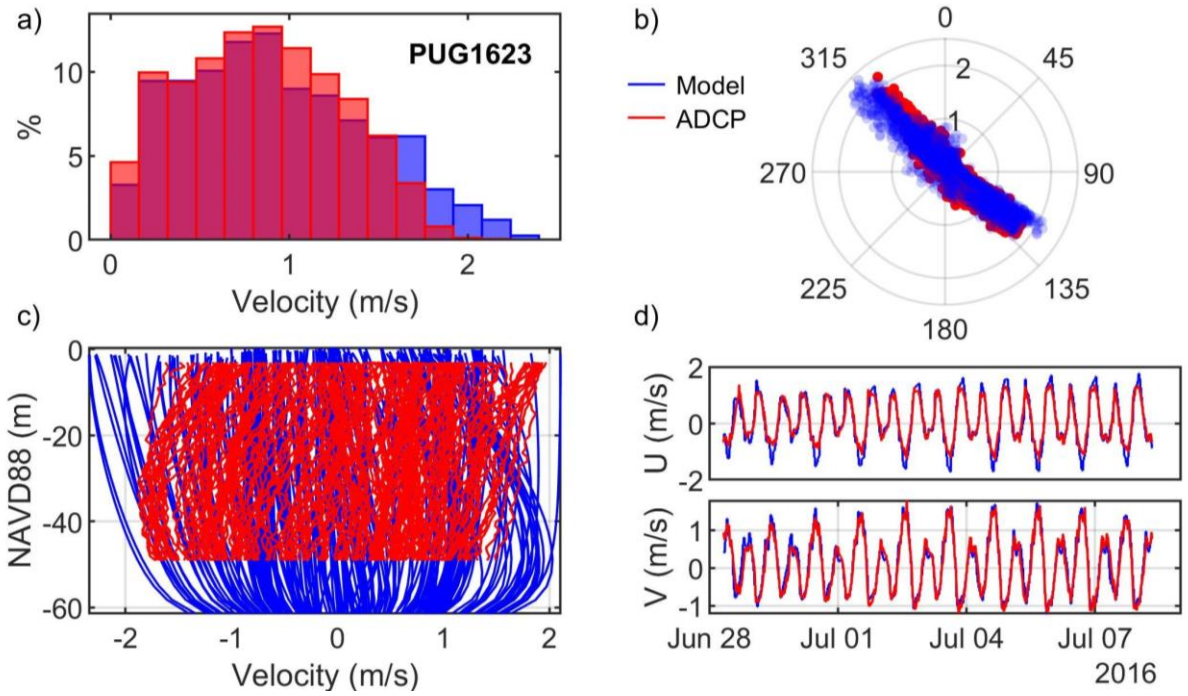

Figure A.70. Comparisons of simulated and observed velocities at Point Wilson A (PUG1623): (a) velocity histograms, (b) scatter plot, (c) vertical profiles, and (d) time series of depth-averaged principal velocities.

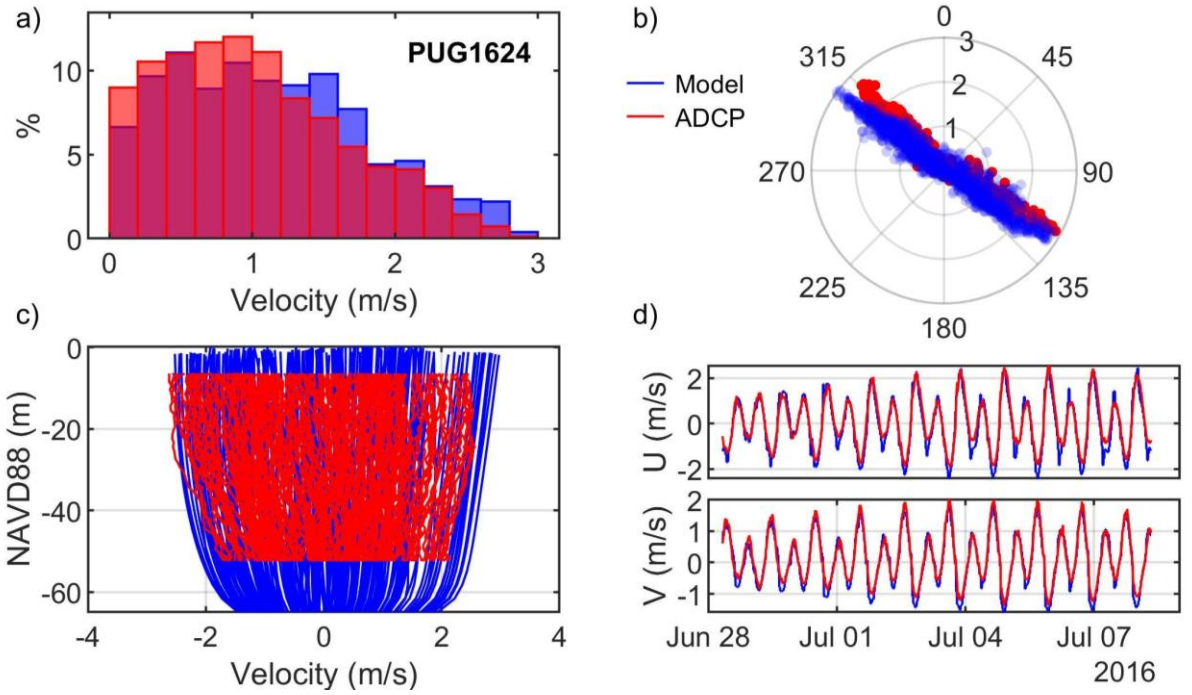

Figure A.71. Comparisons of simulated and observed velocities at Point Wilson B (PUG1624): (a) velocity histograms, (b) scatter plot, (c) vertical profiles, and (d) time series of depth-averaged principal velocities.

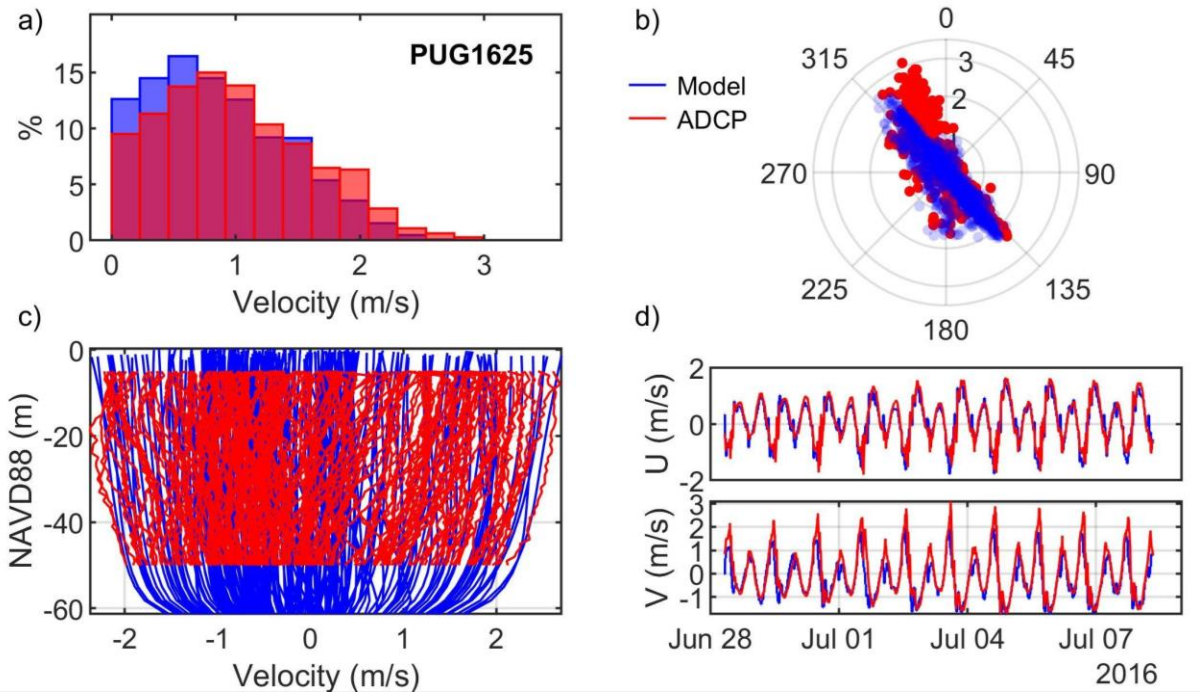

Figure A.72. Comparisons of simulated and observed velocities at Point Wilson C (PUG1625): (a) velocity histograms, (b) scatter plot, (c) vertical profiles, and (d) time series of depth-averaged principal velocities.

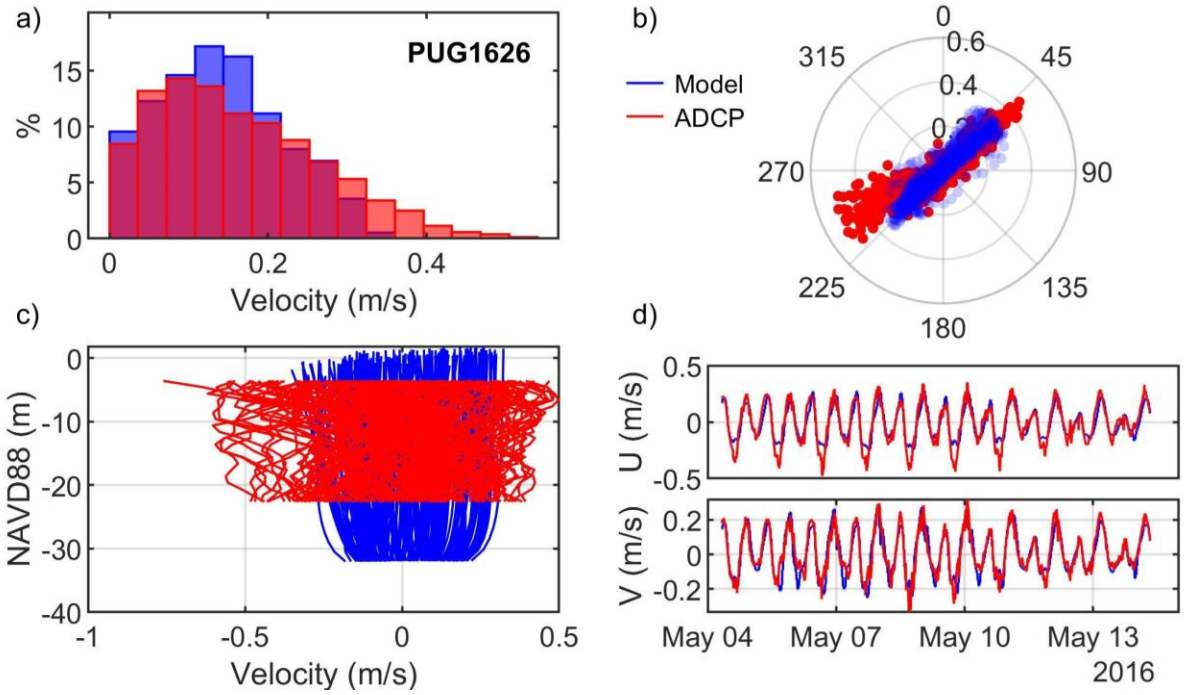

Figure A.73. Comparisons of simulated and observed velocities at Skagit Bay (PUG1626): (a) velocity histograms, (b) scatter plot, (c) vertical profiles, and (d) time series of depth-averaged principal velocities.

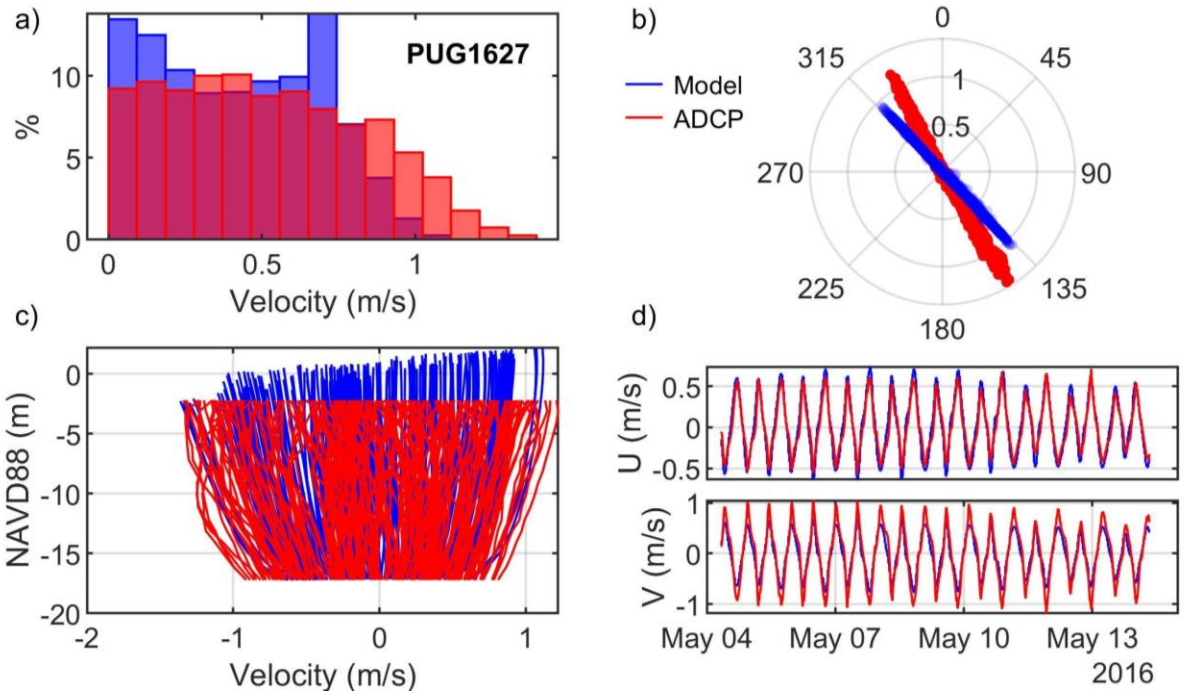

Figure A.74. Comparisons of simulated and observed velocities at Skagit Bay (PUG1627): (a) velocity histograms, (b) scatter plot, (c) vertical profiles, and (d) time series of depth-averaged principal velocities.

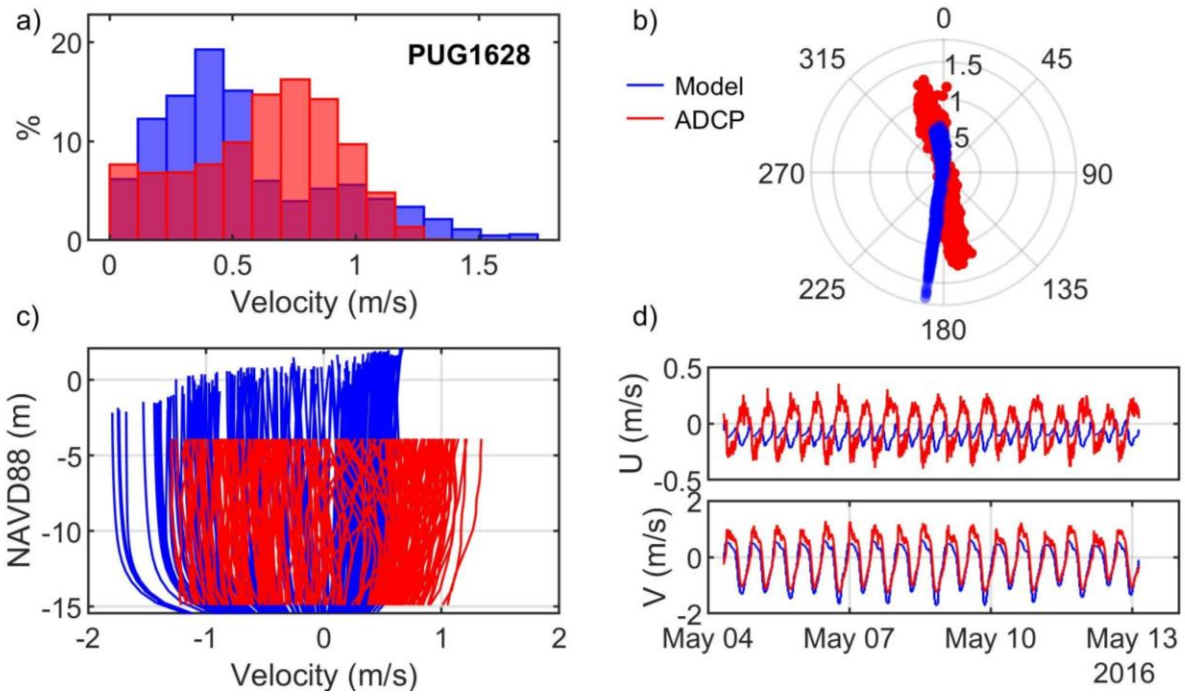

Figure A.75. Comparisons of simulated and observed velocities at Skagit Bay (PUG1628): (a) velocity histograms, (b) scatter plot, (c) vertical profiles, and (d) time series of depth-averaged principal velocities.

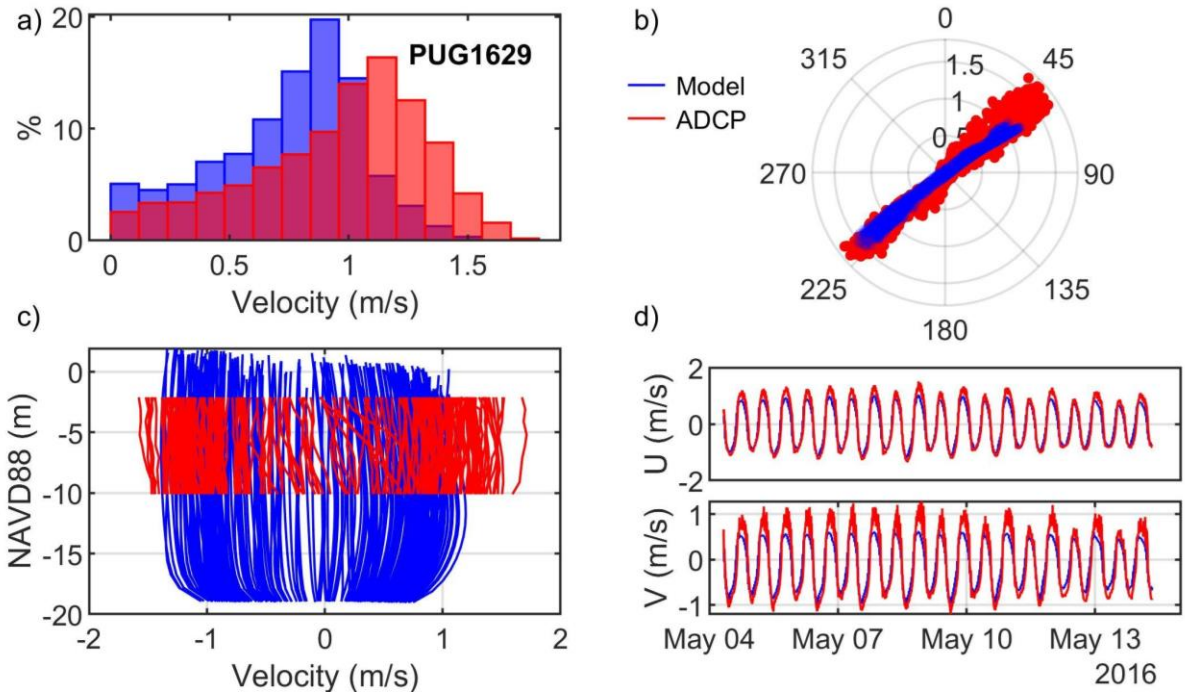

Figure A.76. Comparisons of simulated and observed velocities at Yokeko Point (PUG1629): (a) velocity histograms, (b) scatter plot, (c) vertical profiles, and (d) time series of depth-averaged principal velocities.

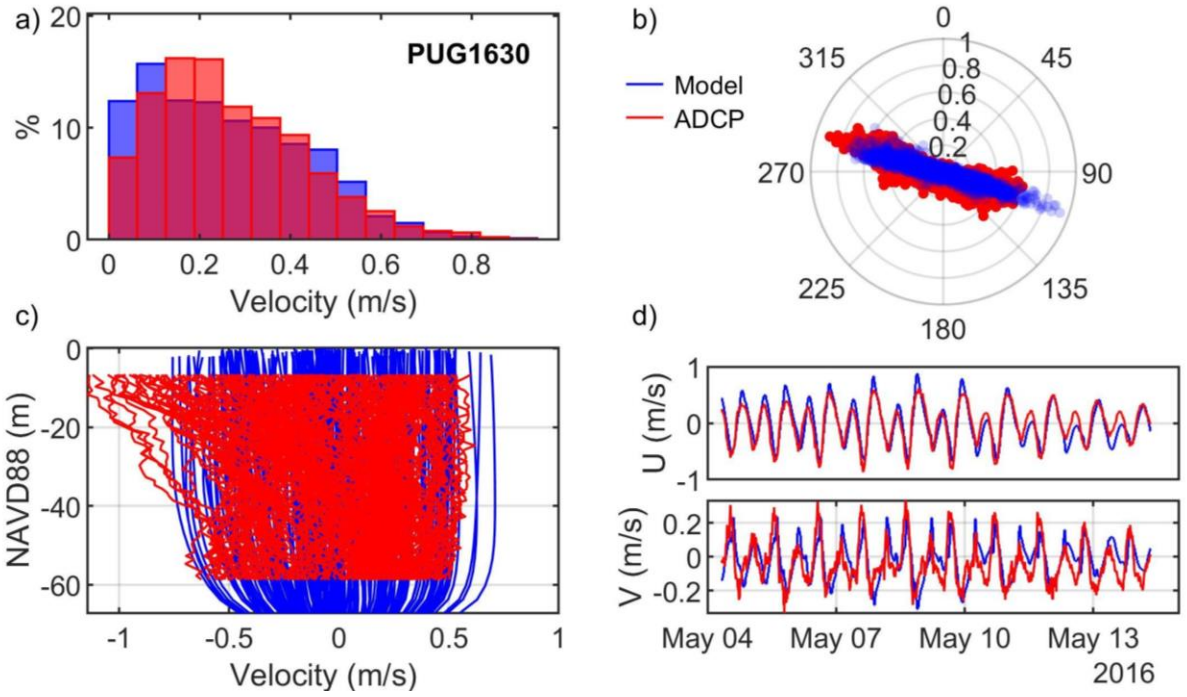

Figure A.77. Comparisons of simulated and observed velocities at Kanem Point (PUG1630): (a) velocity histograms, (b) scatter plot, (c) vertical profiles, and (d) time series of depth-averaged principal velocities.

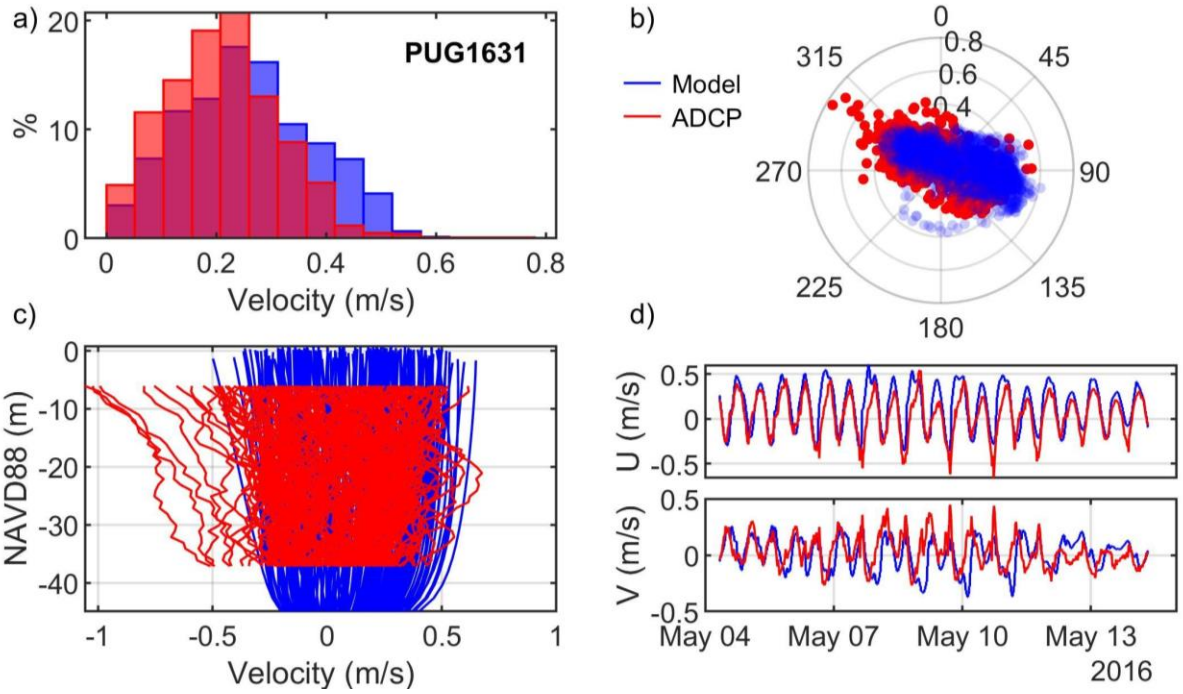

Figure A.78. Comparisons of simulated and observed velocities at Violet Point (PUG1631): (a) velocity histograms, (b) scatter plot, (c) vertical profiles, and (d) time series of depth-averaged principal velocities.

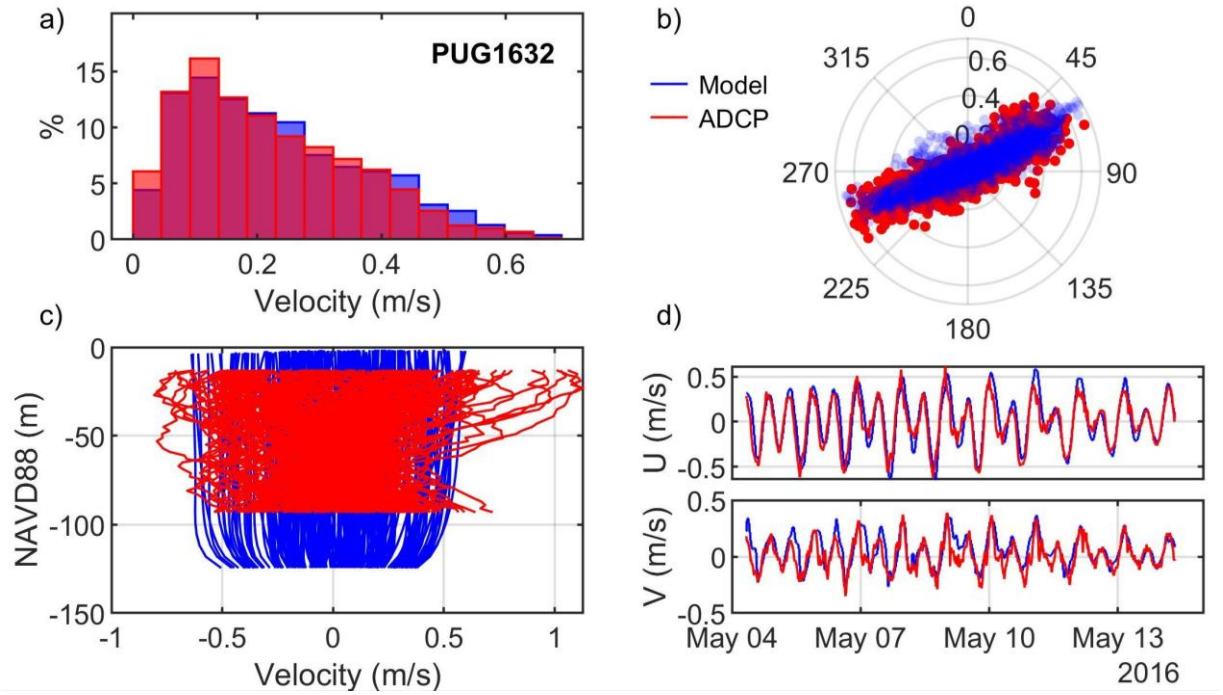

Figure A.79. Comparisons of simulated and observed velocities at Smith Island (PUG1632): (a) velocity histograms, (b) scatter plot, (c) vertical profiles, and (d) time series of depth-averaged principal velocities.

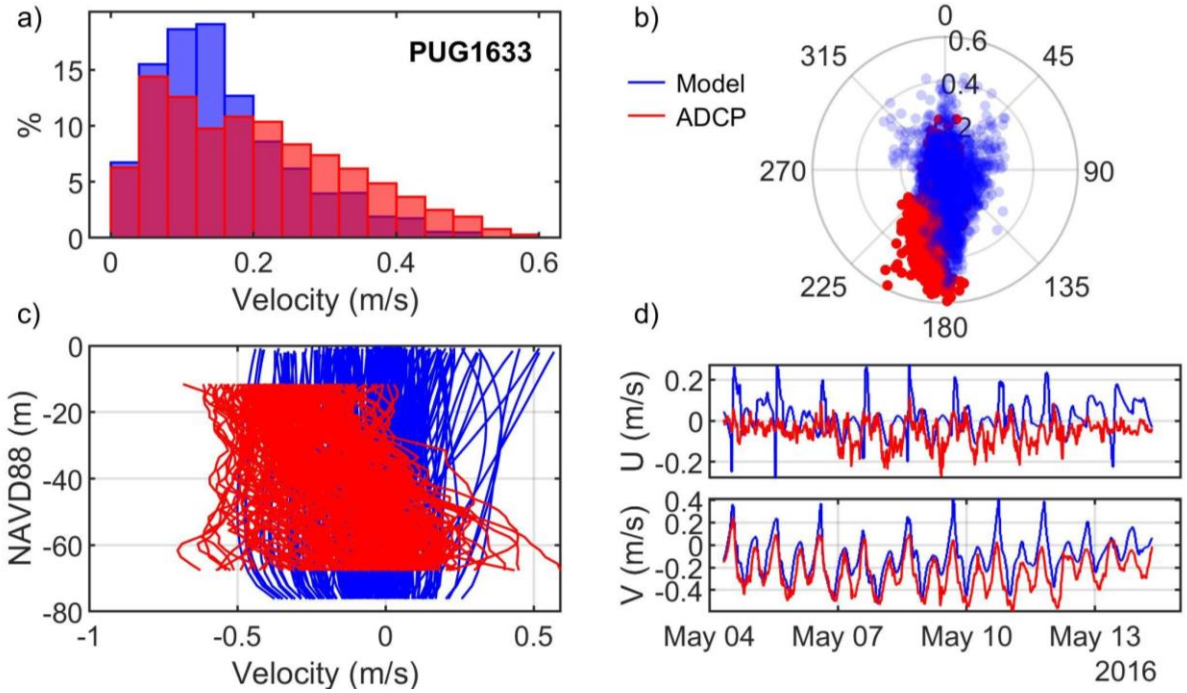

Figure A.80. Comparisons of simulated and observed velocities at Point Partridge (PUG1633): (a) velocity histograms, (b) scatter plot, (c) vertical profiles, and (d) time series of depth-averaged principal velocities.

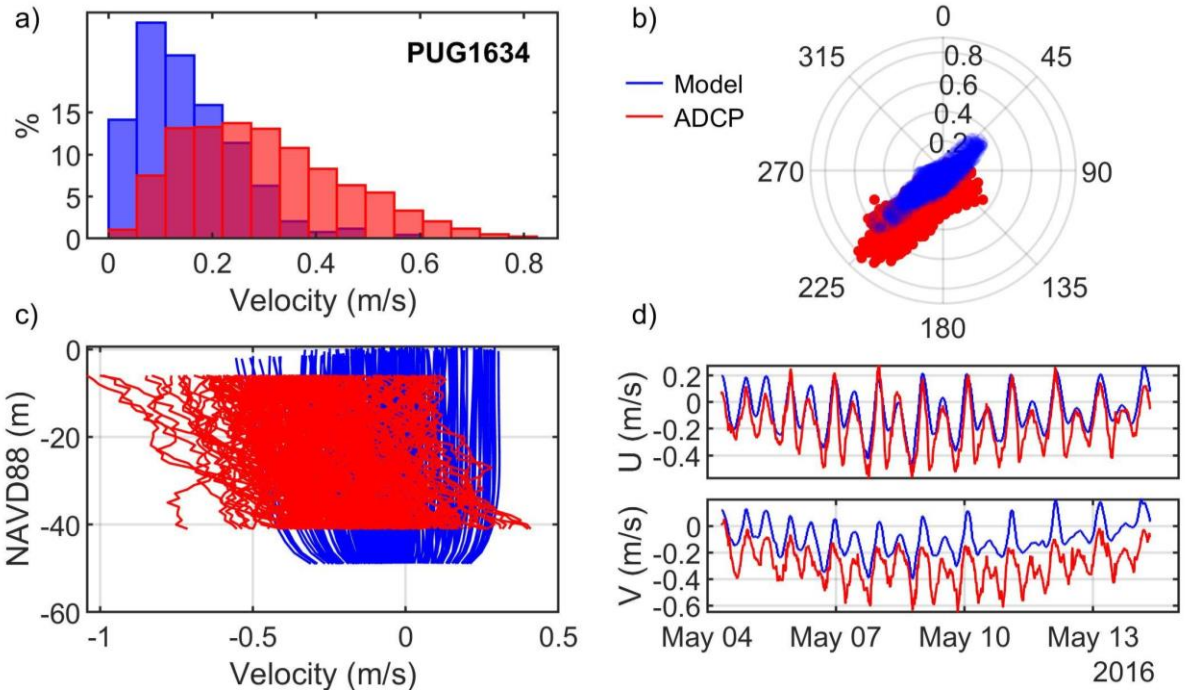

Figure A.81. Comparisons of simulated and observed velocities at Smith Island (PUG1634): (a) velocity histograms, (b) scatter plot, (c) vertical profiles, and (d) time series of depth-averaged principal velocities.

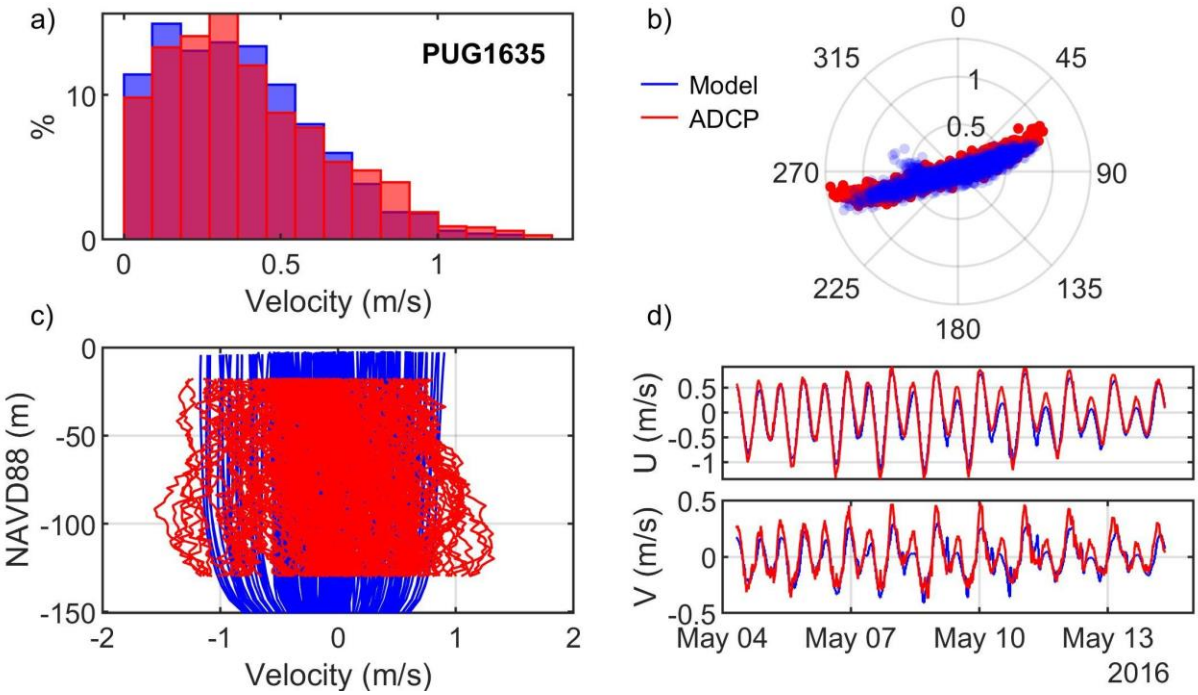

Figure A.82. Comparisons of simulated and observed velocities at New Dungeness Light (PUG1635): (a) velocity histograms, (b) scatter plot, (c) vertical profiles, and (d) time series of depth-averaged principal velocities.

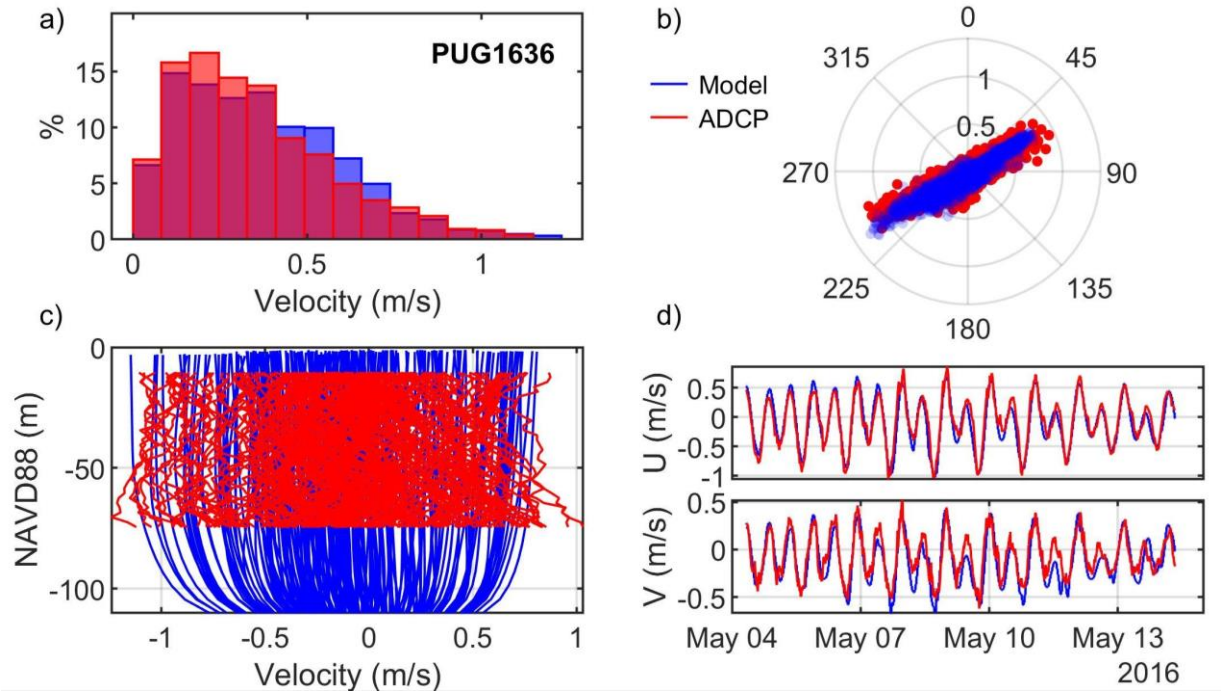

Figure A.83. Comparisons of simulated and observed velocities at Discovery Island (PUG1636): (a) velocity histograms, (b) scatter plot, (c) vertical profiles, and (d) time series of depth-averaged principal velocities.

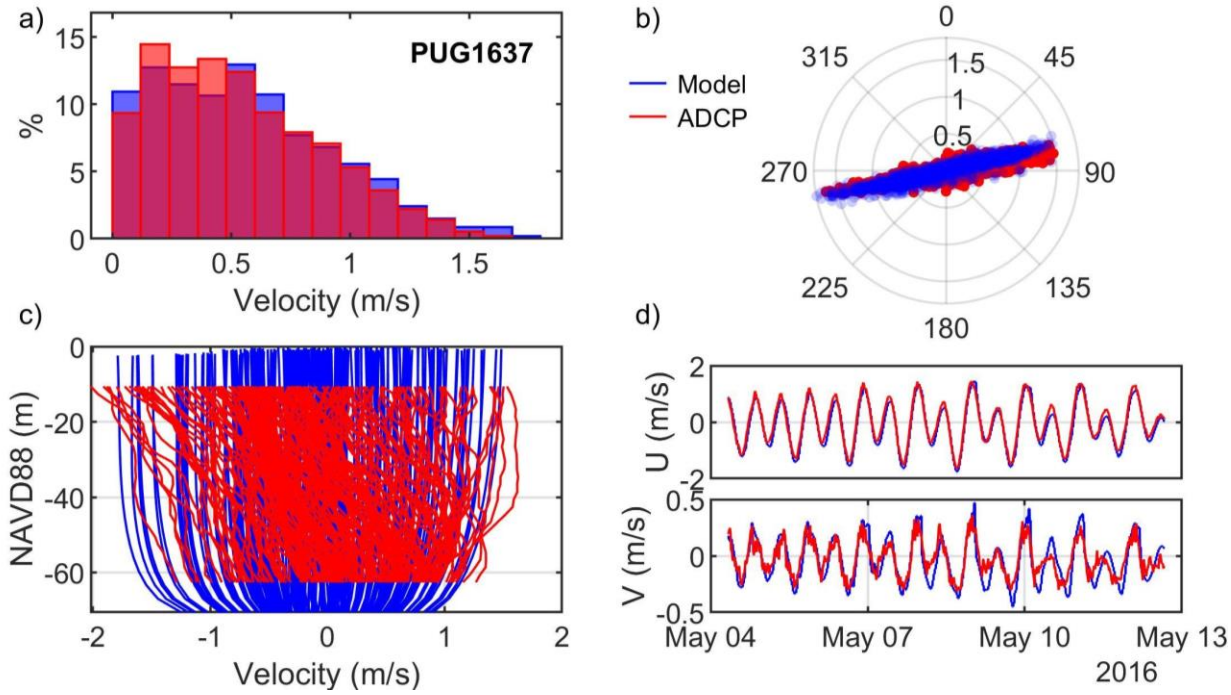

Figure A.84. Comparisons of simulated and observed velocities at Ediz Hook (PUG1637): (a) velocity histograms, (b) scatter plot, (c) vertical profiles, and (d) time series of depth-averaged principal velocities.

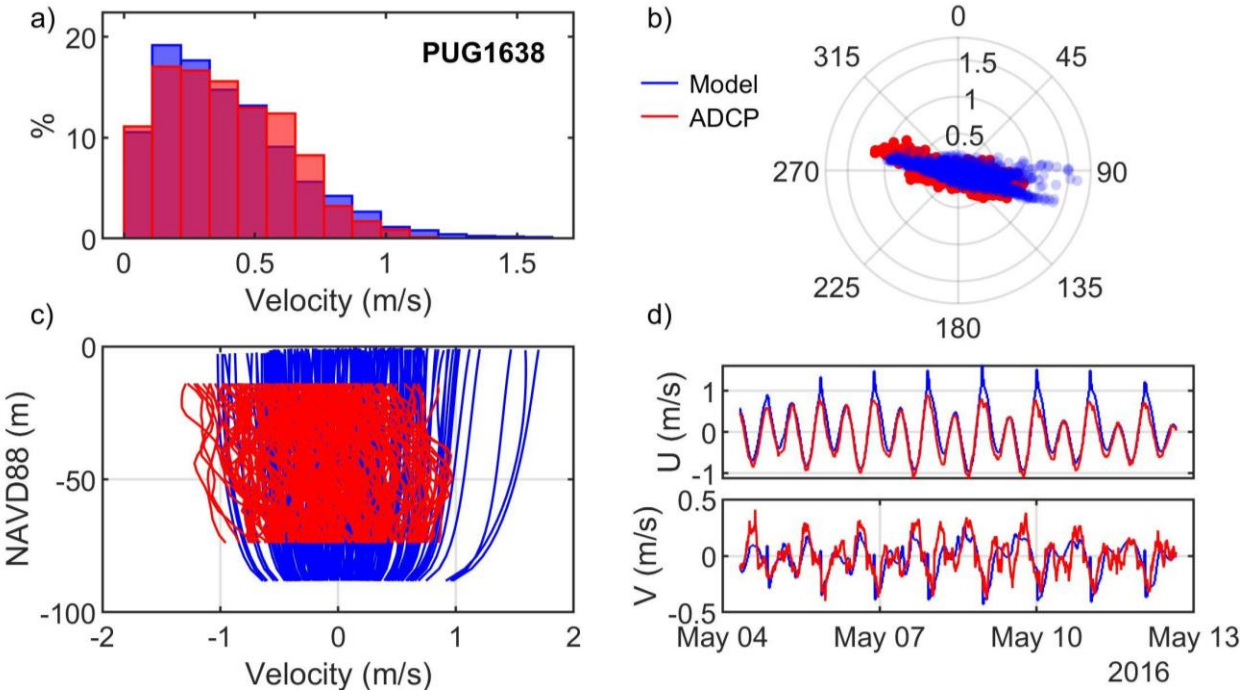

Figure A.85. Comparisons of simulated and observed velocities at Ediz Hook (PUG1638): (a) velocity histograms, (b) scatter plot, (c) vertical profiles, and (d) time series of depth-averaged principal velocities.

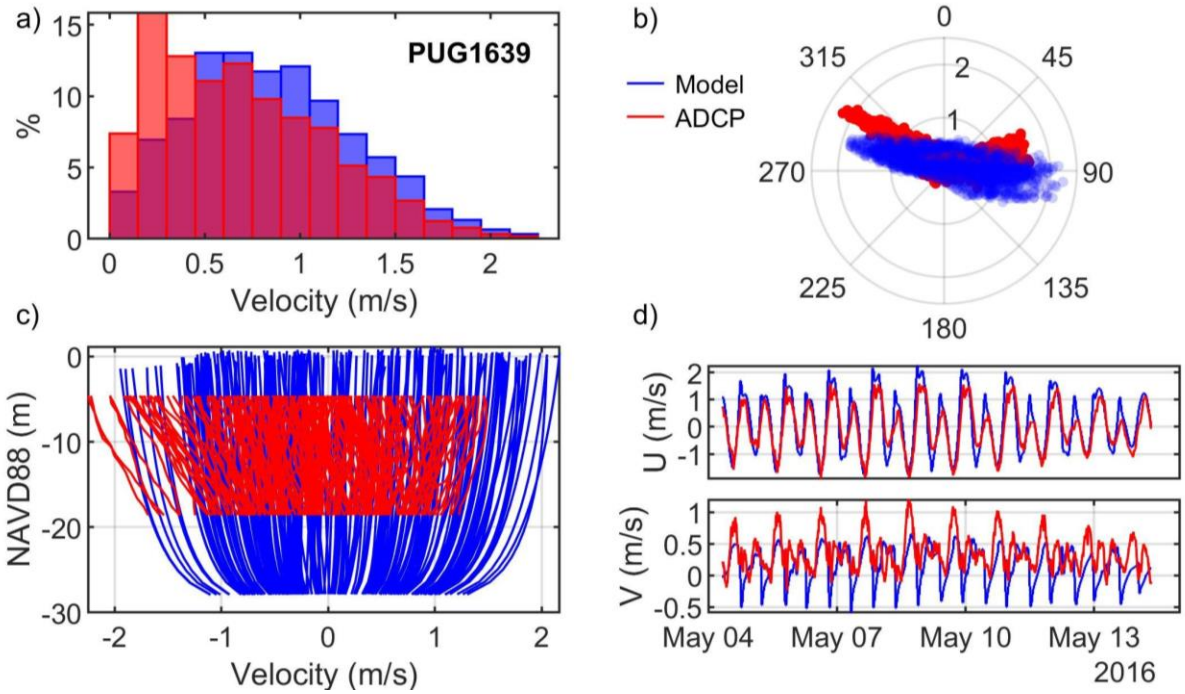

Figure A.86. Comparisons of simulated and observed velocities at Angeles Pt. (PUG1639): (a) velocity histograms, (b) scatter plot, (c) vertical profiles, and (d) time series of depth-averaged principal velocities.

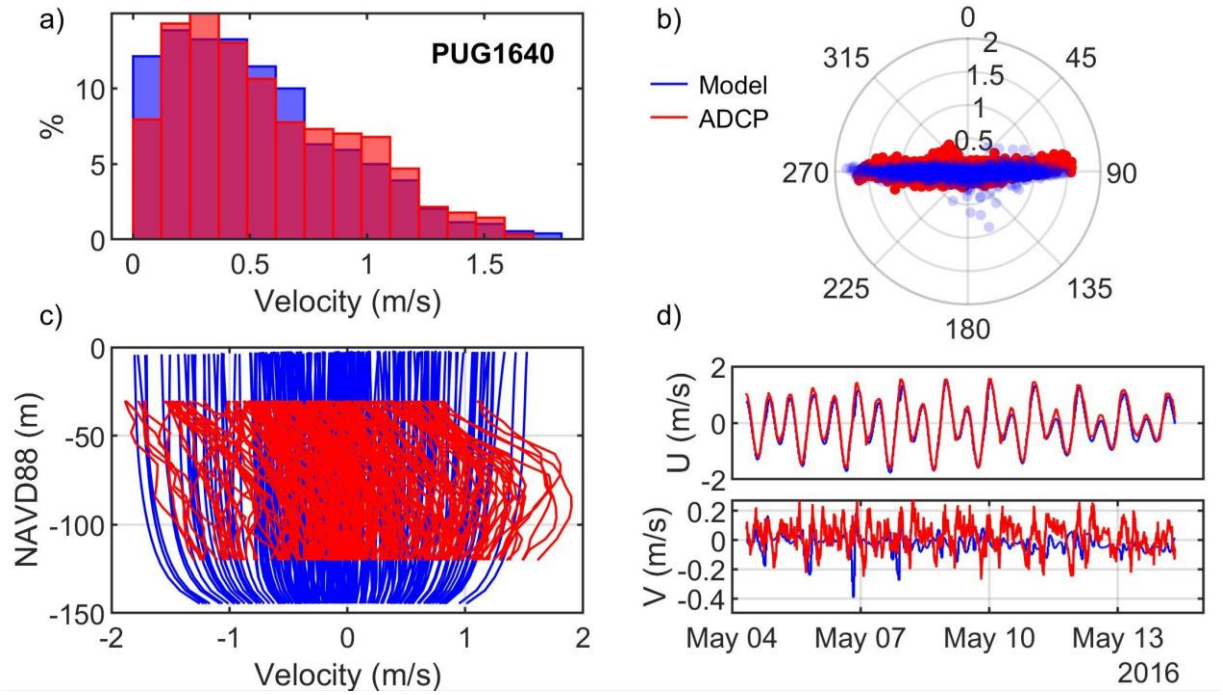

Figure A.87. Comparisons of simulated and observed velocities at Race Rocks (PUG1640): (a) velocity histograms, (b) scatter plot, (c) vertical profiles, and (d) time series of depth-averaged principal velocities.

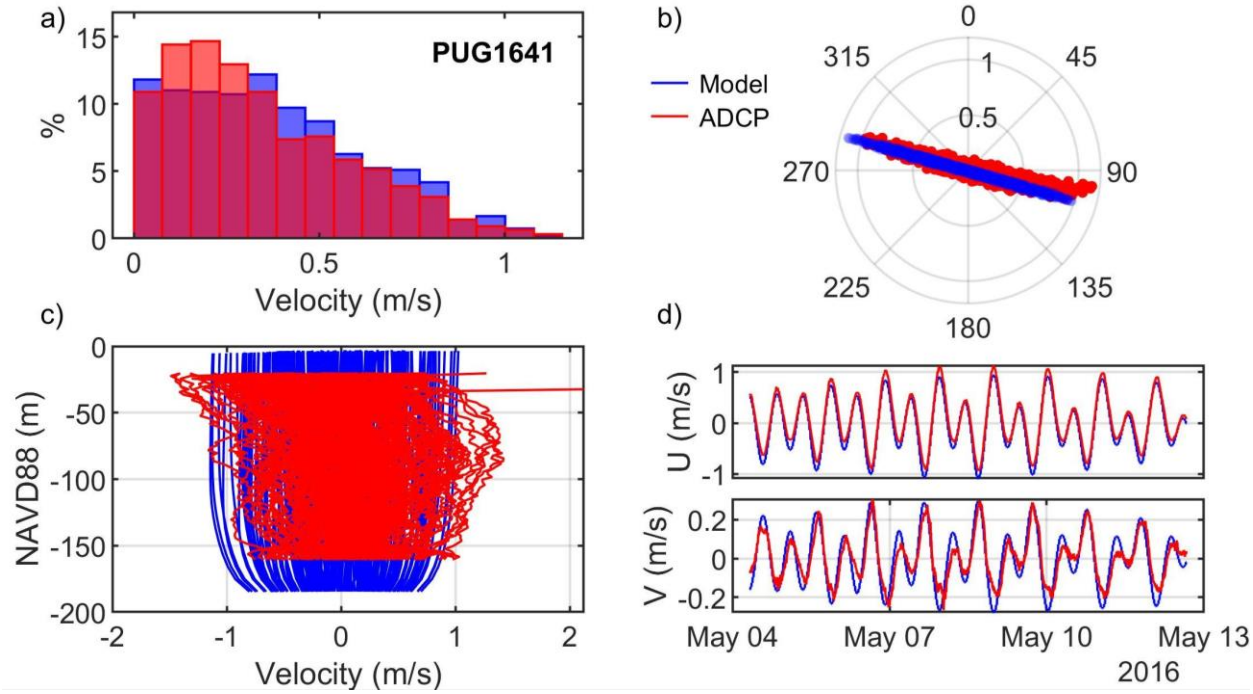

Figure A.88. Comparisons of simulated and observed velocities at Pillar Point (PUG1641): (a) velocity histograms, (b) scatter plot, (c) vertical profiles, and (d) time series of depth-averaged principal velocities.

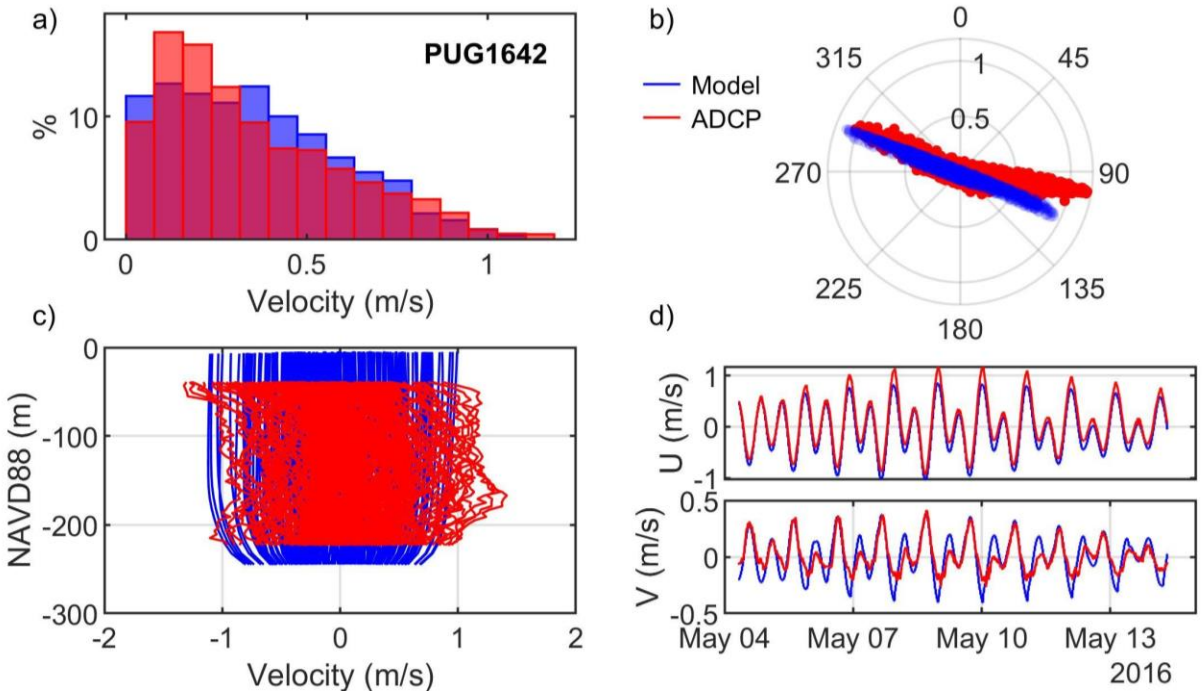

Figure A.89. Comparisons of simulated and observed velocities at Strait of Juan de Fuca (PUG1642): (a) velocity histograms, (b) scatter plot, (c) vertical profiles, and (d) time series of depth-averaged principal velocities.

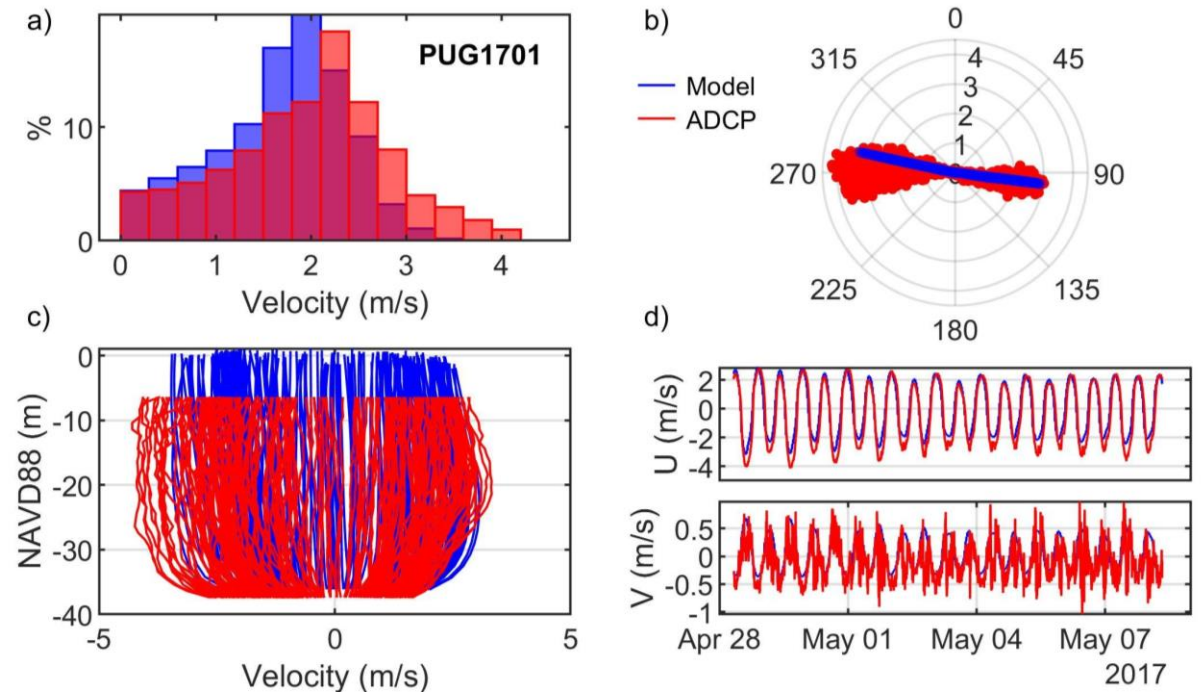

Figure A.90. Comparisons of simulated and observed velocities at Deception Pass (PUG1701): (a) velocity histograms, (b) scatter plot, (c) vertical profiles, and (d) time series of depth-averaged principal velocities.

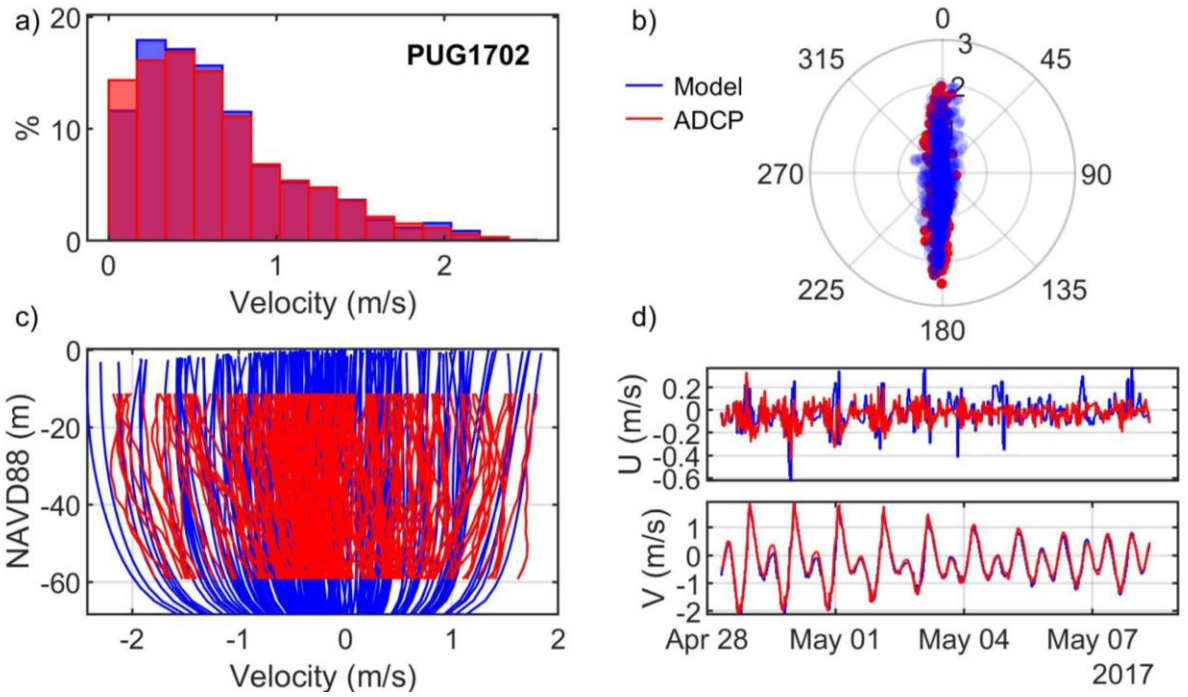

Figure A.91. Comparisons of simulated and observed velocities at Rosario Strait (PUG1702): (a) velocity histograms, (b) scatter plot, (c) vertical profiles, and (d) time series of depth-averaged principal velocities.

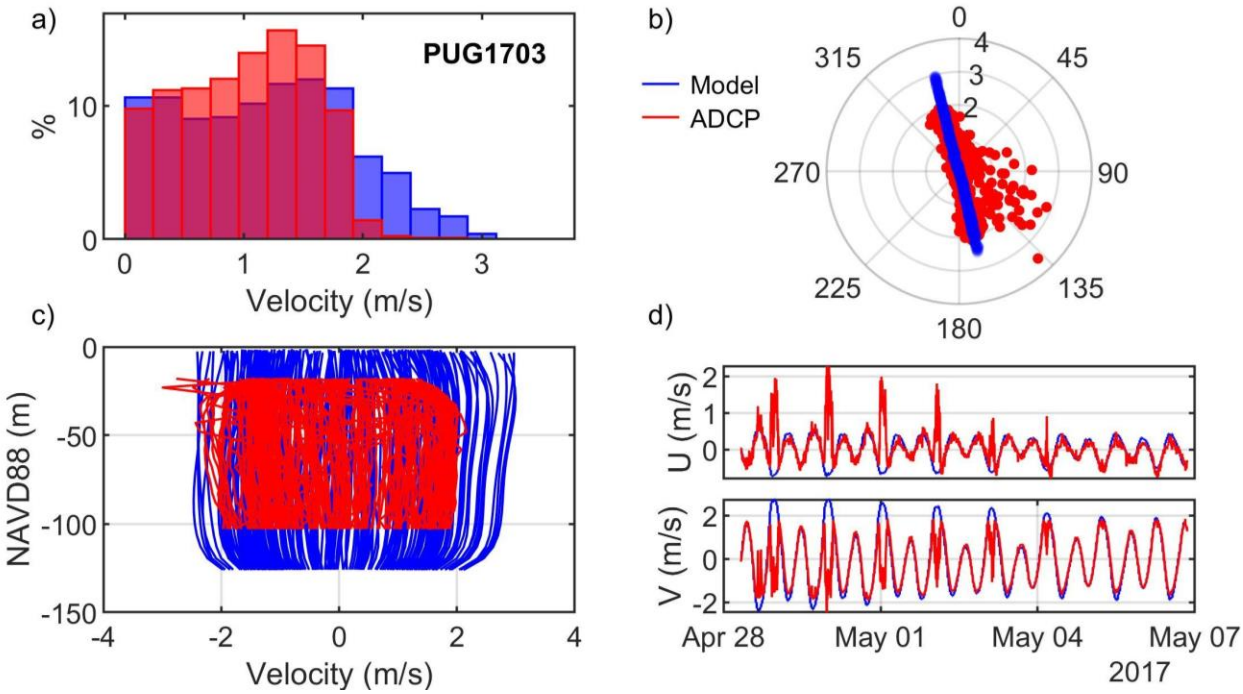

Figure A.92. Comparisons of simulated and observed velocities at San Juan Channel (PUG1703): (a) velocity histograms, (b) scatter plot, (c) vertical profiles, and (d) time series of depth-averaged principal velocities.

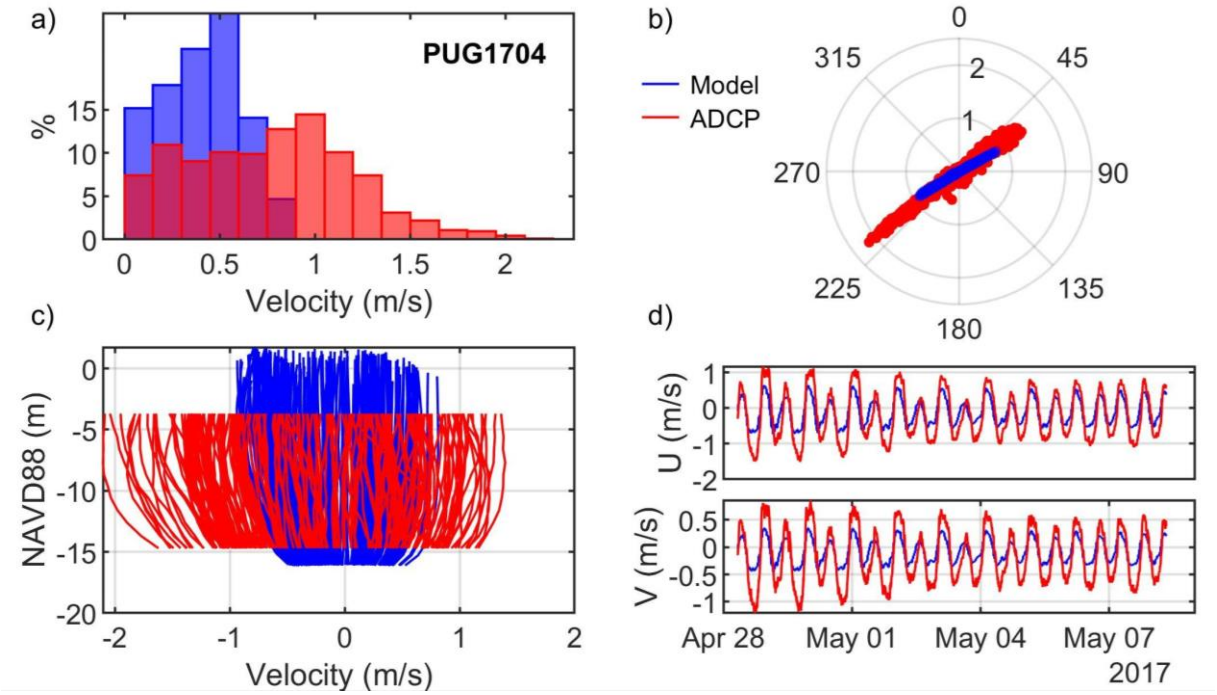

Figure A.93. Comparisons of simulated and observed velocities at Peavine Pass (PUG1704): (a) velocity histograms, (b) scatter plot, (c) vertical profiles, and (d) time series of depth-averaged principal velocities.

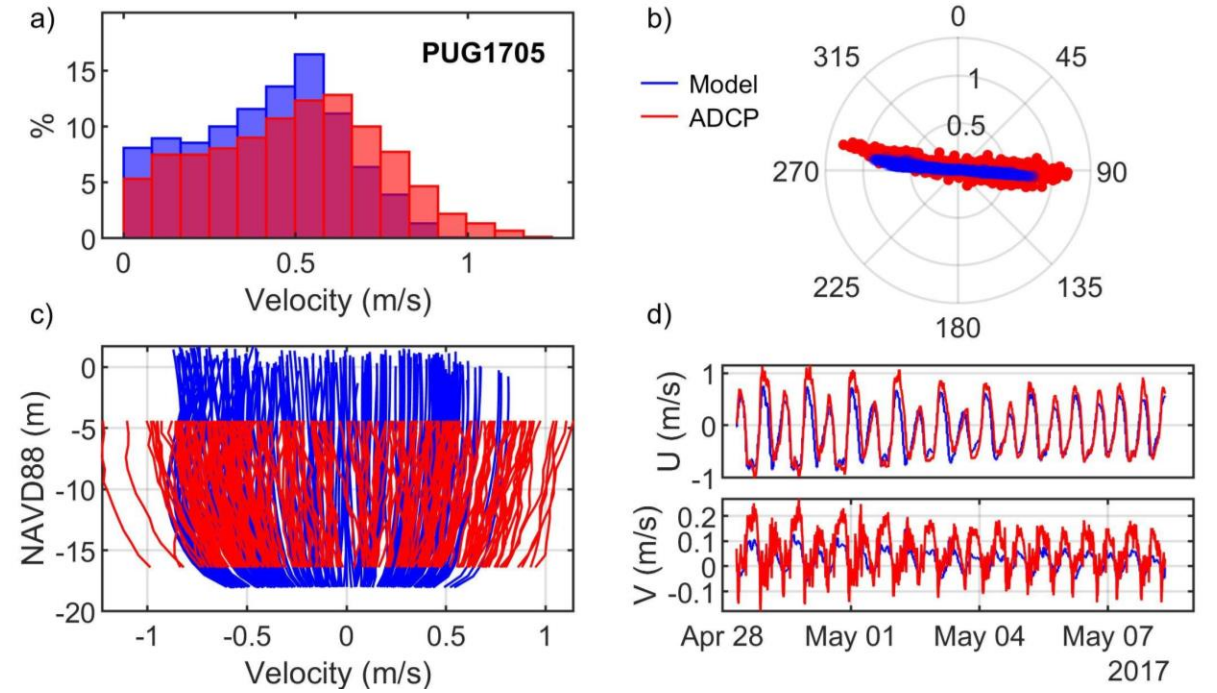

Figure A.94. Comparisons of simulated and observed velocities at Obstruction Pass (PUG1705): (a) velocity histograms, (b) scatter plot, (c) vertical profiles, and (d) time series of depth-averaged principal velocities.

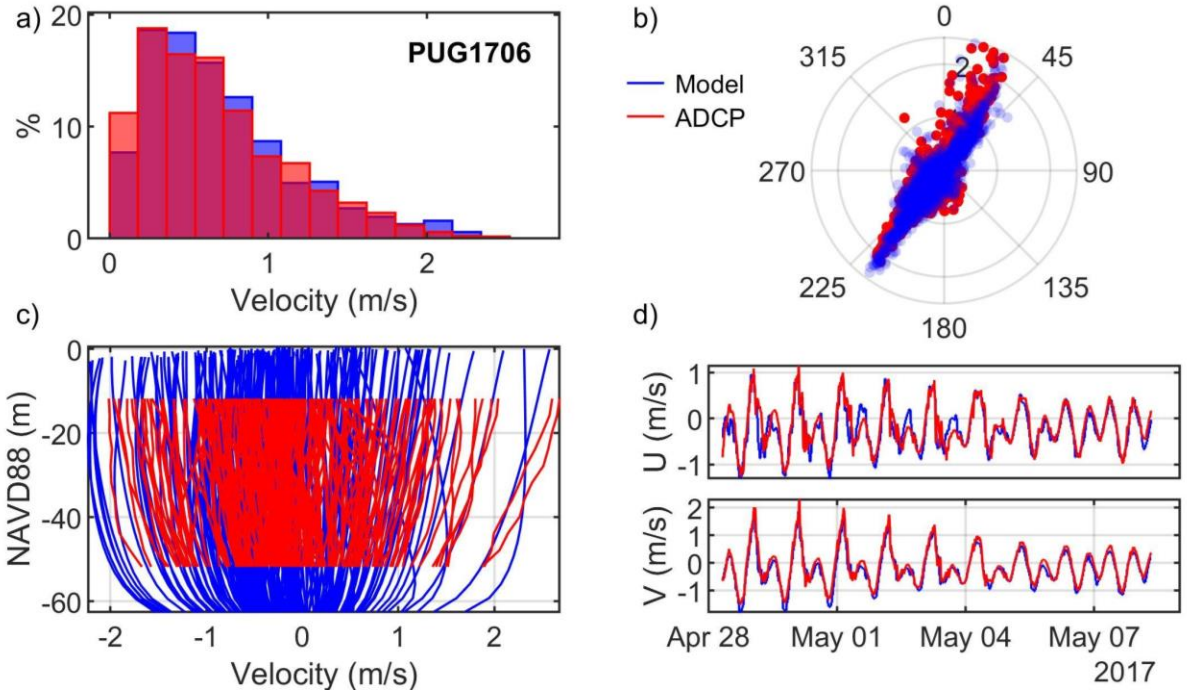

Figure A.95. Comparisons of simulated and observed velocities at Peapod Rocks (PUG1706): (a) velocity histograms, (b) scatter plot, (c) vertical profiles, and (d) time series of depth-averaged principal velocities.

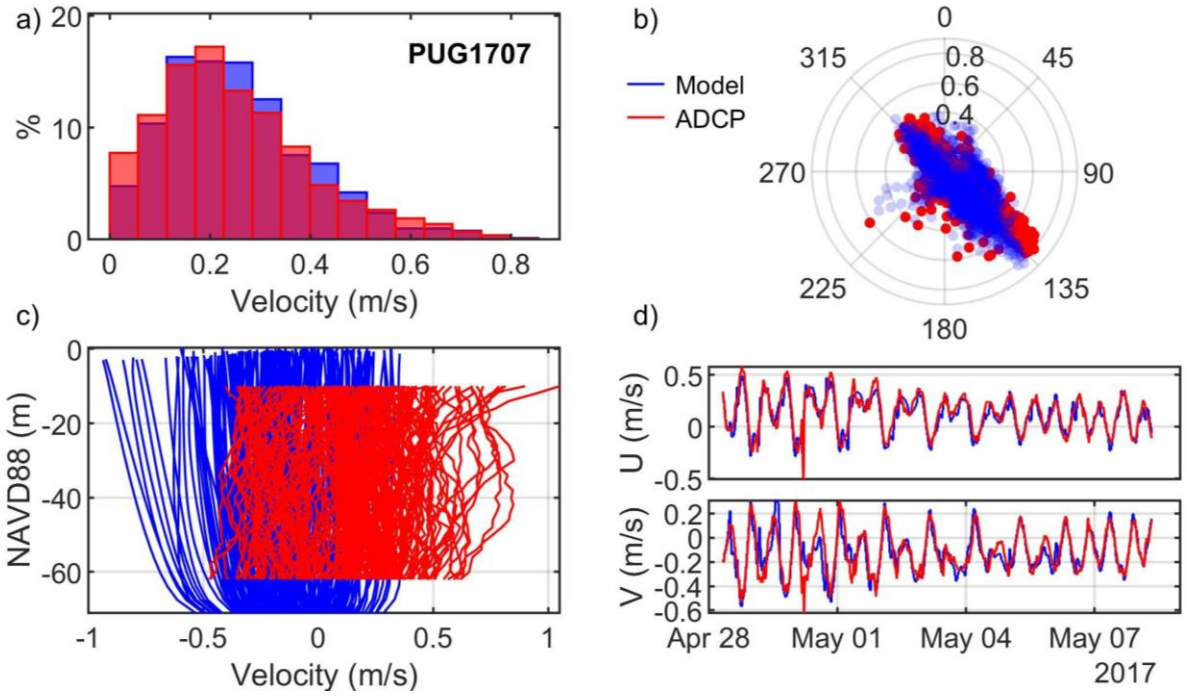

Figure A.96. Comparisons of simulated and observed velocities at Sinclair Island (PUG1707): (a) velocity histograms, (b) scatter plot, (c) vertical profiles, and (d) time series of depth-averaged principal velocities.

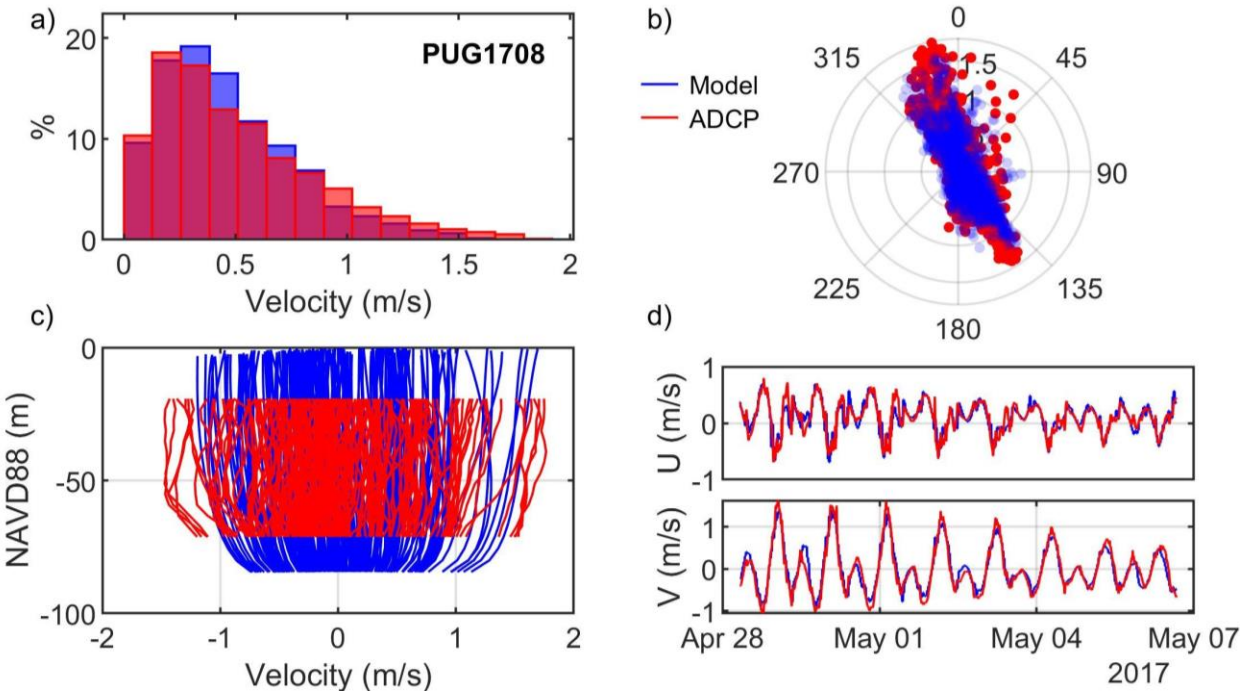

Figure A.97. Comparisons of simulated and observed velocities at Lawrence Point (PUG1708): (a) velocity histograms, (b) scatter plot, (c) vertical profiles, and (d) time series of depth-averaged principal velocities.

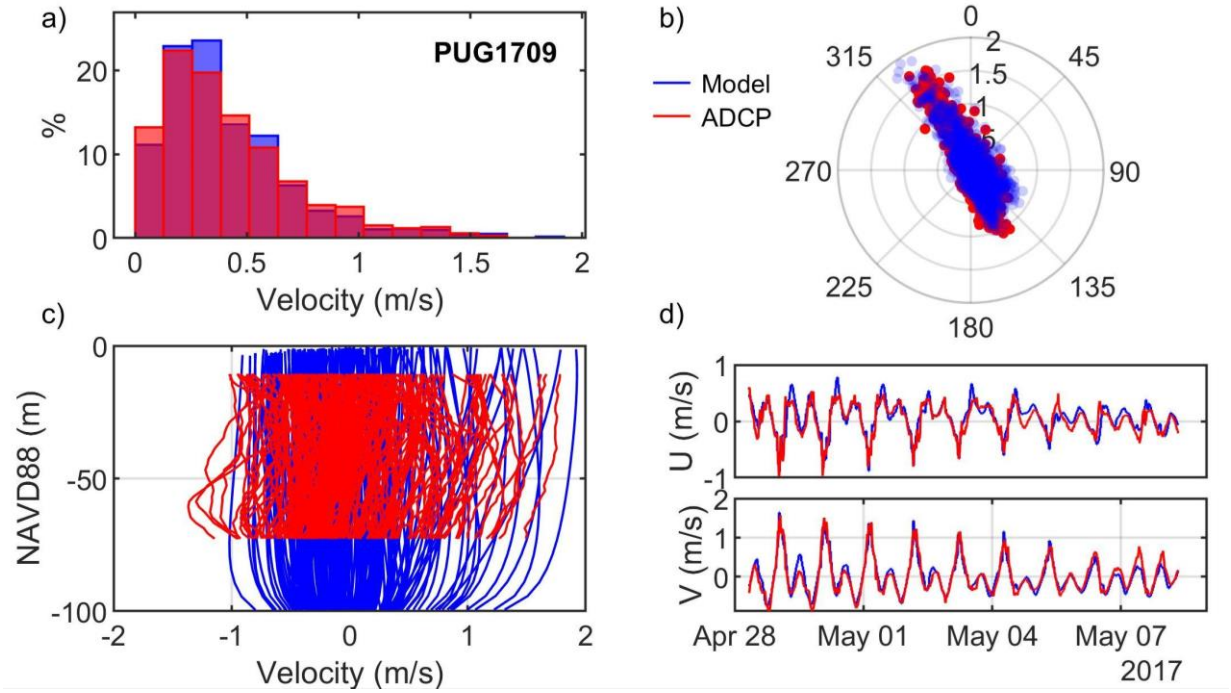

Figure A.98. Comparisons of simulated and observed velocities at Clark Island (PUG1709): (a) velocity histograms, (b) scatter plot, (c) vertical profiles, and (d) time series of depth-averaged principal velocities.

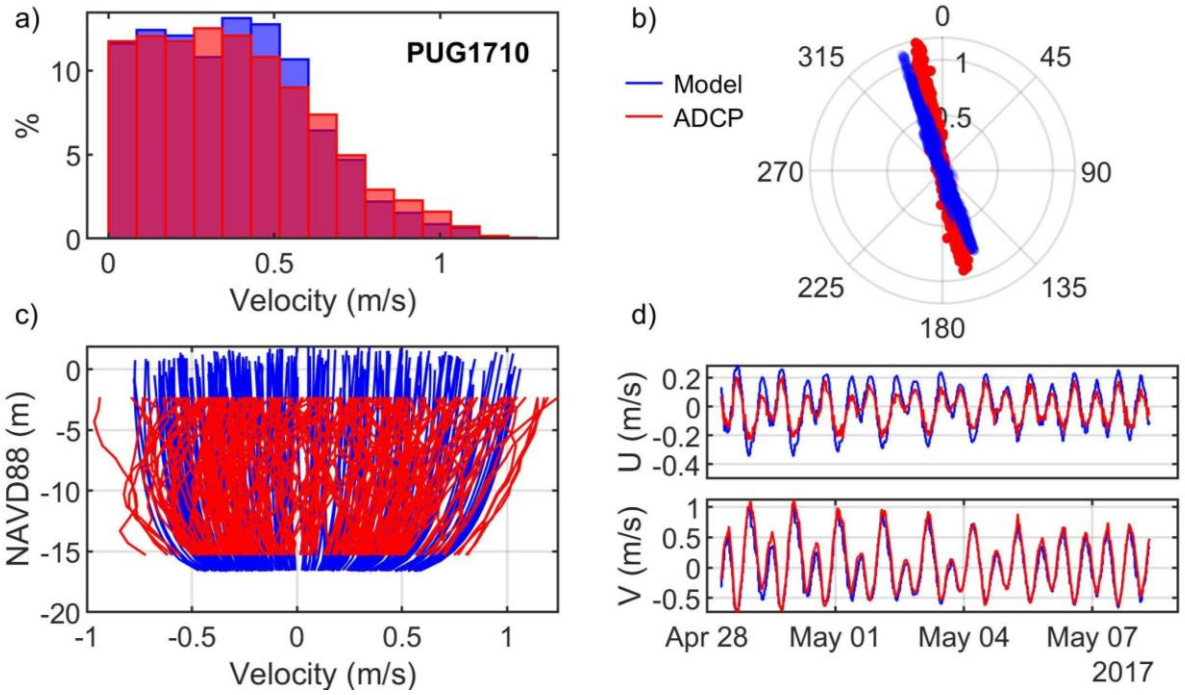

Figure A.99. Comparisons of simulated and observed velocities at Hale Passage (PUG1710): (a) velocity histograms, (b) scatter plot, (c) vertical profiles, and (d) time series of depth-averaged principal velocities.

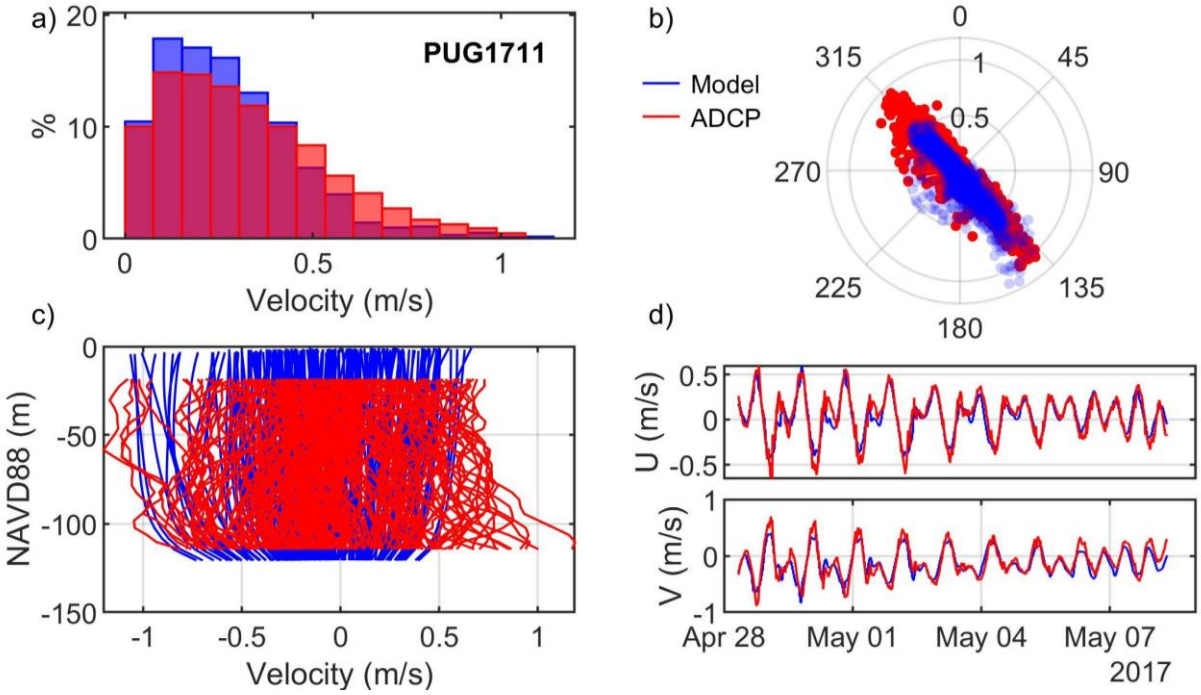

Figure A.100. Comparisons of simulated and observed velocities at Matia Island (PUG1711): (a) velocity histograms, (b) scatter plot, (c) vertical profiles, and (d) time series of depth-averaged principal velocities.

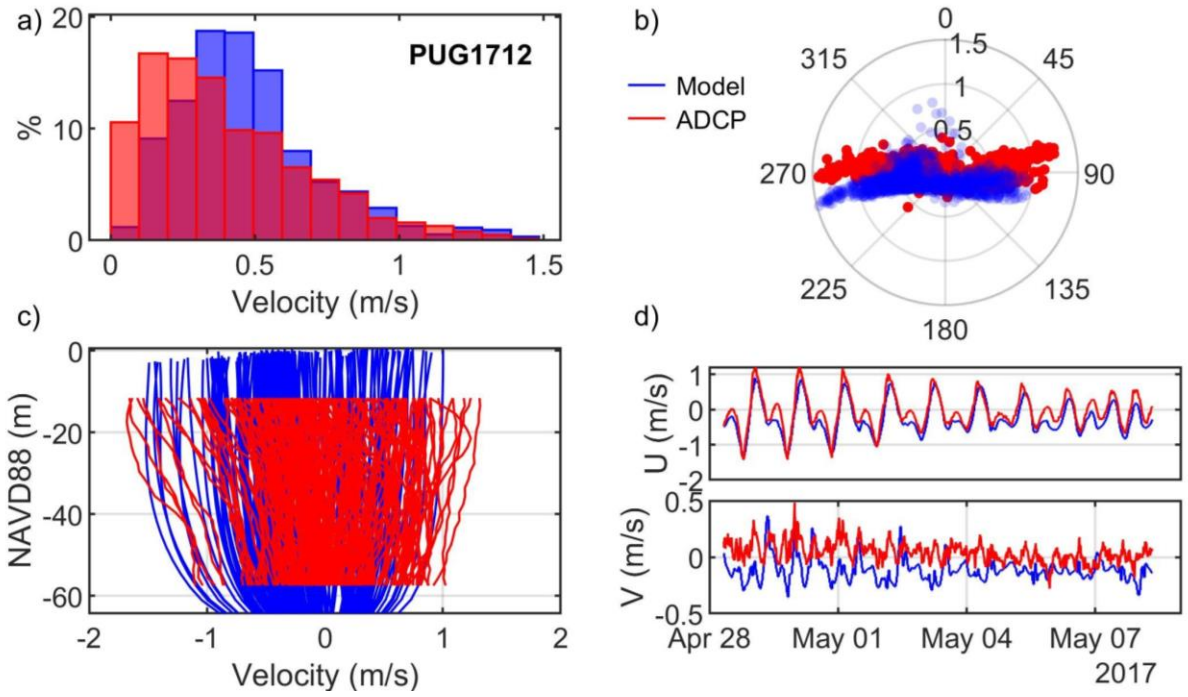

Figure A.101. Comparisons of simulated and observed velocities at Parker Reef (PUG1712): (a) velocity histograms, (b) scatter plot, (c) vertical profiles, and (d) time series of depth-averaged principal velocities.

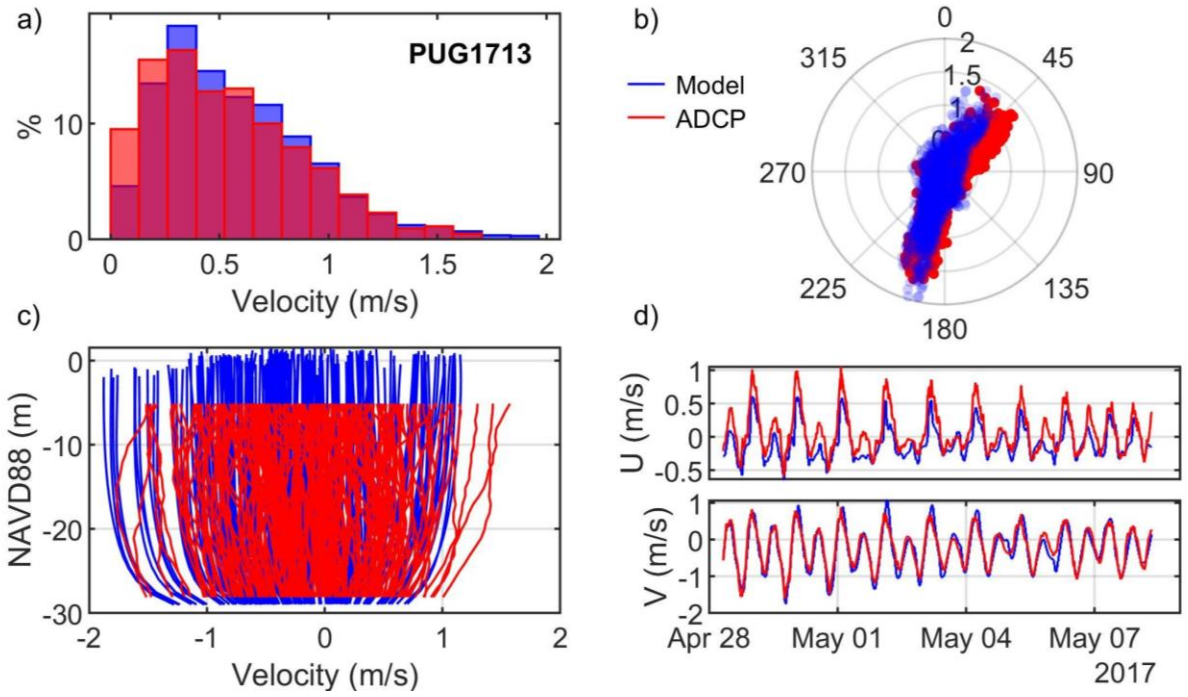

Figure A.102. Comparisons of simulated and observed velocities at Patos Island (PUG1713): (a) velocity histograms, (b) scatter plot, (c) vertical profiles, and (d) time series of depth-averaged principal velocities.

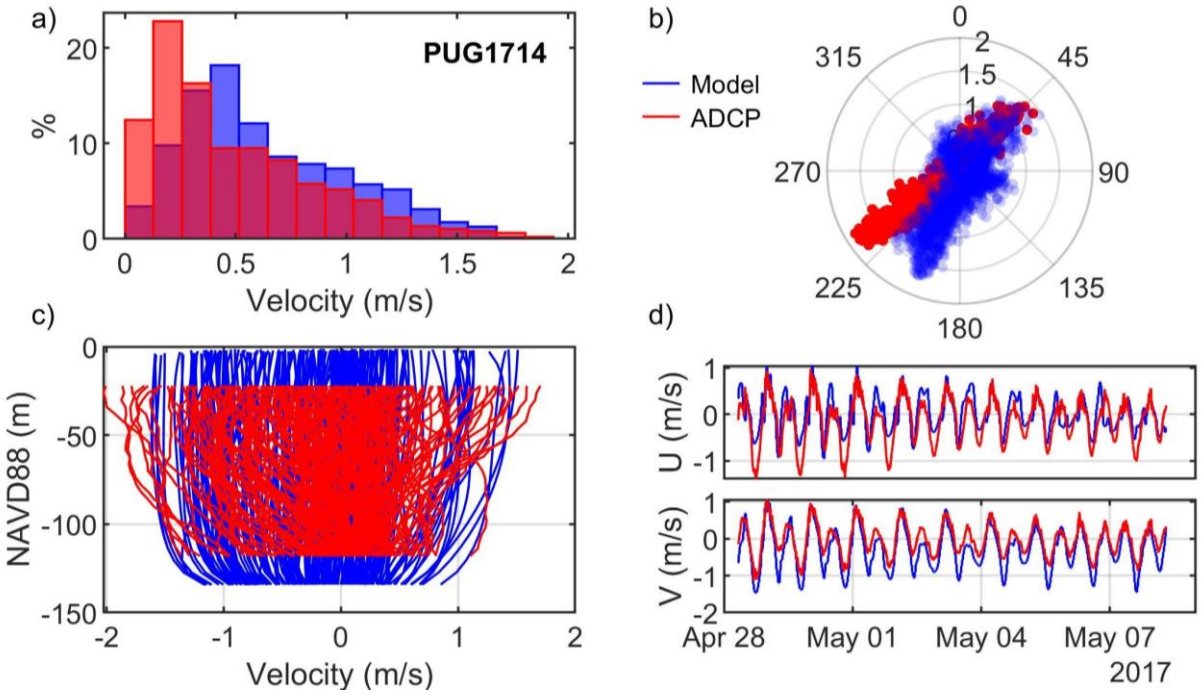

Figure A.103. Comparisons of simulated and observed velocities at Patos Island (PUG1714): (a) velocity histograms, (b) scatter plot, (c) vertical profiles, and (d) time series of depth-averaged principal velocities.

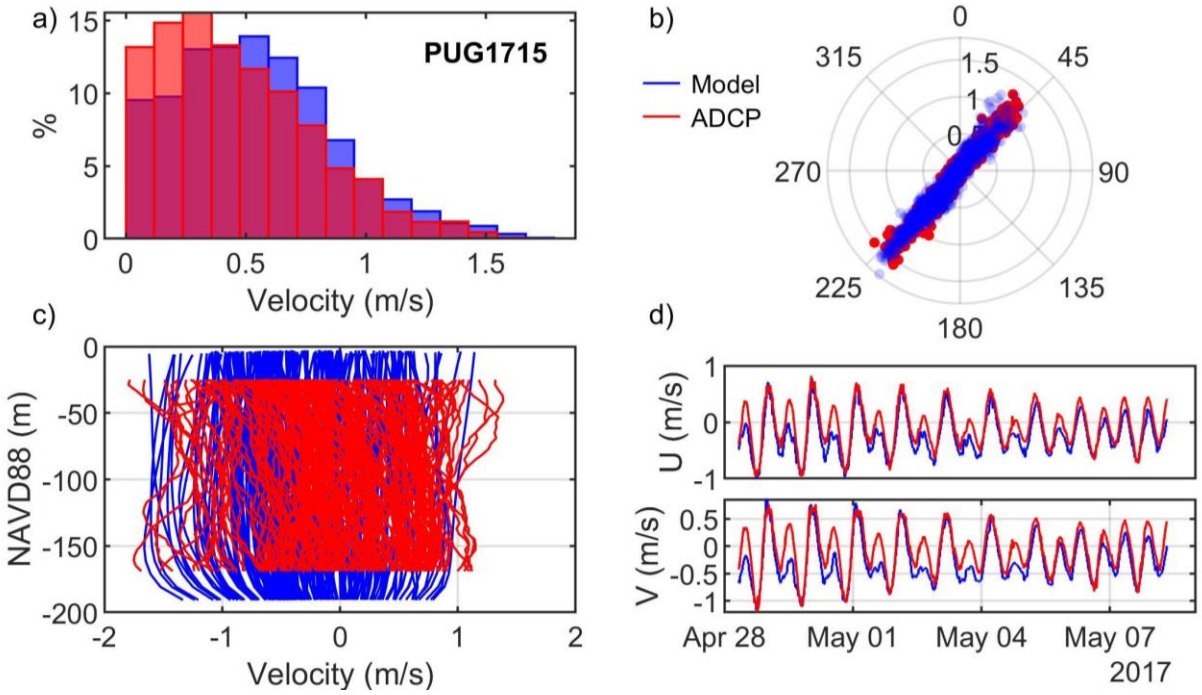

Figure A.104. Comparisons of simulated and observed velocities at President Channel (PUG1715): (a) velocity histograms, (b) scatter plot, (c) vertical profiles, and (d) time series of depth-averaged principal velocities.

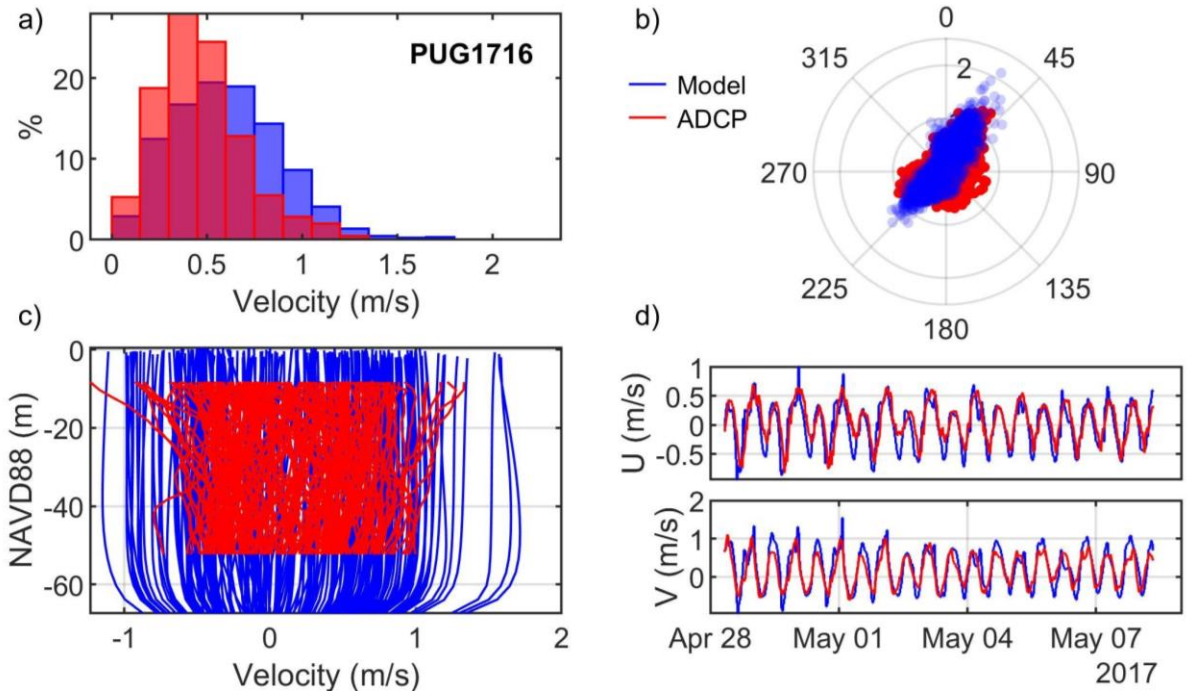

Figure A.105. Comparisons of simulated and observed velocities at Waldron Island (PUG1716): (a) velocity histograms, (b) scatter plot, (c) vertical profiles, and (d) time series of depth-averaged principal velocities.

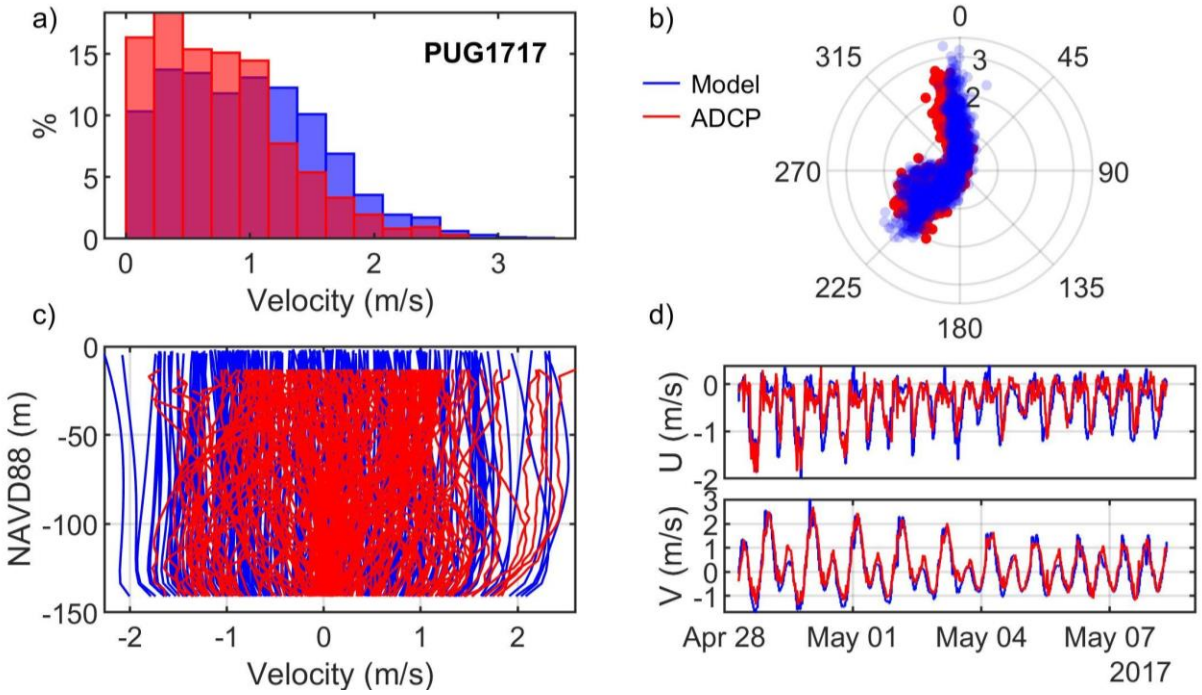

Figure A.106. Comparisons of simulated and observed velocities at Turn Point (PUG1717): (a) velocity histograms, (b) scatter plot, (c) vertical profiles, and (d) time series of depth-averaged principal velocities.

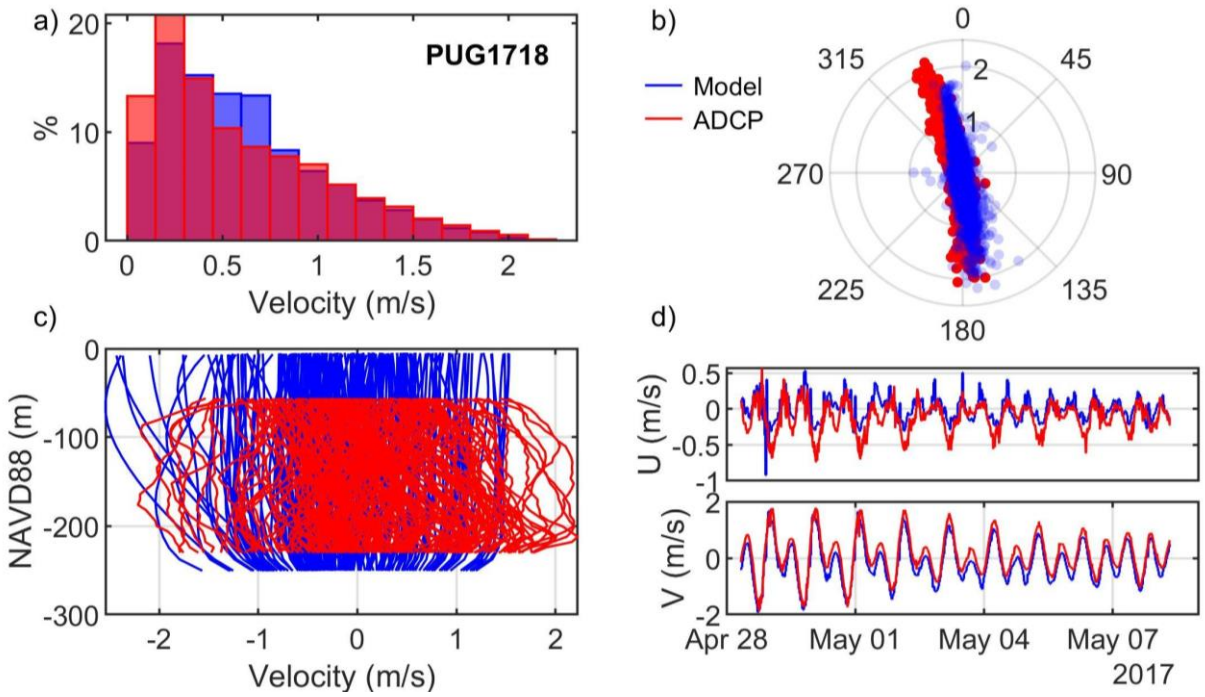

Figure A.107. Comparisons of simulated and observed velocities at Haro Strait (PUG1718): (a) velocity histograms, (b) scatter plot, (c) vertical profiles, and (d) time series of depth-averaged principal velocities.

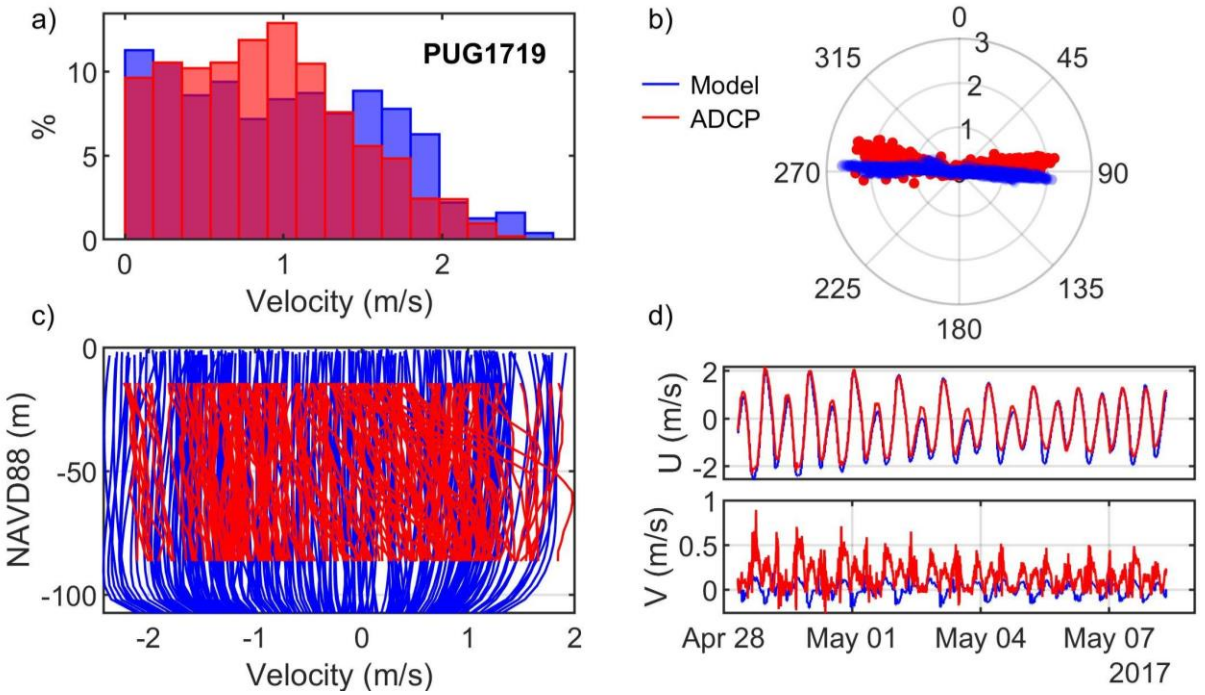

Figure A.108. Comparisons of simulated and observed velocities at Spieden Channel (PUG1719): (a) velocity histograms, (b) scatter plot, (c) vertical profiles, and (d) time series of depth-averaged principal velocities.

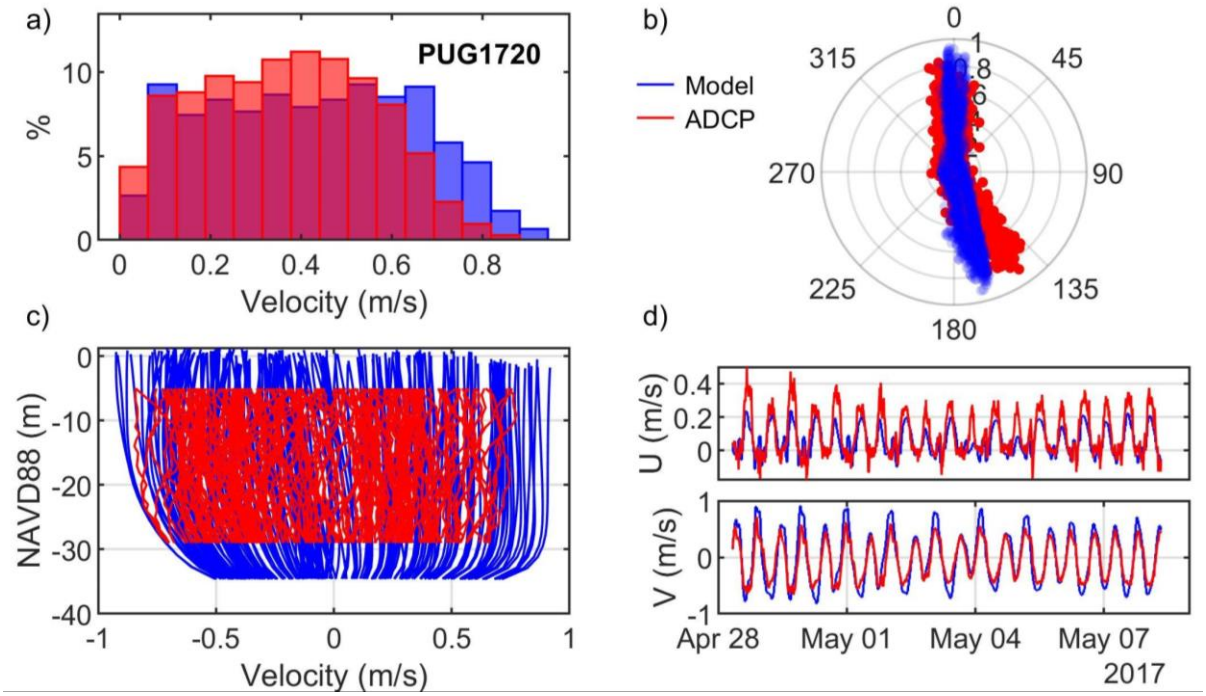

Figure A.109. Comparisons of simulated and observed velocities at Spring Passage (PUG1720): (a) velocity histograms, (b) scatter plot, (c) vertical profiles, and (d) time series of depth-averaged principal velocities.

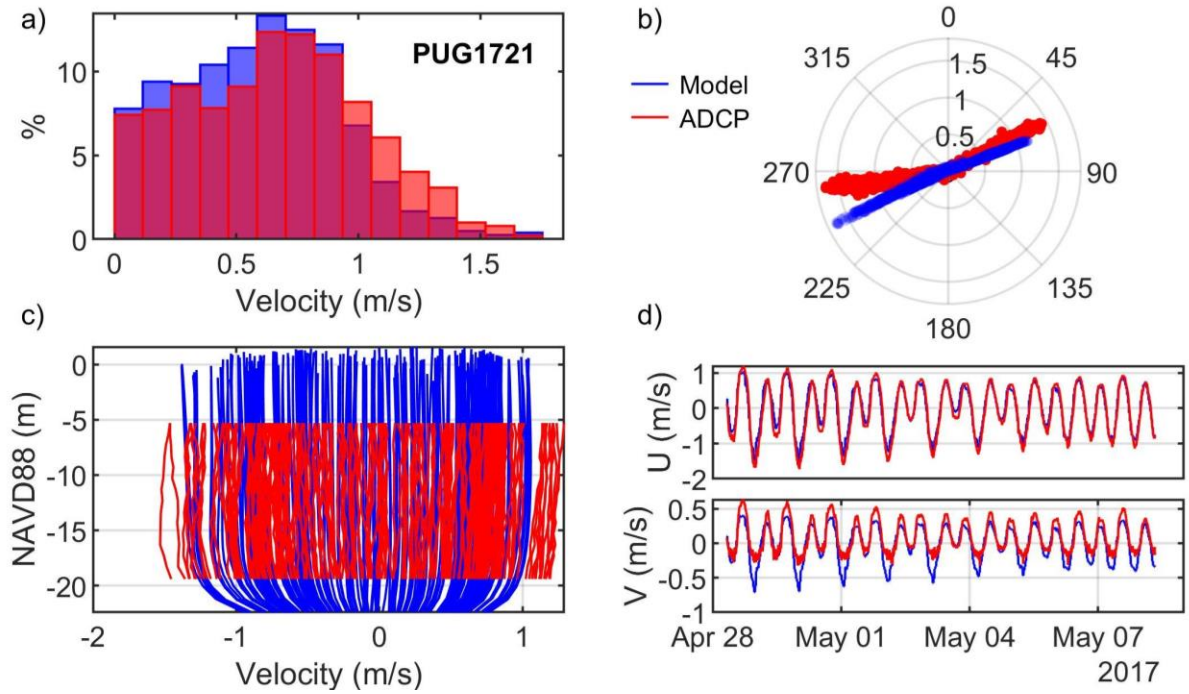

Figure A.110. Comparisons of simulated and observed velocities at Wasp Passage (PUG1721): (a) velocity histograms, (b) scatter plot, (c) vertical profiles, and (d) time series of depth-averaged principal velocities.

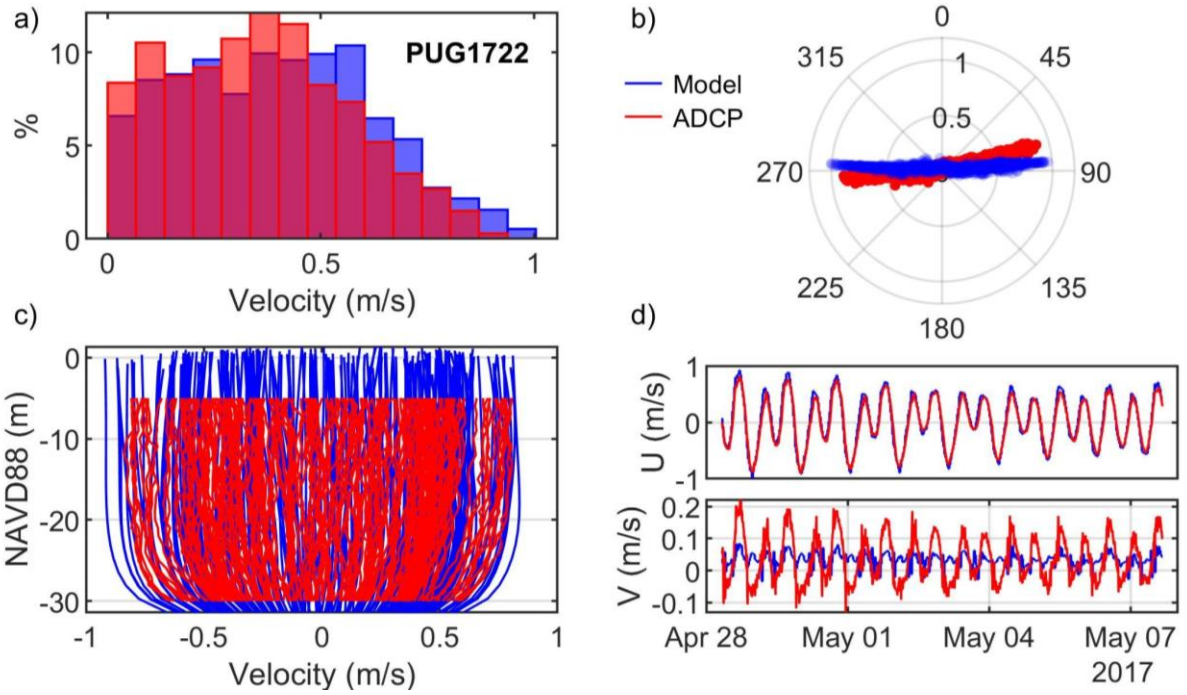

Figure A.111. Comparisons of simulated and observed velocities at Harney Channel (PUG1722): (a) velocity histograms, (b) scatter plot, (c) vertical profiles, and (d) time series of depth-averaged principal velocities.

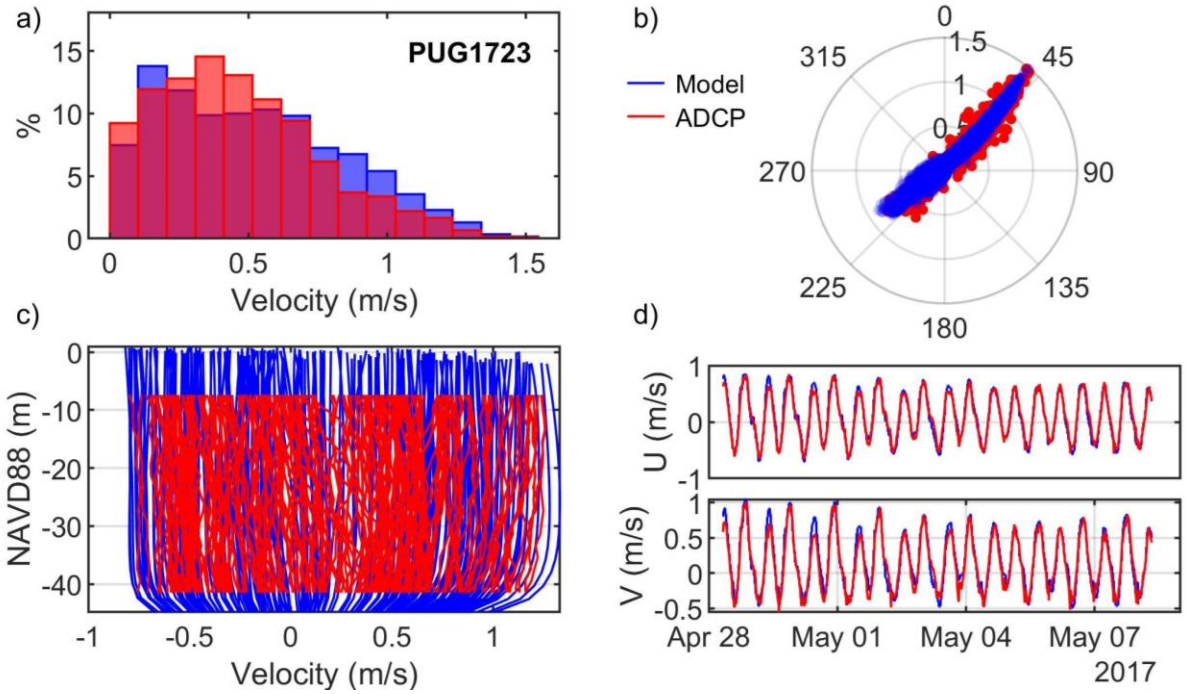

Figure A.112. Comparisons of simulated and observed velocities at Upright Channel (PUG1723): (a) velocity histograms, (b) scatter plot, (c) vertical profiles, and (d) time series of depth-averaged principal velocities.

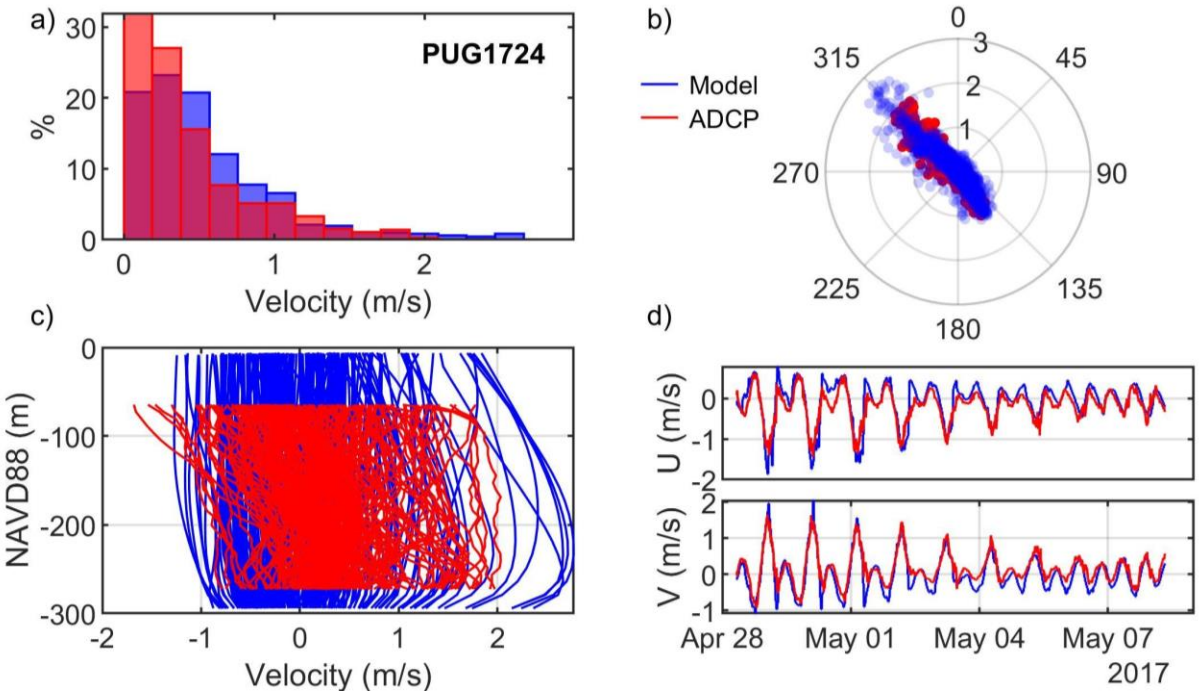

Figure A.113. Comparisons of simulated and observed velocities at South Haro Strait (PUG1724): (a) velocity histograms, (b) scatter plot, (c) vertical profiles, and (d) time series of depth-averaged principal velocities.

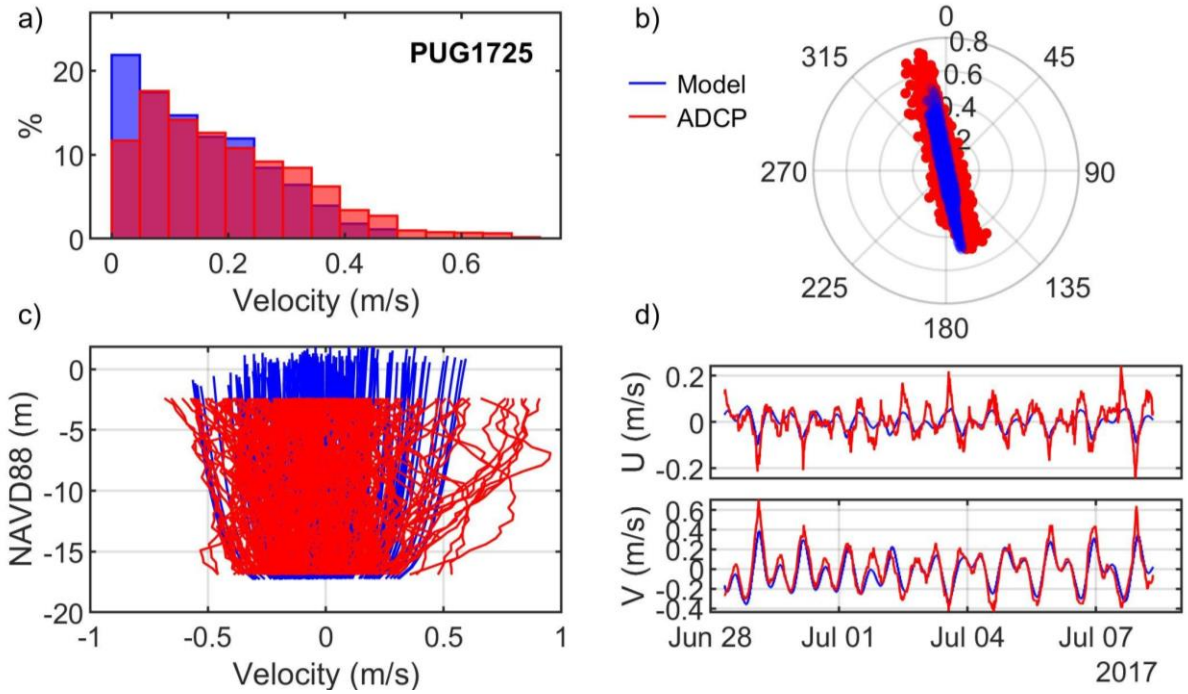

Figure A.114. Comparisons of simulated and observed velocities at Cherry Point (PUG1725): (a) velocity histograms, (b) scatter plot, (c) vertical profiles, and (d) time series of depth-averaged principal velocities.

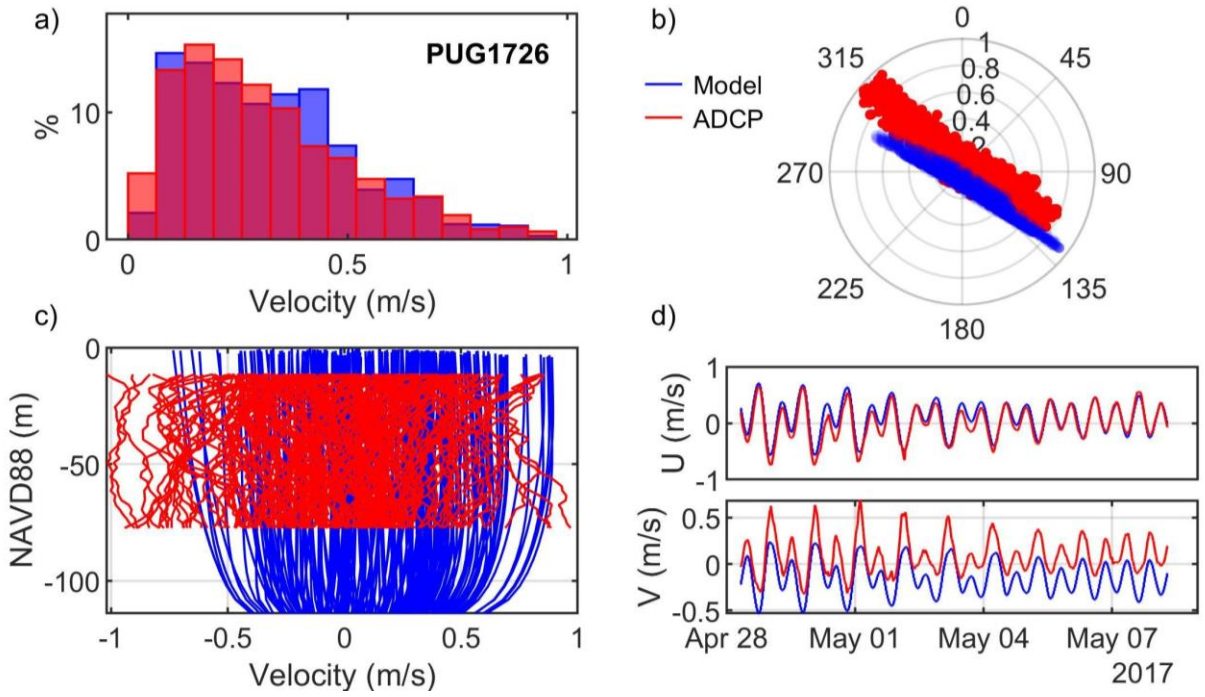

Figure A.115. Comparisons of simulated and observed velocities at Strait of Georgia (PUG1726): (a) velocity histograms, (b) scatter plot, (c) vertical profiles, and (d) time series of depth-averaged principal velocities.

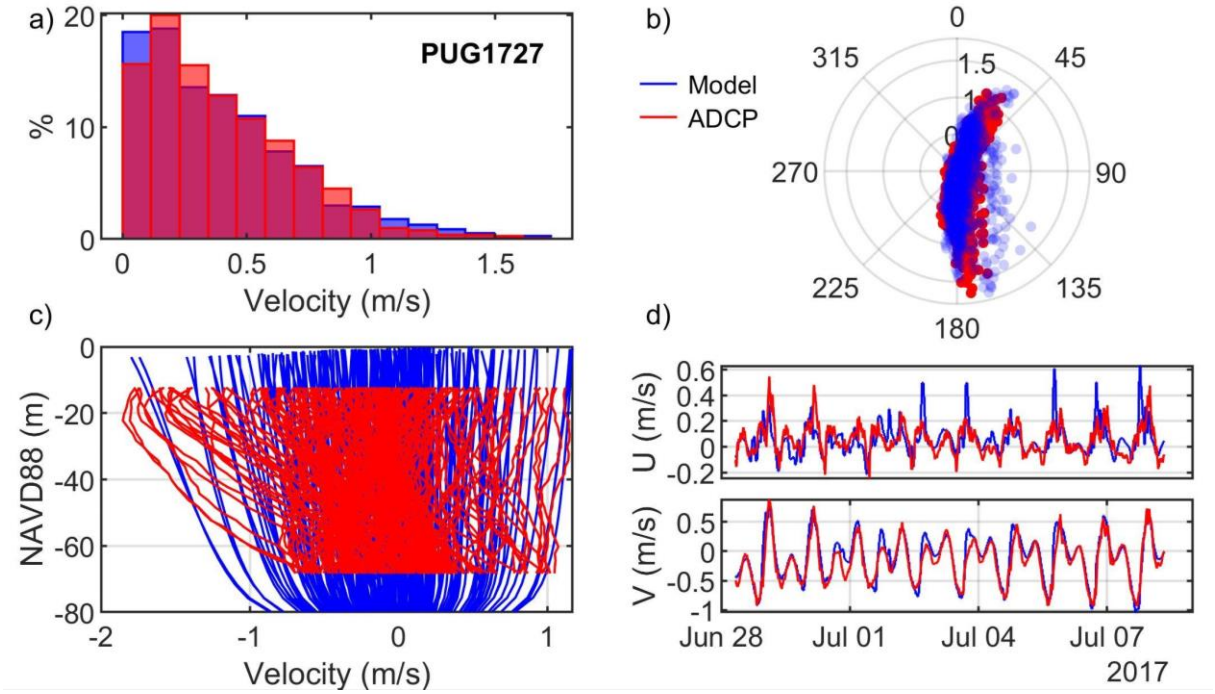

Figure A.116. Comparisons of simulated and observed velocities at Point Colville (PUG1727): (a) velocity histograms, (b) scatter plot, (c) vertical profiles, and (d) time series of depth-averaged principal velocities.

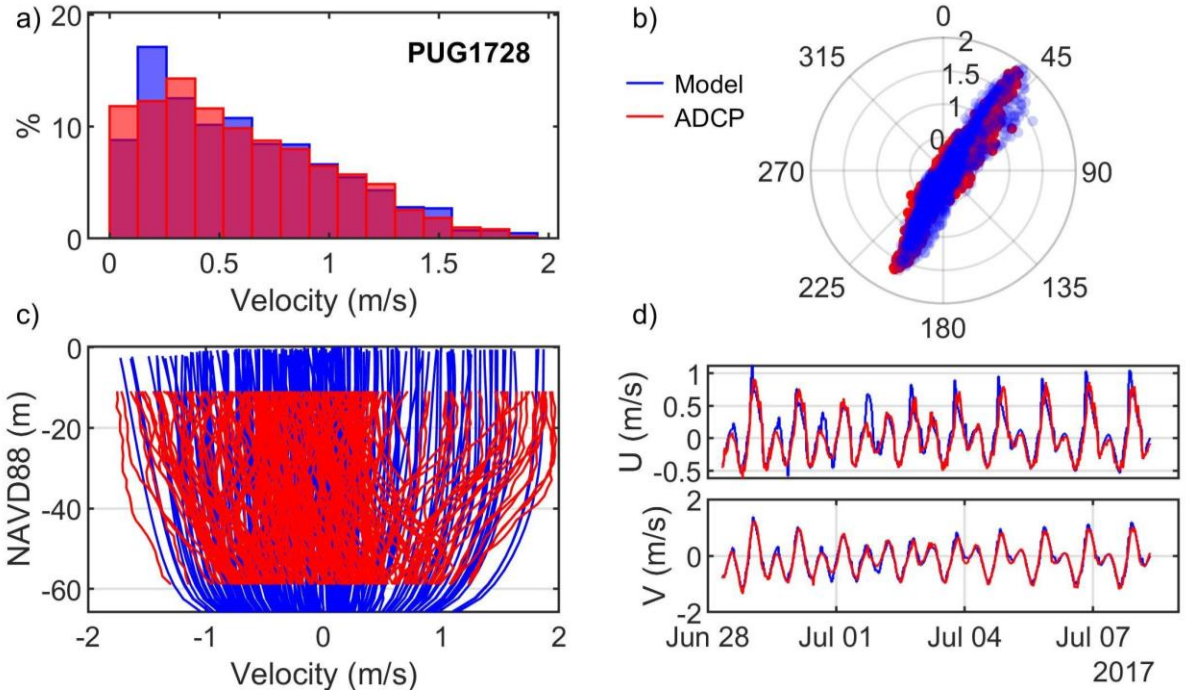

Figure A.117. Comparisons of simulated and observed velocities at Point Colville (PUG1728): (a) velocity histograms, (b) scatter plot, (c) vertical profiles, and (d) time series of depth-averaged principal velocities.

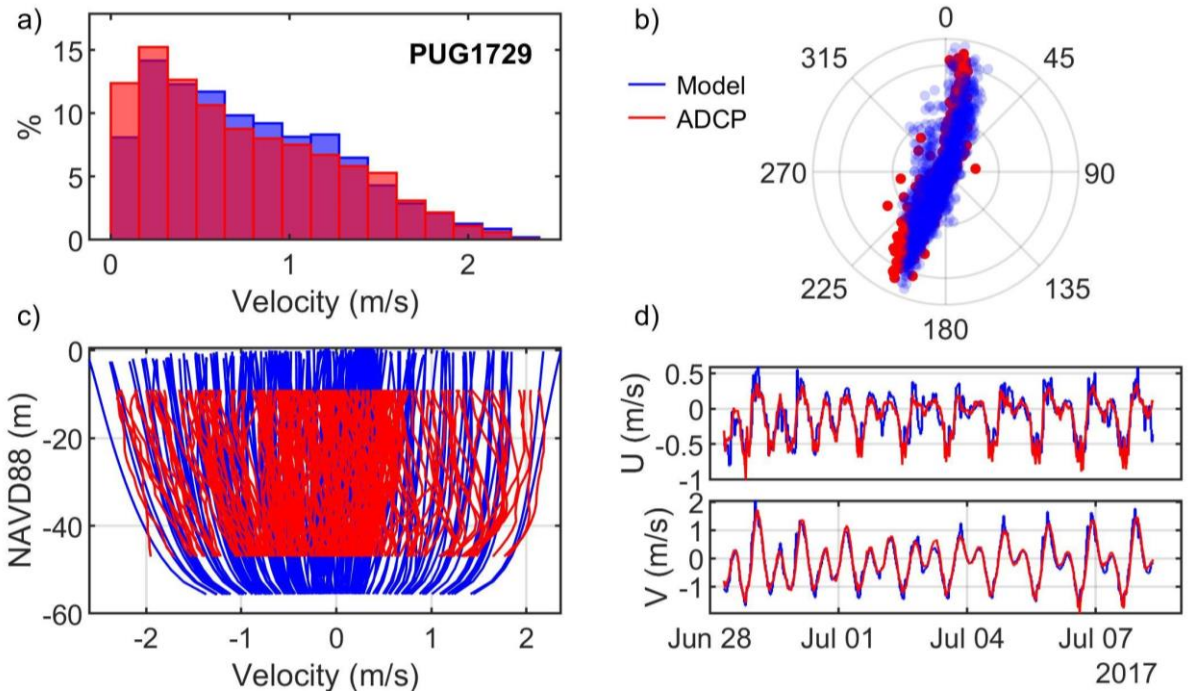

Figure A.118. Comparisons of simulated and observed velocities at Belle Rock Lighthouse (PUG1729): (a) velocity histograms, (b) scatter plot, (c) vertical profiles, and (d) time series of depth-averaged principal velocities.

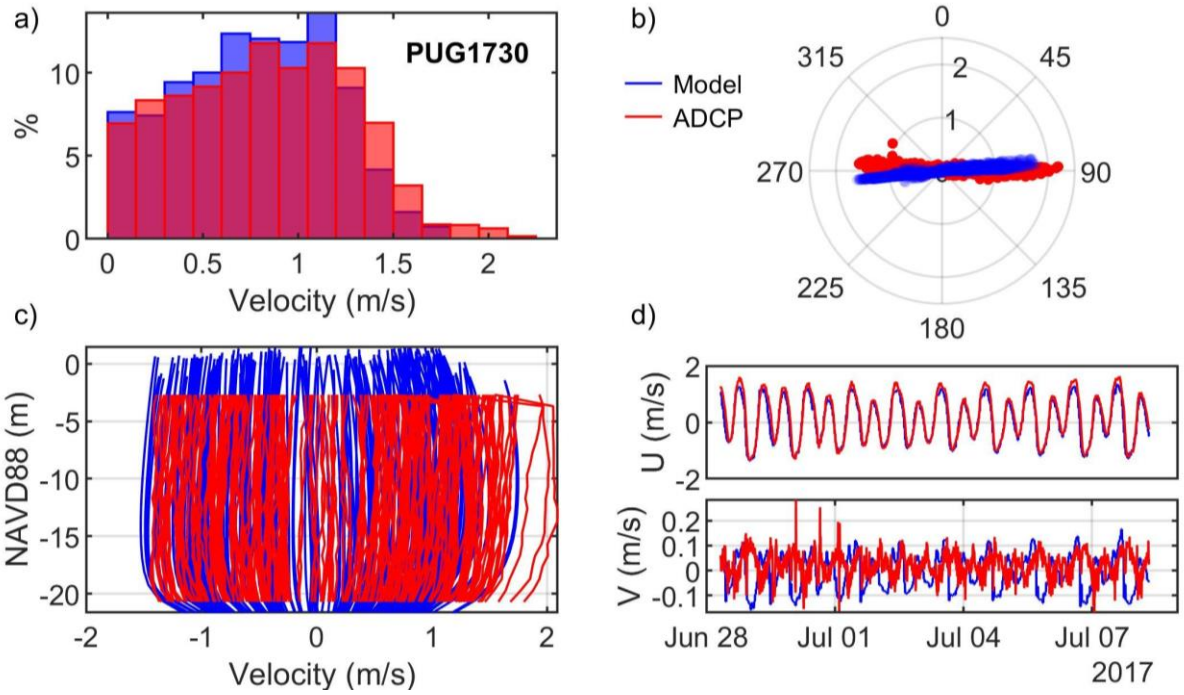

Figure A.119. Comparisons of simulated and observed velocities at Lopez Pass (PUG1730): (a) velocity histograms, (b) scatter plot, (c) vertical profiles, and (d) time series of depth-averaged principal velocities.

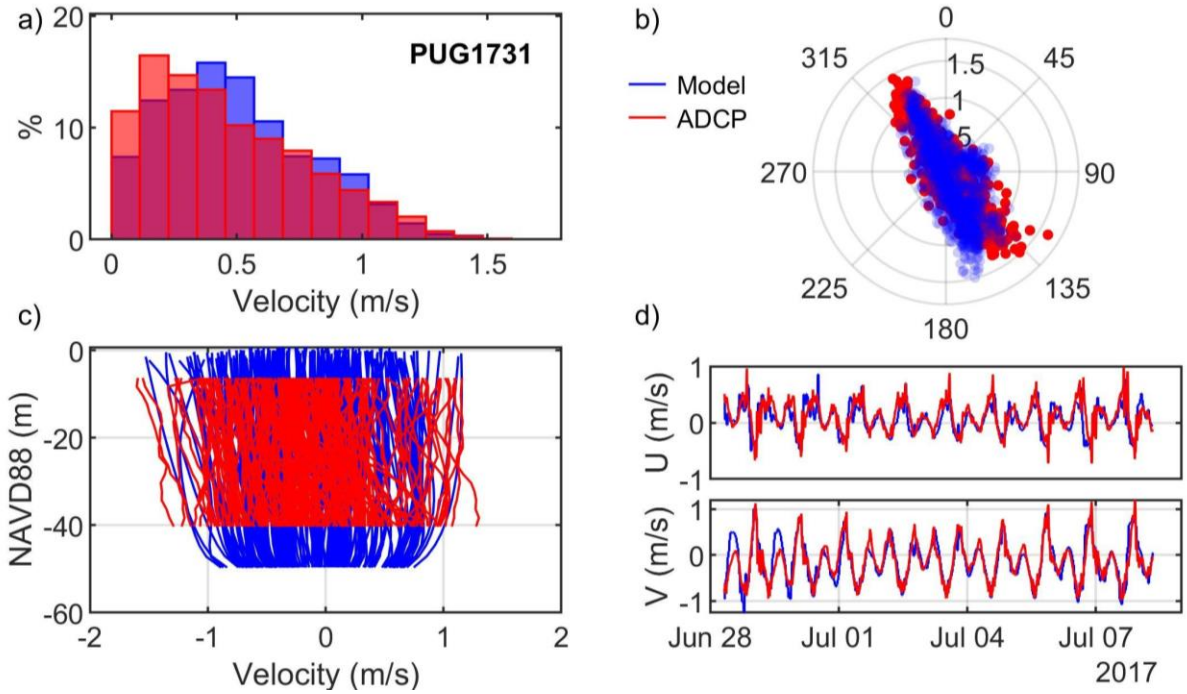

Figure A.120. Comparisons of simulated and observed velocities at Fauntleroy Point Lighthouse (PUG1731): (a) velocity histograms, (b) scatter plot, (c) vertical profiles, and (d) time series of depth-averaged principal velocities.

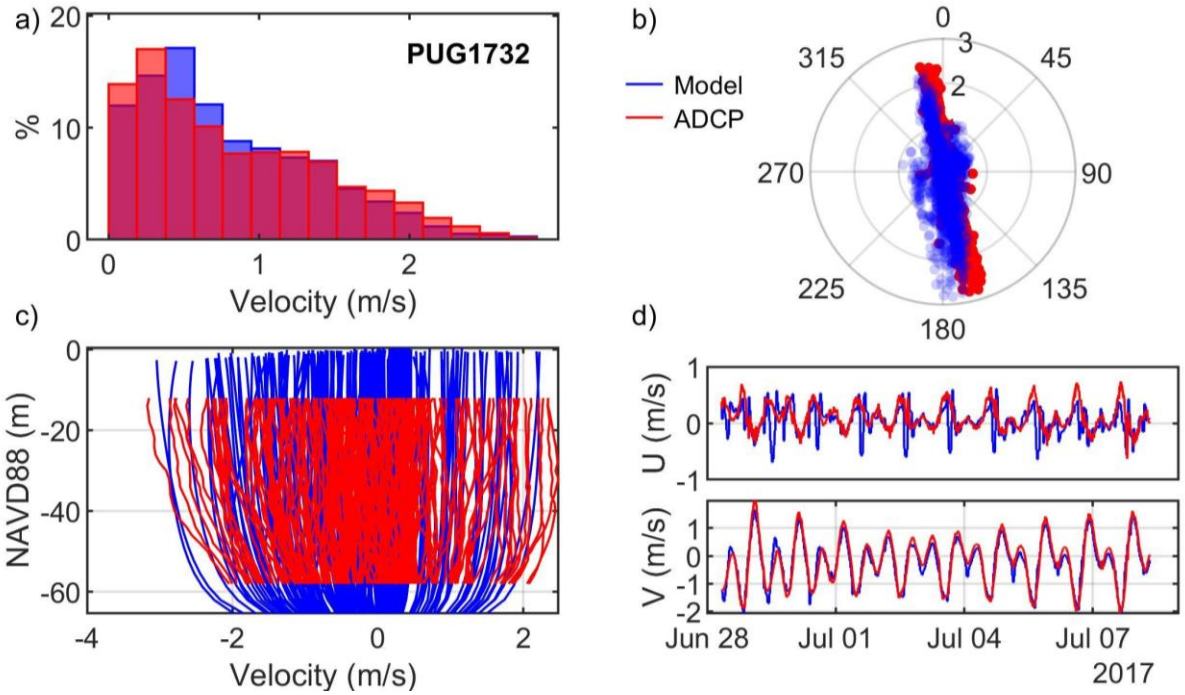

Figure A.121. Comparisons of simulated and observed velocities at Strawberry Island (PUG1732): (a) velocity histograms, (b) scatter plot, (c) vertical profiles, and (d) time series of depth-averaged principal velocities.

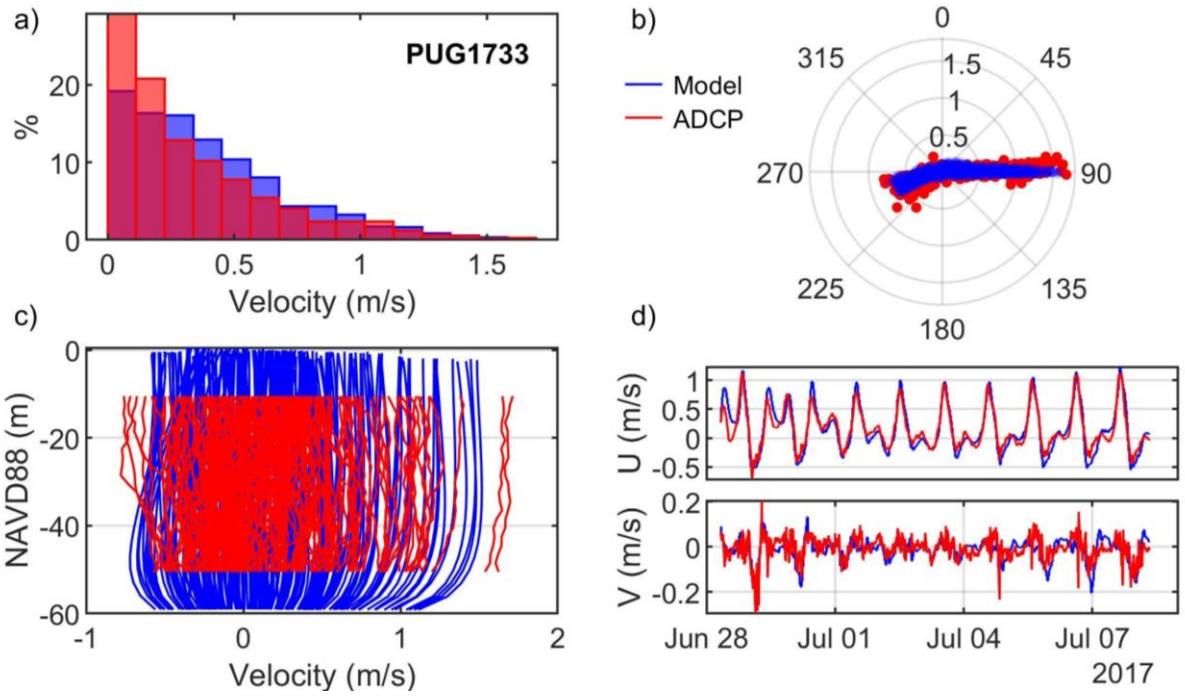

Figure A.122. Comparisons of simulated and observed velocities at Thatcher Pass (PUG1733): (a) velocity histograms, (b) scatter plot, (c) vertical profiles, and (d) time series of depth-averaged principal velocities.

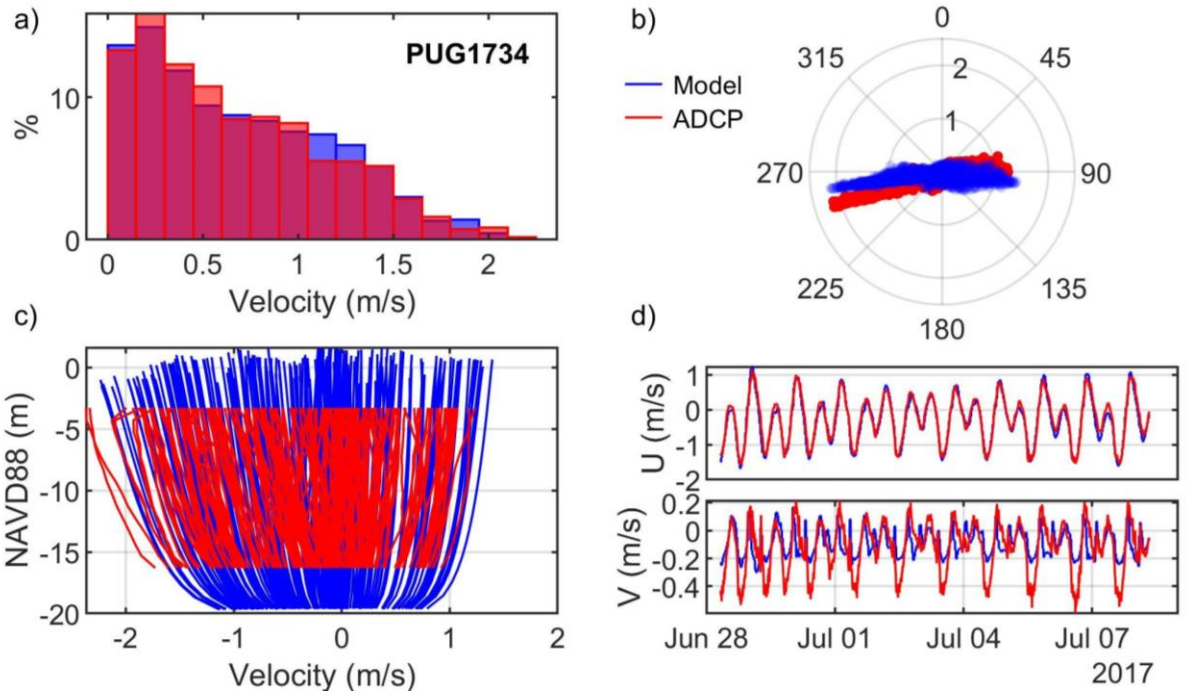

Figure A.123. Comparisons of simulated and observed velocities at Guemes Channel (PUG1734): (a) velocity histograms, (b) scatter plot, (c) vertical profiles, and (d) time series of depth-averaged principal velocities.

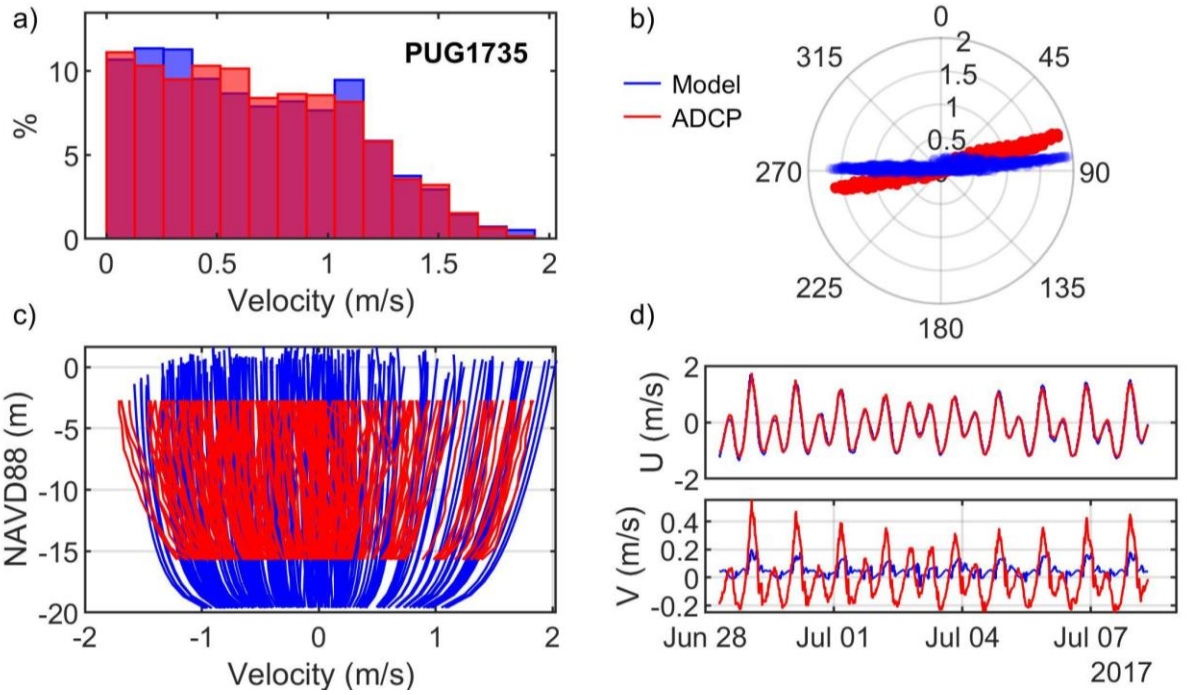

Figure A.124. Comparisons of simulated and observed velocities at Guemes Channel (PUG1735): (a) velocity histograms, (b) scatter plot, (c) vertical profiles, and (d) time series of depth-averaged principal velocities.

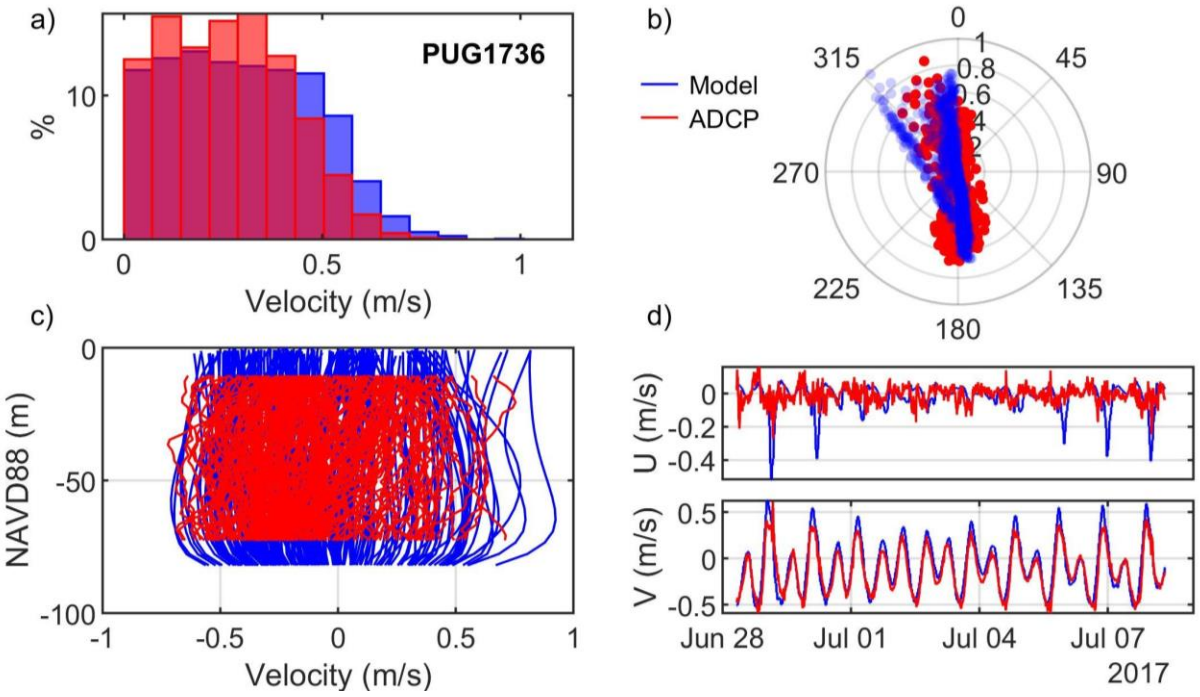

Figure A.125. Comparisons of simulated and observed velocities at Saddle Bag Island (PUG1736): (a) velocity histograms, (b) scatter plot, (c) vertical profiles, and (d) time series of depth-averaged principal velocities.

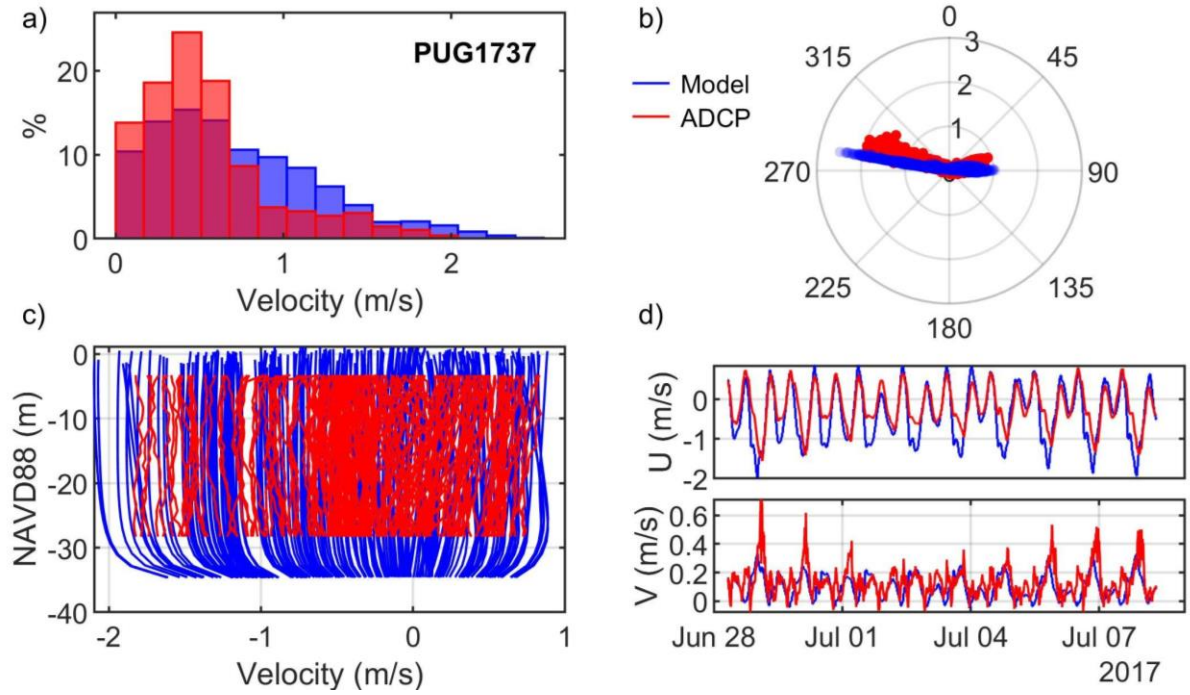

Figure A.126. Comparisons of simulated and observed velocities at Allan Pass (PUG1737): (a) velocity histograms, (b) scatter plot, (c) vertical profiles, and (d) time series of depth-averaged principal velocities.

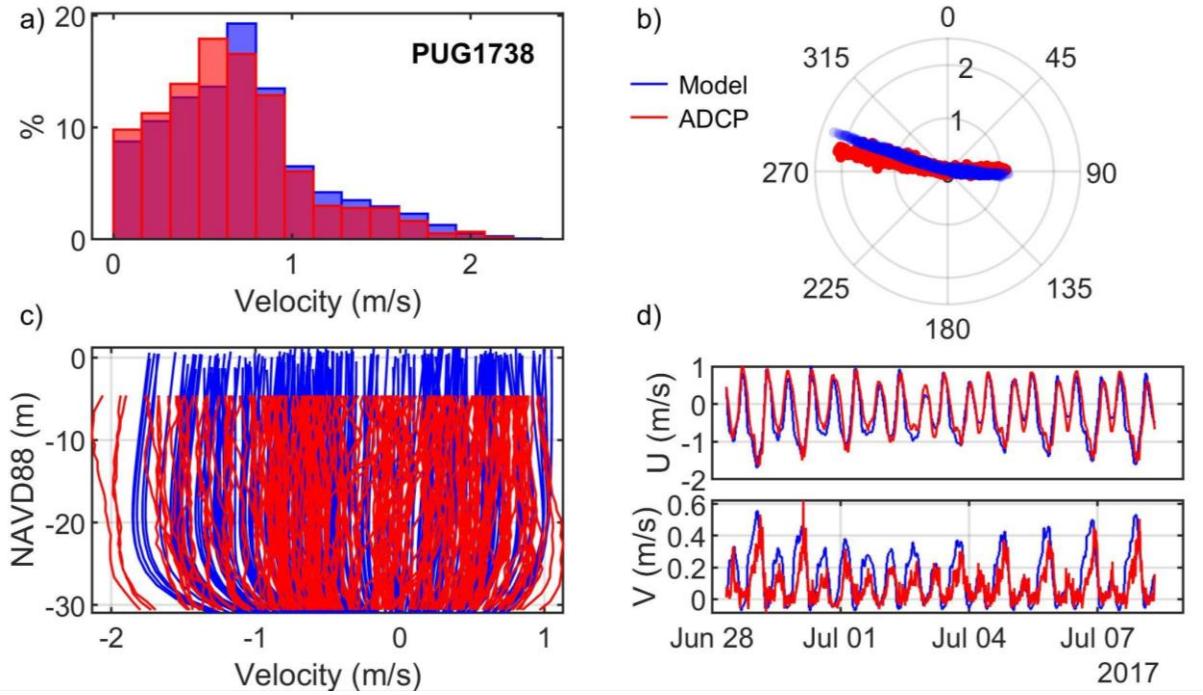

Figure A.127. Comparisons of simulated and observed velocities at Burrows Pass (PUG1738): (a) velocity histograms, (b) scatter plot, (c) vertical profiles, and (d) time series of depth-averaged principal velocities.

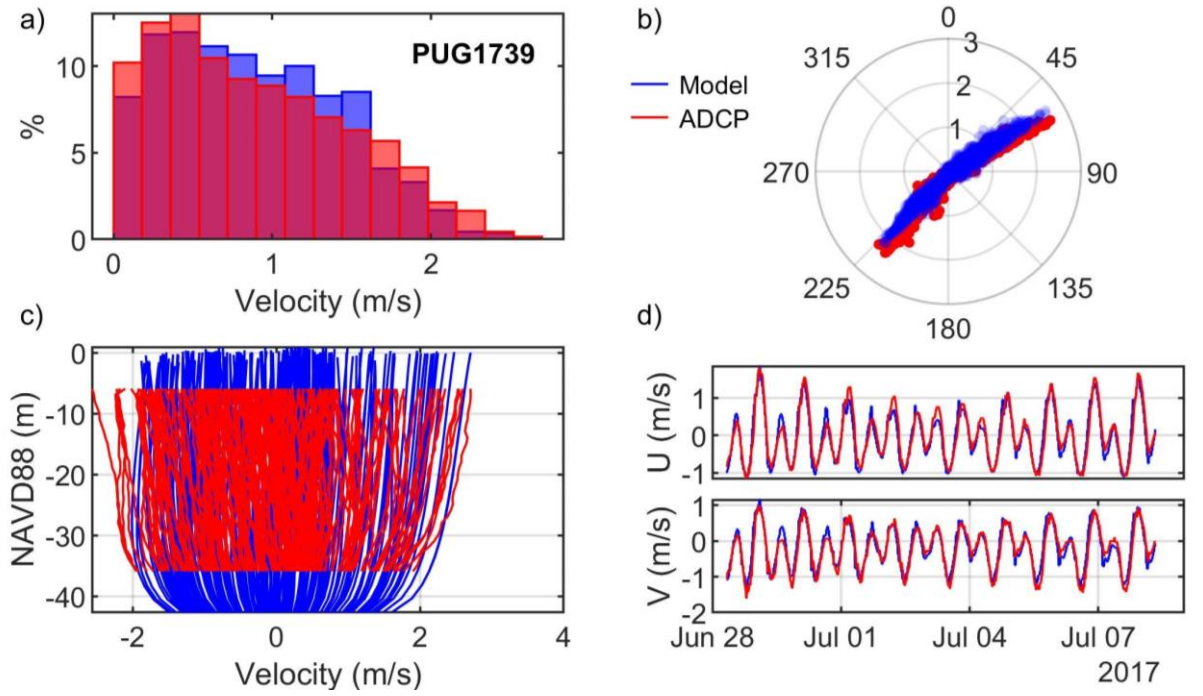

Figure A.128. Comparisons of simulated and observed velocities at Bellingham Channel (PUG1739): (a) velocity histograms, (b) scatter plot, (c) vertical profiles, and (d) time series of depth-averaged principal velocities.

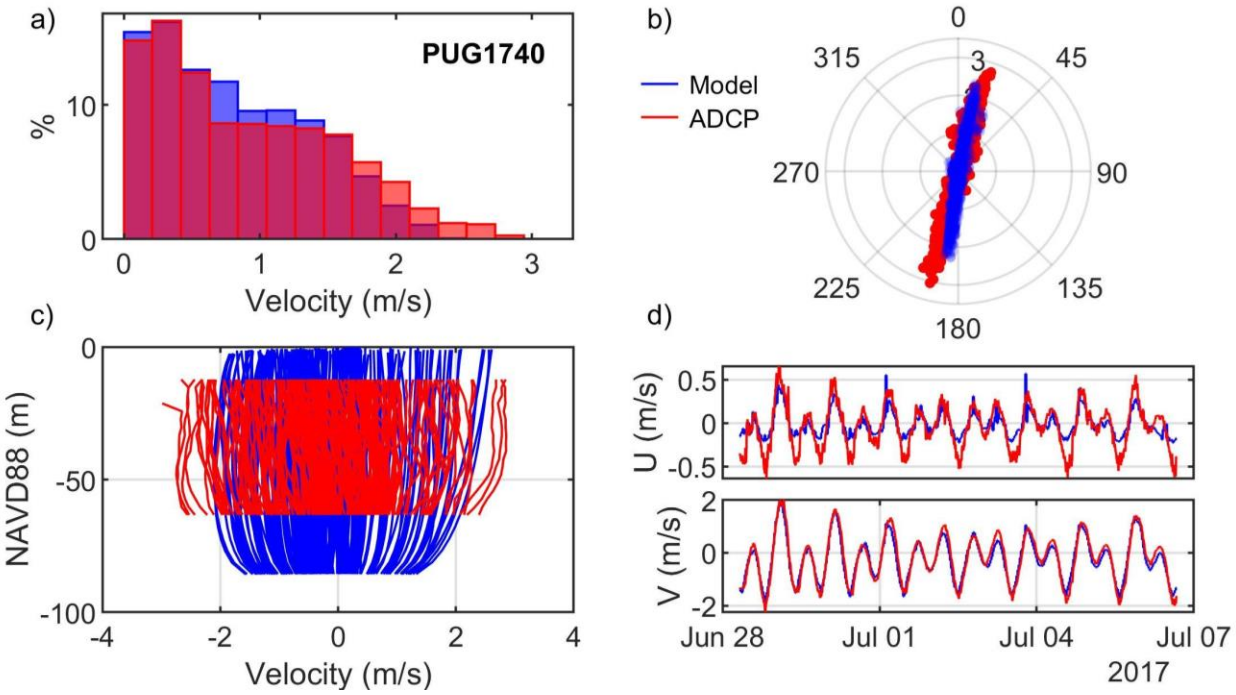

Figure A.129. Comparisons of simulated and observed velocities at Bellingham Channel (PUG1740): (a) velocity histograms, (b) scatter plot, (c) vertical profiles, and (d) time series of depth-averaged principal velocities.

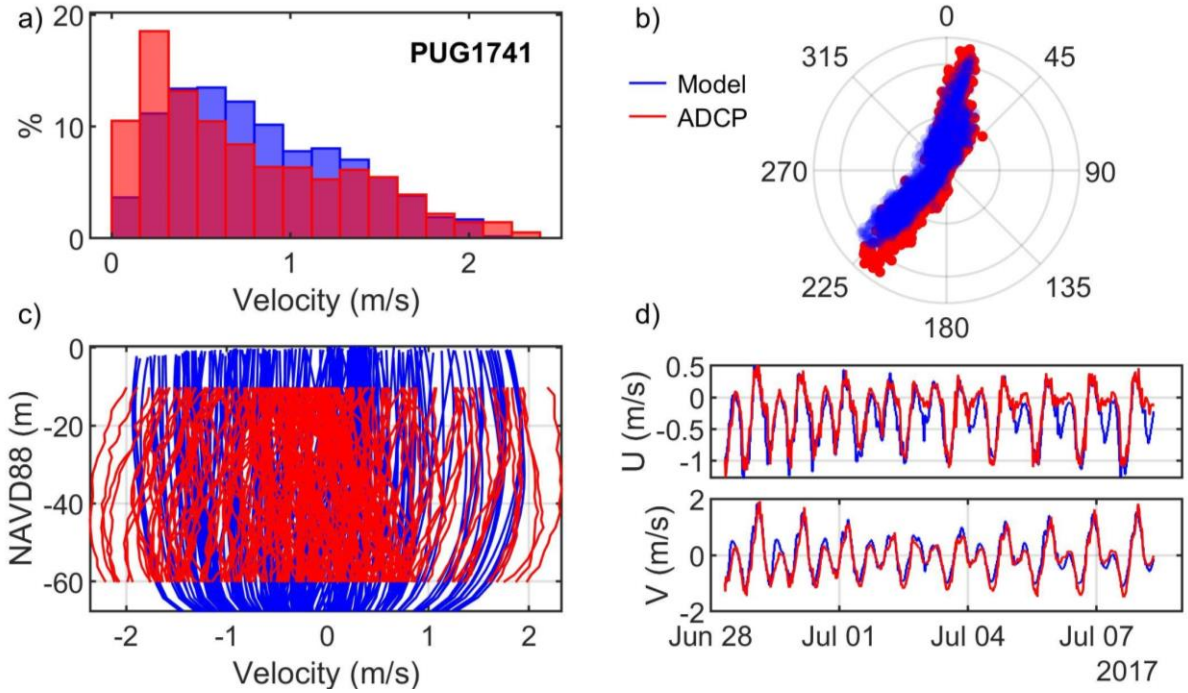

Figure A.130. Comparisons of simulated and observed velocities at Bellingham Channel (PUG1741): (a) velocity histograms, (b) scatter plot, (c) vertical profiles, and (d) time series of depth-averaged principal velocities.

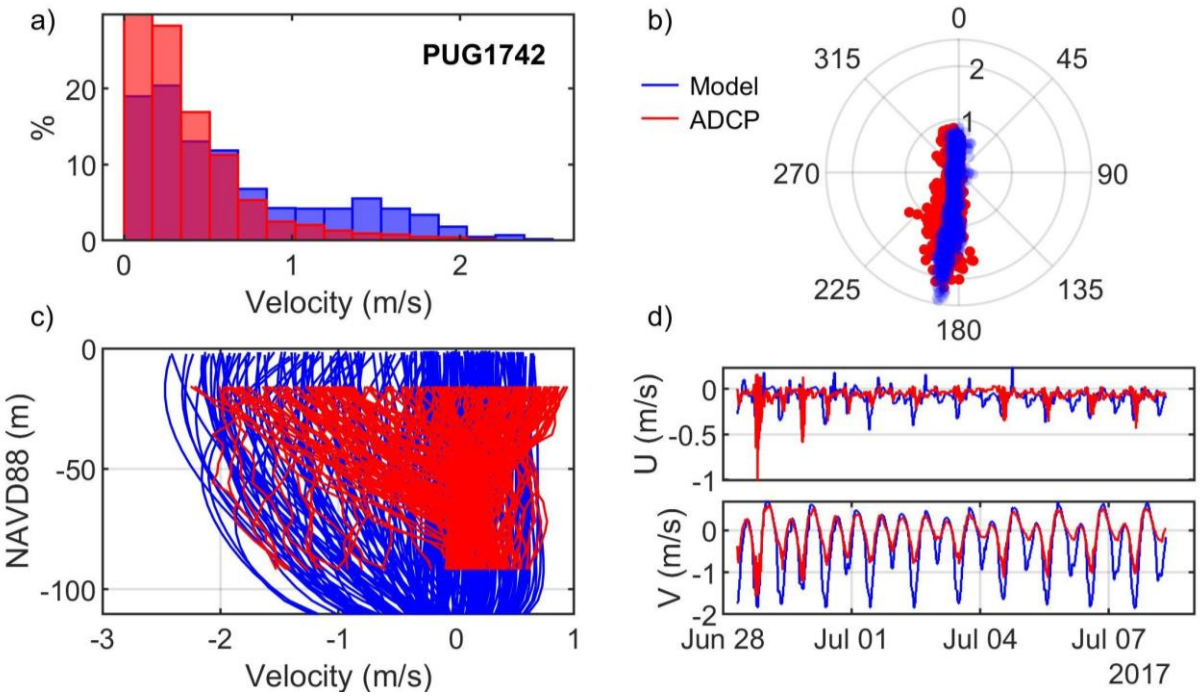

Figure A.131. Comparisons of simulated and observed velocities at Cattle Point (PUG1742): (a) velocity histograms, (b) scatter plot, (c) vertical profiles, and (d) time series of depth-averaged principal velocities.

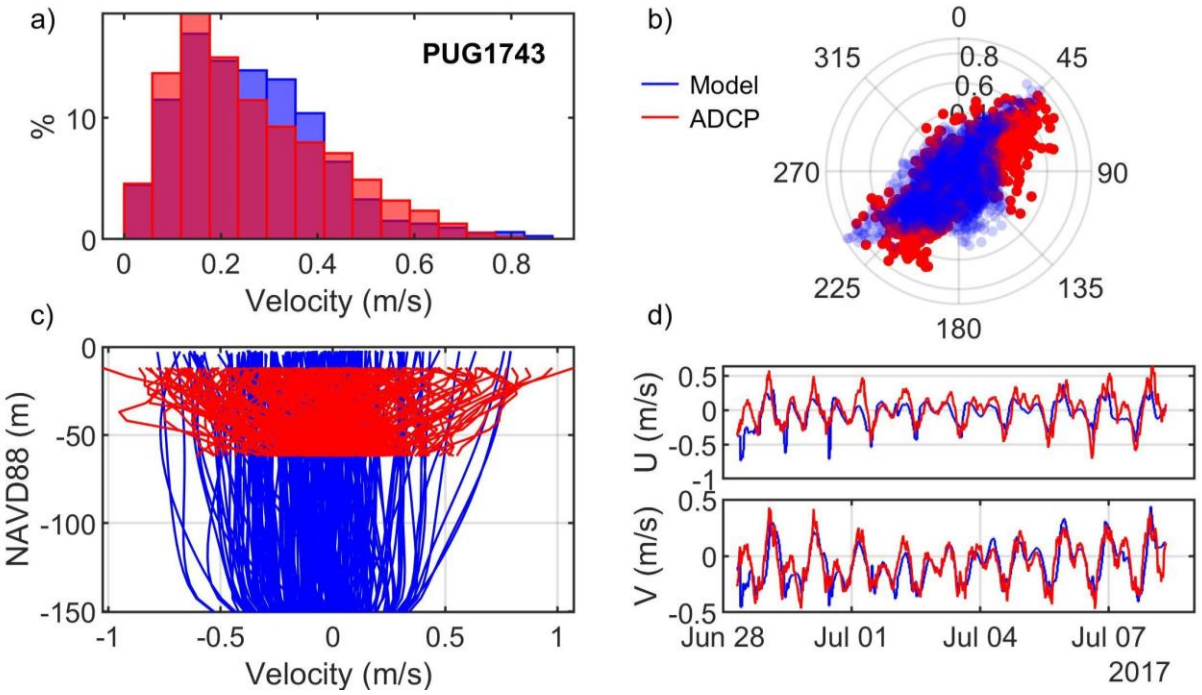

Figure A.132. Comparisons of simulated and observed velocities at Cattle Point (PUG1743): (a) velocity histograms, (b) scatter plot, (c) vertical profiles, and (d) time series of depth-averaged principal velocities.

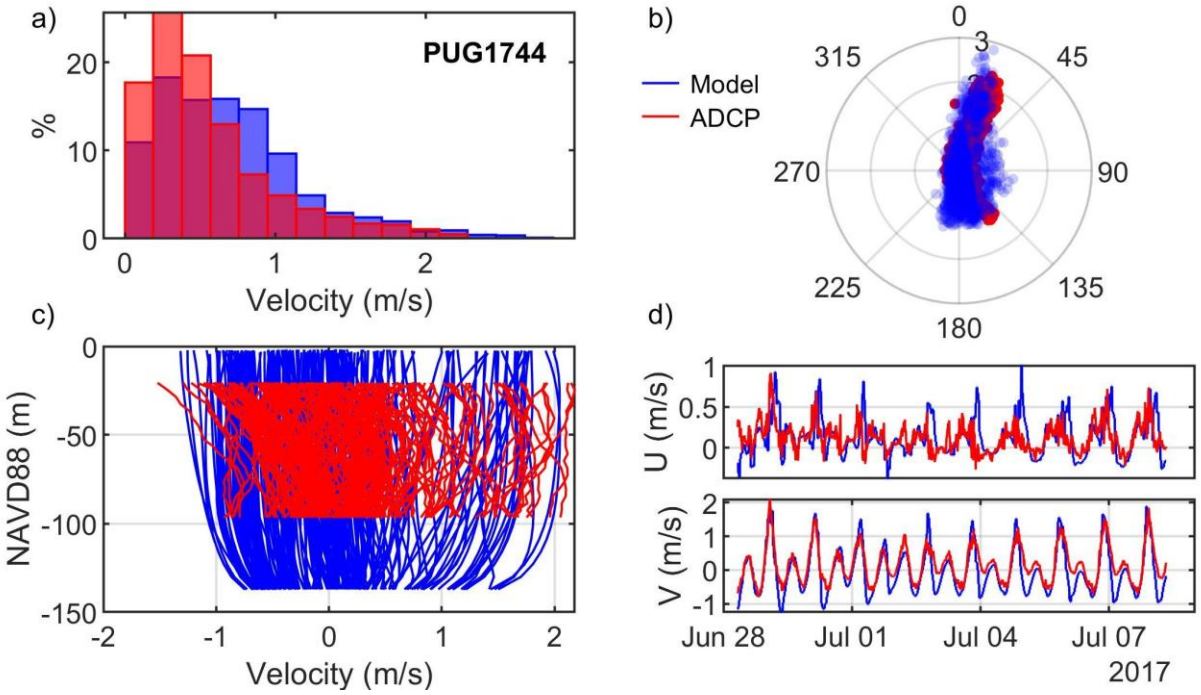

Figure A.133. Comparisons of simulated and observed velocities at Discovery Island (PUG1744): (a) velocity histograms, (b) scatter plot, (c) vertical profiles, and (d) time series of depth-averaged principal velocities.

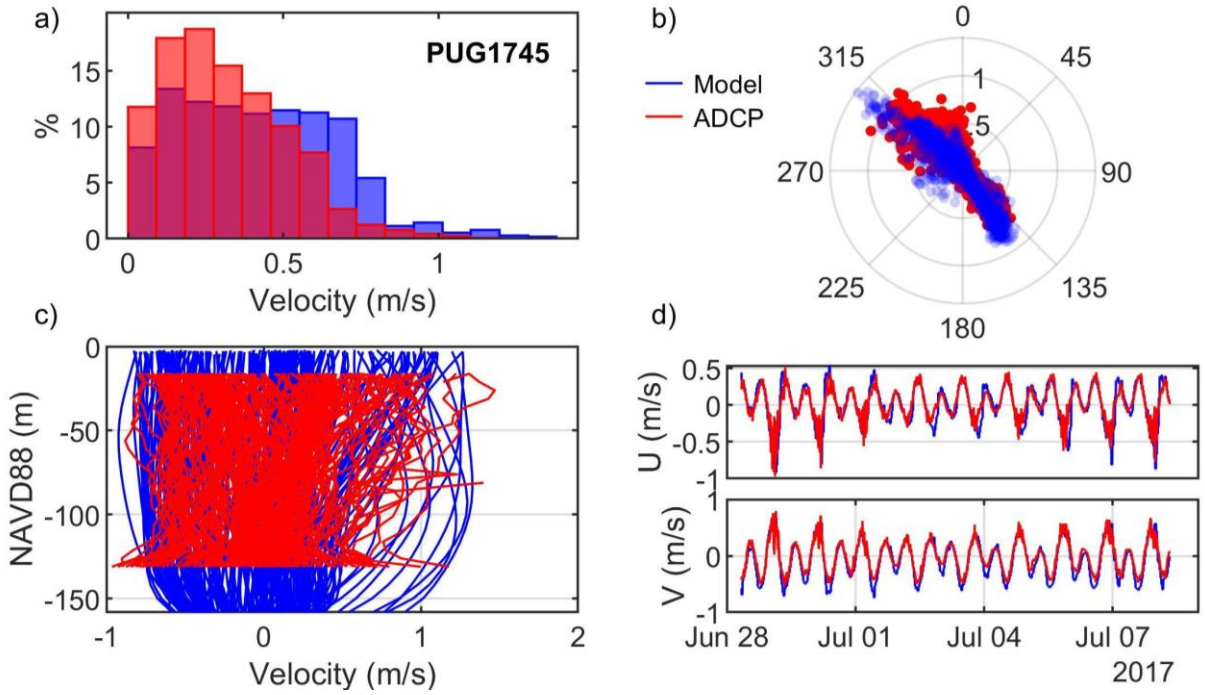

Figure A.134. Comparisons of simulated and observed velocities at Point George (PUG1745): (a) velocity histograms, (b) scatter plot, (c) vertical profiles, and (d) time series of depth-averaged principal velocities.

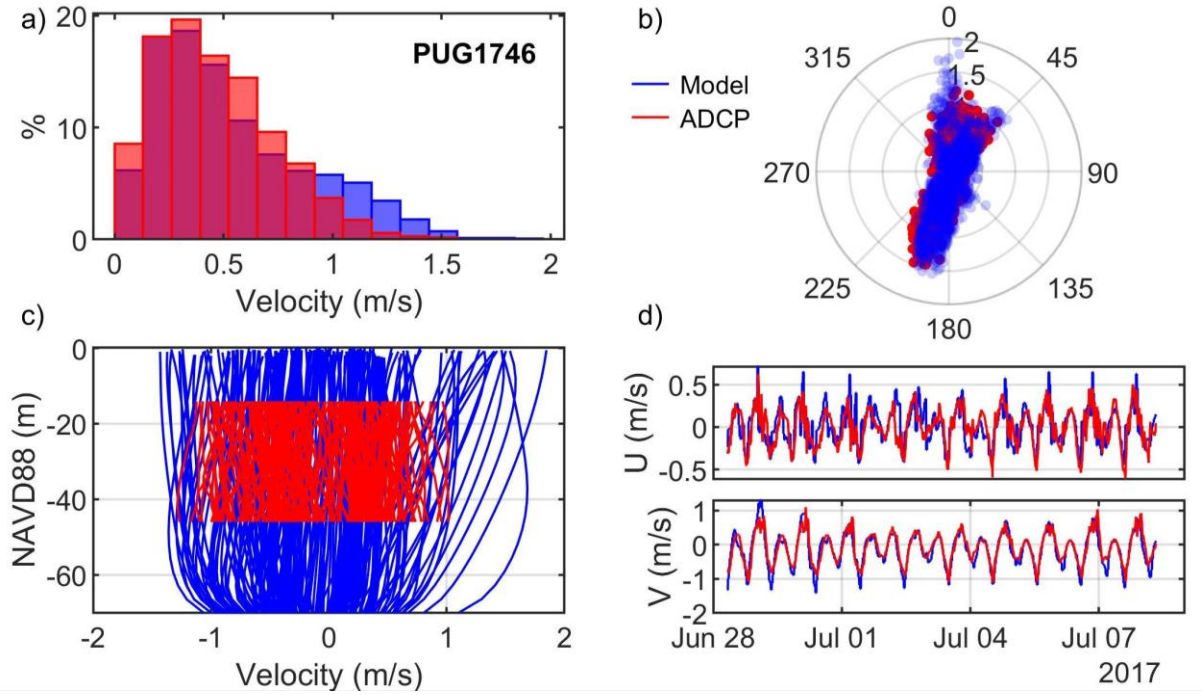

Figure A.135. Comparisons of simulated and observed velocities at Pear Point (PUG1746): (a) velocity histograms, (b) scatter plot, (c) vertical profiles, and (d) time series of depth-averaged principal velocities.

Appendix B – Error Statistics Parameters

This appendix summarizes the error statistics parameters of simulated velocities at all 135 acoustic Doppler current profiler stations.

Table B.1. Error statistics for modeled tidal currents.

	RMSE (m/s)			SI			Bias (m/s)			R		
ID	top	mid	bot	top	mid	bot	top	mid	bot	top	mid	bot
1501	0.26	0.24	0.21	0.29	0.29	0.30	-0.03	-0.02	0.00	0.97	0.97	0.97
1502	0.17	0.09	0.17	0.90	0.67	0.93	-0.15	0.06	0.14	0.81	0.89	0.86
1503	0.20	0.08	0.14	1.14	0.48	0.76	-0.17	0.02	0.10	0.78	0.91	0.85
1504	0.06	0.06	0.03	1.25	1.16	0.76	0.03	0.05	0.01	0.29	0.73	0.18
1505	0.05	0.04	0.04	0.79	0.77	1.00	0.00	-0.01	-0.02	0.83	0.82	0.66
1506	0.06	0.05	0.05	1.00	1.33	1.43	-0.03	0.01	0.01	0.70	0.70	0.51
1507	0.09	0.06	0.08	0.93	0.77	0.99	-0.04	0.05	0.07	0.79	0.92	0.80
1508	0.08	0.08	0.07	0.30	0.30	0.30	0.00	0.03	0.03	0.98	0.98	0.97
1509	0.27	0.21	0.16	0.86	0.67	0.54	-0.15	-0.08	-0.02	0.82	0.86	0.90
1510	0.38	0.31	0.26	0.43	0.37	0.35	-0.04	-0.02	-0.01	0.99	0.99	0.99
1511	0.20	0.08	0.13	1.07	0.50	0.69	-0.15	-0.01	0.11	0.73	0.91	0.92
1512	0.27	0.22	0.17	1.15	1.02	0.84	-0.19	-0.13	-0.05	0.83	0.90	0.92
1513	0.18	0.18	0.17	0.75	0.71	0.67	-0.03	-0.02	-0.01	0.82	0.82	0.83
1514	0.14	0.13	0.13	0.17	0.16	0.17	-0.05	-0.05	-0.04	0.99	0.99	0.99
1515	0.24	0.20	0.19	1.25	1.01	1.04	0.04	0.05	0.03	0.75	0.84	0.84
1516	0.20	0.18	0.15	0.99	0.86	0.62	-0.07	-0.05	0.01	0.82	0.84	0.89
1517	0.12	0.12	0.17	0.36	0.43	0.72	0.01	0.07	0.12	0.92	0.94	0.89
1518	0.09	0.08	0.13	0.30	0.28	0.49	-0.01	0.01	0.07	0.94	0.95	0.93
1519	0.19	0.13	0.24	0.62	0.39	0.72	0.07	0.05	0.11	0.77	0.90	0.75
1520	0.15	0.09	0.10	0.99	0.96	1.14	-0.04	0.01	0.03	0.73	0.67	0.53
1521	0.12	0.11	0.12	0.88	0.84	0.90	-0.01	-0.04	-0.03	0.62	0.72	0.67
1522	0.18	0.15	0.22	0.61	0.52	0.69	0.00	-0.05	-0.13	0.76	0.87	0.90
1523	0.14	0.15	0.13	0.66	0.63	0.64	-0.02	-0.01	0.00	0.84	0.86	0.84
1524	0.25	0.19	0.19	0.26	0.19	0.20	0.02	0.01	-0.01	0.98	0.99	0.99
1525	0.24	0.23	0.22	0.25	0.25	0.27	-0.01	-0.01	0.00	0.93	0.93	0.92
1526	0.33	0.26	0.22	0.41	0.33	0.30	-0.08	-0.02	0.04	0.93	0.95	0.96
1527	0.35	0.28	0.24	0.26	0.22	0.22	-0.16	-0.06	0.00	0.98	0.98	0.99
1528	0.30	0.26	0.24	0.24	0.22	0.23	-0.11	-0.04	-0.01	0.98	0.99	0.98
1529	0.19	0.11	0.16	0.78	0.50	0.74	0.11	0.00	-0.09	0.89	0.92	0.86
1530	0.18	0.18	0.15	0.35	0.36	0.38	0.08	0.10	0.06	0.97	0.96	0.94
1531	0.45	0.42	0.35	0.63	0.55	0.52	-0.10	-0.01	0.03	0.88	0.89	0.90

	RMSE (m/s)			SI			Bias (m/s)			R		
ID	top	mid	bot	top	mid	bot	top	mid	bot	top	mid	bot
1532	0.20	0.21	0.23	1.53	1.73	1.82	-0.02	0.09	0.10	0.25	0.31	0.27
1533	0.16	0.12	0.12	1.23	1.11	0.78	-0.11	-0.01	0.02	0.76	0.72	0.75
1534	0.21	0.26	0.28	0.47	0.58	0.72	-0.03	0.00	0.00	0.92	0.87	0.82
1535	0.33	0.34	0.32	0.49	0.52	0.62	0.03	0.02	0.01	0.92	0.91	0.90
1536	0.16	0.15	0.13	0.43	0.41	0.41	0.03	0.02	0.01	0.94	0.94	0.94
1537	0.09	0.10	0.10	0.66	0.74	0.85	-0.02	0.02	-0.02	0.86	0.84	0.79
1538	0.16	0.09	0.09	1.02	0.58	0.53	0.11	-0.03	-0.03	0.78	0.88	0.91
1539	0.19	0.16	0.16	0.30	0.24	0.26	-0.07	-0.03	0.03	0.97	0.98	0.98
1540	0.07	0.08	0.09	0.50	0.64	0.85	0.02	0.03	0.04	0.92	0.91	0.86
1541	0.09	0.11	0.11	0.62	0.77	0.98	0.00	0.00	-0.01	0.85	0.76	0.66
1542	0.16	0.15	0.14	0.97	1.04	1.13	0.01	-0.02	-0.02	0.68	0.64	0.59
1543	0.29	0.29	0.28	0.60	0.60	0.62	0.03	0.04	0.05	0.87	0.87	0.87
1544	0.23	0.21	0.21	0.58	0.54	0.55	0.00	0.05	0.05	0.89	0.90	0.89
1545	0.74	0.70	0.59	0.81	0.82	0.79	-0.13	-0.06	-0.03	0.85	0.83	0.82
1546	0.29	0.28	0.24	0.54	0.57	0.58	0.02	0.06	0.07	0.89	0.88	0.88
1547	0.26	0.27	0.23	0.55	0.59	0.60	0.03	0.05	0.05	0.91	0.89	0.89
1548	0.09	0.13	0.17	0.46	0.62	0.77	-0.01	0.02	0.02	0.93	0.86	0.77
1601	0.10	0.09	0.07	0.47	0.42	0.34	-0.02	-0.03	0.00	0.92	0.95	0.96
1602	0.12	0.10	0.11	0.42	0.37	0.44	-0.08	0.02	0.07	0.96	0.96	0.95
1603	0.11	0.10	0.12	0.41	0.33	0.39	-0.04	0.03	0.01	0.96	0.97	0.95
1604	0.13	0.12	0.14	0.48	0.44	0.51	0.03	0.04	0.06	0.92	0.94	0.92
1605	0.09	0.08	0.06	0.72	0.76	0.56	-0.06	-0.06	-0.01	0.89	0.90	0.89
1606	0.35	0.19	0.37	1.00	0.61	1.17	-0.25	0.01	0.25	0.87	0.90	0.67
1607	0.25	0.18	0.23	0.78	0.54	0.63	0.15	0.06	-0.11	0.89	0.92	0.89
1608	0.18	0.10	0.16	0.65	0.43	0.65	-0.13	0.01	0.04	0.92	0.94	0.84
1609	0.09	0.05	0.05	0.68	0.44	0.46	-0.04	0.00	0.00	0.87	0.93	0.92
1610	0.25	0.18	0.22	0.37	0.29	0.36	0.13	0.01	-0.11	0.97	0.97	0.96
1611	0.32	0.19	0.17	0.97	0.56	0.54	-0.21	-0.07	0.01	0.85	0.91	0.89
1612	0.10	0.07	0.09	0.92	0.57	0.58	0.03	0.00	0.00	0.77	0.88	0.90
1613	0.06	0.04	0.04	1.34	1.17	1.30	0.02	0.01	0.01	0.21	0.34	0.19
1614	0.35	0.38	0.34	0.30	0.33	0.35	0.00	-0.01	-0.06	0.96	0.95	0.95
1615	0.56	0.45	0.28	0.74	0.64	0.55	-0.36	-0.27	-0.12	0.89	0.91	0.92
1616	0.33	0.20	0.28	0.44	0.27	0.41	-0.18	0.05	0.18	0.95	0.97	0.96
1617	0.36	0.30	0.31	0.45	0.36	0.39	-0.09	0.06	0.14	0.95	0.96	0.95
1618	0.10	0.06	0.07	0.64	0.51	0.66	0.02	0.01	0.00	0.87	0.91	0.85
1619	0.37	0.26	0.31	0.37	0.28	0.38	-0.10	0.04	0.11	0.95	0.98	0.96
1620	0.32	0.22	0.28	0.37	0.29	0.39	-0.20	-0.01	0.14	0.97	0.98	0.97

	RMSE (m/s)			SI			Bias (m/s)			R		
ID	top	mid	bot	top	mid	bot	top	mid	bot	top	mid	bot
1622	0.06	0.04	0.04	0.60	0.44	0.42	0.01	0.00	-0.01	0.88	0.93	0.95
1623	0.42	0.29	0.25	0.55	0.35	0.31	0.03	-0.06	-0.08	0.91	0.96	0.97
1624	0.33	0.28	0.38	0.30	0.27	0.46	0.08	-0.06	-0.14	0.97	0.98	0.97
1625	0.56	0.48	0.39	0.54	0.49	0.47	-0.23	-0.15	-0.03	0.91	0.92	0.92
1626	0.13	0.10	0.12	0.74	0.62	0.68	0.02	-0.01	0.00	0.81	0.87	0.82
1627	0.21	0.17	0.19	0.36	0.34	0.43	0.00	-0.01	-0.02	0.96	0.97	0.97
1628	0.36	0.39	0.34	0.55	0.62	0.63	-0.24	-0.23	-0.15	0.93	0.89	0.86
1629	0.36	0.33	0.30	0.38	0.35	0.32	-0.04	-0.04	-0.03	0.96	0.96	0.97
1630	0.22	0.17	0.22	0.62	0.68	0.93	0.09	-0.04	-0.07	0.89	0.85	0.71
1631	0.21	0.14	0.15	0.87	0.70	0.98	0.09	0.06	0.06	0.78	0.86	0.75
1632	0.19	0.17	0.23	0.58	0.85	1.08	0.02	0.04	-0.02	0.89	0.80	0.60
1633	0.31	0.17	0.15	0.95	0.83	1.02	0.28	0.13	-0.02	0.71	0.77	0.65
1634	0.30	0.23	0.16	0.87	0.82	0.81	0.27	0.21	0.08	0.79	0.87	0.71
1635	0.21	0.19	0.28	0.53	0.44	0.71	0.12	-0.09	-0.17	0.93	0.95	0.88
1636	0.16	0.14	0.21	0.49	0.40	0.61	-0.02	-0.01	-0.08	0.93	0.94	0.89
1637	0.29	0.20	0.41	0.44	0.37	0.80	0.23	-0.09	-0.36	0.97	0.96	0.94
1638	0.35	0.21	0.18	0.86	0.52	0.51	0.28	0.14	0.06	0.90	0.95	0.92
1639	0.56	0.46	0.40	0.83	0.73	0.76	0.31	0.20	0.14	0.87	0.90	0.92
1640	0.24	0.27	0.30	0.44	0.46	0.56	0.17	-0.21	-0.25	0.96	0.97	0.97
1641	0.26	0.23	0.17	0.64	0.57	0.61	0.17	-0.18	-0.14	0.90	0.95	0.97
1642	0.20	0.19	0.13	0.52	0.52	0.41	0.16	-0.17	-0.11	0.95	0.98	0.98
1701	0.58	0.68	0.58	0.29	0.34	0.39	0.18	0.33	0.29	0.97	0.97	0.95
1702	0.19	0.17	0.22	0.27	0.26	0.41	-0.05	-0.08	-0.13	0.98	0.98	0.97
1703	0.73	0.59	0.58	0.97	0.70	0.66	0.10	-0.01	-0.13	0.82	0.90	0.89
1704	0.50	0.50	0.43	0.63	0.65	0.67	0.16	0.14	0.12	0.91	0.91	0.91
1705	0.25	0.23	0.20	0.46	0.45	0.47	-0.07	-0.08	-0.07	0.93	0.93	0.93
1706	0.24	0.24	0.25	0.35	0.37	0.46	-0.12	-0.15	-0.17	0.97	0.97	0.97
1707	0.13	0.11	0.12	0.54	0.43	0.52	0.00	-0.01	0.00	0.87	0.91	0.86
1708	0.19	0.18	0.16	0.39	0.37	0.37	-0.04	-0.01	0.02	0.96	0.96	0.95
1709	0.22	0.19	0.23	0.53	0.45	0.56	-0.04	-0.05	0.07	0.91	0.94	0.90
1710	0.18	0.11	0.09	0.43	0.29	0.32	-0.11	-0.05	-0.03	0.96	0.98	0.97
1711	0.19	0.20	0.24	0.65	0.62	0.74	-0.04	-0.04	-0.08	0.85	0.87	0.85
1712	0.30	0.38	0.31	0.66	0.95	1.03	-0.18	-0.30	-0.24	0.90	0.88	0.86
1713	0.28	0.27	0.23	0.53	0.56	0.57	-0.10	-0.15	-0.13	0.91	0.93	0.92
1714	0.26	0.28	0.50	0.43	0.55	1.78	-0.01	-0.07	-0.32	0.93	0.91	0.74
1715	0.27	0.39	0.45	0.50	0.86	0.97	-0.12	-0.34	-0.37	0.92	0.94	0.88
1716	0.42	0.32	0.30	1.03	0.78	0.81	0.08	0.00	0.03	0.74	0.86	0.88

	RMSE (m/s)			SI			Bias (m/s)			R		
ID	top	mid	bot	top	mid	bot	top	mid	bot	top	mid	bot
1717	0.46	0.51	0.43	0.69	0.76	0.68	-0.19	-0.24	-0.24	0.90	0.91	0.92
1718	0.34	0.38	0.49	0.63	0.65	0.81	-0.14	-0.31	-0.35	0.91	0.95	0.88
1719	0.37	0.34	0.39	0.43	0.38	0.44	0.04	-0.11	-0.25	0.95	0.96	0.96
1720	0.20	0.16	0.15	0.56	0.45	0.48	0.02	0.01	0.03	0.91	0.95	0.95
1721	0.14	0.14	0.15	0.22	0.22	0.23	-0.02	-0.01	-0.01	0.98	0.98	0.98
1722	0.08	0.08	0.09	0.23	0.23	0.31	0.00	0.01	0.02	0.99	0.99	0.98
1723	0.17	0.17	0.16	0.37	0.36	0.36	0.04	0.01	-0.01	0.96	0.96	0.96
1724	0.35	0.40	0.60	0.66	0.87	1.21	0.02	-0.21	-0.32	0.86	0.89	0.68
1725	0.16	0.11	0.08	0.71	0.54	0.55	-0.01	-0.01	0.01	0.84	0.92	0.90
1726	0.23	0.21	0.22	0.75	0.73	0.78	0.13	0.20	0.19	0.86	0.97	0.96
1727	0.25	0.17	0.29	0.50	0.45	0.90	0.12	0.06	-0.12	0.93	0.94	0.78
1728	0.29	0.17	0.21	0.43	0.29	0.44	0.10	0.07	-0.06	0.94	0.98	0.95
1729	0.28	0.21	0.20	0.36	0.29	0.33	0.03	-0.03	-0.04	0.96	0.97	0.97
1730	0.24	0.20	0.22	0.29	0.24	0.30	-0.14	-0.11	-0.12	0.98	0.98	0.98
1731	0.29	0.26	0.25	0.60	0.57	0.58	0.05	0.04	-0.02	0.87	0.89	0.88
1732	0.29	0.28	0.27	0.32	0.33	0.38	0.00	-0.05	-0.10	0.97	0.97	0.96
1733	0.18	0.18	0.20	0.49	0.52	0.63	-0.02	0.02	0.05	0.92	0.93	0.90
1734	0.14	0.15	0.16	0.19	0.23	0.31	-0.01	-0.04	-0.06	0.99	0.98	0.97
1735	0.12	0.11	0.13	0.16	0.16	0.24	0.00	-0.01	-0.05	0.99	0.99	0.99
1736	0.12	0.12	0.19	0.51	0.47	0.67	0.00	0.03	0.09	0.93	0.93	0.84
1737	0.46	0.40	0.39	0.86	0.75	0.79	-0.19	-0.17	-0.14	0.84	0.89	0.88
1738	0.34	0.31	0.23	0.51	0.47	0.40	-0.14	-0.14	-0.05	0.91	0.93	0.94
1739	0.33	0.25	0.25	0.35	0.29	0.34	0.10	-0.01	-0.09	0.96	0.97	0.97
1740	0.29	0.29	0.33	0.31	0.31	0.40	0.08	-0.06	-0.16	0.98	0.97	0.96
1741	0.29	0.28	0.38	0.43	0.38	0.53	0.06	0.02	-0.04	0.95	0.95	0.90
1742	0.32	0.59	0.61	0.42	1.81	3.46	-0.15	-0.29	-0.28	0.95	0.78	0.44
1743	0.25	0.23	0.23	0.82	0.92	1.33	-0.02	-0.06	-0.12	0.74	0.70	0.62
1744	0.46	0.38	0.40	0.79	0.74	0.98	-0.04	-0.21	-0.23	0.83	0.92	0.92
1745	0.24	0.21	0.25	0.55	0.67	0.82	0.03	-0.05	-0.03	0.90	0.92	0.80
1746	0.29	0.25	0.24	0.66	0.56	0.56	0.04	-0.02	-0.08	0.89	0.92	0.92

PNNL-30448

Pacific Northwest National Laboratory

902 Battelle Boulevard
P.O. Box 999
Richland, WA 99354
1-888-375-PNNL (7665)

www.pnnl.gov